Colorado
School of Mines

Quaternary Geology and Neotectonics of the West Flank of the Northern Sangre de Cristo Mountains, South-Central Colorado

James P. McCalpin

July 1982

Quarterly
vol. 77 no. 3

COLORADO SCHOOL OF MINES QUARTERLY

Volume 77 July 1982 Number 3

Quaternary Geology and Neotectonics of the West Flank of the Northern Sangre de Cristo Mountains, South-Central Colorado

James McCalpin
Department of Geology

Utah State University

$12.00

Guy T. McBride, Jr.
President

© 1983 Colorado School of Mines

CONTENTS

FIGURES

TABLES

PLATES

ABSTRACT

The Quaternary history of the northern Sangre de Cristo Mountains was dominated by at least four, and possibly five, episodes of alpine glaciation. Relative-dating (RD) data from 75 stations on moraines and rock glaciers suggest correlation of the four glacial advances with the Bull Lake, early Pinedale, mid-late Pinedale, and early Neoglacial episodes of the Rocky Mountains. Geomorphic evidence indicates that alluvial fan surfaces at the base of the mountains formed at the same time as terminal moraines and are primarily glacial outwash features. Postglacial (Holocene) alluvial fan deposition is restricted to much smaller areas than was full-glacial deposition.

The northern Sangre de Cristo Mountains and adjacent San Luis Valley are major horst and graben, respectively, of the Rio Grande Rift Zone in Colorado. Quaternary faulting on the 120-km-long Sangre de Cristo Fault Zone and on the 10-km-long Villa Grove Fault Zone has repeatedly offset the glacial and alluvial deposits. A total of 153 detailed scarp profiles and five backhoe trenches were utilized to reconstruct the history of Quaternary faulting on the two fault zones.

The Villa Grove Fault Zone is an intrabasin swarm of about 40 discontinuous, en echelon, basin-facing scarps that traverse northwestward across the northern San Luis Valley. Individual scarps range from 0.3 m to 14.0 m high. Vertical displacements of 0.8 to 1.4 m per fault event have estimated recurrence intervals of 60,000 to 100,000 years. Length of surface rupture and displacement per event suggest Quaternary earthquakes of Richter magnitude (M_L) 6.6 to 7.0. The last earthquake occurred less than about 13,000 years ago.

The range-bounding Sangre de Cristo Fault Zone displays evidence of recurrent surface faulting from pre-Bull Lake to early Holocene time. Scarp heights range from 2 m in Holocene to 87 m in pre-Bull Lake deposits. Average displacements of 1.2 m to 2.9 m per event, deduced from scarp profile and trench data, suggest Quaternary earthquakes of magnitude (M_L) 6.8 to 7.4. Long-term recurrence intervals for surface-faulting events range from about 10,000 to 47,500 years; however, distribution in time is nonuniform. Radiocarbon dates indicate events can occur within as little as 2500 years of each other. The two most recent events are dated by ^{14}C; the first occurred between about 13,000 and 10,100 $\pm$ 110 years ago, and the second shortly before 7600 $\pm$ 120 years ago.

The deduced frequency and magnitude of Quaternary earthquakes is not readily compatible with the lack of historic seismicity in the Sangre de Cristo Mountains. In the 110-year history of the study area, shocks up to magnitude 4.6 should have occurred if standard earthquake frequency-magnitude relations are assumed. The lack of such events indicates that the two studied faults may resemble other Basin and Range faults, which display a "seismic cycle" of thousands of years from one large earthquake to the next. Between large events, seismicity falls to very low levels.

ACKNOWLEDGMENTS

Field research for this study was supported by National Science Foundation Grant EAR 79-12446. The author is indebted to Thomas L.T. Grose, Steve Colman, R. Ernest Anderson, Rahe Junge, and Robert Kirkham for field reviews and interpretation of trench exposures excavated across fault scarps. Jim Yenter and Ted Barnhart assisted in data interpretation. Gratitude is expressed to landowners and managers for permission to trench, especially Stan Pavlin, Malcolm Stewart, and Maurice Strong. Neil and Terry Seitz and Doug and Sioux Bishop provided excellent field and moral support.

GLOSSARY

α Fan surface slope (Wallace 1980).
β Fault dip (Wallace 1980).
γ Rotation angle.
ϕ Rotation angle.
θ Maximum scarp slope angle (Bucknam and Anderson 1979).

ns Net dip slip.
h_1 Fault throw (vertical component of displacement).
h_{1t} True fault throw across fault zone (same as h_{nt}, H_t).
h_{1a} Apparent fault throw at main scarp.
h_2 Scarp height.
h_3 Scarp height levelled.
h_4 Scarp height, modified levelling.

h_{mt} True displacement, main scarp.
h_{ma} Apparent displacement, main scarp.
h_{at} True displacement, antithetic scarp.
h_{aa} Apparent displacement, antithetic scarp.
h_d Vertical component of drag.
h_f Vertical component of displacement due to flexure.
h_{sf} Vertical displacement due to rotation of the fault-bounded zone.

so Surface offset.
so_f Surface offset due to rotation (flexure).

W_c Width of scarp crest (horizontal distance that encompasses 50 percent of the total angular curvature between θ and α, roughly centered on scarp crest).
R_c Retreat of scarp crest (horizontal distance between projected original crest and present crest).
W_f Width of rotated zone.

H Scarp head (edge of uneroded original fan surface).
C Scarp crest (segment junction of maximum curvature below head).
B Scarp base (segment junction of maximum curvature above toe).
T Scarp toe (edge of uncolluviated original fan surface).

INTRODUCTION

BACKGROUND

Location

The study area is located in south-central Colorado, on the eastern margin of the San Luis Valley (figure 1). The adjacent mountains, the Sangre de Cristo Range, are the northern segment of a linear mountain chain which extends from central New Mexico to central Colorado. This lofty range, elevated by late Cenozoic tectonism, contains seven of Colorado's 53 peaks over 4269 m (14,000 ft).

The mapped area includes the entire western flank of the northern Sangre de Cristo Mountains, as well as a portion of the adjacent alluvial slope of the eastern San Luis Valley (figure 2). The main structural feature of the area, the Sangre de Cristo Fault, coincides with the physiographic boundary between the mountains and valley.

Purpose and Strategy

The purpose of this study is threefold: first, to map Quaternary deposits in the area in greater detail than was previously done; second, to establish the chronology of Quaternary depositional episodes; and third, to determine the sequence and magnitude of neotectonic faulting that has deformed the deposits. An additional objective is to supplement estimates of seismic risk for the State of Colorado and the Rio Grande Rift Zone (RGRZ) by supplying new data on Quaternary tectonism. As Allen (1975) has noted, analysis of historical seismicity without regard for the visible Quaternary record is often unreliable for estimating earthquake potential.

The strategy adopted to achieve these goals is also threefold. First, the distribution of glacial and alluvial deposits has been determined by photogeologic mapping and field checking. Second, collection of stratigraphic, morphologic, and weathering data from deposits permits definition of an age sequence of deposits. Finally, detailed mapping of the distribution of fault scarps and their interaction with Quaternary deposits, and collection of scarp profile data, provide estimates of the timing of Quaternary faulting. The field program carried out in 1979 and 1980 essentially followed this strategy.

Previous Investigations

Early reports by Siebenthal (1907, 1910) provided generalized descriptions of the geology of the Sangre de Cristo Range and San Luis Valley. A hiatus in publications followed until the late 1930s, when Burbank and Goddard (1937) reviewed the structural history of the Sangre de Cristo Mountains, and Bryan (1938) described the geology of the San Luis Valley. Upson (1938, 1941) was the first to note Quaternary faulting in the eastern San Luis Valley and gave a broad overview of the valley's geomorphology (Upson 1939). Detailed mapping of the Sangre de Cristo Range began in the 1950s as thesis projects, each of which covered a small portion of the range (Gableman 1952; Clement 1952; Toulmin 1953; Litsey 1954; Munger 1959; Koch 1963; Karig 1964; Volckmann 1965; Nolting 1970; Wychgram 1972). Recent theses have synthesized data from throughout the area (Knepper 1974; Huntley 1977). Scott and others (1976) mapped and subdivided surficial deposits in part of the area and introduced the nomenclature of the Rocky Mountain Quaternary chronology (Blackwelder 1915; Richmond 1965) into the study area.

Dr. McCalpin earned his Ph.D. from Colorado School of Mines in geology in 1981. He is currently assistant professor of geology at Utah State University.

0163-9153/82/7703-0001 $00.20/0

© 1983 Colorado School of Mines

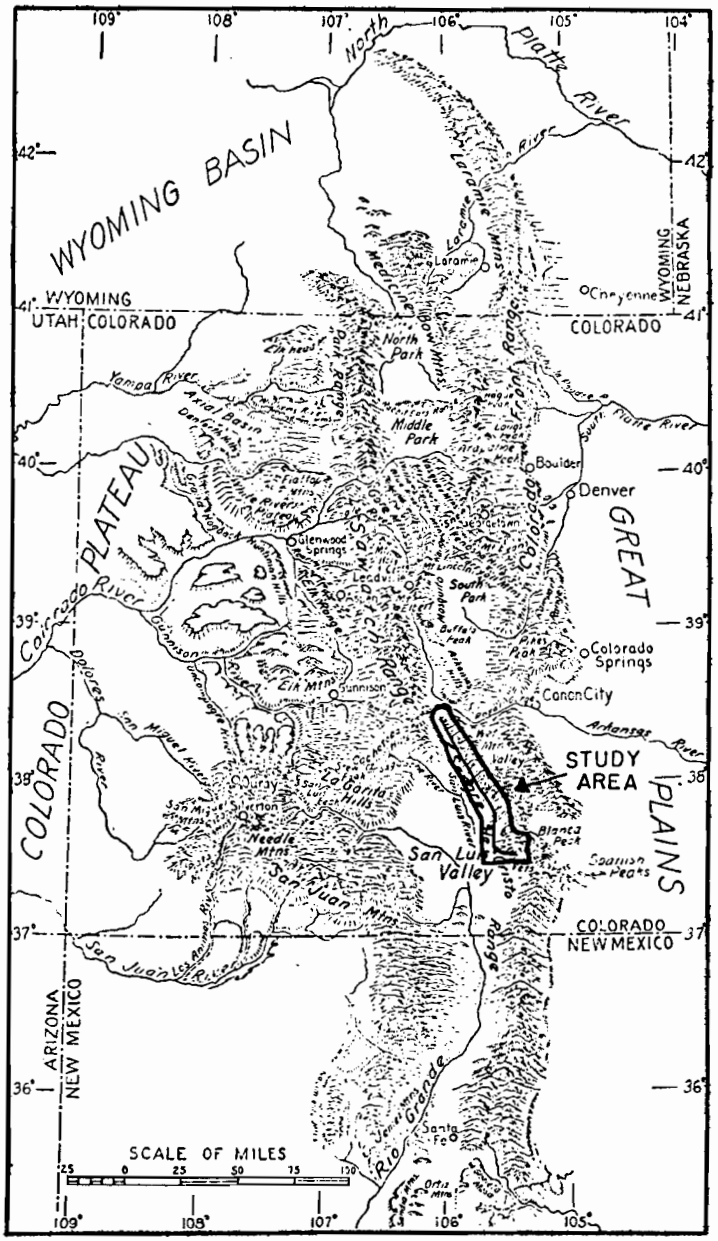

Figure 1.—Location map of the study area. Physiographic drawing by Guy Harold-Smith, from Atwood (1939).

Geophysical data collected in the San Luis Valley area (Gaca and Karig 1966; Stoughton 1977; Davis and Stoughton 1979) have contributed to understanding of subsurface geology. Jordan (1974) and Pearl and Barret (1976) discussed the geothermal potential of the valley. Previous works addressing Quaternary tectonism of the area are Scott (1970), Kirkham and Rogers (1981), and Peterson (1979). For an overview of RGRZ tectonics, the reader is referred to two recent comprehensive surveys (Hawley 1978; Riecker 1979).

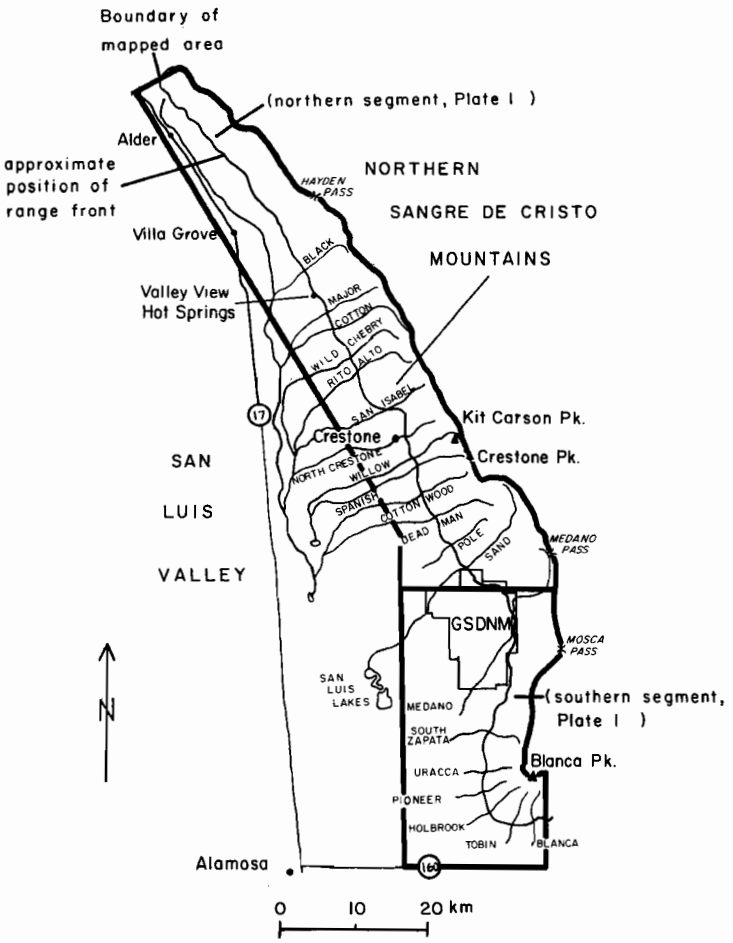

Figure 2.—Index map of the study area, showing geographic names.

Climate

Strong gradients of both temperature and precipitation exist between the floor of the San Luis Valley (elevation 2285 m) and the high peaks of the Sangre de Cristo Mountains (elevation 3660 m—4270 m). These gradients are reflected in vegetation, weathering rates, and physical processes at work in the study area.

Precipitation falls largely as winter snow or summer thunder showers. Annual precipitation ranges from 178 mm per year on the valley floor to 1016 mm per year on the highest mountain peaks (figure 3). Temperatures likewise exhibit an extreme range. At Alamosa, immediately southwest of the study area, mean monthly temperatures range from −8°C (January) to 18°C (July): extreme temperatures of −40°C to over 38°C have been recorded (Huntley 1977). Potential evapotranspiration varies widely over the study area, dependent mainly on local values of temperature. In general, precipitation exceeds evapotranspiration in the Sangre de Cristo Mountains, whereas the reverse is true in the San Luis Valley.

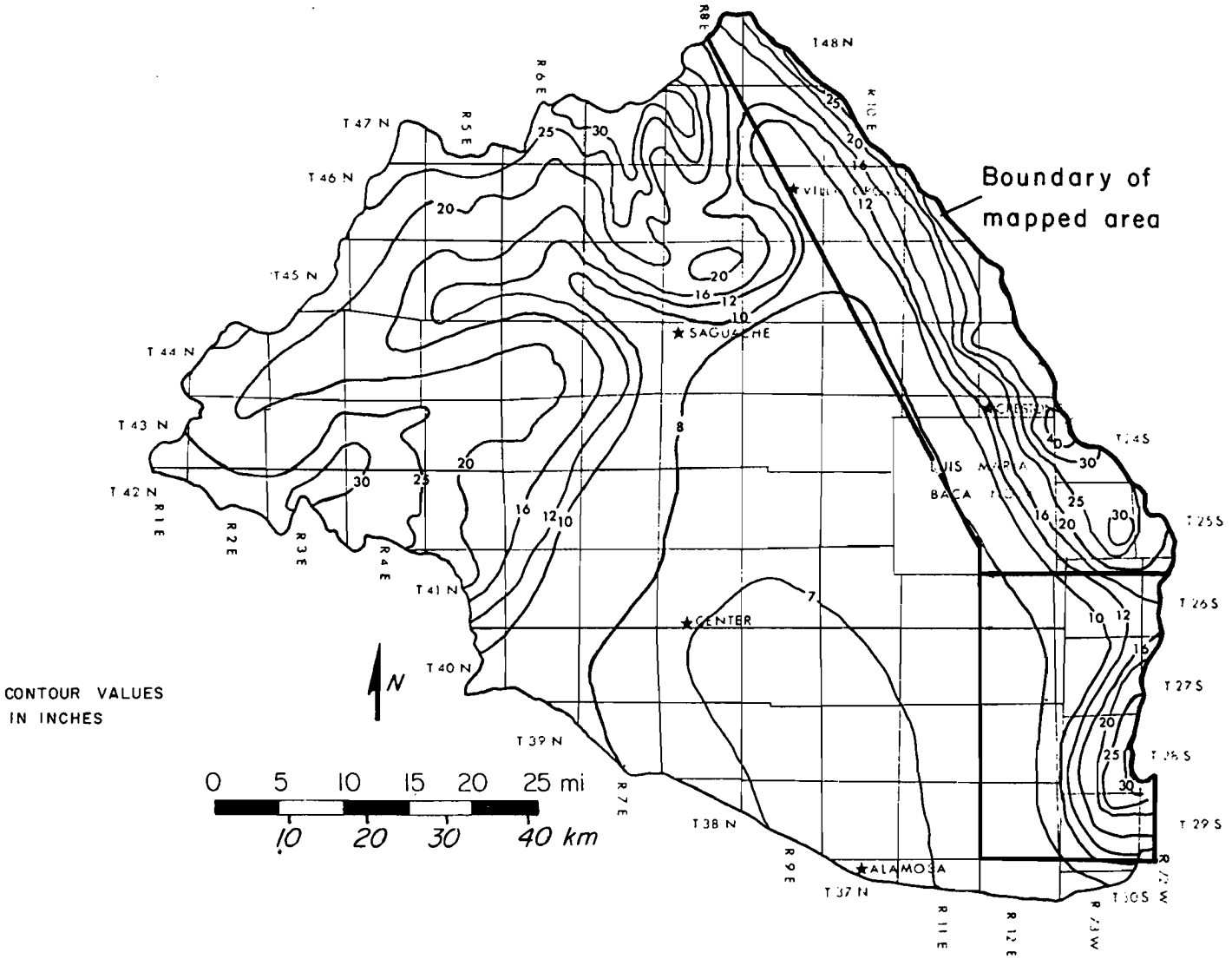

Figure 3.—Map of mean annual precipitation in the San Luis Valley, Colorado. Modified after Huntley 1977; data from U.S. Department of Commerce.

Vegetation and Soils

The study area encompasses five of the six life zones of Merriam (1897), from the Upper Sonoran (lowest) to the Arctic-Alpine (highest). The distribution of these zones in the study area, and their characteristic vegetation, are schematically shown in figure 4. The boundaries of the life zones, which roughly parallel elevation contours, are controlled by elevation, temperature, slope, aspect, wind, and available moisture. At lower elevations available moisture seems to be the primary control on boundaries, whereas temperature, aspect, and wind become more important at higher elevations.

Within each zone, distribution of individual plant species is sometimes sensitive to geologic or pedologic parameters. In the mountains, aspen (*Populus tremuloides*) dominate on glacial deposits in the Canadian Zone, whereas bedrock slopes of similar elevation and aspect carry a Douglas fir cover (*Pseudotsuga menzeiesii*). At the toe of slopes, the pinyon-juniper community (*Pinus edulis-Juniperus scopolorum*) occupies sites with young, stony soils; older, more clay-rich soils support scrub oak (*Quercus gambelli*).

Strong gradients of precipitation, evapotranspiration, and temperature traversing the study area from west to east (figures 3 and 4) have seemingly affected soil development and morphology. Richmond (1962, page 25) observed that "In the Rocky Mountains, climatic provinces are telescoped in narrow altitude zones, to which the great soil groups correspond . . . ." Effects due to climate in soil profiles of the San Luis Valley are superimposed upon those due to time. These climatic effects can be examined by describing soils on surfaces of a single age across a climatic transect. The resulting soil sequence is known as a climosequence.

Two soil climosequences, developed in deposits of Pinedale and Bull Lake age (defined later in the Quaternary Chronology section), are shown diagrammatically in figure 5. In each cli-

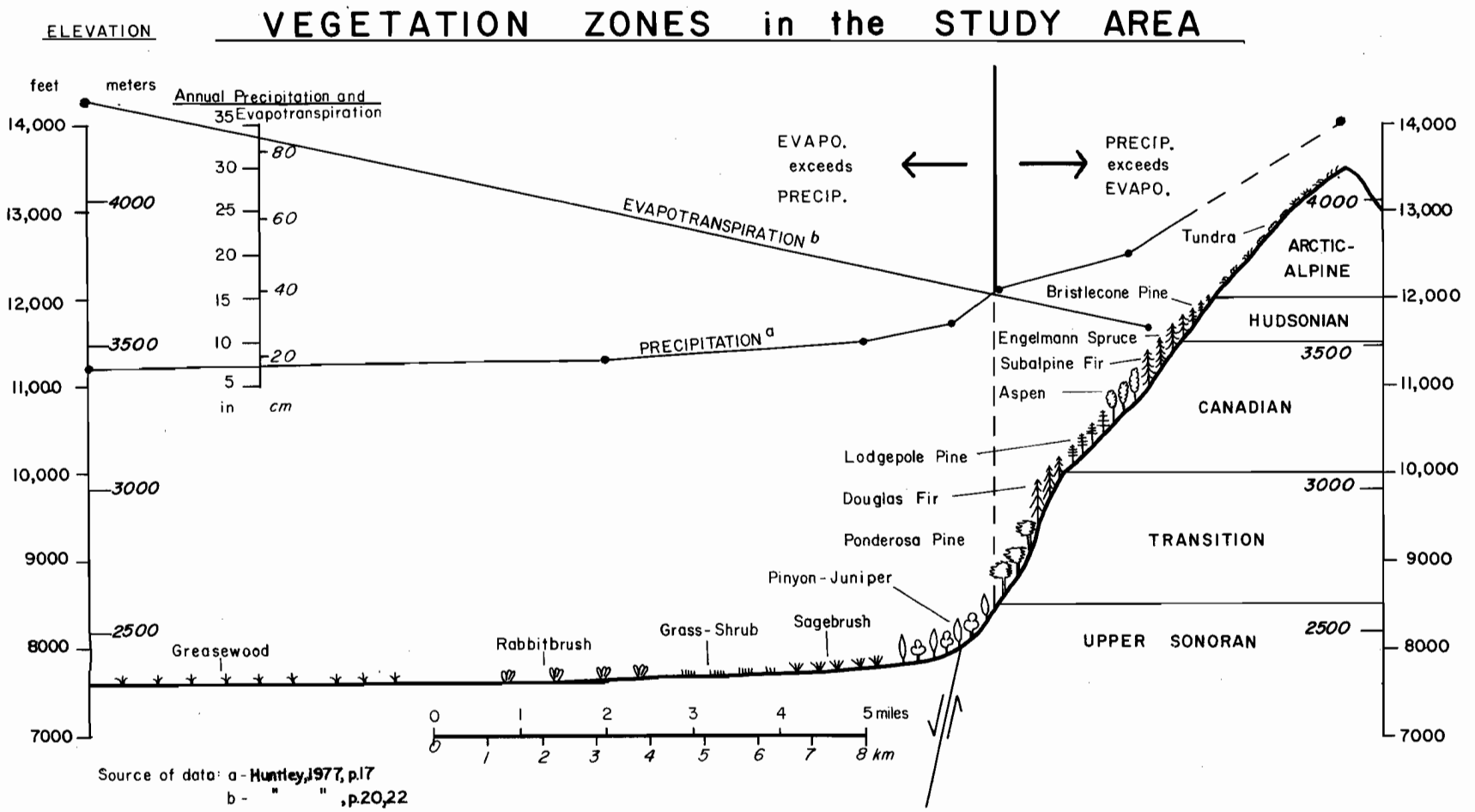

Figure 4.—Schematic profile of vegetation zones in the study area. Distribution of plants and zones is adapted from Dixon (1971) and from field observations in this study.

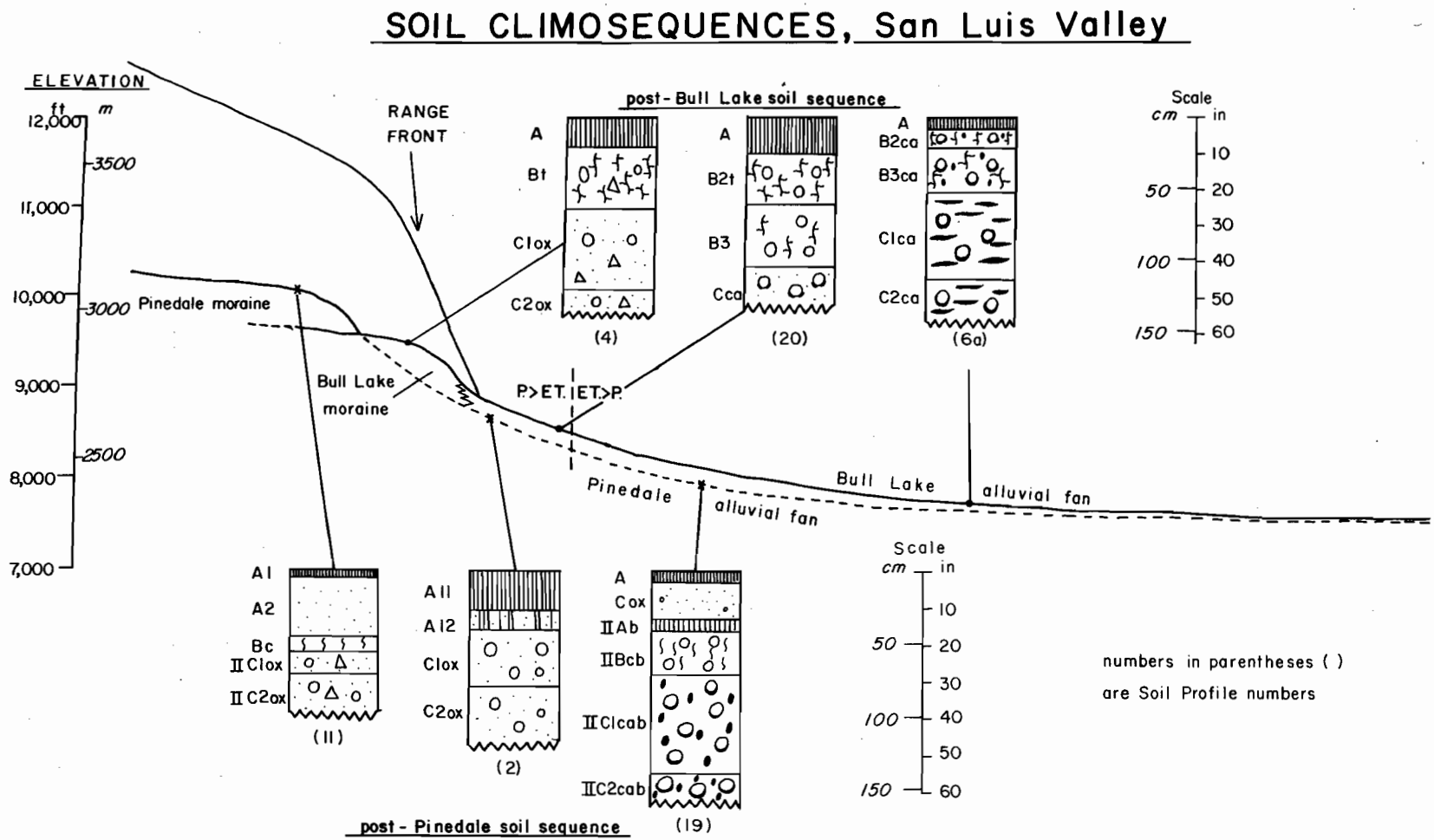

Figure 5.—Diagram showing effect of elevation and climate on Quaternary soil profile development, San Luis Valley. Profile symbols are explained in Appendix A.

mosequence, the effect of decreased precipitation and soil water infiltration with decreasing altitude is apparent. Soil carbonate becomes better developed and shallower in the profiles approaching the valley floor. Soils of post-Pinedale age contain no secondary $CaCO_3$ above the modern line where precipitation equals evapotranspiration (P = ET, figure 4), but do contain increasing amounts of secondary $CaCO_3$ with increasing drop below that elevation. By contrast, post-Bull Lake soils display secondary $CaCO_3$ at elevations higher than the modern P = ET elevation. A higher elevation for the pedocal-pedalfer boundary for older Quaternary soils is common in the Rocky Mountains (Richmond 1972, figure 2). The mechanism responsible for this is probably the development of clayey B horizons and subsequent greater water-holding capacity in the older soils (Birkeland 1974, page 243).

REGIONAL GEOLOGY AND TECTONIC SETTING

Regional Geology

The northern Sangre de Cristo Mountains are a Neogene block uplift comprised mainly of Upper Paleozoic clastic sedimentary rocks, with minor Precambrian crystalline rocks, Lower to Middle Paleozoic sedimentary rocks, and rare Tertiary intrusives. Large anticlines and synclines in the thick (up to 5500 m) Upper Paleozoic section trend roughly parallel to present range boundaries and dominate the structure of the northern portion of the range. The southern portion, including the Blanca Peak Massif, is predominantly Precambrian metamorphic rocks (figure 6).

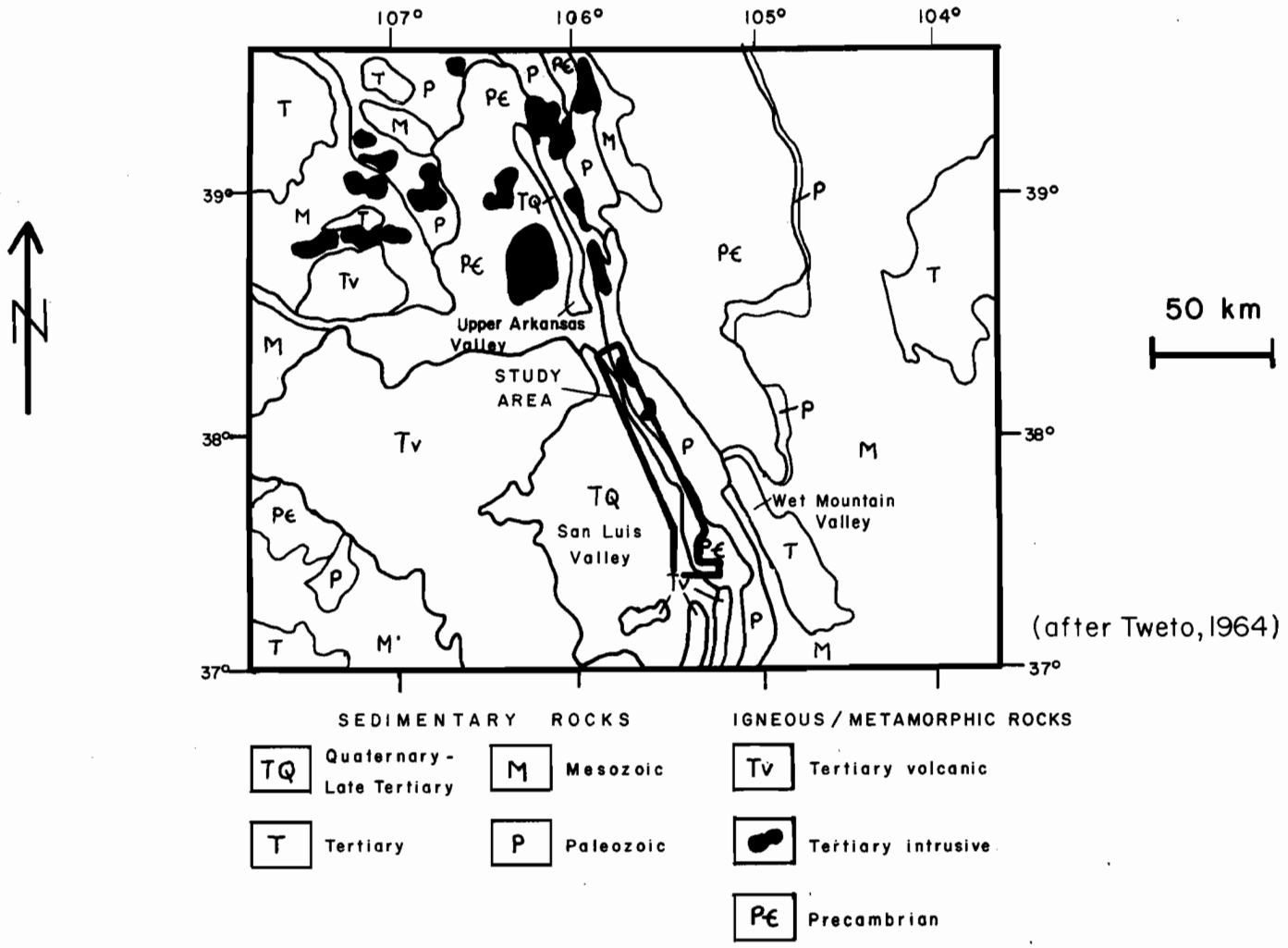

Figure 6.—Regional geologic map of south-central Colorado, after Tweto (1964).

Flanking the Sangre de Cristo Range on the west is the San Luis Valley, a Neogene asymmetric graben (figure 6). Continuous syntectonic sedimentation since at least mid-Tertiary time has filled this graben with up to 5000 m of volcanoclastic and arkosic sediments, plus intercalated volcanic flows (Huntley 1979).

Tectonic Setting

The northern Sangre de Cristo Mountains and San Luis Valley are integral parts of the Rio Grande Rift Zone (RGRZ, figure 7). Structurally the RGRZ is an intracratonic continental rift superimposed during the late Cenozoic upon previously deformed terranes of Colorado and New Mexico. With the cessation of the Laramide orogeny in early Tertiary time, erosion beveled the Laramide folds to produce a widespread low-relief erosion surface over much of central Colorado (Epis and others, 1976). This surface was well developed by late Eocene. Its further development was arrested in early Oligocene by outpouring of andesitic volcanics from the San Juan Volcanic Field and other locales. Andesitic and rhyolitic flows crossed the site of the present Sangre de Cristo Range north of 38° N latitude from west to east, indicating that no continuous topographic barrier existed at that time (Taylor 1975; Epis and others 1976, figure 8).

Sometime after early Oligocene time the Rio Grande Rift began to form. Simplistically, the RGRZ can be viewed as a giant "pull-apart" structure formed by the separation of the Colorado Plateau on the west from the interior craton on the east. The previous widespread Eocene erosion surface and its overlying volcanic cover were displaced by normal faulting, with displacements measured today ranging from 50 m to 1000+ m (Epis and others 1976). Knepper (1974) outlined five stages of rift development in central Colorado, the first three associated with north-trending structures, and the last two by northwest-trending structures. The present topographic features of this study area have resulted from the latter two stages (Pliocene to Holocene).

The geometry of the San Luis Basin is shown in figure 8. Basin-fill strata are disrupted by intragraben normal faults, as well as by the Sangre de Cristo Fault at the eastern basin margin. Thinning of basin-fill strata over buried horsts (figure 8) suggests that rifting may have been contemporaneous with deposition of these beds. Palynomorphs from arkosic basin-fill sediments overlying Precambrian basement indicate a Paleocene to Oligocene age for the oldest basin-fill sediments. Based on such evidence Tweto (1975, page 5) has hypothesized that rifting in Colorado may have begun as early as Paleocene, or considerably before the classical inception of Rio Grande rifting in late Oligocene (Lipman and Mehnert 1973; Chapin and Seager 1975, pages 299-304).

Intragraben faults die out in the Plio-Pleistocene Alamosa Formation and do not offset the surface (figure 8). The only surficial evidence of Quaternary faulting occurs at the Sangre de Cristo Fault Zone (SCFZ), at the base of the Sangre de Cristo Range. The geometry of the Alamosa Formation as a simple unfaulted wedge, which thickens steadily from west to east across the San Luis Basin, suggests that faulting during and after its deposition has been mainly downdropping along the Sangre de Cristo Fault, with subsequent eastward tilting of the San Luis Valley graben. The present position of the lowest part of interior drainage near the eastern margin of the valley, and the presence of conspicuous fault scarps at the base of the Sangre de Cristo Mountains, suggest that such tilting is still active today.

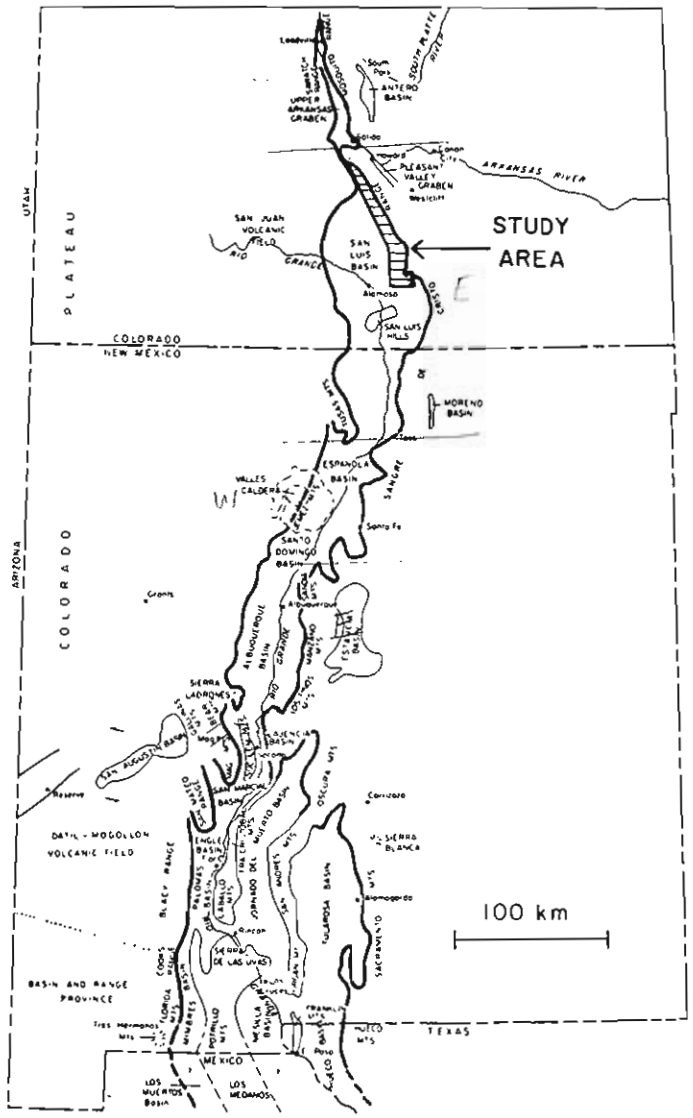

Figure 7.—Generalized map of the Rio Grande Rift Zone, Colorado and New Mexico. Modified from Chapin (1971). Marginal faults are marked by a heavy line.

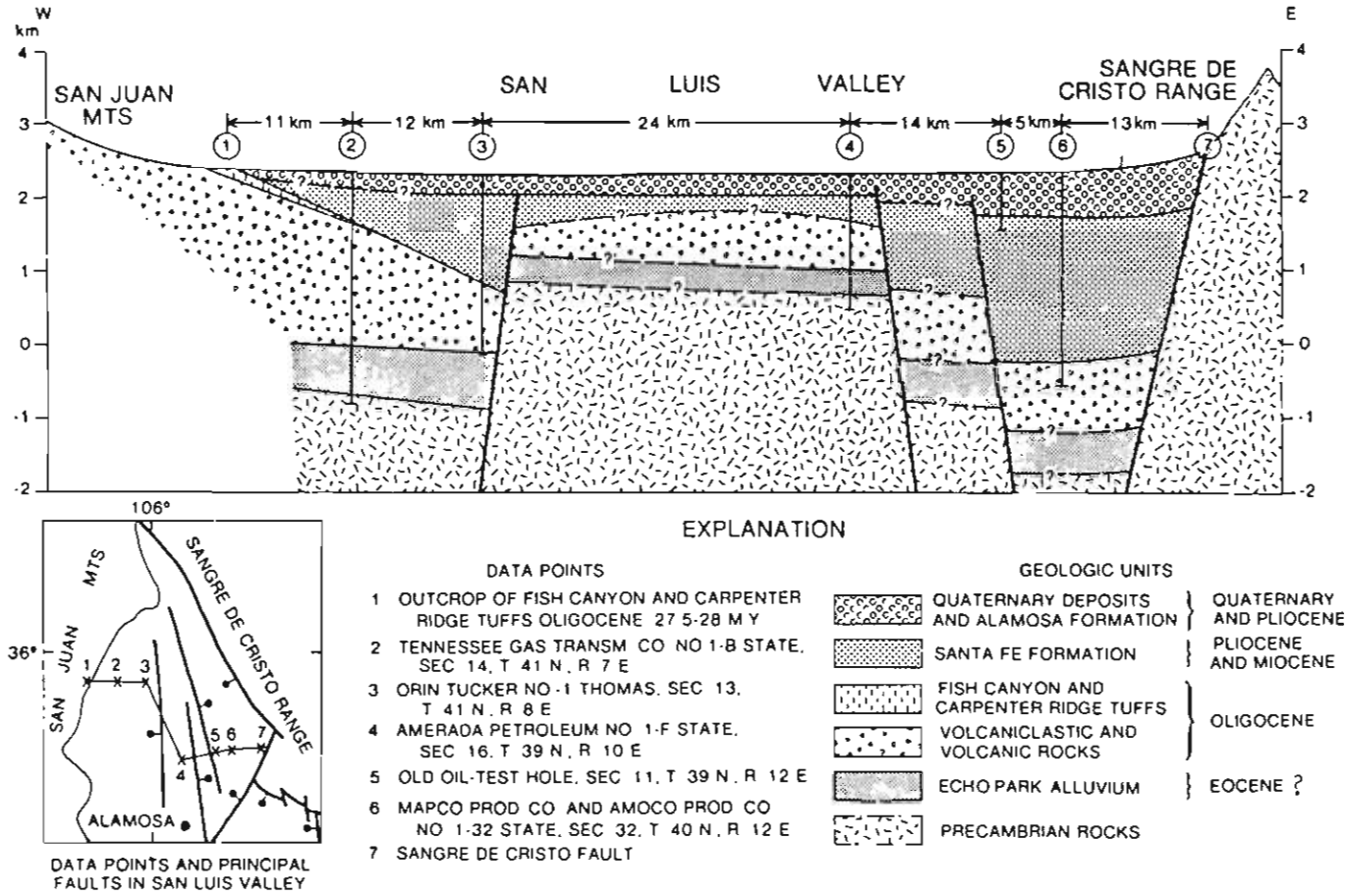

Figure 8.—Diagrammatic cross section of the San Luis Valley from Tweto (1979). Intrabasin faults die out within the Plio-Pleistoene Alamosa Formation; only the range-bounding Sangre de Cristo Fault offsets late Pleistocene deposits.

PART ONE: QUATERNARY GEOLOGY

INTRODUCTION

Quaternary deposits in the study area fall into two broad categories: (1) glacial, lacustrine, and mass-movement deposits in the Sangre de Cristo Mountains, and (2) alluvial fan deposits of the adjacent San Luis Valley. The distribution, morphology, sedimentology, and weathering characteristics of Quaternary deposits are described by category in the following sections. Quantifiable morphologic and weathering parameters form the basis for a relative-age chronology that is presented at the end of the description section. Deposits are informally named by reference to correlated equivalents which are widespead in the Rocky Mountains (Pinedale, Bull Lake, pre-Bull Lake). Usage in this report follows the earlier introduction of the Pinedale-Bull Lake terminology into part of the study area by Scott (1970), Scott and Taylor (1975) and Scott and others (1976).

METHODS

Quaternary deposits were identified and delineated by photogeologic mapping from various imagery sources: (1) 1:100,000 (nominal) color and color infrared aerial photographs; (2) 1:50,000 (nominal) color infrared aerial photographs; and (3) 1:15,840 black-and-white aerial photographs. Deposit boundaries were inferred from the outlines of well-defined landforms such as lateral and terminal moraines and alluvial fans. Boundaries were modified during field checking, and, in addition, deposits with poor morphologic expression were mapped. Weathering and morphologic data were collected from stations located on crests of moraines, rock glaciers, and alluvial fan surfaces.

In determining the chronology of Quaternary deposits heavy reliance was placed on collection of relative-dating (RD) data collected at stations. RD data cover a broad range of measurements on surface clast weathering and deposit morphology. Proponents of the RD method have concluded "the chances of arriving at a valid subdivision and correct correlations are greatly enhanced if a variety of surface and subsurface RD parameters are measured" (Birkeland and others 1979b, page 534). Accordingly, 15 RD parameters were measured in this study at each of 75 RD stations [RD station locations are given in McCalpin (1981, plate 1)]. Parameters measured were chosen from a comprehensive list compiled by Burke and Birkeland (1979), and are listed and defined in table 1.

GLACIAL DEPOSITS

Quaternary glacial deposits occur in 25 of the larger drainages on the west flank of the northern Sangre de Cristo Mountains. Glacial ice appears to have concentrated in two areas: (1) in the north-central part of the range, centered about Kit Carson (4317 m) and Crestone (4357 m) Peaks, and (2) in the Blanca Peak Massif at the south end of the range, a large uplift that includes four summits higher than 4269 m (figure 2). From these two centers of accumulation, glacial ice filled valley-head cirques and flowed down valley as valley glaciers.

In the northern section of the range, most glaciers did not advance to the tectonic mountain front. Hence their terminal deposits occur within steep-walled canyons cut into the Sangre de Cristo Range. To the south, the six radial glaciers of the Sierra Blanca reached the mountain front and extended as much as 0.5 km out onto the alluvial slope. Because glacier dynamics and till deposition differed considerably between the north and south segments of the range, deposits in each area are described separately.

Table 1.—Definitions and measurement techniques for relative-dating (RD) parameters [modified from Burke and Birkeland (1979)]

NOTE that parameters (1)-(8) describe surface clast weathering, parameters (9)-(12) describe deposit morphology, and parameters (13)-(14) describe subsurface weathering. (At each station 25 stones were sampled, most from 5 to 15 cm in diameter.)

(1) POS—Percentage of oxidized stones. The percentage of sampled stones on the moraine surface which exhibit brownish or reddish oxidation discoloration over more than 50 percent of the stone surface.

(2) PPS—Percentage of pitted stones. The percentage of sampled stones on the moraine surface which exhibit concave weathering pits formed by granular disintegration of rock grains or crystals.

(3) MPD—Maximum pit depth. The maximum depth (in mm) of a weathering pit formed by granular disintegration on sampled stones, measured perpendicular to the stone surface.

(4) PSWR—Percentage of stones with weathering rinds. The percentage of sampled stones on the moraine surface which exhibit measurable rinds of oxidation or alteration beneath the stone surface. The lower measurement limit in this study was 0.5 mm.

(5) MRT—Maximum rind thickness. The maximum thickness (in mm) of weathering rinds on all sampled stones, as defined above.

(6) ART—Average rind thickness. The mean of all measurable weathering rind thicknesses on sampled stones, as defined above. Zero values (for stones with no rinds) were not included.

(7) MPLC—Maximum percentage of lichen cover. The maximum percentage of surface area of sampled boulders that is covered by any species of lichen; visually estimated.

(8) MLD—Maximum lichen diameter. The maximum measured diameter (in mm) of individual lichen of the species *Rhizocarpon geographicum* on the surface of sampled boulders.

(9) SBF—Surface boulder frequency. The number of boulders greater than 30 cm in diameter exposed at or on the surface within a 30 m by 6 m area on the moraine crest. Areas were chosen that seemed representative of the entire moraine surface.

(10) BBF—Boulder burial factor. The product of (1) the percentage of boulders partially buried on the moraine crest, multiplied by (2) the average volume percentage burial of boulders (visual estimate). Possible range of values is 0 (all boulders sitting loose on surface) to 1.0 (no boulders exposed at surface). This term is introduced in this paper.

(11) MCW—Moraine crest width. The average horizontal width (in m) of the surface zone at the top of a moraine which has a surface slope of 5° or less.

(12) MMSAO and MMSAI—Maximum moraine slope angles, outer and inner. The maximum measured slope (in degrees) of the present outer and inner slopes of morainal ridges.

(13) SPD—Soil profile development. The degree of subsurface weathering and soil horizonation which has occurred at the moraine surface since deposition. Soil profiles are described according to standardized U.S. Soil Conservation Service terminology (Soil Survey Staff 1975).

(14) SWS—Subsurface weathering of stones. The relative abundance of fresh, moderately weathered (grussified) and strongly weathered (grussified) clasts within glacial deposits. Usually measured within 1.0 m of the ground surface.

Pre-Bull Lake Till

Although pre-Bull Lake till (undivided) has been mapped on the east side of the Sangre de Cristo Range (Scott and Taylor 1975; Scott and others 1976), none was found within the present study area. Assuming that pre-Bull Lake glaciers also existed on the west side of the range, there are several possibilities for the failure to map contemporaneous deposits: (1) till was removed by erosion, (2) till was deposited on the down-dropping San Luis Valley block, and is now buried by younger deposits, (3) till does exist, but could not be distinguished from Bull Lake till.

Bull Lake Till

Northern Segment. Till of Bull Lake age exists in the lower parts of glaciated valleys from Black Canyon to Pole Creek (figure 2 and plate 1). Morphology of till deposits includes massive, hummocky lobes, high-level till-veneered benches, and distinct lateral and terminal moraines. All deposits have been modified and subdued by weathering. RD stations are limited to the better-preserved moraines, where sites relatively undisturbed by erosion could be located. Table 2 lists RD data from Bull Lake moraines.

A stream cut into Bull Lake till on the banks of Willow Creek exposes 43 m of oxidized till. The material is composed of unsorted boulders and cobbles in a brown (7.5YR6-7/4 Munsell) matrix of compact, hard, sandy silt. Boulders assume random attitudes in the lower part of the outcrop, but weak stratification is visible near the surface. Coarse-grained igneous clasts are completely grussified while fine-grained clasts are only partially grussified. Surface soil profiles, where exposed, exhibit textural B horizons.

Multiple moraines of Bull Lake age occur only at Spanish Creek (figure 2; plate 1). RD data from stations on both moraines failed to demonstrate significant weathering differences between the two (table 2, Stations 47 and 48). The general lack of multiple moraines, together with the uniformity of RD data, suggests that only a single Bull Lake glacial advance occurred in the study area. Recent reexamination of the type locality of the Bull Lake glaciation in Wyoming by Roy and Hall (1980) has shown that RD parameters show no difference among Bull Lake moraines. Absolute age of the Bull Lake glaciation is currently disputed (e.g., Richmond and Obradovich 1971; Pierce and others 1976); estimates range from 80,000 to 140,000 years BP.

Southern Segment. Bull Lake till exists in every glacial valley of the Sierra Blanca (plate 1). The morphology of all terminal moraine complexes is strikingly similar (figure 9), and argues for similar glacial histories in each valley. Subdued knob-and-kettle topography, characterized by infilled and partially breached kettles, indicate substantial postdepositional modification of moraines. Low benches fronting the massive lobes of Bull Lake till at South Zapata and Pioneer Creeks (figure 9), at first suspected of recording an early advance, have RD and morphological features very similar to those of the massive lobes (table 2, Stations 61 and 69). A probable explanation is that these benches represent rotational landslides of ice-rich Bull Lake till which slid off the steep frontal moraine slope during or soon after deposition.

Early Pinedale Till

Northern Segment. Moraines exhibiting steep slopes, abundant surface boulders and slight surface weathering commonly occur within the lower parts of glaciated valleys in the northern segment, and are ascribed to early Pinedale deposition. Early Pinedale till, where exposed in rare cuts, is bouldery, unsorted, slightly oxidized, and carries a weakly developed surface soil. Subsurface

Table 2.—RD data: Bull Lake moraines (see parameter definitions, table 1)

RD Parameter No. and Acronym	(1) POS	(2) PPS	(3) MPD	(4) PSWR	(5) MRT	(6) ART	(9) SBF	(10) BBF	(11) MCW	(12) MMSAO	(12) MMSAI	
Station No.[a]	(%)	(%)	(mm)	(%)	(mm)	(mm)			(m)	(deg)	(deg)	Station Elevation (m)
Northern Segment												
01	——	48	15	68	11	4.0	30	——	12	15	17	2994
03	——	36	15	96	11	3.8	48	——	11	18	37	2908
04	——	36	8	100	10	3.0	65	——	13	25	20	2934
10	——	——	50	100	8	5.0	——	.45	19	——	22	?
25	36	40	13	84	8	3.3	68	.36	11	29	35	3463
26	48	32	24	88	8	3.0	69	——	24	28	35	3585
36B	84	36	20	96	10	3.8	90	.60	20	27	24	2780
45	68	32	——	76	15	4.4	85	.15	19	28	37	3488
47[b]	56	16	——	96	6	2.4	59	.54	11	26	27	3158
48[c]	40	28	——	76	7	2.3	42	.58	14	32	26	3079
58	72	24	30	100	7	3.9	78	.32	14	——	32	2951
Mean	**58**	**33**	**22**	**89**	**9**	**3.5**	**63**	**.43**	**14**	**25**	**28**	**2846**
Southern Segment												
61[d]	32	0	——	100	10	4.7	87	.24	7	18	24	2811
62	56	0	——	100	12	5.3	110	.40	10	28	22	2869
65	16	0	——	100	22	6.0	75	.40	13	18	26	2957
66	24	0	——	100	7	5.1	84	.38	14	28	31	3037
68	——	——	——	——	——	——	——	.65	15	17	23	2982
69[d]	28	0	——	100	11	5.6	29	.40	10	26	13	2915
70B	24	0	——	100	16	6.6	122	.28	10	19	15	2884
72	30	0	——	100	35	12.2	20	——	12	37	16	2805
73	56	0	——	100	9	4.9	67	.39	11	27	29	2908
75	44	0	——	96	18	7.2	94	.70	14	23	14	2994
Mean	**35**	**0**	**——**	**99**	**16**	**6.4**	**76**	**.43**	**12**	**25**	**21**	**2928**

[a] RD station locations are given in McCalpin (1981, Plate 1a, northern segment; Plate 1b, southern segment).
[b] Inner moraine, Spanish Creek.
[c] Outer moraine, Spanish Creek.
[d] Frontal till bench, Blanca Massif.

stones are commonly oxidized, but are rarely grussified. RD data from stations on early Pinedale moraines are given in table 3. Vigorous postglacial erosion by streams has removed much of the terminal parts of early Pinedale moraines. Two exceptions are well preserved at the mouths of South Crestone and Willow Creeks (figure 10), where multiple lobate Pinedale moraines exist. Each moraine complex consists of a massive, single-crested outer till embankment (figure 11) with smaller multiple morainal ridges inset within it. The smallest and innermost moraine in each complex encloses a level, marshy meadow.

RD data from these two localities, as well as from other valleys where a similar sequence is more poorly preserved, show that the inner moraines are significantly less weathered than the outer moraines. The amount of the difference in weathering varies with the parameter measured, as discussed later in the Quaternary chronology section, but in most cases it is comparable to the difference between early Pinedale and the much older Bull Lake moraines. The large weathering difference suggests that the inner moraines, as a group, are considerably younger than the large outer moraine and are not simply recessionals within the same stade. Accordingly, the large, single-crested moraines are interpreted as the deposits of long-established glaciers at their maximum extent since Bull Lake time. Following a long period of stability, glacier ice retreated an unknown distance up valley, and then re-advanced at some later time (post-early Pinedale) to form the nested inner moraines. Retreat of the second advance created proglacial lakes, which filled to form the present marshy meadows.

Southern Segment. Linear, single-crested moraines which commonly overlie and cross cut large Bull Lake moraines (figure 9) are ascribed to early Pinedale glaciation. Extensive post-Pinedale landsliding has created many excellent exposures of fresh till at deeply incised fanheads. The till is an unstratified mixture of boulders and cobbles in a gray unoxidized matrix of sandy silt. RD values from stations on early Pinedale moraines are given in table 3.

The position of early Pinedale moraines on the flank (usually north flank) of Bull Lake moraine complexes suggest that early Pinedale ice advanced through stream breaches at the valley sides, between the pre-existing moraines and the bedrock valley wall (figure 9). Preference for the north valley side may reflect more insolation, ice melting, marginal meltwater discharge, and till erosion at the base of these south-facing slopes during deglaciation. Within terminal zones, till grades abruptly into coarse glacial outwash of the alluvial fans. Weak sorting and stratification in the outwash are the main field criteria to distinguish it from till (figure 12).

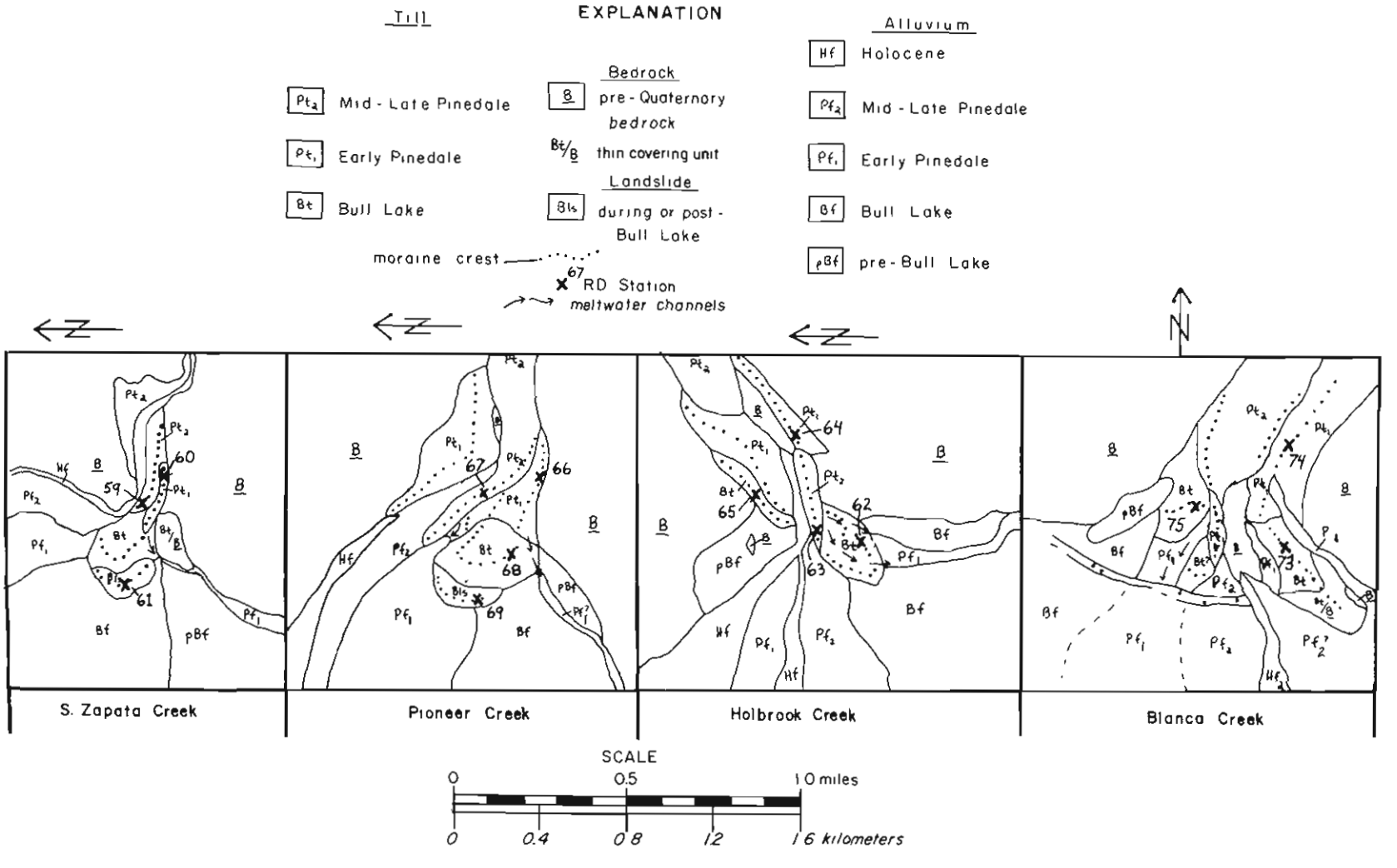

Figure 9.—Glacial geologic maps of four valley mouths, Blanca Massif. Massive Bull Lake moraines are commonly overlain and cross cut by younger linear Pinedale moraines of two ages. RD data from stations are given in tables 2,3, and 4.

Table 3.—RD data: Early Pinedale moraines (see parameter definitions, table 1)

RD Parameter No. and Acronym	(1) POS	(2) PPS	(3) MPD	(4) PSWR	(5) MRT	(6) ART	(9) SBF	(10) BBF	(11) MCW	(12) MMSAO	(12) MMSAI	
Station No.[a]	(%)	(%)	(mm)	(%)	(mm)	(mm)			(m)	(deg)	(deg)	Station Elevation (m)
Northern Segment												
02	—	12	30	72	5	2.4	54	—	8	25	31	3006
05	—	22	5	77	10	2.7	84	—	6	28	30	3091
09	—	38	4	77	10	4.2	67	.59	14	24	33	3030
16	4	12	5	52	6	2.0	67	.12	4	25	31	2957
22	56	36	15	100	20	5.5	29	.75	6	23	29	3165
23	72	48	—	100	12	4.4	20	.52	8	23	28	3121
24	36	40	12	76	4	2.7	37	.30	8	36	30	2945
32[b]	36	24	6	56	2	1.2	86	.34	5	35	35	3152
34[b]	56	4	—	68	4	2.3	97	—	8	32	27	3177
37[b]	36	0	48	56	4	1.7	151	.15	6	29	37	3073
40[b]	72	12	56	76	4	2.1	90	.24	5	33	28	2982
46	40	16	—	72	6	2.3	96	.52	8	28	33	3268
51	52	24	40	68	3	1.4	57	.22	6	25	34	3366
52	40	20	12	80	2	1.2	69	.29	8	26	34	3378
53	52	16	10	68	4	1.4	51	.20	7	28	32	3036
57	40	0	—	50	5	3.4	127	.30	6	34	32	3104
Mean	**46**	**20**	**20**	**72**	**6**	**2.6**	**74**	**.35**	**7**	**28**	**32**	**3116**
Southern Segment												
60	52	8	8	100	9	4.8	109	.40	5	24	32	2912
64	16	0	—	96	10	5.3	80	.40	8	31	41	3098
67	8	0	—	100	7	5.0	70	.22	5	20	37	3018
71	12	0	—	92	5	3.4	130	.22	11	26	35	3012
74	24	0	—	96	7	4.0	101	.18	4	33	36	3091
Mean	**22**	**1**	**8**	**97**	**8**	**4.5**	**98**	**.28**	**7**	**27**	**36**	**3026**

[a] RD station locations are given in McCalpin (1981, plate 1).
[b] At the South Crestone Creek/Willow Creek Terminal moraine complexes.

Table 4.—RD data: Mid-late Pinedale moraines (see parameter definitions, table 1)

RD Parameter No. and Acronym	(1) POS	(2) PPS	(3) MPD	(4) PSWR	(5) MRT	(6) ART	(9) SBF	(10) BBF	(11) MCW	(12) MMSAO	(12) MMSAI	
Station No.[a]	(%)	(%)	(mm)	(%)	(mm)	(mm)			(m)	(deg)	(deg)	Station Elevation (m)
Northern Segment												
High Elevation												
08	—	32	5	88	6	3.9	97	—	4	32	28	3308
12	40	40	—	92	9	3.8	—	—	5	16	27	3341
21	56	40	58	100	15	4.9	89	.54	4	25	27	3354
30	72	24	20	88	10	3.0	182	.17	8	35	14	3341
43	92	20	22	88	12	2.0	128	—	12	26	31	3790
Mean	**65**	**31**	**26**	**91**	**10**	**3.5**	**124**	**.36**	**6**	**27**	**25**	**3427**
Low Elevation												
15	8	28	—	60	4	2.0	90	—	8	28	37	2939
31	32	16	12	44	8	2.2	48	.31	6	16	18	3152
33[b]	44	24	8	52	3	1.7	88	.27	6	23	30	3134
38[b]	40	8	28	64	8	2.6	98	.26	11	28	26	2982
39[b]	68	8	8	72	7	2.8	125	.24	6	28	25	2988
44	—	—	—	—	—	—	66	.45	5	26	40	3036
54	24	12	25	60	6	2.0	105	.13	5	—	30	2957
56	28	0	—	60	6	2.8	146	.15	5	34	29	3158
Mean	**35**	**14**	**16**	**59**	**6**	**2.3**	**96**	**.26**	**6**	**26**	**29**	**3043**
Southern Segment												
59	52	0	—	84	7	3.3	116	.36	4	20	36	2887
63	16	0	—	96	7	4.7	107	.24	5	20	38	2884
Mean	**34**	**0**	**—**	**90**	**7**	**4.0**	**111**	**.30**	**4**	**20**	**37**	**2885**

[a] RD station loations are given in McCalpin (1981, plate 1).
[b] At the South Crestone Creek/Willow Creek terminal moraine complexes.

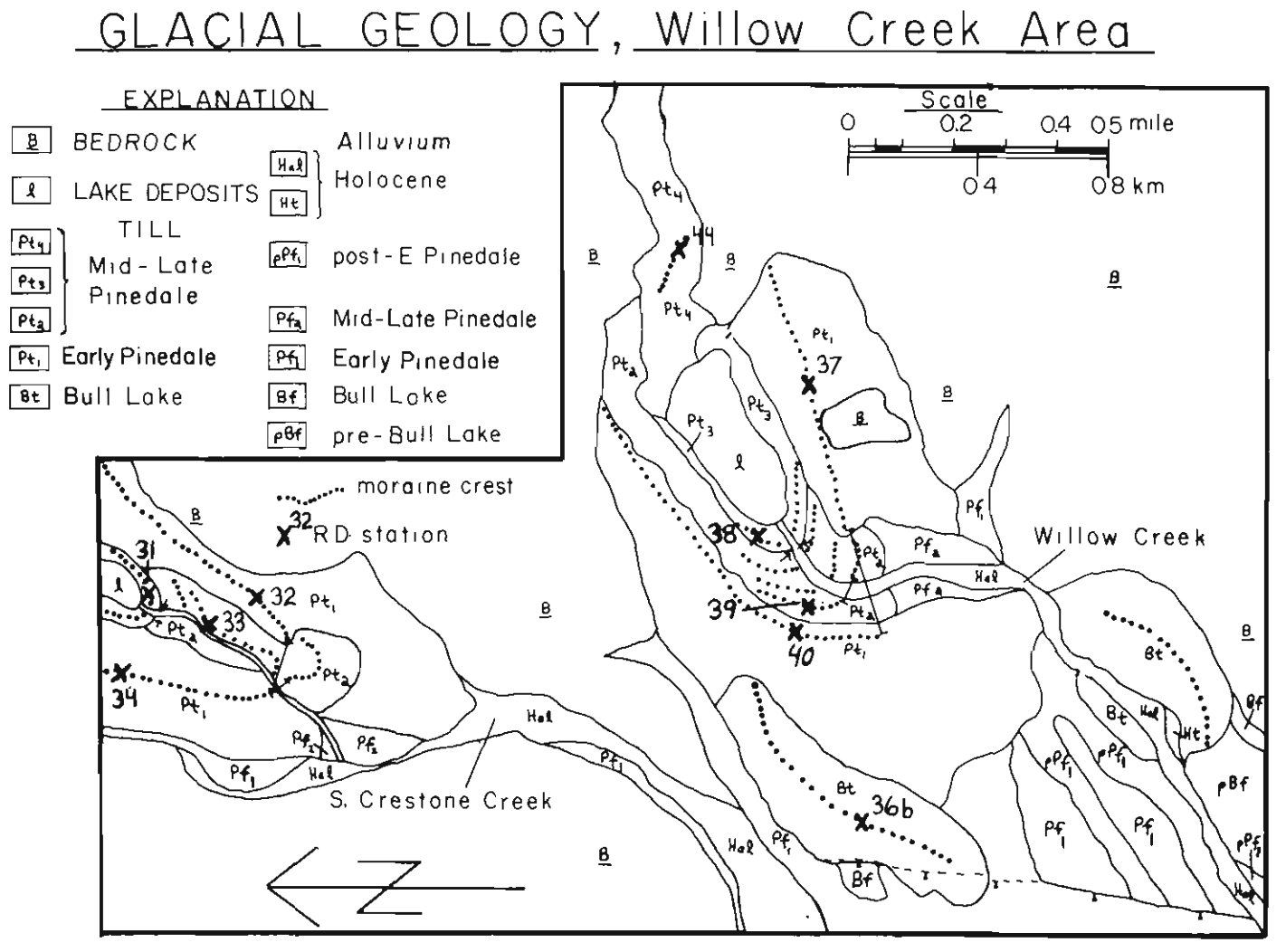

Figure 10.—Glacial geologic map, Willow Creek area. Well-preserved lobate Pinedale moraine complexes record multiple ice advances. RD data from stations (tables 2, 3, and 4) reveal large weathering differences between Bt, Pt_1 and Pt_2, Pt_3, Pt_4.

Mid-Late Pinedale Till

Northern Segment. Small moraines nested within larger early Pinedale terminal or lateral moraines occur in most of the glacial valleys of the northern segment (plate 1). RD data (table 4) indicate these moraines have significantly less weathered surfaces than do early Pinedale moraines. Lack of significant post-glacial dissection prevented fresh exposures of this younger Pinedale till from being observed. Lacustrine basins impounded by these moraines suggest they represent the last major Pinedale ice advance.

In the upper parts of some glacial valleys, low cross-valley moraines occur (plate 1, Cotton Creek, Willow Creek). Their position and small size suggest they resulted from minor re-advances or stillstands amid overall late-Pinedale glacial retreat. Both in position and morphology, the moraines are very similar to late-Pinedale moraines described by Richmond (1960) elsewhere in the Rocky Mountains. RD data from these high-altitude moraines (table 4) suggest that they are *older* than either early or mid-late Pinedale moraines farther down valley. More rapid oxidation rates at high altitudes than at low altitudes are believed to be responsible for the apparent age reversal. A similar phenomenon was reported by Birkeland and others (1979a) for Quaternary moraines in the Sierra Nevada, California.

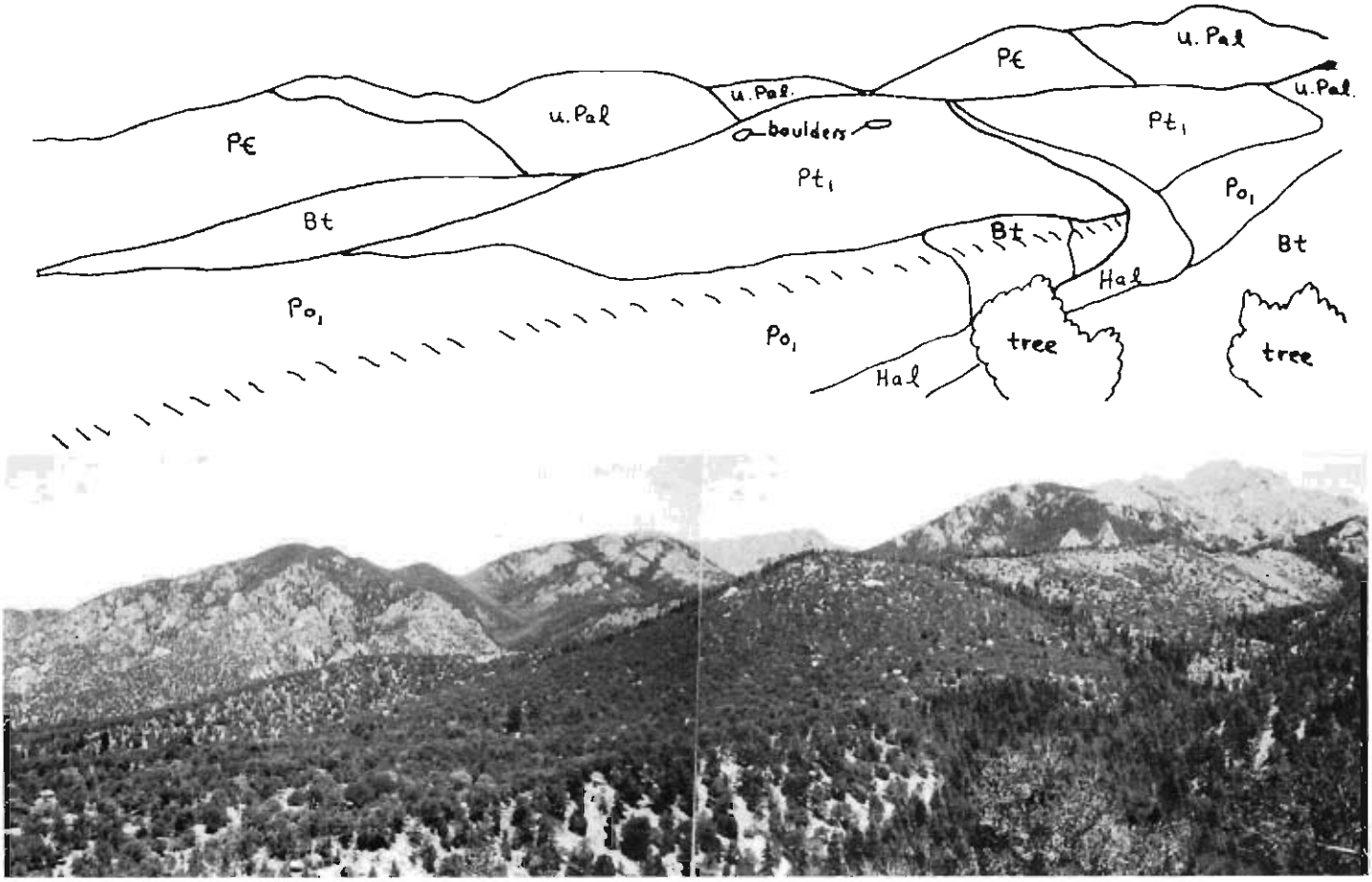

Figure 11.—Panoramic photograph of the Willow Creek terminal moraine complex, looking NE. Bull Lake terminal moraines (left center, and lower right corner) were once continuous across the center area. Interglacial erosion by Willow Creek presumably breached the moraine.

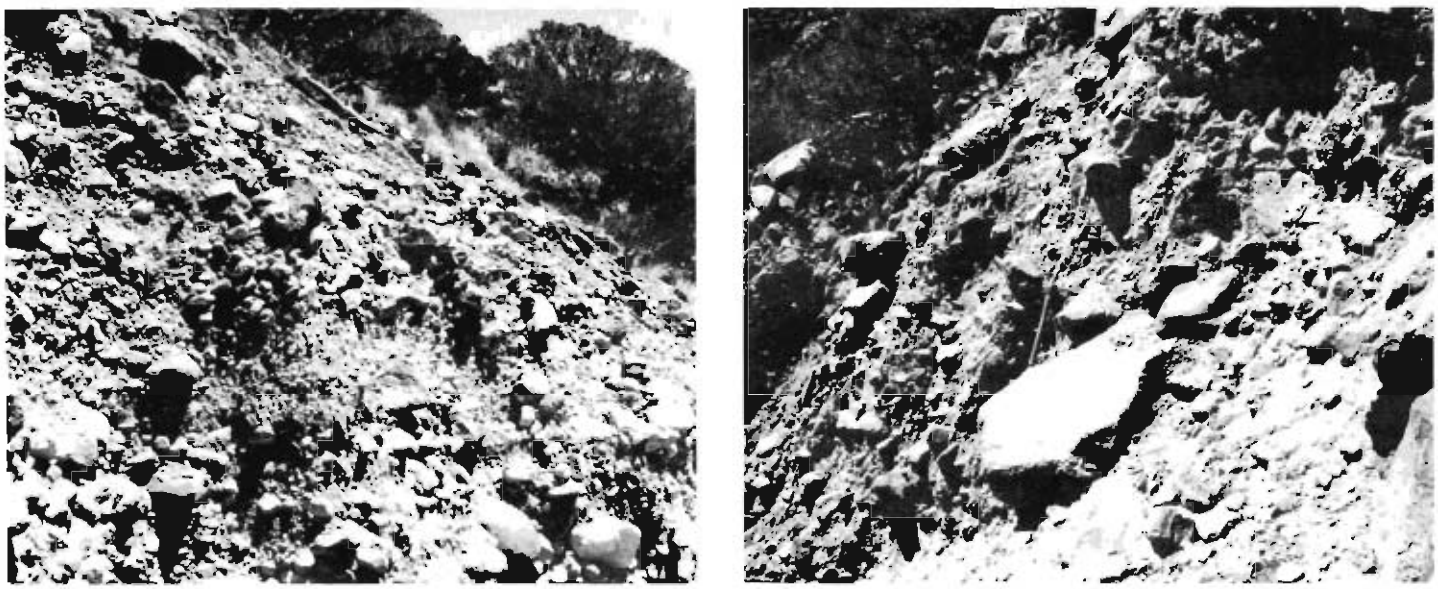

Figure 12.—Typical exposures of early Pinedale till and outwash.
(a) Crudely stratified Pinedale outwash, mouth of Blanca Creek. (b) Unstratified, unoxidized Pinedale till, mouth of South Zapata Creek. Mattock is 40 cm long.

Southern Segment. Moraines of a second Pinedale advance are found in all glacial valleys of the Sierra Blanca, where they are usually nested within the larger early-Pinedale terminal moraines. At two localities (Holbrook and Blanca Creeks, figure 9), moraines of the second Pinedale advance cross cut and extend farther down valley than those of the first advance. Landslide exposures reveal till to be unsorted bouldery debris with a silty matrix. Oxidation and soil development on the till are very weak. As in the northern segment, RD data (table 4) indicate the second Pinedale advance is significantly younger than the first.

Neoglacial Till and Rock Glaciers

Northern Segment. Small cirque moraines and rock glaciers exist in many valley heads, well below the limits of Pinedale glacier ice. The restriction of cirque moraines to deeply shaded, north-facing cirques indicates that post-Pinedale climatic conditions were marginal for glacier formation in the Sangre de Cristo Range. In less favorable topographic settings, rock glaciers occupy valley heads. Tongue-shaped rock glaciers are common in high cirque basins, whereas lobate rock glaciers occur at the bases of oversteepened glacial valley walls (plate 1; see also Nolting 1970). RD data (table 5) suggest that most sampled cirque moraines and active rock glaciers may date from the early Neoglacial stade. Inactive rock glaciers appear older as a group, and may date from the late Pinedale deglaciation.

Sedimentologic data from a post-Pinedale lake basin at Willow Park (figure 13) shed light on later Neoglacial climatic fluctuations. A 3.5-m-deep auger hole in the basin penetrated a succession of organic-rich silty clays interstratified with beds of peat. Values for ^{14}C dates from two peat horizons at 130 cm and 250 cm below the surface are similar to dates compiled by Benedict (1973) for major Neoglacial interstades (figure 13). The stratigraphic sequence of sediments suggests that lacustrine conditions prevailed in Willow Park during Neoglacial advances and that silty clays were deposited. During interstades, water levels probably fell and peat encroached out over the lake basin. At present (interstadial) the water table is within about 1 m of the surface, and peaty sediments are accumulating.

Southern Segment. No Neoglacial moraines were recognized in the mapped valleys of the Blanca Massif. Rock glaciers are also rare, but become more common in the eastern part of the massif beyond the limits of this study (plate 1). Detailed work by Morris (1979) suggests that rock glaciers of the eastern Blanca Massif began to form in latest Pinedale (i.e., pre-Altithermal) time, as debris covered stagnant glacial ice.

Table 5.—RD data: Neoglacial moraines and rock glaciers (see parameter definitions, table 1)

RD Parameter No. Acronym / Station Number[a]	(1) POS (%)	(2) PPS (%)	(3) MPD (mm)	(4) PSWR (%)	(5) MRT (mm)	(6) ART (mm)	(7) MPLC (%)	(8) MLD (mm)	(11) MCW (m)	(12) MMSAO (deg)	(12) MMSAI (deg)	Station Elevation (m)
Neoglacial Moraines												
14	12	24	—	84	3	1.3	—	—	8	26	19	3597
18	64	40	10	96	2	0.9	60	65	5	41	—	3707
19	16	24	6	68	1	0.8	45	38	5	44	—	3683
42	64	36	20	60	2	1.0	60	60	6	26	28	3829
55	52	16	20	36	1	0.7	60	73	4	34	39	3695
Mean	**42**	**28**	**14**	**69**	**2**	**0.9**	**56**	**59**	**6**	**34**	**29**	**3702**
Inactive Rock Glaciers												
06	—	92	89	64	6	3.0	85	.75	—	28	—	3518
17	—	76	25	75	7	—	70	78	—	38	—	3573
11	—	56	50	92	6	2.1	70	63	—	23	—	3280
13	72	56	48	96	4	1.8	80	90	—	42	—	3536
17	—	99	—	80	3	1.7	85	73	—	—	—	3286
20	96	68	12	100	13	4.4	—	—	—	—	—	3597
27	90	28	41	76	2	0.9	75	88	—	40	—	3671
29	88	36	23	100	6	2.9	80	113	—	35	—	3646
36A	68	24	10	92	5	1.5	85	125	—	34	—	3524
41	40	8	6	40	1	0.6	60	50	—	36	—	3896
49	100	60	40	100	2	0.9	75	75	—	35	—	3476
Mean	**72**	**55**	**34**	**83**	**5**	**2.0**	**76**	**83**	**—**	**35**	**—**	**3545**
Active Rock Glaciers												
28	40	44	30	36	4	1.6	90	80	—	37	—	3756
35	60	16	8	72	2	1.2	60	58	—	38	—	—
50	93	13	12	80	1	0.6	60	40	—	37	—	3634
Mean	**64**	**24**	**17**	**63**	**2**	**1.1**	**70**	**59**	**—**	**37**	**—**	**3695**

[a] RD station locations are given in McCalpin (1981, plate 1).

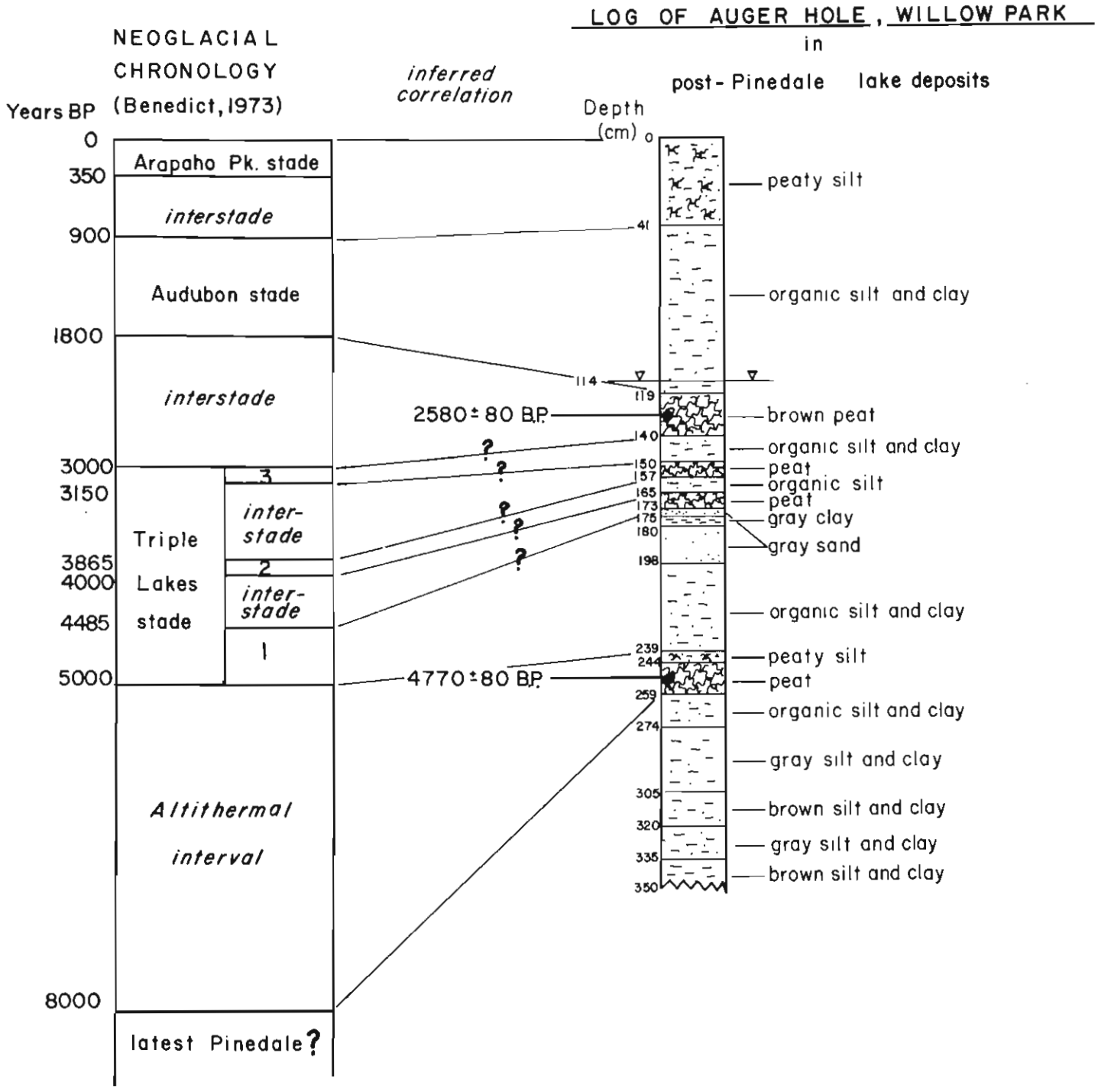

Figure 13.—Stratigraphy and correlation of post-Pinedale lacustrine deposits, Willow Park. Data are from a 3-in. diameter auger hole located 0.2 km east of Station 38, figure 10. Two dates at center are radiocarbon dates on peat.

FEATURES OF GLACIAL EROSION

The retreat of Pinedale glaciers exposed many features of glacial erosion in the Sangre de Cristo Range. Valleys are commonly U-shaped in cross section above terminal moraines, but deeply V-shaped below them. This shape criterion is useful for defining ice limits in valleys where erosion has removed terminal deposits (*e.g., Sand Creek, plate 1*). Near the terminal moraine valley floors are usually till covered, but middle and upper parts of valleys display widespead bedrock erosional features such as ice-molded slabs (roches moutonees) (figure 14). The good preservation of striated outcrops (figure 15) and glacial polish (figure 16) attests to the recency of deglaciation. There is no evidence to suggest that modern bedrock valley floors were ever covered by more than thin, discontinuous glacial debris. This observation implies that in the middle and upper valleys clean glacier ice stagnated in place, and that an active glacier snout did not retreat far into the valley heads during deglaciation.

NONGLACIAL ALPINE DEPOSITS

Deposits of nonglacial origin in the alpine parts of the study area include talus, alpine fans, landslides, and rockfalls. Conditions prevailing during and immediately after deglaciation gave rise to most of these deposits, but many deposits are still forming today.

Figure 14.—Scoured bedrock slabs (roches moutonees) on the floor of Cottonwood Creek at 3600 m elevation. The U-shaped glacial valley is 500 m wide here. Pinedale ice thickness was about 120 m, ice flow was from left to right. Talus cones with prominent mudflow levees in background are post-Pinedale.

Figure 15.—Glacially grooved outcrops of Precambrian gneiss, upper Deadman Creek. Ice flowed from lower left to upper right. Hammer is 32 cm long.

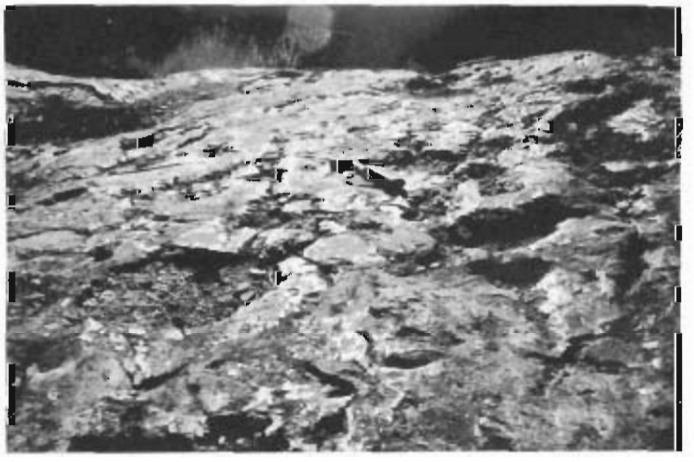

Figure 16.—Discontinuous glacial polish on a slab of Permo-Pennsylvanian Crestone Conglomerate (Sangre de Cristo Formation). Ice flowed toward observer. Hammer is 32 cm long.

Figure 17.—Coarse rubble fan from the debris flow of September 8, 1980, buries the road to the USFS North Crestone Campground with up to 2 m of boulders. Intense local rainfall of 75 mm in 45 minutes triggered this event; evidence for older flows at the same location was noted.

Talus and Alpine Fan Debris

With the retreat of latest Pinedale glaciers, oversteepened cliffs were exposed to frost shattering and gravity failure. Abundant debris accumulated at the bases of valley and cirque walls as a series of coalescing talus cones. Where fluvial processes were significant, cones resemble small alluvial fans, complete with distributary channels and levees. A continuum exists between deposits formed solely by gravity fall (talus) and deposits formed solely by fluvial and debris-flow processes—in fact, evidence of both processes can be found on a single landform (figure 14).

There was evidence that significant debris-flow deposition continues currently. On September 8, 1980, intense local precipitation (75 mm in 45 minutes) north of the town of Crestone (figure 2) triggered multiple debris flows in tributaries of North Crestone Creek. Alpine fan debris buried the U.S. Forest Service access road with up to 1.5 m of angular boulders, some up to 1 m in diameter (figure 17). At least one older vegetated debris flow lobe was partially overridden at the site, suggesting that periodic debris flowage may be the normal mode of sediment transport in such steep, rubble-filled tributary valleys.

Landslides and Rockfall Deposits

Deposits of coarse angular rubble are common in valley heads in the Sangre de Cristo Range. Deposits that exhibit signs of down valley flowage are mapped as rock glaciers. Other deposits, lacking flow evidence, are mapped as landslide and rockfall debris. Diameter of individual clasts is often 5 m to 10 m and appears to be related to the spacing of bedding planes and joints in the bedrock of adjacent oversteepened valley walls. Furthermore, many coarse rubble deposits occur at the base of conspicuous landslide scars, where it appears that huge slabs of sandstone and conglomerate have slid into valleys (figure 18).

Retreat of Pinedale ice from glaciated valley heads is inferred to have exposed steep walls cut into dipping Upper Paleozoic strata. Many valleys are aligned along strike or occupy axes of synclines so that strata dip steeply into the valley on one or both sides. With the removal of ice support, large slabs may have undergone bedding-plane detachment and slid into valleys. RD data were not collected for most rubble deposits, but data collected on some inactive rock glaciers below landslide scars indicate that at least the rock glacier deposits probably predate the Neoglaciation. This indication is consistent with the hypothesis that many rubble deposits formed in late Pinedale time by landslide burial of stagnant glacier ice.

Landslides were not observed in alpine areas of the Sierra Blanca, where bedrock is a closely jointed Precambrian gneiss. However, several large landslides do occur along the range front between the Great Sand Dunes National Mounument and Blanca Peak. Surface morphology indicates that both rotational slumping and chaotic ground breaking and flowage have occurred near the mountain front. Soil profile development on the large landslide north of Pioneer Creek suggests this landslide predates the Bull Lake glaciation in the study area. Restriction of large slides to the frontal fault zone area of the southern segment suggests that tectonic shearing of bedrock and earthquake shaking may be responsible for landslide activity in this area.

Figure 18.—Panoramic photograph of steep dip slopes in Upper Paleozoic strata (upper left and center) above coarse rubble deposits choking valley floors. Angular conglomerate blocks in right foreground (up to 6 m in diameter) mantle an inactive rock glacier. View is SSE up the southern glacial tributary of Rito Alto Creek.

ALLUVIAL DEPOSITS

Like many other fault-bounded mountain blocks in semi-arid climates, the northern Sangre de Cristo Mountains are flanked by a continuous belt of coalescing alluvial fans that spread out into the San Luis Valley. Five topographic levels of alluvial fans are recognizable, correlated with the glacial stades recognized in the Sangre de Cristo range. Correlation is based on: (1) physical continuity with moraines, (2) similar number of relative-age subdivisions in the glacial and alluvial sequences, and (3) close correspondence of RD data between individual units of the glacial versus alluvial relative-age sequences. Units mapped include pre-Bull Lake, Bull Lake, early Pinedale, mid-late Pinedale, and Holocene alluvium. In addition, small alluvial deposits of tectonic origin (post-Bull Lake, post-Pinedale) have been mapped near fault scarps. Morphologic and weathering data for the five inferred alluvial units are summarized in table 6. The distribution, sedimentology, surface morphology, weathering characteristics, and relation to adjacent units of each alluvial deposit are described in the following section.

Pre-Bull Lake Alluvium

Northern Segment. Fan alluvium of pre-Bull Lake age is restricted to small areas in the northern San Luis Valley and interfan remnants or fault-bounded blocks along the Sangre de Cristo and Villa Grove Fault Zones (plate 1). Pre-Bull Lake surfaces usually slope more steeply than all younger surfaces, and are thus overlapped by younger deposits toward the valley center. Progressive tilting of alluvial surfaces by tectonism could explain steeper slopes in successively older surfaces. Moderate-to-severe dissection, ubiquitous surface clast oxidation, and strong-to-very-strong soil development characterize all pre-Bull Lake alluvial deposits (table 6).

Stratigraphic relations of pre-Bull Lake alluvium are well exposed in a mine tunnel 0.3 km northwest of the mouth of Wild Cherry Creek (figure 2; plate 1). At the tunnel site, faulted Bull Lake alluvium carrying a moderately developed soil is underlain by pre-Bull Lake alluvium also carrying a moderately developed soil (figure 19). Discontinuous pods of fluvially reworked volcanic ash in the lower alluvium have been identified as the

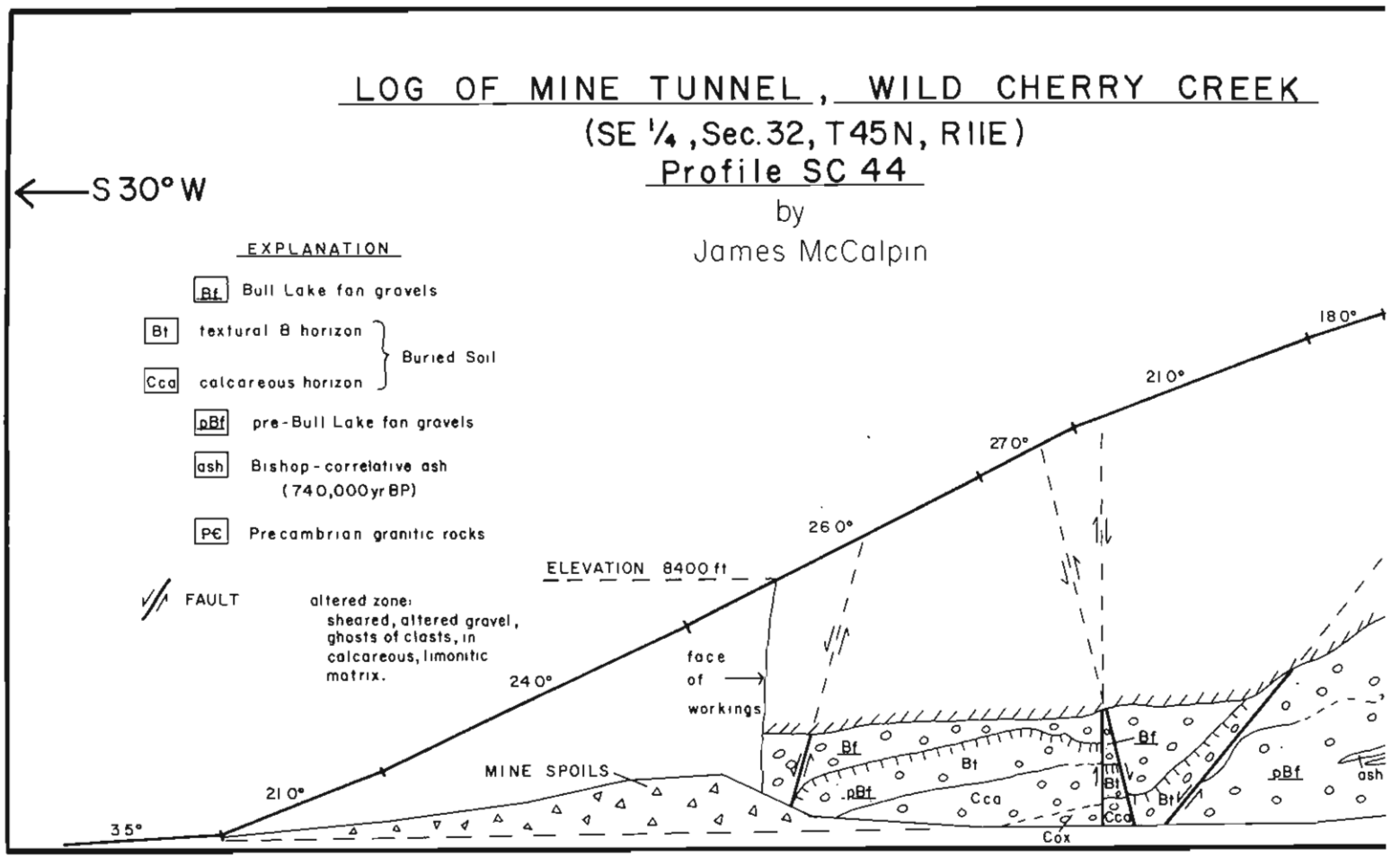

Figure 19.—Log of mine tunnel, Wild Cherry Creek area. Tunnel is driven into the base of a Quaternary fault scarp in Bull Lake gravels, perpendicular to scarp strike. Exposed normal faults steepen and cut younger units to the southwest (valley-ward).

Bishop Ash (0.7×10^6 years old), based on the index of refraction of glass shards, shard shape, vesicle fluid, and chemical composition (G. Izett, personal communication, 1980). Presence of the dated ash confirms a pre-Bull Lake age for the lower alluvium.

Southern Segment. Pediment gravels of pre-Bull Lake age approximately 15 m thick overlie an erosional surface that truncates steeply dipping beds of the Santa Fe Formation on the north banks of Uracca Creek, 0.8 km north of the Uracca Pioneer Cemetery (plate 1). Pre-Bull Lake sediments at other fan heads (e.g., Blanca Creek, figure 15) are more poorly exposed, but also appear to be pediment gravels rather than thick fills. Severe dissection and highly calcareous surface soils typify all pre-Bull Lake deposits of the Sierra Blanca and point to considerable antiquity for the alluvium.

Bull Lake Alluvium

Northern Segment. Alluvium of Bull Lake age dominates the bajada north of Valley View Hot Springs. To the south, Bull Lake deposits are restricted to interfan remnants and fault-bounded blocks near the range front (plate 1). Relict bouldery paleochannels and large isolated boulders are conspicuous on Bull Lake fan surfaces. The advanced state of chemical and physical degradation displayed by the boulders (figure 20) indicates long exposure to subaerial weathering. Widespread pitting, spalling, splitting, and surface oxidation typify exposed clasts on Bull Lake alluvial surfaces (figure 21). The high proportion of resistant quartzite boulders of the Ordovician Harding Formation, despite the small outcrop area of the unit, suggests that less resistant boulder lithologies have largely disintegrated since Bull Lake time. Trains of large boulders trend radially downfan on the Steel Canyon and Black Canyon fans, and contain individual clasts up to 31 m^3 in volume with an estimated weight of 81,000 kg. These boulders have been transported up to 1.3 km from canyon mouths on slopes averaging only 5°. The writer favors a debris-flow mechanism for transport; however, no traces of typical debris-flow morphology such as marginal levees were observed. Positive relief of some coarse channel deposits above finer-grained adjacent alluvium suggests that possibly a reversal of topography has occurred since deposition. This and

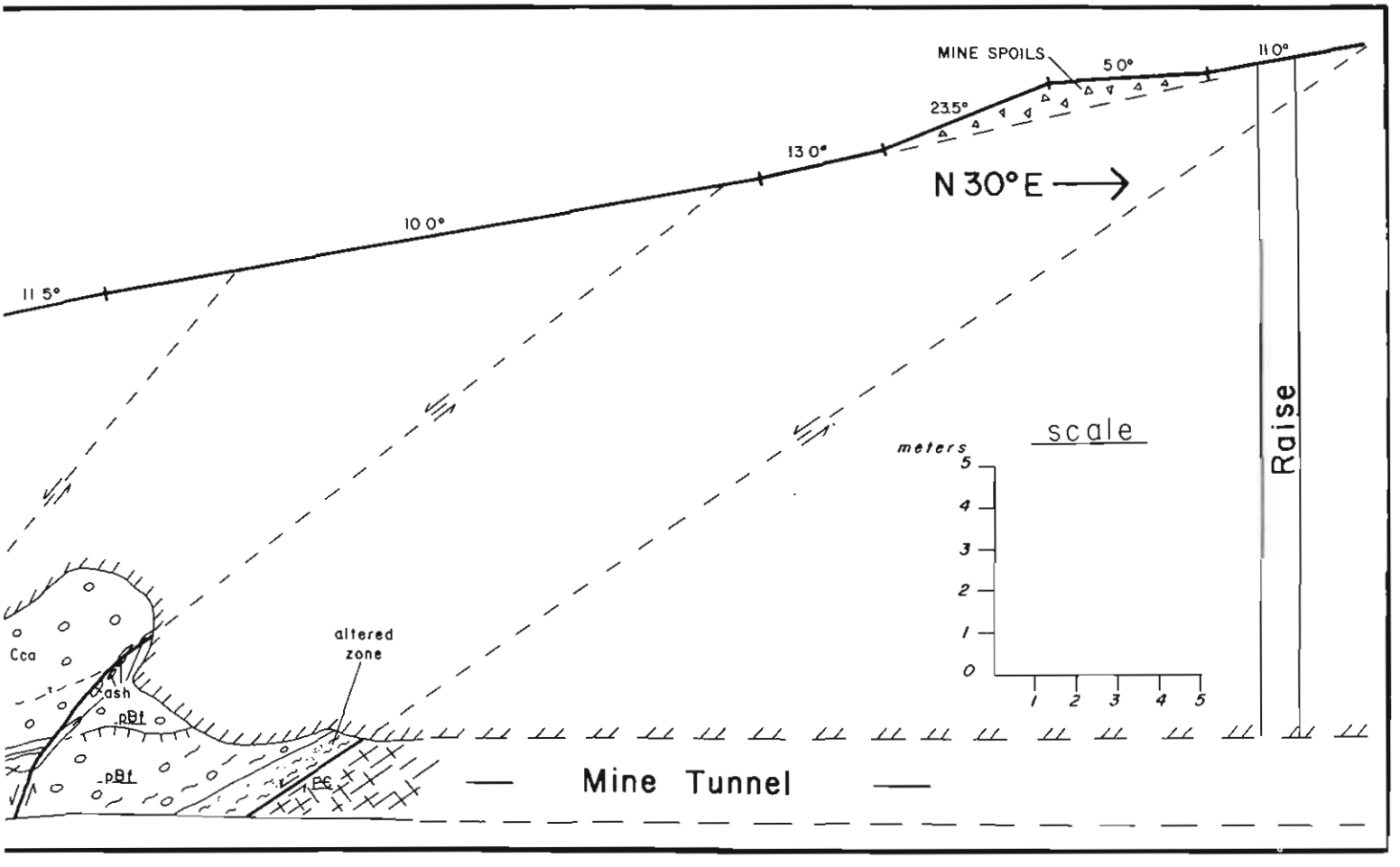

Table 6.—Alluvial deposits: weathering and morphologic characteristics

Age of Deposit[a]	Morphology	Slope	Eolian Cover	Soil Development	Clast Weathering	Dissection	Surface Morphology	Direct Connection to Moraines
				Northern Segment				
Ha	linear flood plain	low	none	azonal	no oxidation	none	active bar-and-swale	No
Pfu	narrow channels	low	variable	weak	slight oxidation	slight	fresh bar-and-swale	No
Pf2	large symmetrical fans	2-5°	thin, discontinuous	very weak	no oxidation	very slight	fresh bar-and-swale	No
Pf1	large symmetrical fans	3-6°	33-75 cm	weak	slight oxidation	slight	smooth alluvial surface	Yes
Bf	broad bajada, interfan ridges	5-6°	variable	moderate	moderate pitting, oxidation	moderate	relict surface with paleochannels	No No
pBf	interfan wedges, fault-bounded fan remnants	7-8°	variable	very strong	severe pitting, oxidation	severe	eroded ridges of alluvium	[b]
				Southern Segment				
Ha	low fans, linear flood plains	low	none	azonal	no oxidation	none	active bar-and-swale	[b]
Pfu	symmetrical fans	——	slight	weak	no oxidation	slight	subdued bar-and-swale	No
Pf2	poorly defined terraces	——	none-slight	——	no oxidation	very slight	fresh bar-and-swale	No
Pf1	narrow terraces	8-10°	none-slight	weak	slight oxidation and spalling	slight oxidation	shallow channels, low bars	Yes
Bf	large symmetrical fans	8-14°	variable	moderate	common splitting and spalling	slight to severe	subdued bar-and-swale	Yes
pBf	pediment gravels, fault-bounded fan remnants	——	variable	very strong	moderate oxidation, spalling	severe	eroded ridges, pediment remnants	[b]

[a] Age of alluvium deposit: Ha is Holocene, Pfu is Pinedale (undivided), Pf2 is mid-late Pinedale, Pf1 is early Pinedale, Bf is Bull Lake, pBf is pre-Bull Lake.
[b] No moraines of this age.

the advanced weathering of clasts suggests that Bull Lake alluvium is probably at least 100,000 years old.

Southern Segment. Bull Lake alluvium covers more than half the bajada surrounding the Sierra Blanca (plate 1). Outwash from Bull Lake glaciers spread out to form large, symmetrical alluvial fans which rise 500 m above the floor of the San Luis Valley at slopes of 8° to 14°. Fans are directly traceable to Bull Lake terminal moraines at several fanheads. Soil and weathering characteristics are also similar between Bull Lake moraines (table 2) and Bull Lake alluvial fans (table 6). Deep incision by modern drainage at fanheads shows Bull Lake till grades into Bull Lake outwash, demonstrating contemporaneity.

Post-Bull Lake Alluvium

Northern Segment. At the mouth of San Isabel Creek, a broad shallow channel incised approximately 3 m into a block of Bull Lake alluvium directly above the fault scarp is mapped as post-Bull Lake alluvium. This channel was probably incised into Bull Lake alluvium in response to post-Bull Lake faulting, and the gravels themselves were subsequently faulted several more times. No soil pits were dug in this unit, but surface weathering

Figure 20.—Granite boulder on the Steel Canyon fan (4.6 m × 3.6 m × 1.9 m), 1.3 km downslope of the canyon mouth (in right background). The tusk-shaped rock in foreground is a weathered spall fragment of the boulder with the hat on it (hat is 30 cm wide).

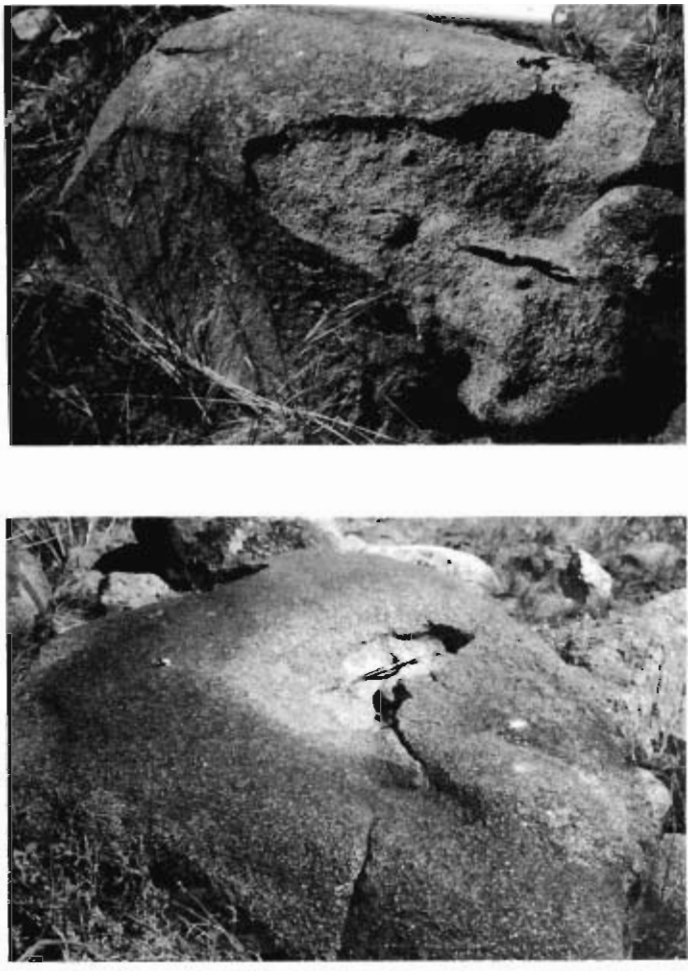

Figure 21.—Typical clast weathering on a Bull Lake alluvial fan surface. Surface spalling and severe granular disintegration of this coarse-grained tonalite boulder have occurred.

characteristics were indistinguishable from surrounding Bull Lake surfaces. Based on the weathering characteristics and morphology of the alluvium, it is suggested that post-Bull Lake gravels were deposited in the waning stages of glaciation or early in the interglacial, when streams were still carrying a heavy sediment load and had not begun to downcut vigorously. Subsequent renewed faulting and stream diversion have led to perching of the relict tectonically induced channels 10 to 20 m above present drainages.

Southern Segment. Alluvium of inferred post-Bull Lake age occurs in a broad channel incised into Bull Lake gravels at the faulted valley mouth of an unnamed valley 3 km west of Blanca Creek (plate 1). Surface clasts on the floor of the 2.5-3-m-deep channel have weathering characteristics similar to adjacent Bull Lake gravels, and much stronger than lower-lying Pinedale gravels. Weathering and channel geometry suggest an origin similar to that for post-Bull Lake alluvium in the northern segments, described above.

Early Pinedale Alluvium

Northern Segment. Large alluvial fans of early Pinedale age front the major glaciated valleys of the northern range segment (plate 1). The large size, low gradient, and surface morphology of these fans suggest they were built primarily by aggrading glacial outwash channels. The smooth, even texture of the fans as seen on airphotos results from a veneer of eolian sand, ranging from 33 to 75 mm thick, which overlies cobble gravels. Weak soil profiles are typically developed in the eolian covers. Physical continuity of the surfaces of early Pinedale alluvial fans with early Pinedale terminal moraines at Willow and South Crestone Creeks (figure 12; plate 1) suggests deposits are contemporaneous.

Southern Segment. Early Pinedale alluvium of the Sierra Blanca is restricted to broad, shallow terraces incised as much as 6 m into the larger Bull Lake outwash fans. Terrace surfaces are typified by flat-floored, anastomosing, shallow paleochannels and low bars that trend downfan. Eolian cover is slight to nonexistent. As in the north, fans of this age can be traced directly to early Pinedale terminal moraines at fanheads (figure 9).

Mid-Late Pinedale Alluvium

Northern Segment. Flanking the early Pinedale alluvial fans are lower, more gently sloping fans inferred to correlate with the mid-late Pinedale stade. Fan surfaces are distinguished by fresh, primary depositional bar-and-swale topography, with minimal (less than 10 cm) eolian cover. Surface weathering and morphologic data (table 6) indicate the fans are distinctly younger than early Pinedale fans. However, in no cases are the fans traceable directly to mid-late Pinedale terminal moraines. Correlation therefore rests mainly on RD criteria.

Southern Segment. Poorly defined low terraces which parallel and separate early Pinedale from Holocene alluvium are ascribed to mid-late Pinedale deposition. The terraces have fresher constructional topography, stonier soils, and less vegetation cover than adjacent early Pinedale terraces. Because of postglacial fanhead erosion, terraces are not in physical contact with mid-late Pinedale terminal moraines (figure 9). Therefore correlation, as in the north, relies on similarities in RD data.

Pinedale Alluvium

Undivided Northern Segment. Pinedale alluvial fans of only a single morphologic aspect front the unglaciated western flank of the Sangre de Cristo Range at the extreme north end of the study area (plate 1). The fans are narrow and slightly incised into Bull Lake deposits near the mountain front, but widen and overlap the older deposits near the valley center. Degree of clast oxidation and soil development suggest that the fans are correlative with Pinedale fans which front glaciated valleys (table 6). Because the two-fold morphology is not present on these nonglacial fans, they are assigned only an undivided Pinedale age.

Undivided Southern Segment. The narrow alluvial slope between Great Sand Dunes National Mounument and South Zapata Creek (figure 2) consists of coalescing small, steep alluvial fans. No drainages contributing to the alluvial slope were glaciated. Accordingly, the individual fans of the slope are smaller, steeper, and lack the twofold morphology of their counterparts which

front glaciated valleys directly to the south (plate 1). Morphologic and weathering characteristics of these fans are more similar to those of early Pinedale than of mid-late Pinedale fans of the glaciated Sierra Blanca (table 6). A similar RD-based correlation exists for nonglacial versus glacial Pinedale alluvial fans on the northern segment. The two correlations suggest a more rigorous climate and greater sediment production in early than in mid-late Pinedale time.

Post-Pinedale Alluvium

At Willow Creek three broad, shallow channels are incised into early Pinedale alluvium above the scarp of the Sangre de Cristo Fault. Gravels deposited in these channels have weathering characteristics similar to nearby early Pinedale gravels. Gravel-filled channels are traceable to the early Pinedale moraine, and are truncated by mid-late Pinedale terraces and the Holocene gorge. This geometry indicates that the tectonically induced channels were cut while discharge was still emanating from the terminal moraine area, and before drainage was diverted southward into the present gorge. A further implication is that, at least in this location, gravels were deposited in the waning stages of early Pinedale glaciation, in response to faulting and creation of a new base level for the upthrown block.

No post-Pinedale alluvium was mapped in the southern segment of the study area.

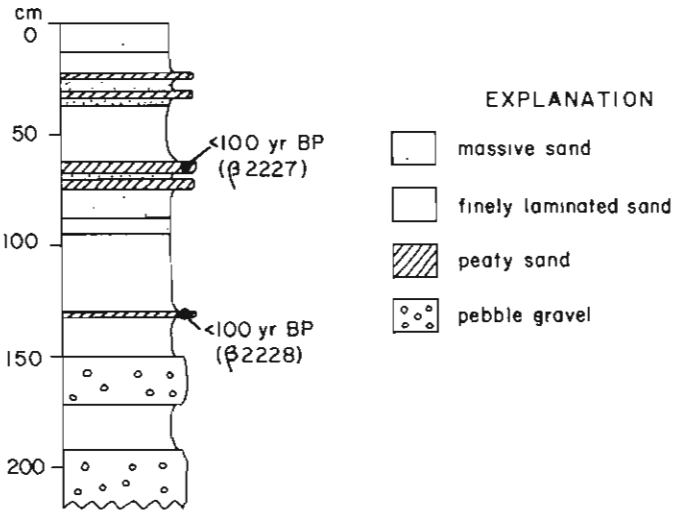

Figure 22.—Stratigraphy of Holocene sandy alluvium reworked from eolian deposits, 3 km SW of the mouth of Spanish Creek. Peaty sands, which cap fining-upward units 20-40 cm thick, have been dated as "modern" (less than 100 radiocarbon years old).

Holocene Alluvium

Holocene alluvium occurs on narrow modern flood plains of the study area. Active Holocene alluvial surfaces are incised several meters below Pinedale surfaces near fanheads, but commonly overlap older deposits and form low alluvial fans near the valley floor. Discernible flood channels, fresh constructional bars of loosely packed gravel, and lack of eolian or lichen cover suggest that most mapped Holocene surfaces are still active.

Nongravelly Holocene alluvium occurs in two localities: (1) on the flood plain of San Luis Creek at the northern end of the study area and (2) near the Great Sand Dunes National Monument (figure 2). In the former area, dark gray, massive silty sand exposed in shallow banks is probably of overbank origin. Near the sand dunes, Holocene channels are filled with reworked eolian sand washed from dunes. Organic layers interstratified with massive to parallel-laminated sand layers in the alluvium (figure 22) demonstrate that deposition is rapid and cyclical. Rare intense precipitation events may be responsible for much of Holocene alluvial deposition.

EOLIAN DEPOSITS

Sandy alluvium on the floor of the San Luis Valley has been extensively reworked by southwesterly winds in Quaternary time. Deposits of eolian sand reach maximum development on the east side of the valley at Great Sand Dunes National Monument (GSDNM) (figure 2), where active dunes rise 213 m above the surrounding alluvial slope. Eolian deposition decreases both north and south of the National Monument.

Northern Segment. Eolian deposits of the northern segment range from a thin veneer of sand and loess overlying fan gravels in the extreme north, to large active and stabilized dunes of the Great Sand Dunes National Monument. Deposit thickness increases from north to south, from 0 at Valley View Hot Springs to 33 cm at Rito Alto Creek, 76 cm at San Isabel Creek, and over 350 cm at Willow Creek. Between Willow Creek and the northern boundary of the national monument low vegetated dunes overlap all but the extreme upper parts of mountain-front alluvial fans (plate 1). Late- and post-glacial drainage channels, filled with fluvially reworked eolian sand, are cut into the stabilized dunes.

The Great Sand Dunes National Monument encompasses about 155 km^2 of spectacular active sand dunes (figure 23) within a larger (385 km^2) field of stabilized and active dunes (plate 1). Subdivision of dune types follows detailed mapping of Johnson (1967). Dune types grade from parabolic dunes of deflation near the valley floor, through fixed parabolic dunes, parabolic dunes of accumulation, and finally transverse and climbing dunes at the mountain front (plate 1). Longitudinal dunes fringe the southern and eastern sides of the dune field. The existence of the dunes is ascribed to three factors: (1) prevailing southwesterly winds, (2) large expanses of loose, fine sediment on the valley floor, and (3) a natural wind funnel at Medano Pass in a re-entrant in the Sangre de Cristo Range. Dunes overlie Pinedale outwash terraces at the mouth of Medano Creek (plate 1) on the eastern boundary of the national monument, indicating that in this area eolian deposition is postglacial.

Southern Segment. South of the national monument eolian sand covers the valley floor as small, vegetated sand hummocks, interspersed with blowout depressions. Hurst (1941) reports that a thin (<1 m) layer of Holocene eolian sand on the valley floor unconformably overlies older Pleistocene alluvium. Sand cover thins toward the Sierra Blanca and is insignificant on most of the steep proglacial alluvial fans (plate 1).

CHRONOLOGY OF QUATERNARY DEPOSITS

Determination of the chronology of Quaternary deposits was a major goal of this study. The chronology as finally adopted was developed in three steps: (1) identification of a fivefold local age subdivision of deposits, (2) correlation of the fivefold sequence to a composite Quaternary chronology for the Rocky Mountains, and (3) assessment of the absolute age of deposits via local ^{14}C dates and correlation to dated deposits elsewhere.

Local Subdivision

The local subdivision of glacial deposits followed natural groupings of moraines by topographic position and by RD parameters (table 7). Deposits in the lower parts of valleys (2850-3050 m elevation) fall into three distinct age groups. Eroded, subdued moraines occurring near valley mouths (Bull Lake) yield the highest weathering values (table 7). Massive, single-crested moraines farther upvalley (early Pinedale) define a significantly less weathered group. Nested smaller moraines directly upvalley (mid-late Pinedale) are even less weathered.

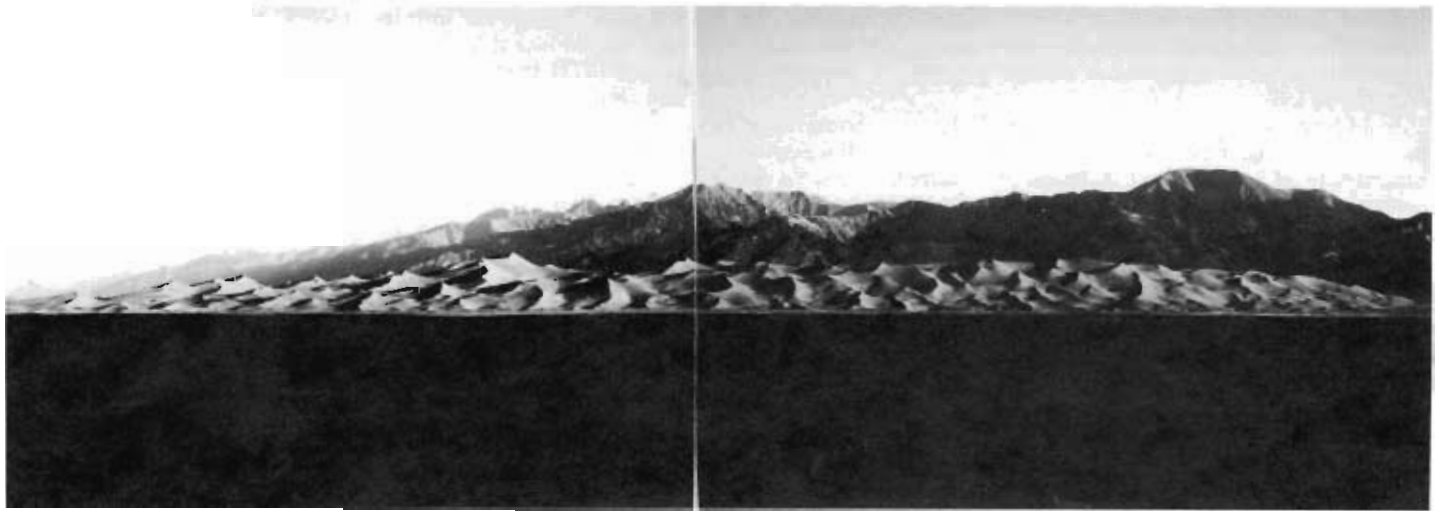

Figure 23.—Panoramic photograph of the large transverse dunefield (Qet) of the Great Sand Dunes National Monument, looking due north. Prevailing wind direction and sand source is from left of photo (southwest). Portion of the dunefield pictures is 6.5 km wide from extreme left to right; highest dunes rise 230 m above Pinedale alluvium (shadowed in foreground).

Table 7.—Summary of RD data on glacial deposits (see parameter definitions, table 1). Values given are means for each age group, as calculated from tables 2-5

Parameter No.	(1)	(2)	(3)	(4)	(5)	(6)	(7)	(8)	(9)	(10)	(11)	(12)	(12)	
Deposit[b] Acronym	POS	PPS	MPD	PSWR	MRT	ART	MPLC	MLD	SBF	BBF	MCW	MMSAO	MMSAI	
	(%)	(%)	(m)	(%)	(mm)	(mm)	(%)	(mm)			(m)	(deg)	(deg)	Station Elevation (m)
Northern Segment														
High Elevation														
Nm	42	28	14	69	2	0.9	56	59	—	—	6	34	—	3702
Nra	64	24	17	63	2	1.1	70	59	—	—	—	37	—	3545
Nri	72	55	34	83	5	2.0	76	83	—	—	—	35	29	3695
Low Elevation														
Pt2h	65	31	26	91	10	3.5	—	—	124	.36	6	27	25	3427
Pt2l	35	14	16	59	6	2.3	—	—	96	.26	6	26	29	3043
Ptl	46	20	20	72	6	2.6	—	—	74	.35	7	28	32	3116
Bt	58	33	22	89	9	3.5	—	—	63	.43	14	25	28	2846
Southern Segment														
Pt2	34	0	—	84	7	3.3	—	—	116	.36	4	20	36	2887
Ptl	24	1	8	97	8	4.5	—	—	96	.28	7	25	34	2990
Bt	35	0	—	99	16	6.6	—	—	75	.45	12	25	21	2928

Deposit identification: Mn is Neoglacial moraine, Nri is inactive Neoglacial rock glacier, Nra is active Neoglacial rock glacier, Pt2h is high-elevation mid-late Pinedale moraine, Pt2l is low-elevation mid-late Pinedale moraine, Pt2 is mid-late Pinedale moraine, Ptl is early Pinedale moraine, Bt is Bull Lake moraine.

The difference in average RD values between each moraine age group was examined to estimate the magnitude of the relative-age differences between deposit groups. Specifically, it was questioned whether the inferred mid-late Pinedale moraines were significantly less weathered than the early Pinedale moraines, or whether they might represent simple recessions in early Pinedale time. A histogram comparing all RD values was therefore constructed, with the early Pinedale value of each parameter arbitrarily set equal to 1.0, and RD values for other age groups plotted as percents of the early Pinedale value (figure 24). The comparison shows that for most RD parameters, the difference between mid-late Pinedale and early Pinedale RD values is nearly equal to the difference between early Pinedale and Bull Lake RD values. At first this may seem surprising, but it should be emphasized that many weathering rates are nonlinear with time, with rapid rates of change followed by slower rates (Birkeland 1974, page 176).

In addition to variable rates of change, RD parameters possess two basically different limitation formats that also influence the magnitude of relative-age differences, referred to herein as *percent-limited* and *unlimited*. *Percent-limited parameters*, such as percent stones with rinds in figure 24 have an absolute limit of 100 percent. Where rind development is rapid, all RD data may be confined in a small range near 100 percent. For example, the range of percentage of stones with rinds in the southern segment of this report is only 84 percent (mid-late Pinedale) to 99 percent (Bull Lake) as shown in table 7. *Unlimited parameters*, by contrast, are measurements of physical dimensions in which the size of the natural upper limit may be far larger than the size of typical field measurements.

For example, moraine crest width values in this study range from about 6 to 14 m, but continued weathering may broaden the moraine crests to a considerable percentage of their basal widths, which are on the order of 100's of meters. Values for pre-Bull Lake moraine widths in other studies have been reported as large as "infinite," meaning the entire moraine surface sloped less than 5° and could all be considered as "crest" (Miller 1971). In the present study, separation of moraine relative age groups was usually better for unlimited RD parameters than for percent-limited parameters, and within the latter category better for slow-developing rather than fast-developing parameters.

Morainal deposits in the upper valley reaches and cirques (3450-3700 m elevation) exhibit clast weathering characteristics equal to or stronger than terminal deposits far down valley, yet

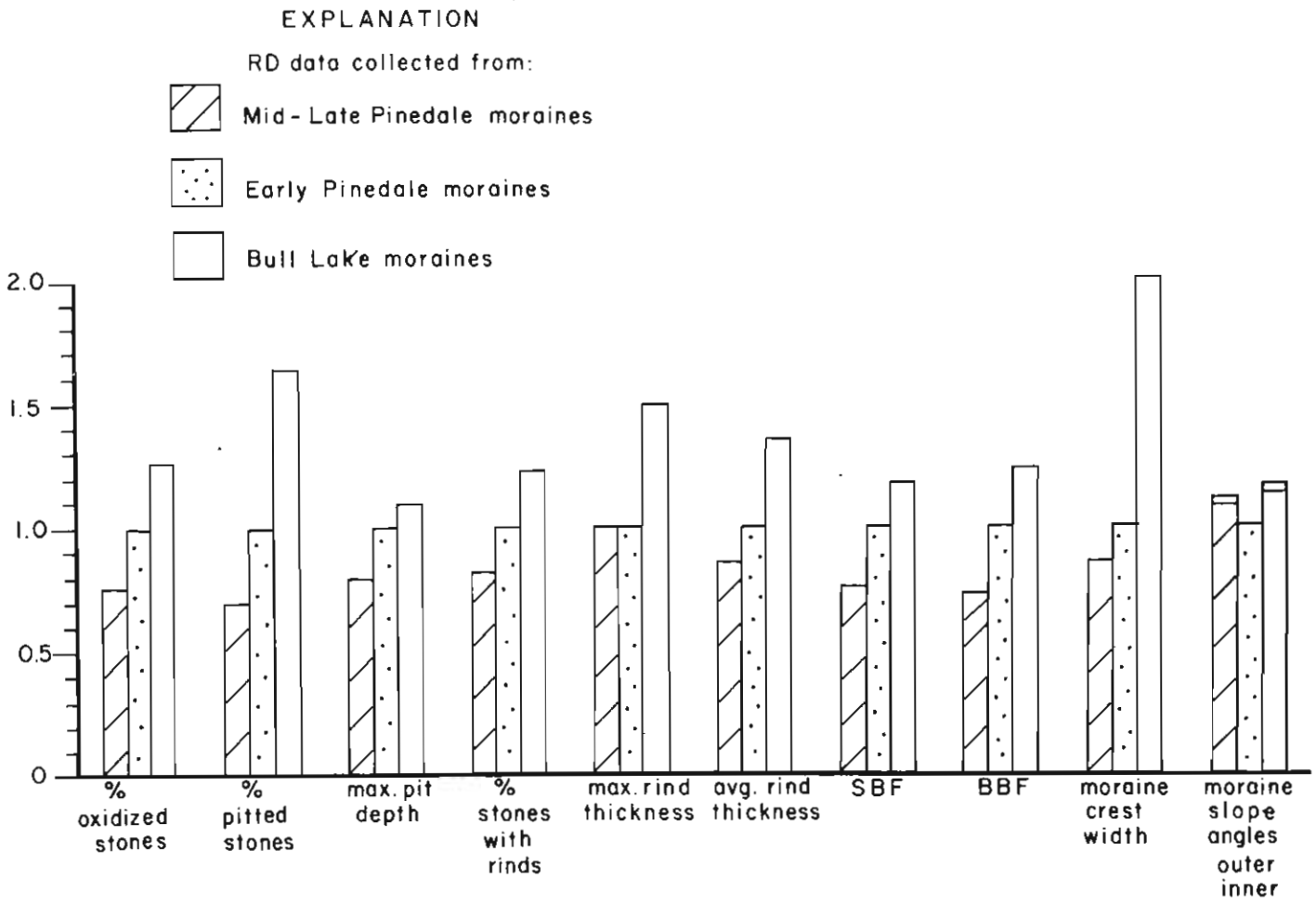

Figure 24.—Ratios of all averaged RD values for three different ages of low-elevation glacial deposits. Ratios are derived from values in table 7 by setting the early Pinedale value equal to 1.0 and representing the other averaged values as percentages of the early Pinedale value.

moraine slope and surface boulder frequency data imply (as does topographic position) that they are significantly younger than terminal deposits (table 7). RD values for high-elevation deposits define two groups: less weathered cirque moraines and rock glaciers and more weathered cross-valley moraines and inactive rock glaciers. A histogram of ratios of various RD parameters, with active rock glacier values arbitrarily set equal to 1.0 shows the grouping (figure 25). RD separation is best for unlimited parameters (maximum pit depth, maximum rind thickness) and worst for percent-limited parameters (percentage of stones with rinds, percentage of lichen cover).

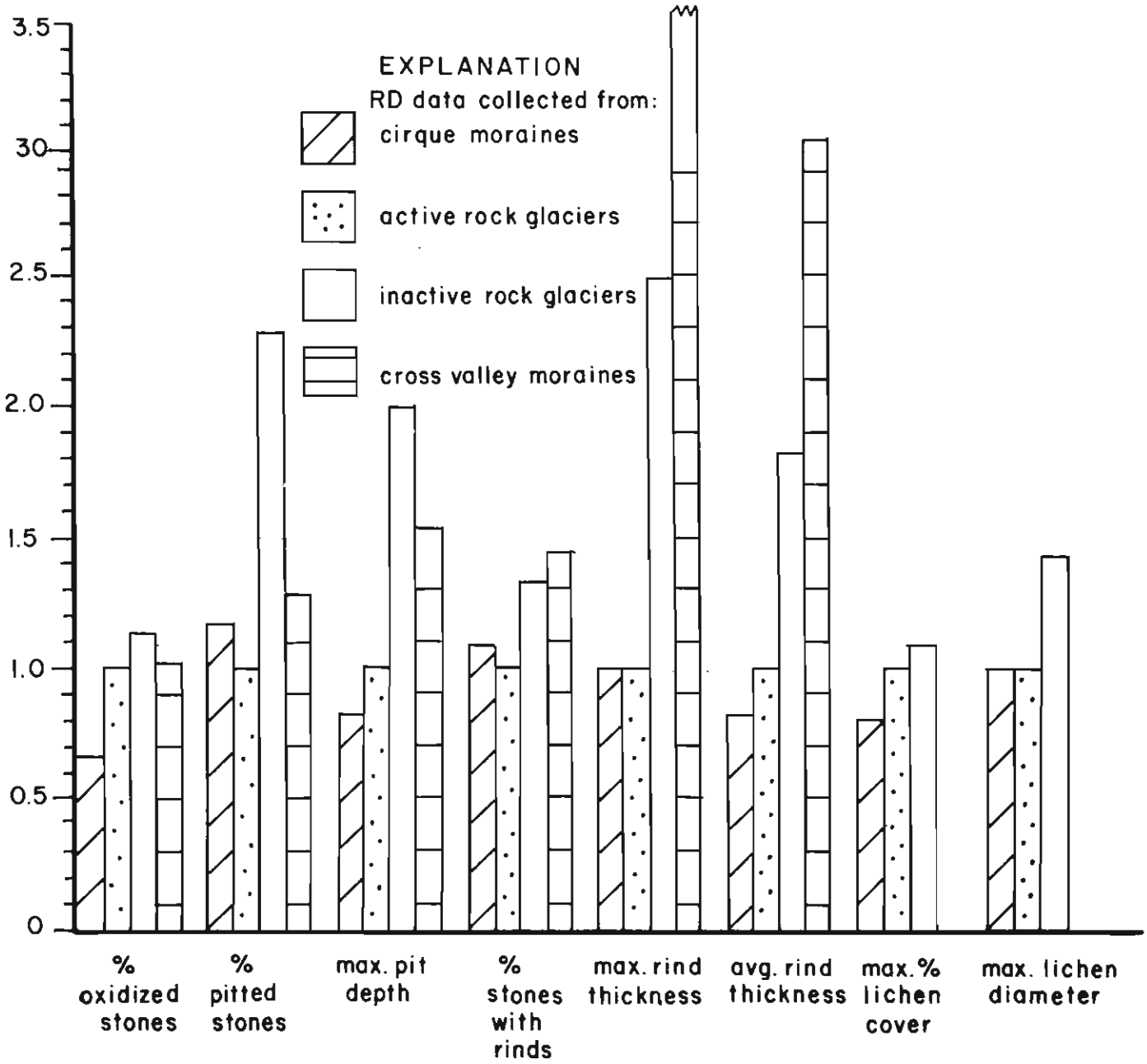

Figure 25.—Ratios of all averaged RD values for four different ages of high-elevation glacial and periglacial deposits. Ratios are derived from values in table 7 by setting the active rock glacier values equal to 1.0 and representing the other averaged values as percentages of the active rock glacier values.

Representative soils from moraines of different inferred age constitute a distinct chronosequence. Calcareous and noncalcareous variants exist within the chronosequence depending on elevation. Soil profiles on glacial deposits show very weak development on mid-late Pinedale moraines, weak development on early Pinedale moraines, and moderate development on Bull Lake moraines (figure 26). The most prominent age-dependent parameters in noncalcareous soils are depth of oxidation and B horizon development (table 8). In calcareous soils the depth of carbonate leaching and thickness of calcareous horizons are the most reliable relative-age indicators.

The five topographic levels of alluvial fan surfaces define a fivefold relative-age sequence in the San Luis Valley. Differences in weathering and erosion characteristics among the five fan levels indicate considerable relative-age difference. The most reliable RD parameter to distinguish fans is soil profile development. Soils are azonal on Holocene deposits, very weak to weak on Pinedale deposits (both ages), moderate to strong on Bull Lake deposits, and very strong on pre-Bull Lake deposits. A chronosequence of typical soils from fan surfaces of four ages is shown in figure 27. For noncalcareous soils, differences in B horizon thickness, B horizon structure, and soil color are most diagnostic (table 9). For calcareous soils, thickness of carbonate horizons and stage of carbonate development increase most notably with age.

Long-Distance Correlation

Correlation of Quaternary deposits in the Sangre de Cristo Range with deposits found elsewhere in glaciated mountains of the western United States is based on similarity of topographic position and various RD parameters. The Pleistocene glacial chronology first worked out by Blackwelder (1915) for the Wind River Mountains of Wyoming has evolved into a widely used Quaternary chronology now recognized throughout the Rocky Mountains. Refinements by many workers (especially Richmond 1960, 1962, 1965) in the last 20 years have resulted in a detailed chronology of six glaciations. Due to differences in climate, vegetation, and lithology between the Sangre de Cristo Range and other mountain ranges, a comparison of RD data may not show an exact match. However, the *magnitude of differences* between units of similar inferred age should be roughly equivalent.

Collection of RD data in the Rocky Mountains has been irregular, and detailed RD data have still not been published for the type areas of the Bull Lake and Pinedale moraines of the Rocky Mountains. However, Burke and Birkeland (1979) have published

Table 8.—Summary of soil profile data on glacial deposits[a]

No. of Profiles	Age of Deposit[b]	B Horizon Thickness	B Horizon Structure[c]	Depth of Oxidation	Maximum Soil Color[d]
2	Pt 2	None	None	34"-42"	2.5 YR-10YR
3	Pt 1	None to 4"	None to Bs (cambic B)	22"-19+"	10YR-7.5YR 4/6
2	Bt	18-23"	wk to mod, sbk	50+"-55+"	10YR-5YR

[a] Values listed are ranges for all soil profiles of the stated age.
[b] Pt 2—mid-late Pinedale, Pt 1—early Pinedale, Bt—Bull Lake.
[c] Abbreviations defined in Appendix A.
[d] Munsell color.

Table 9.—Summary of soil profile data on alluvial deposits[a]

No. of Profiles	Age of Deposit[b]	B Horizon Thickness	B Horizon Structure[c]	Maximum Soil Color[d]	Calcareous Horizon Thickness	Calcareous Horizon Stage[e]
3	Hf	None	None	10YR 5/3-10YR 5/8	46"	I
11	Pf	None to 14"	None to Bs (cambic B)	10YR 5/3-7.5YR 5/4	23"-74"	I-II
9	Bf	5"-43"	wk to str, sbk	10YR 5/4-7.5YR 5/6	50"-75"	II-III
5	pBf	47+"-71"	str abk to str columnar	5YR 4/4-5YR 5/6	77"-149"	III-III+

Total = 28

[a] Values listed are ranges for all soil profiles of the stated age.
[b] Hf—Holocene, Pf—Pinedale, Bf—Bull Lake, pBf—pre-Bull Lake.
[c] Abbreviations defined in Appendix A.
[d] Munsell color.
[e] Carbonate stages after Gile and others 1966.

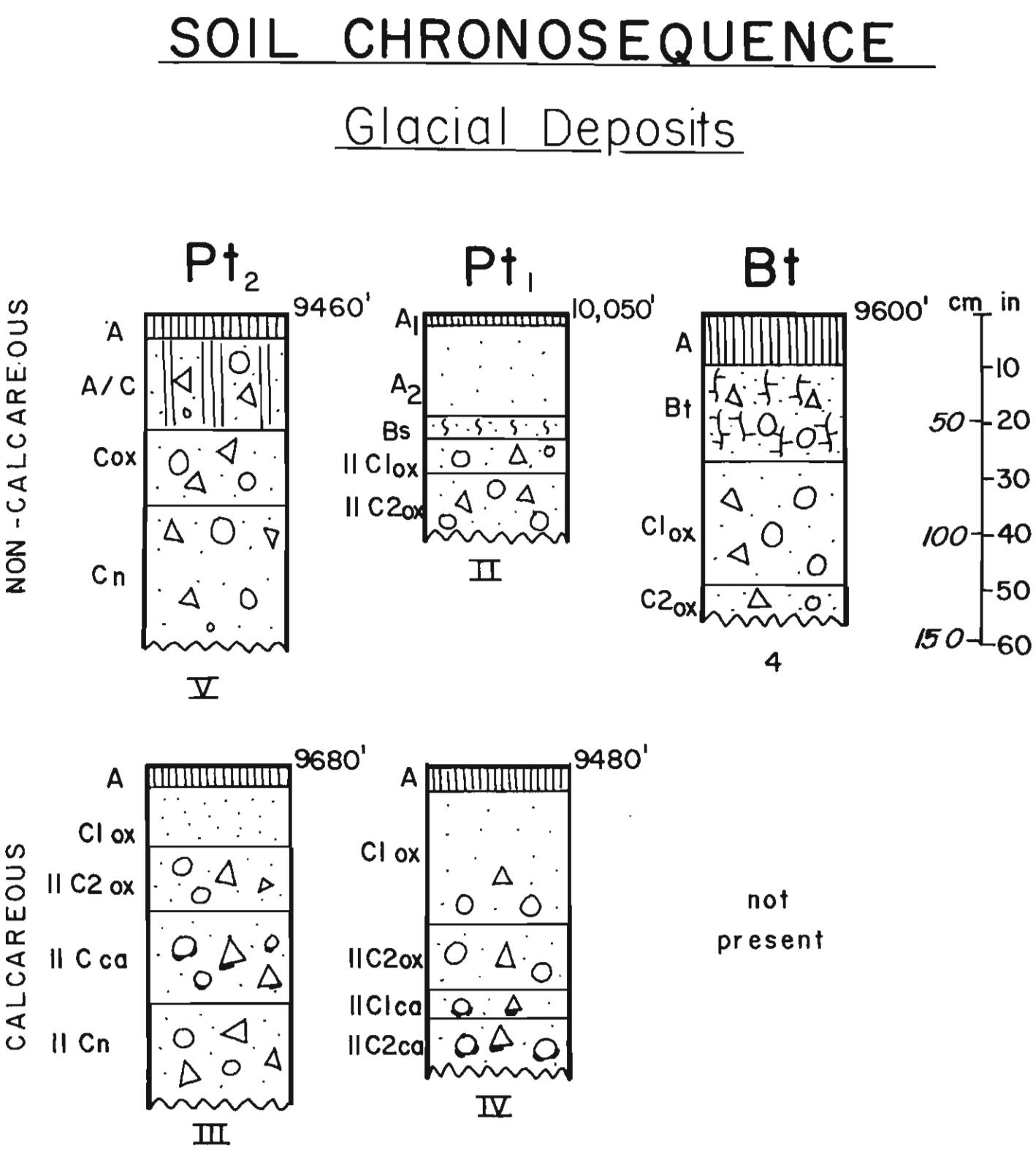

Figure 26.—Soil chronosequence of typical soils, glacial deposits.

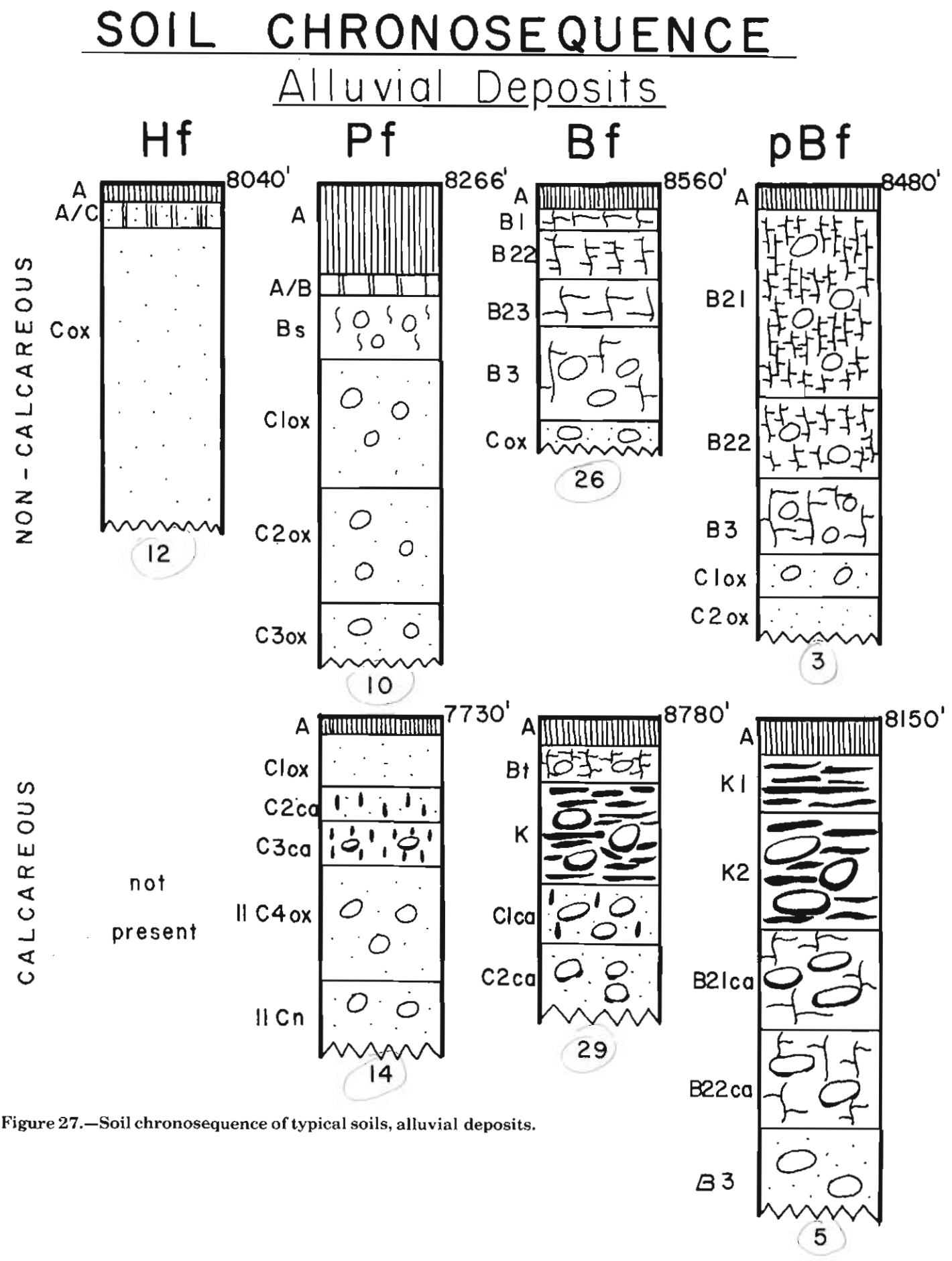

Figure 27.—Soil chronosequence of typical soils, alluvial deposits.

a complete suite of RD observations from the type area of the Tahoe and Tioga moraines of the Sierra Nevada moraines, which have been repeatedly correlated with the Bull Lake and Pinedale moraines, respectively, of the Rocky Mountains. Comparison of four RD parameters from the Sangre de Cristo Range with the same parameters from the Sierra Nevada (figure 28) shows that the *magnitude of differences* between the older and younger moraines is quite similar in both areas. Weathering rinds are slightly more common and thicker in the Sangre de Cristo Mountains, on deposits of both ages. The difference may represent greater susceptibility to chemical weathering for Sangre de Cristo sandstone clasts than for Sierra Nevada granitic clasts. Moraine slope angles are also lower in the Sangre de Cristo Range, suggesting that local moraines are more susceptible to physical erosional processes as well.

The general extent of soil development and the difference in development between soils of different inferred age in this study area are similar to that exhibited by Pinedale and Bull Lake soils elsewhere in the Rocky Mountains as described by Richmond (1962, figure 55). Based on RD and soil profile data, the Bull Lake moraines in the Sangre de Cristo range are therefore correlated with the type Bull Lake moraines of the Rocky Mountain Quaternary chronology. Older and younger Pinedale moraines in the study are correlated with early Pinedale and mid-late Pinedale deposits found widely in the Rocky Mountains (Richmond 1965).

Long-distance correlation of Neoglacial deposits is based on degree of lichen development on boulders. A comparison of lichen data from the study area with data from localities elsewhere in the Rocky Mountains (figure 29) suggests that cirque moraines and active rock glaciers probably originated in Early Neoglacial time. The more weathered inactive rock glaciers may also date from this interval, but weathering data presented previously (table 7) indicate inactive rock glaciers are more weathered than active rock glaciers. The older inactive rock glaciers may date from the last stages of Pinedale glaciation, formed as debris from steep valley walls locally buried stagnant glacier ice.

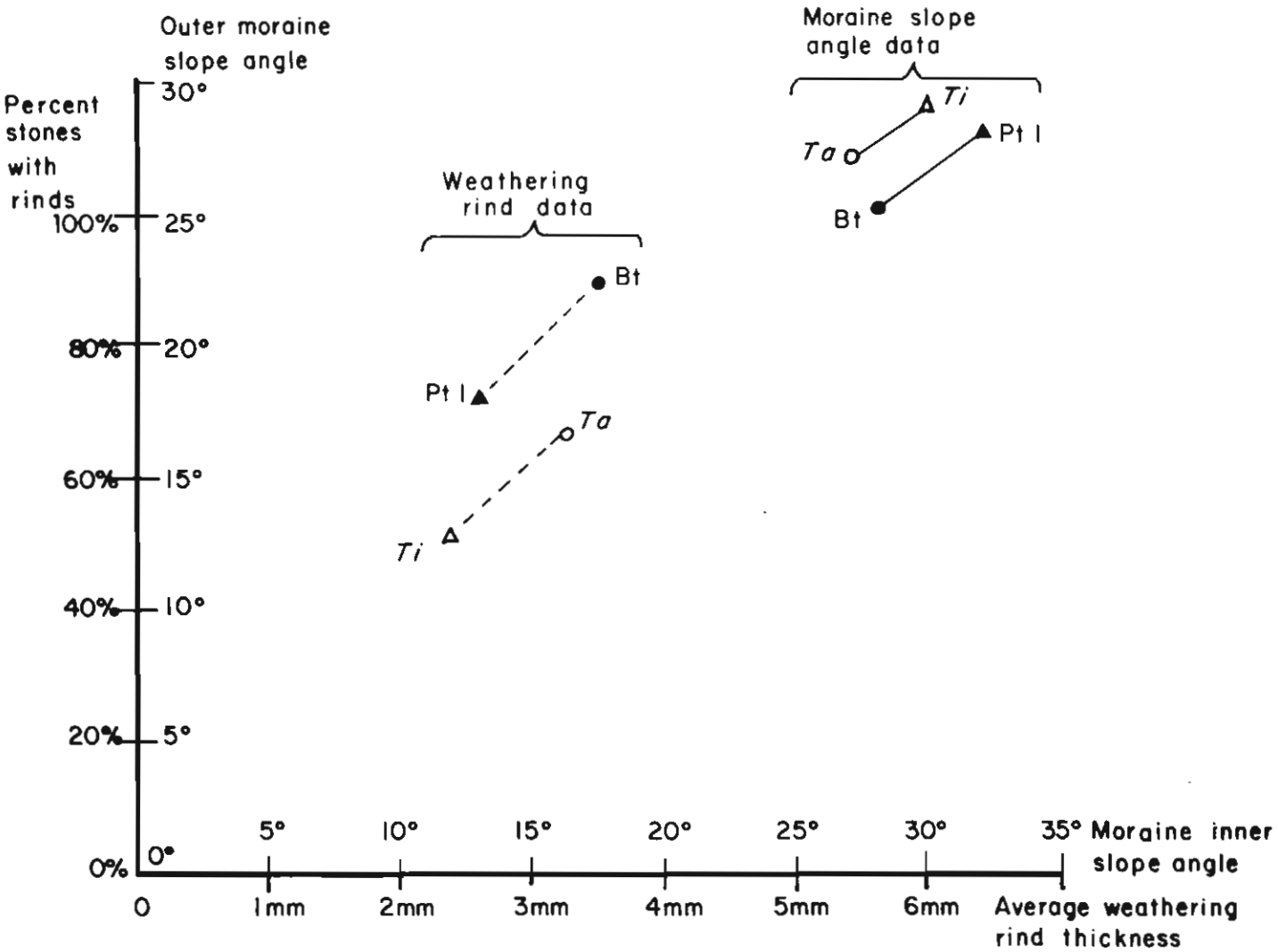

Figure 28.—Comparison of four selected parameters from Sangre de Cristo glacial deposits with those from the Sierra Nevada, California (data from Burke and Birkeland 1979).

Relative Timing of Glacial and Fluvial Deposition

Where dating of alluvial fan surfaces is accomplished indirectly by correlation to dated glacial deposits, as in the study area, it is important to understand the relative timing of glacial versus fluvial deposition. Field evidence that bears on this question was examined at a key fan-head location. At Willow Creek, the early Pinedale alluvial surface is directly traceable to the early Pinedale terminal moraine through a 0.5-km-wide breach eroded in the earlier Bull Lake terminal moraine (figure 10). RD and soil characteristics of the alluvial surface are similar to those of the terminal moraine, suggesting similar age. After the Willow Creek glacier retreated from its terminal position, glacier runoff breached the south wall of the moraine loop and established an outlet channel. This channel is presently incised about 50 m below the early Pinedale outwash surface. The interpretation proposed here is that early Pinedale outwash gravels were deposited throughout the early and maximum stages of glacier advance, but that the broad outwash surface was abandoned when the glacier retreated behind its terminal moraine, after which runoff was directed southward into the present channel. The alluvial slope was therefore mainly a product of early-and-full-glacial deposition.

Similar observations have been made for modern glacier-outwash systems. Describing sandurs (outwash plains) fronting glaciers in Iceland, Embleton and King (1975, page 526) state "The sandur reaches its maximum elevation when the ice front becomes stationary and terminal moraines are forming." Similar situations are reported from Baffin Island (Church 1972) and New Zealand (Speight 1963). These observations indicate that the bulk of outwash gravels are deposited before and during the maximum advance and that the outwash surface itself becomes subject to lowering (erosion) in late stages of glaciation. Conceptual modeling of Pleistocene fluvial processes by Schumm (1965, page 790, table 2) reveals that for basins partly occupied by valley glaciers, early-and-full-glacial times should be marked by deposition, and late-glacial and interglacial times by erosion.

In summary, evidence suggests that alluvial fan surfaces of the San Luis Valley formed during early-and-full-glacial times as braided outwash streams deposited coarse gravels. Abandonment and incision of these surfaces probably began after ice

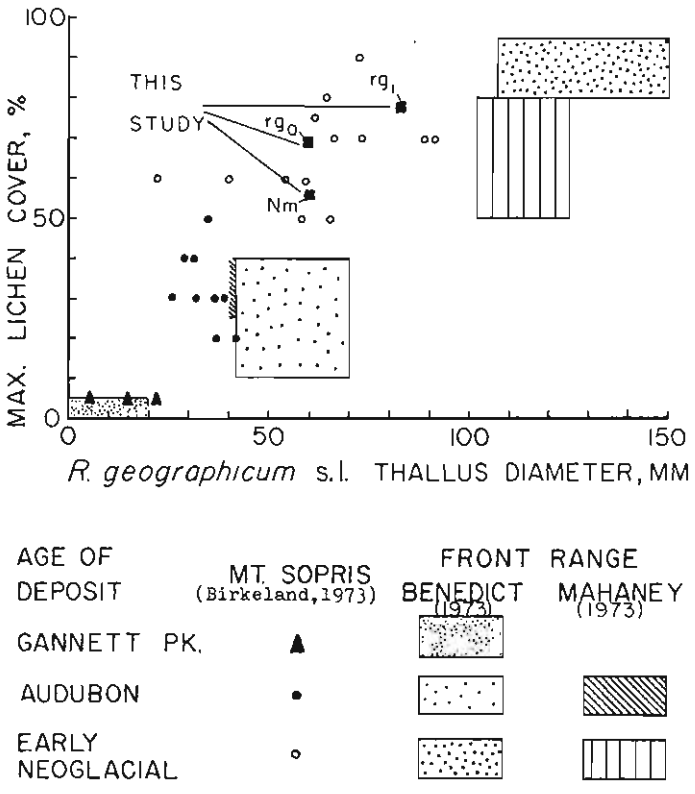

Figure 29.—Comparison of lichen data from the Sangre de Cristo range with data from elsewhere in the Rocky Mountains.

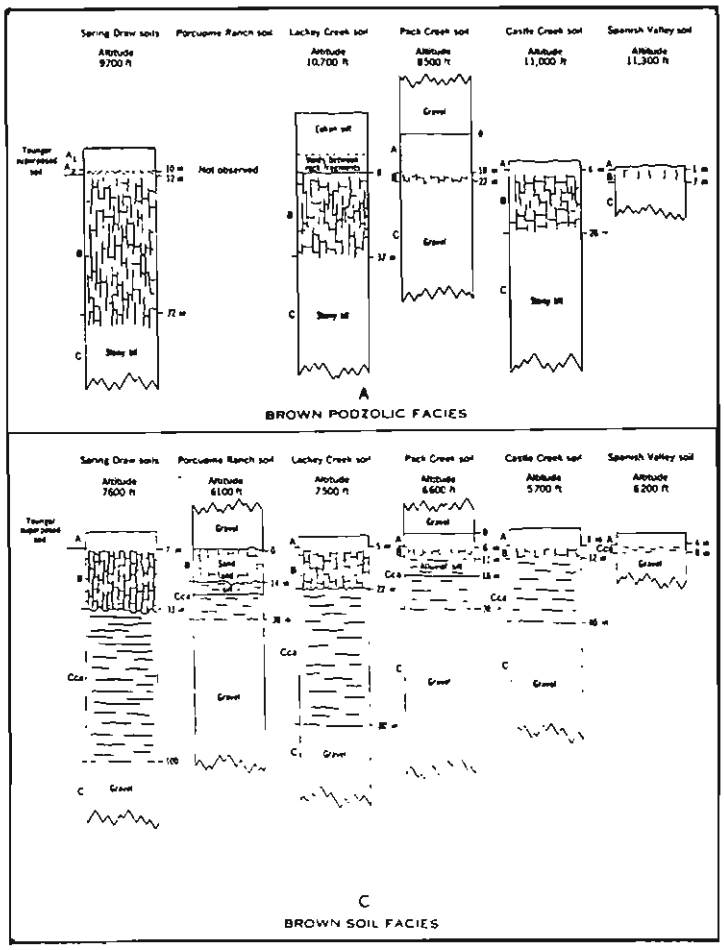

Figure 30.—Soil chronosequences from the La Sal Mountains, Utah (after Richmond 1962, figure 55). Compare with study area soils in figure 27.

retreated from terminal moraines. If true, this sequence of events implies that the presently preserved fan *surfaces* of each age were last active at about the same time as terminal moraines were formed, and that dates on terminal moraine deposition apply equally to correlative fan surfaces. This conclusion bears on alluvial fan-fault scarp age relations because scarps displacing a given fan surface would only be well preserved if they were formed after the fan surface had largely become abandoned.

Fan deposits are therefore correlated with deposits in the composite Rocky Mountain chronology based on: (1) continuity of fans with previously correlated moraines, and (2) similarity of soil development between the local fan sequence, the local moraine sequence, and the composite Quaternary sequence. One of the most detailed studies of Pinedale and Bull Lake soil profiles which includes effects due to both time and climate is that of Richmond (1962) in the La Sal Mountains, Utah. Because of the similarity of climate and vegetation between the Sangre de Cristo Mountains and the La Sal Mountains, soil chronosequences in the two areas can be compared in detail. The soil chronosequence of the La Sal Mountains is shown in figure 30. In each group, soils are strikingly similar to those in the San Luis Valley (figure 27). A correlation chart comparing deposits and soils of the Sangre de Cristo, La Sal, and Wind River Mountains is shown in figure 31.

Absolute Age of Deposits

Knowledge of the absolute age of various deposits is important for precisely dating surface-faulting events. The age limits for deposits of the composite chronology are assumed to broadly apply to correlated deposits of the study area. The temporal relation of moraine deposition to fan formation was previously discussed. Five ^{14}C dates from local alluvial and lacustrine units (table 10) are compatible with the proposed correlation, yet only provide age control for post-Pinedale history. A date of 7660 ± 120 yr BP is younger than mid-late Pinedale deposition, and a date of 10,100 ± 110 yr BP may represent late phases of that period. Other limiting dates for the Pinedale and Bull Lake glaciations are inferred from correlation to the dated composite sequence (figure 32).

The age limits for pre-Bull Lake deposits are especially critical, since these deposits contain the longest record of fault activity in the area, yet are the most poorly age-controlled units in the Quaternary chronology. Absolute age of pre-Bull Lake deposits is circumscribed by several observations: (1) presence of 700,000-year-old ash several meters below the top of the alluvium, (2) development of a soil between pre-Bull Lake and Bull Lake deposits of similar strength to the post-Bull Lake soil, which has developed over roughly 120,000-140,000 years, and (3) correlation with dated paleosols in similar settings. Old alluvial surfaces in southwest Utah carrying soil profiles similar to those in pre-Bull Lake deposits of the San Luis Valley have been U series dated by Sterr (1981) as about 240,000 and 400,000 years old, equivalent to cool stages 8 and 12 of the marine oxygen isotope record (Berggren and others 1980).

From the above data we can conclude that (1) pre-Bull Lake deposition continued after 700,000 years BP, (2) soil formation had commenced on a presumably stable surface roughly 120,000

Figure 31.—Correlation of Quaternary deposits and soils in the study area with sequences elsewhere in the Rocky Mountains. Modified from Richmond (1962, page 87).

Midcontinent region time-stratigraphic standard	La Sal Mountains, Utah (Richmond 1962)		Wind River Mountains, Wyoming (Blackwelder 1915; Richmond 1948; Moss 1949, 1951)		Sangre de Cristo Mountains, Colorado (this report)
Recent Series	Gold Basin Formation	Upper Member Spanish Valley Soil Lower Member	Modern Moraines Very Weak Soil Temple Lake Stage		Azonal Soil Early Neoglacial Deposit
		Castle Creek Soil	Moderate Soil		Very Weak Soil
Pleistocene Series					
Late Wisconsin	Beaver Basin Formation	Upper Member Pack Creek Soil Lower Member	Pinedale Stage Stage	Upper Till ——— Lower Till	Mid-late Pinedale Deposit Weak Soil Early Pinedale Deposit
Mid-Wisconsin	Lackey Creek Soil			Strong Soil	Moderate-Strong Soil
Early Wisconsin Illinoian	Placer Creek Formation	Upper Member Porcupine Ranch Soil Lower Member	Bull Lake Stage	Upper Till — Lower Till	Bull Lake Deposit
Pre-Wisconsin	Harpole Mesa Formation	Upper Spring Draw Soil Upper Member Middle Spring Draw Soil Middle Member Lower Spring Draw Soil Lower Member	Buffalo Stage	Very Strong Soil Post-Canyon Till (?) ——— Pre-Canyon Till (?) ——— Pre-Canyon Till (?)	Very Strong Soil ——— Pre-Bull Lake Deposit ——— ————

QUATERNARY CHRONOLOGY

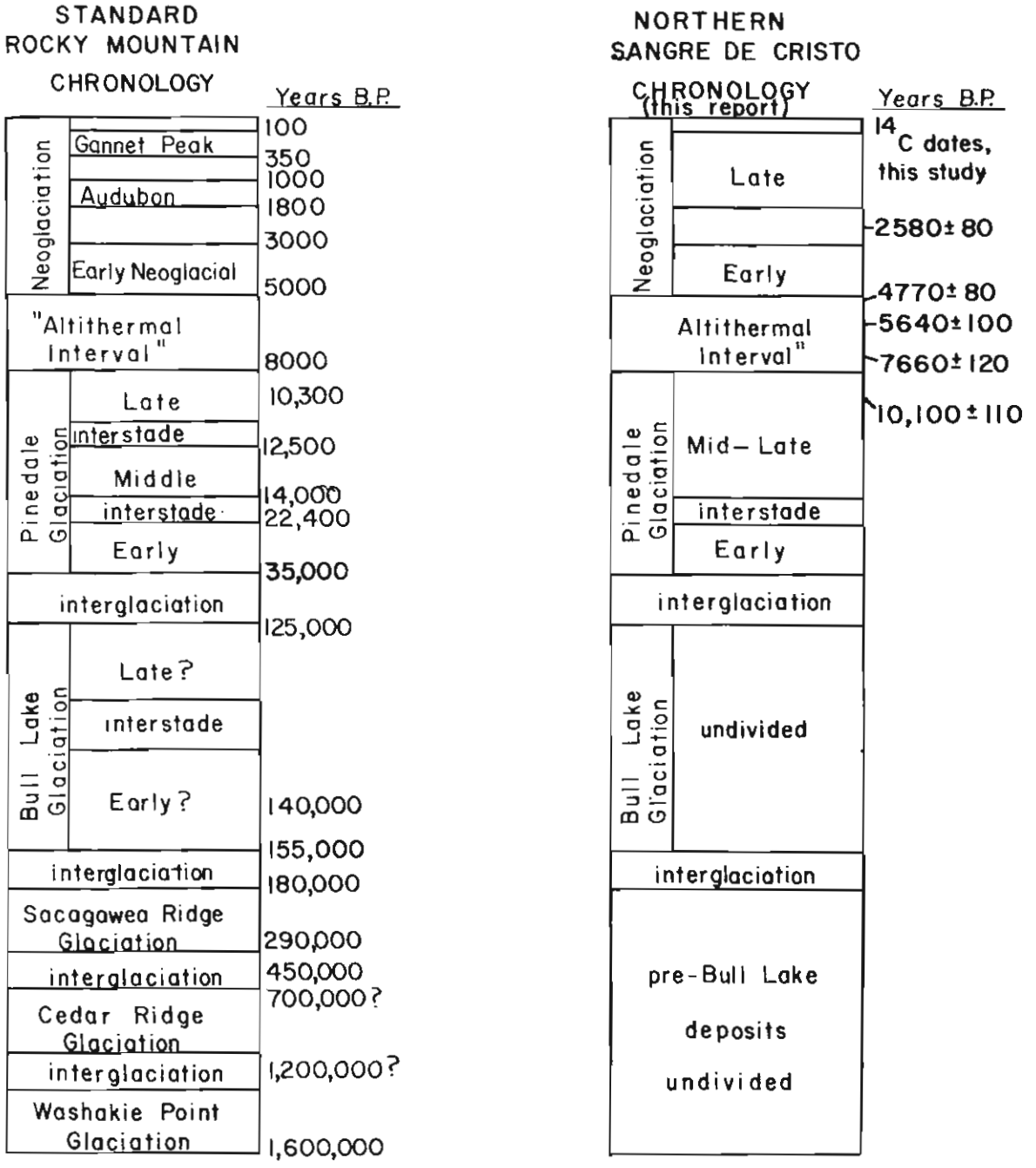

Figure 32.—Composite Quaternary chronology of the Rocky Mountains and correlative chronology derived for the Sangre de Cristo Mountains. Sources: Anderson 1978; Benedict 1973; Currey 1974, 1980; Lineback and Wickham 1978; Madsen and Currey 1979; Nelson 1976; Pierce and others 1976; Richmond and Obradovich 1972; Scott and others 1980; West 1978.

Table 10.—Radiocarbon dates and stratigraphic information

Sample No.	Lab No.	Age (Yr BP)	Unit	Location and Stratigraphic Setting
			Glacial—Lacustrine Deposits	
Auger hole 1 47-53"	β-2234	2580 ± 80	Lacustrine sediments	Willow Park basin; dates a 20-cm-thick interstadial peat bed interstratified with stadial lacustrine silts and clays
Auger hole 1 96-102"	β-2233	4770 ± 80	Lacustrine sediments	Willow Park basin; dates a 15-cm-thick interstadial peat interstratified with stadial lacustrine silts and clays
			Alluvial-Colluvial Deposits	
80JMC007	β-2227	modern (< 100 yr BP)	Holocene alluvium	3 km southwest of mouth of Spanish Creek; dates thin organic layers interstratified with fluvially reworked Holocene eolian sands
80JMC008	β-2228	modern (< 100 yr BP)	Holocene alluvium	3 km southwest of mouth of Spanish Creek; dates thin organic layers interstratified with fluvially reworked Holocene eolian sands
80JMC030	β-2229	5640 ± 100	Holocene alluvium	Mouth of Uracca Creek (trench site); dates a buried A horizon in colluvium overlying faulted Holocene alluvium
80JMC932	β-2230	7660 ± 120	Holocene colluvium	Mouth of Major Creek (trench site); dates a buried A horizon on tectonically derived colluvium overlying faulted mid-late Pinedale alluvium.
80JMC033	β-2231	10,000 ± 110	Holocene colluvium	Mouth of Major Creek (trench site); dates a buried organic horizon in tectonic graben fill overlying mid-late Pinedale alluvium

to 140,000 years before Bull Lake time, i.e., 240,000 to 280,000 years BP, and (3) the alluvial surfaces may have been deposited about 240,000 or 400,000 years ago. The amount of age uncertainty represented by these statements compelled an independent absolute age estimate using quantitative soils analysis.

Most soil parameter values, when plotted against linear time, yield curves which show a rapid increase for about 20,000 years, followed by a more gradual increase with time, finally reaching a constant value (Birkeland 1974, figures 8-17). Marchand and Harden (1976, page 19) state that "the time for attainment of the constant value varies with the parameter—about 100,000 years or less for bulk density; and about 500,000 years for B horizon thickness, depth to fresh parent material, and clay content; and 1 million years or more for color and pH changes."

Prominent age-dependent parameters of total soil pedogenic clay and total pedogenic carbonate were measured in the representative profiles of the alluvial soil chronosequence (figures 33, 34). The values were computed by multiplying the percentage of pedogenic clay or carbonate by weight (total clay or carbonate in each horizon *minus* an assumed original clay or carbonate content), times the bulk density, times the horizon thickness, for each enriched horizon. The sum of the products from all enriched horizons of a single profile yields the total pedogenic clay or carbonate, per unit area of the soil column (expressed in gm/cm^2).

Quantitative analysis of total pedogenic clay in the noncalcareous alluvial soil chronosequence reveals a progressive increase in clay with age (figure 33). Total soil carbonate in the calcareous alluvial soil chronosequence also increases with age (figure 34). Plotted against linear time, the measured values define an S-shaped curve (figure 35) similar to conceptual curves proposed by Birkeland (1974, figures 8-17). If the minimum age of pre-Bull Lake alluvium based on geologic evidence is assumed (280,000-240,000 years BP), the curves show little tendency toward the steady-state. A correlated age of approximately 400,000 years, however, produces a more S-shaped curve. Based on this analysis, an age of about 400,000 years is inferred for most pre-Bull Lake alluvium in the study area.

SUMMARY OF QUATERNARY DEPOSITS

Quaternary deposits of the study area include till, rock glacier rubble, and mass movement deposits in the Sangre de Cristo Mountains, and an alluvial fan deposit in the adjacent San Luis Valley. Moraines and alluvial fans are separable into relative-age groups by topographic position, morphology, and weathering data. The age groups correlate well with those of the widespread Pinedale-Bull Lake chronology of the Rocky Mountains. Sparse ^{14}C dates from local lacustrine and alluvial deposits support the correlation from late Pinedale time to present. Relative-dating and soil data support correlation of older deposits. The absolute age of Quaternary deposits in the study area cannot be definitely established, but correlation to a composite Quaternary chronology gives broad age limits that probably apply to local deposits. These age estimates will be utilized in the following sections to infer the probable history of tectonic events that offset the Quaternary deposits.

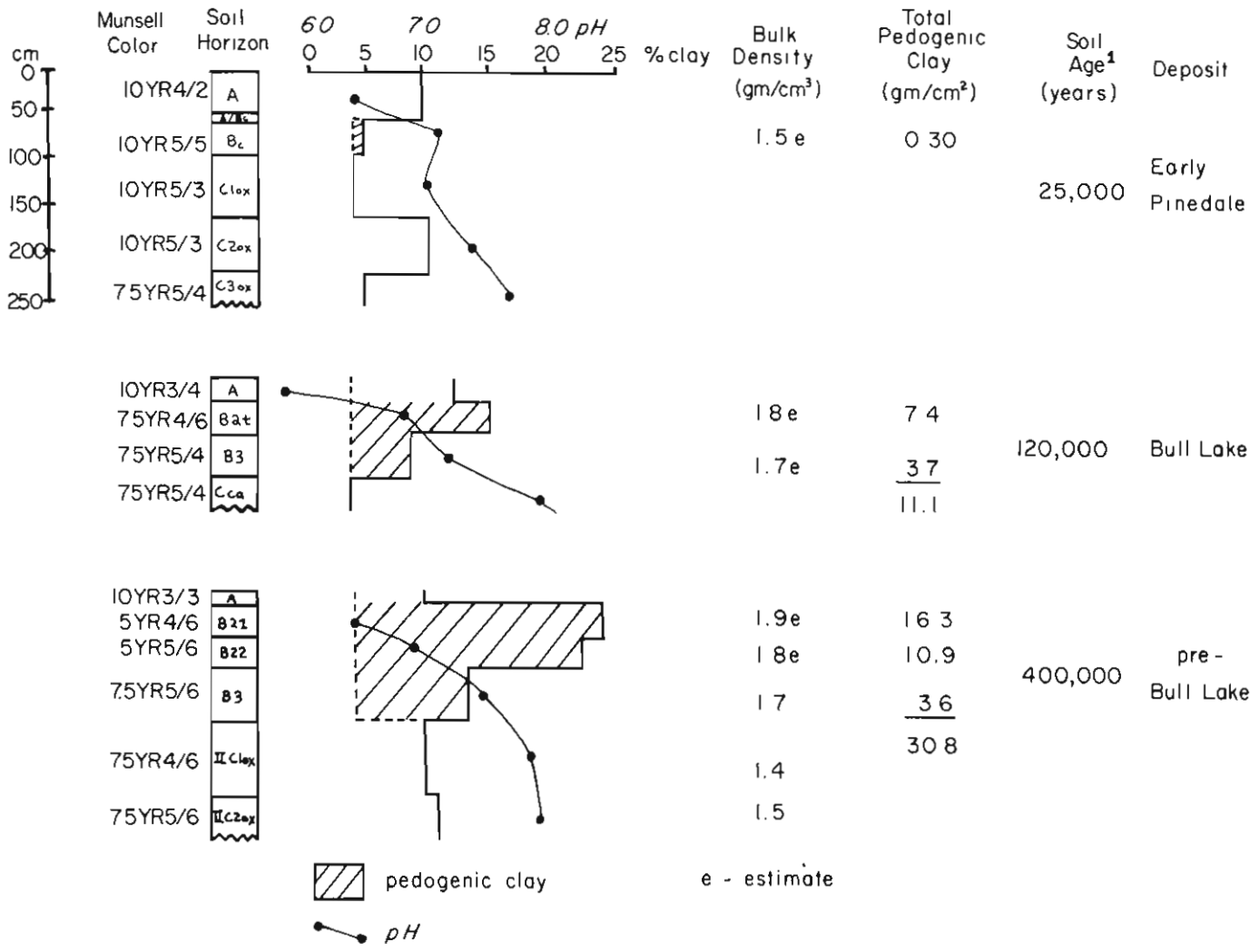

Figure 33.—Quantitative soil profile data, noncalcareous alluvial chronosequence. Pedogenic clay content increases with soil age. Age estimates from correlation (figure 32).

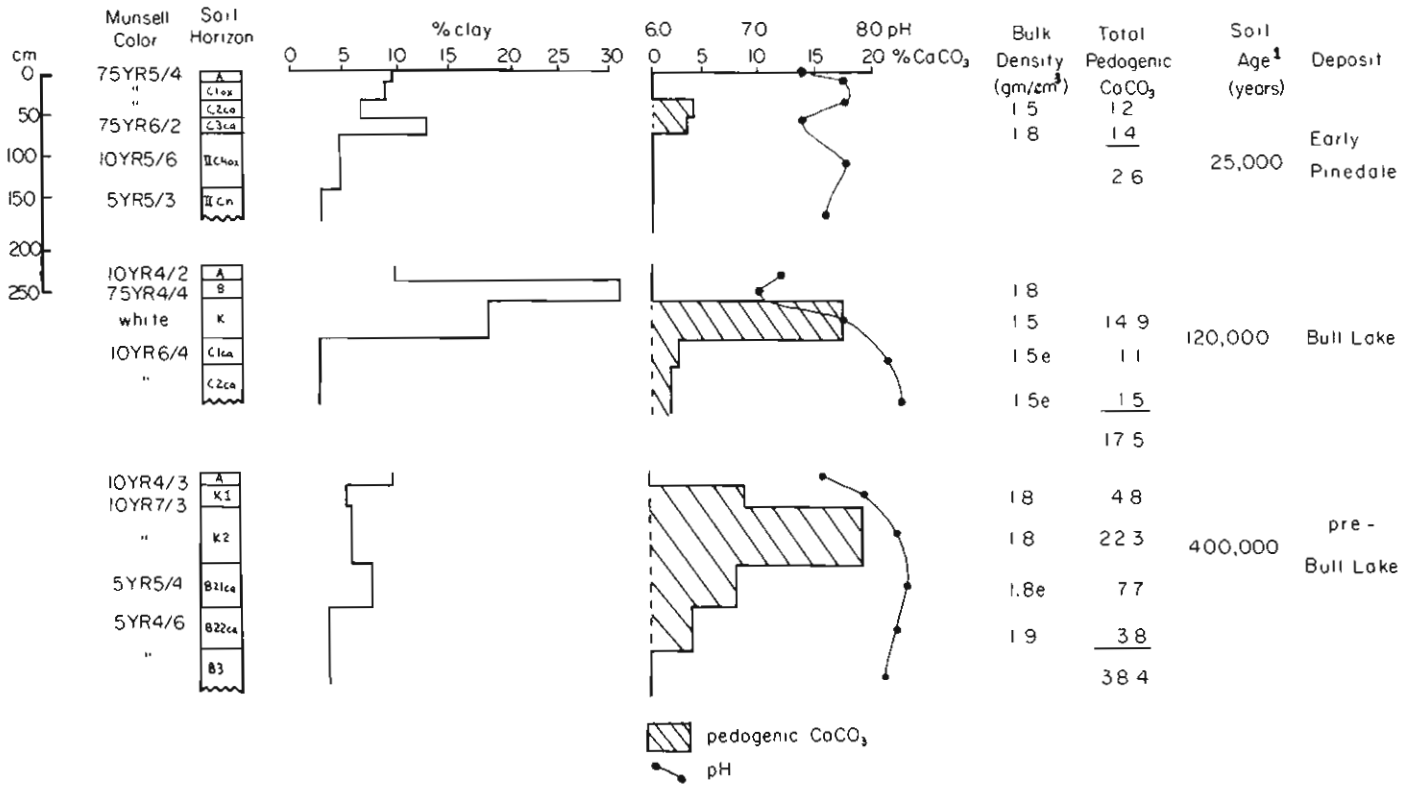

Figure 34.—Quantitative soil profile data, calcareous alluvial chronosequence. Pedogenic carbonate increases with soil age. Age estimates from correlation (figure 32).

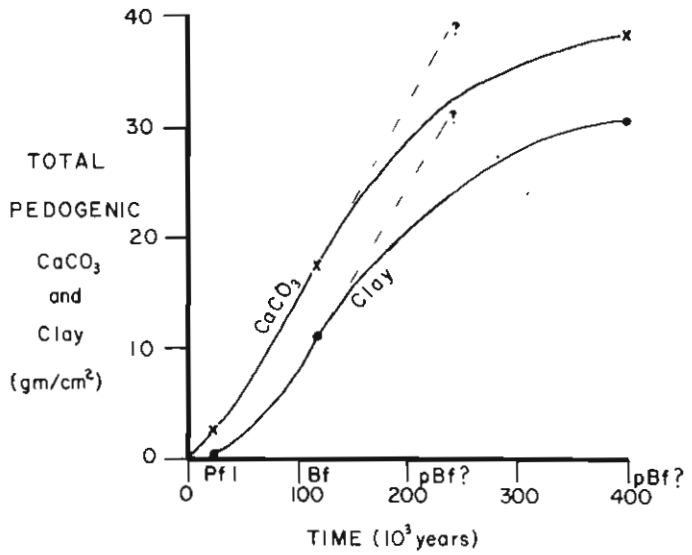

Figure 35.—Plot of increasing pedogenic $CaCO_3$ and clay with soil age, for study area chronosequences. Data are derived from figures 33 and 34. An age of about 400,000 years for pre-Bull Lake deposits produces an S-shaped curve (solid lines), whereas an age of 240,000 years (dashed lines) shows a linear increase with time.

PART TWO: NEOTECTONICS

INTRODUCTION

The northern Sangre de Cristo Mountains and adjacent San Luis Valley constitute major horst and graben, respectively, of the 950-km-long RGRZ (figure 9). Normal displacement on the range-bounding SCFZ has resulted in up to 7015 m of vertical basement offset since Early to Mid-Tertiary time (Huntley 1977). Quaternary glacial and alluvial deposits which cross the range-bounding fault are commonly offset by well-preserved basin-facing scarps. Scarps offsetting successively older deposits are progressively higher, ranging from 2 m high in Holocene to up to 87 m high in pre-Bull Lake deposits. The geometry of increasing scarp height across older Quaternary deposits suggests recurrent Quaternary movement on the Sangre de Cristo Fault. Similar evidence for recurrent faulting occurs on the VGFZ, a 10-km-long swarm of scarps within the northern San Luis Valley. The distribution, morphology, and geometry of fault scarps and their interaction with Quaternary deposits is examined in detail to reconstruct the neotectonic history of this part of the RGRZ.

METHODS

Fault scarps were initially located on large-scale (1:15,840) black-and-white aerial photographs. Vegetation and hydrologic anomalies associated with scarps allowed features as small as 30 cm high to be located. Surface profiles of 153 scarps along the SCFZ and VGFZ were measured by standard field methods (Bucknam and Anderson 1979, page 12), using an extendable 4 m-long stadia rod and an Abney level. All field measurements are reproduced in Appendix B (VGFZ) and Appendix C (SCFZ). Profiles were aligned perpendicular to the fault scarp without regard to the local slope of the faulted surface. Wide deformation zones often necessitated extending the profile 40 m or more above and below the prominent scarp to attain undisturbed alluvial surfaces. Five trenches (one on the VGFZ, four on the SCFZ) were excavated across fault scarps by small backhoes with 60 cm-wide buckets. Trench lengths ranged from 15 to 35 m, aligned perpendicular to scarp strike; depths averaged 2.5-3.5 m. Trench walls were mapped at a scale of 1:40, from a 1 m by 1 m grid system.

Before any descriptions of fault scarps are made, terminology and measurements must be defined as used in this report (refer to Glossary). The relation of these field measurements to scarp morphology and original fault displacement will be examined explicitly by use of geometric models.

Scarp Terminology and Measurements

Geometrically, fault scarps can be simple or complex. A simple scarp (after Slemmons 1957, page 367) is defined as a scarp produced by simple translational offset along a single fault plane. Scarp terminology and measurements for simple scarps as used in this study are shown in figures 36 and 37. These parameters, adopted from various authors, are necessary for estimating scarp age and measuring the "size" of the scarp. Several kinds of complex fault scarps can form over normal faults (figure 38) by: (1) tilting of the downthrown block, (2) rifting of the downthrown block, or (3) stepfaulting of the upthrown block (Gilbert 1890; Slemmons 1957). In addition, erosion and deposition over long periods of time can modify scarp geometry. Field studies (Wallace 1977) have shown that as the scarp declines with time: (1) maximum scarp slope angle decreases, (2) retreat and width of scarp crest increases, and (3) scarp height increases, if on a nonhorizontal surface.

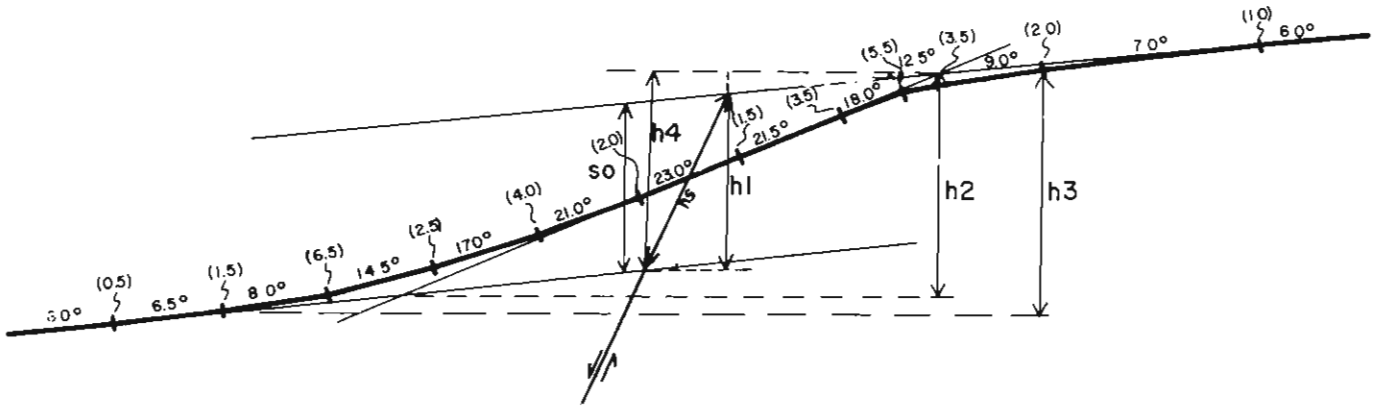

Figure 36.—Scarp height measurements for simple scarps (terms defined in Glossary).

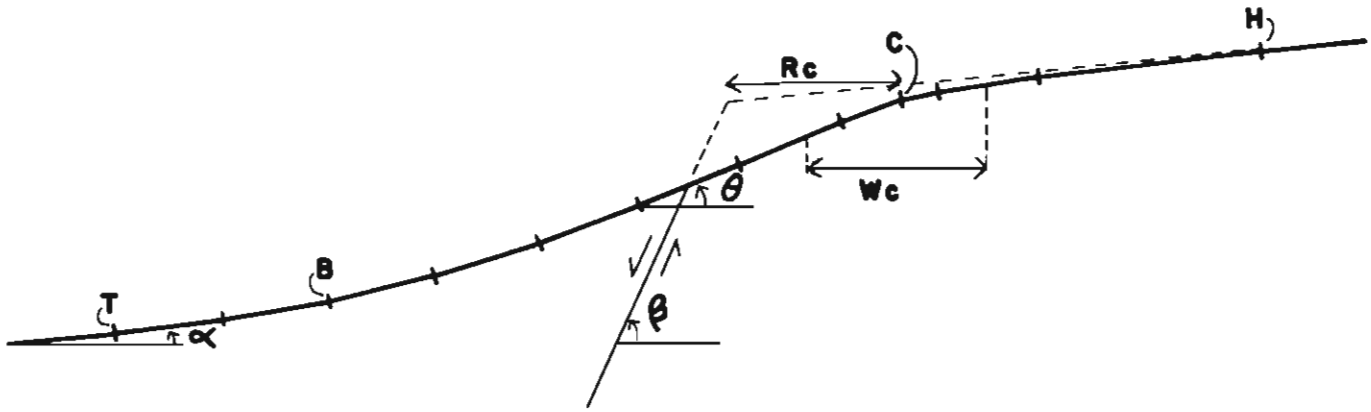

Figure 37.—Scarp morphologic terms for simple scarps; same scarp profile as in figure 36 (terms defined in Glossary).

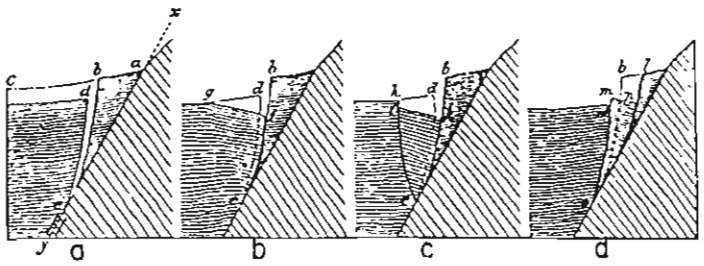

Figure 38.—Illustration of Gilbert's theory for the formation of complex fault scarps (Gilbert 1890, page 355). Terms are defined in Glossary.

Scarp Geometric Modeling

For interpreting temporal and spacial variations in fault displacement throughout the study area, a method was needed which would identify and compensate for effects of different scarp types and different amounts of scarp degradation on scarp height. Geometric models of simple and complex scarps were therefore developed to allow calculation of the vertical component of fault displacement (hereafter referred to as fault throw) on each measured scarp profile. The reduction of all scarp height data to fault throw values had several advantages: (1) it allows comparison of fault displacement data from throughout the study area regardless of scarp type or degree of modification, (2) displacement values can be compared to displacements on worldwide historic scarps to estimate magnitude of Quaternary earthquakes, and (3) vertical displacement in Quaternary time can be compared to vertical displacement of dated pre-Quaternary horizons. Because of the importance of this method in tectonic reconstruction, its development is presented in detail in the following section.

For simple scarps, the relation between fault throw and surface offset at any time can be derived trigonometrically. Table 11 shows the derivation of Equation (1) which quantitatively interrelates original fault throw (h_1) with scarp surface offset (so):

$$so = h_1(1 - \cot\beta \tan\alpha) \tag{1}$$

(Terms are defined in Glossary). The relation between fault throw and surface offset depends only on fault dip (β) and fan slope (α); because these two terms are time invariant, the relation is also time invariant. The relation between fault throw and scarp height as commonly defined (Bucknam and Anderson 1979) is more complex, since scarp height is determined by interaction of maximum scarp angle (β) and fan slope (α). Table 12 shows the derivation of Equation (2), which relates throw and scarp height:

$$h_2 = h_1 \left\{ \frac{\sin\theta \sin(\beta - \alpha)}{\sin\beta \sin(\theta - \alpha)} \right\} \tag{2}$$

In both the above formulas, all quantities can be measured from surface profiles except β. For most fault scarps β cannot be directly measured except in trench exposures and therefore must be estimated. Values for β vary over a range of 10° or more in study area trenches, so this amount of uncertainty is introduced into all calculations in which β is assumed.

Note that as the scarp broadens, scarp height becomes progressively larger than fault throw. The relation of Equation (2) is time dependent, since the maximum scarp slope angle changes with time.

In summary, the original fault throw of any degraded simple fault scarp can be calculated by measuring a single height parameter and two or three angular parameters and assuming a fault dip angle. However, near-surface deformation is often more complicated than the simple scarp model assumes. Four tectonic and two geomorphic processes can lead to a combination of situations where Equations (1) and (2) must be modified, as discussed below.

Rotation of the downthrown block toward the fault plane (figure 38) can result in a scarp whose height exceeds the net throw across the deformation zone. The term "reverse drag" is often applied to this situation, although examination of figure 38 will show that the geometry actually results from slumping under tension rather than from any frictional drag. The additional throw added solely by rotation (h_f) can be calculated trigonometrically (table 13, figure 39), resulting in Equation (3):

$$h_f = \frac{W_f\{\tan\alpha + \tan(\phi - \alpha)\}\cos\alpha \sin\beta}{\sin(\beta - \alpha)} \tag{3}$$

Table 11.—Derivation of the relationship between surface offset and fault throw for simple fault scarps (so is surface offset and h_1 is fault throw)

Combining the three relationships

$x = h_1 - so,$

$y = h_1 \tan(90° - \beta,)$

$x/y = \tan\alpha$

and solving for so gives

$x = h_1 - so = h_1 \cot\beta \tan\alpha.$

$so = h_1(1 - \cot\beta \tan\alpha).$

Table 12.—Derivation of the relation between scarp height and fault throw for simple fault scarps (h_2 is scarp height and h_1 is fault throw)

Combining the four relationships

$\sin\theta = 1/2h_2R,\ Y/R = \sin(\theta - \alpha),$

$\sin\beta = 1/2h_1/r,\ y/r = \sin(\beta - \alpha),$

solve for h_2:

$$h_2 = 2R\sin\theta; \quad R = \frac{Y}{\sin(\theta - \alpha)}, \quad h_2 = \frac{2\sin\theta Y}{\sin(\theta - \alpha)},$$

then solve for Y:

$$r = \frac{h_1}{2\sin\beta} = \frac{Y}{\sin(\beta - \alpha)}, \text{ or } Y = \frac{h_1 \sin(\beta - \alpha)}{2\sin\beta}.$$

Substituting h_2 for Y gives

$$h_2 = \frac{2\sin\theta}{\sin(\theta - \alpha)} \times \frac{h_1 \sin(\beta - \alpha)}{2\sin\beta} = h_1 \left\{ \frac{\sin\theta \sin(\beta - \alpha)}{\sin(\theta - \alpha)\sin\beta} \right\}$$

Table 13.—Derivation of the component of fault throw introduced by surface rotation for a complex fault scarp (h_f is surface rotation). Refer to figure 39

Combine the three relationships

$so_f = X + Y, \quad X = w_f \tan\alpha, \text{ and } Y = w_f \tan(\phi - \alpha)$

to get $so_f = w_f[\tan\ \alpha + \tan(\phi - \alpha)].$

From the Law of Sines, $\frac{s}{\sin(90° - \beta)} = \frac{so_f}{\sin(\beta - \alpha)}$

Since $s = h_f/\sin\beta$ and $\sin(90° + \alpha) = \cos\alpha$

then $s = \frac{so_f \sin(90° + \alpha)}{\sin(\beta - \alpha)} = \frac{so_f \cos\alpha}{\sin(\beta - \alpha)} = h_f/\sin\beta.$

Substituting for so_f and solving for h_f:

$$h_f = \frac{w_f[\tan\alpha + \tan(\phi - \alpha)]\cos\alpha \sin\beta}{\sin(\beta - \alpha)}.$$

The true net throw (h_{lt}) is then calculated by subtracting h_f from the calculated throw of the scarp from Equations (1) or (2) (h_{lm}). In other words:

$$h_{lt} = h_{lm} - h_f \quad (4)$$

Near-fault drag of strata into fault planes can contribute to fault throw as calculated by Equations (1) or (2) (figure 40). However, the origin of drag is uncertain. It could represent: (1) sudden drag during a surface-faulting earthquake, (2) flexure only over an earthquake displacement at depth, or (3) slow seismic creep over a fault. If (3) is true, then the vertical component of drag (h_d in figure 40) should not be included in displacement calculations used for earthquake magnitude estimation. However, field evidence to distinguish (1), (2), and (3) is usually lacking.

If tensional stresses are severe in the near-surface environment, the downthrown block may develop single or multiple graben structures (figure 41). As with surface rotation, graben formation creates a scarp whose height exceeds the net vertical displacement across the fault. The amount of exaggeration is great when the graben is wide, or when the offset surface is steep.

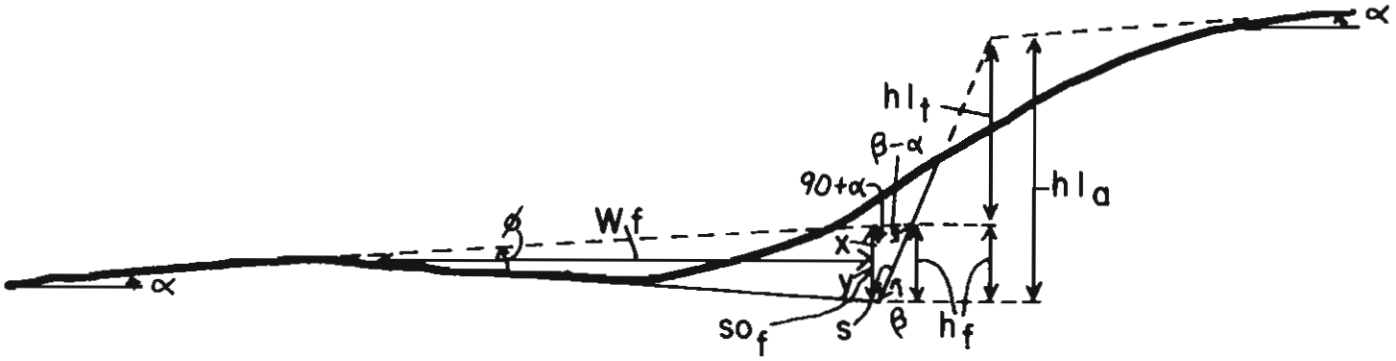

Figure 39.—Geometric relation of lower surface rotation (flexing) to overall scarp geometry (terms defined in Glossary).

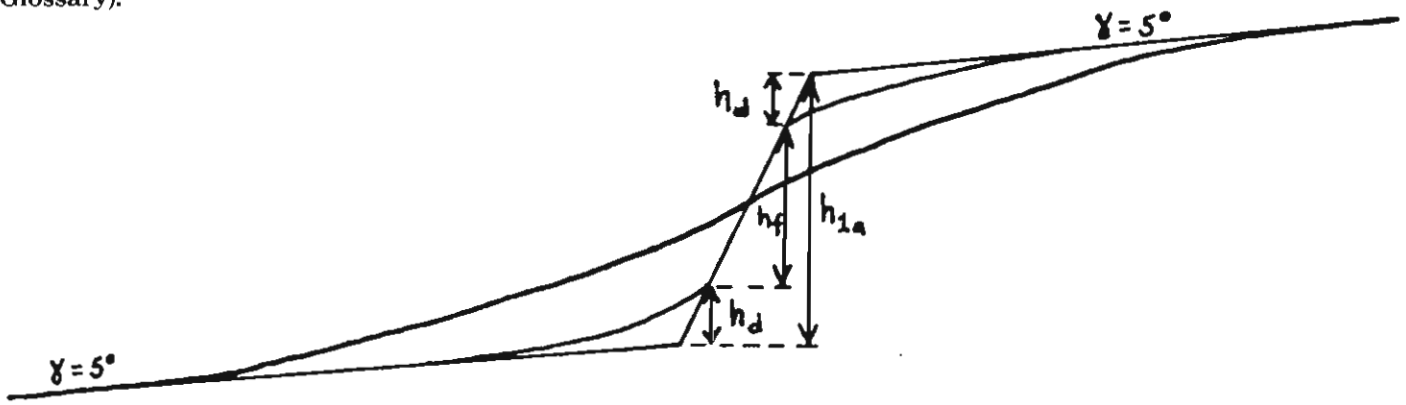

Figure 40.—Geometric relation between vertical component of drag and fault displacement (terms defined in Glossary).

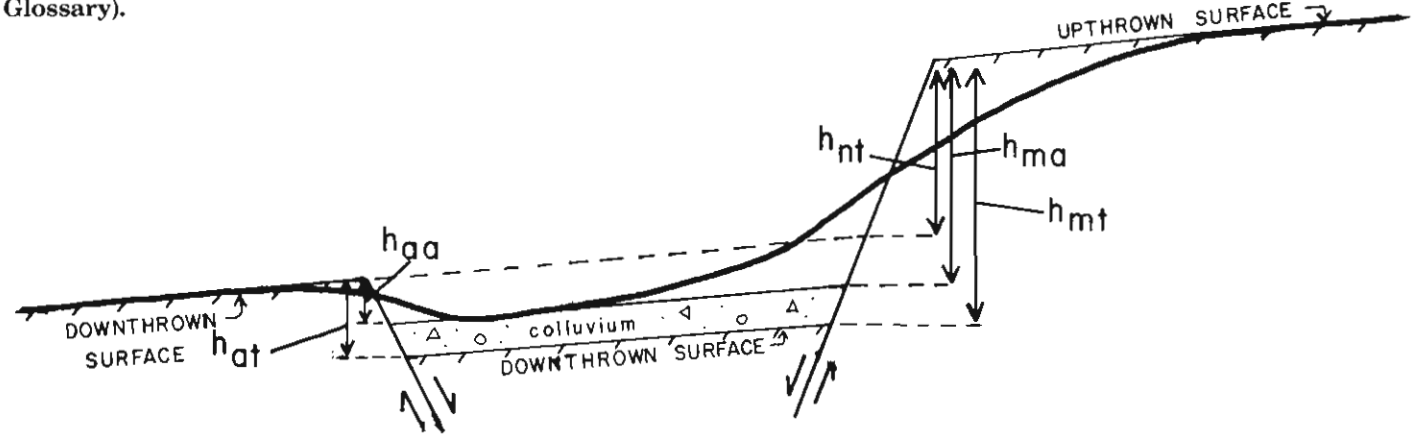

Figure 41.—Effect of graben formation on the geometry of a hypothetical fault scarp (terms defined in Glossary).

True net throw can be calculated mathematically by summing positive and negative vertical displacements across the graben zone (figure 41). However, because of graben colluviation, graben tilting, and multiple faulting, the mathematical procedure can be tedious. A simpler method is graphical projection of the lower faulted surface to the fault scarp, and subsequent graphical measurement of net vertical displacement (figure 41).

Failure of the upthrown alluvial block during faulting can create longitudinal step-faults which parallel the main fault (figure 38). If no rotation of fault slivers occurs, then the sum of individual fault displacements will total net displacement. However, both forwards and backwards rotations have been observed on historic faults (Gilbert 1890; Slemmons 1957). For backwards rotations the sum overestimates, and for forwards, it underestimates, the true net displacement (figure 42). The amount of error increases as the fault slivers become wider, and/or as the rotation angle becomes larger.

If extensive eolian-augmented colluviation occurs at the scarp base, the downthrown block may be buried by colluvium for considerable distances from the scarp. Figure 43 shows how this situation leads to an underestimate of true fault displacement by use of Equations (1) or (2). By adding the colluvium thickness at the scarp toe (C) to the apparent fault throw (h_{1a}), the true throw (h_{1t}) is approximated. As described later, colluvium thickness increases with time.

On old scarps, the entire upthrown surface may be lowered by erosional processes such as sheetwash, rillwash, and eolian deflation (Cooke and Warren 1975, page 124). Figure 43 shows how the thickness of material stripped from the upper block (E) decreases the apparent fault throw (h_{1a}) relative to the true throw (h_{1t}). Erosion is inferred to have affected scarps of the SCFZ and VGFZ that offset pre-Bull Lake deposits, but exact measurement of erosion depth is difficult due to lack of reference points. Because surface soil profiles on older surfaces are well developed, rate of stripping probably did not exceed rate of downward weathering development. The implication is that surface erosion rates are slow, and probably less important geometrically than colluviation effects.

In summary, features of fault scarp geometry have been described to emphasize that scarp height does not always truly represent fault displacement. To analyze Quaternary displacement trends spatially and temporally, all complicating geometric, tectonic, and geomorphic factors must be identified and corrected for *on each scarp profile*. In the following tectonic analyses, quoted fault displacements have been calculated using the simple scarp model and appropriate corrections made for complicating factors, when identifiable.

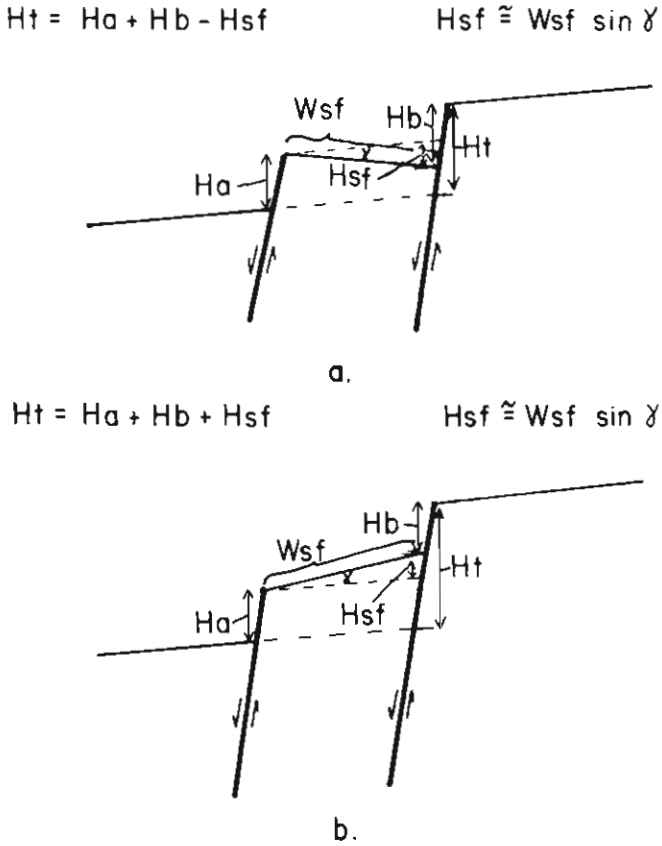

Figure 42.—Effects of longitudinal stepfaulting on fault scarp geometry (terms defined in Glossary).

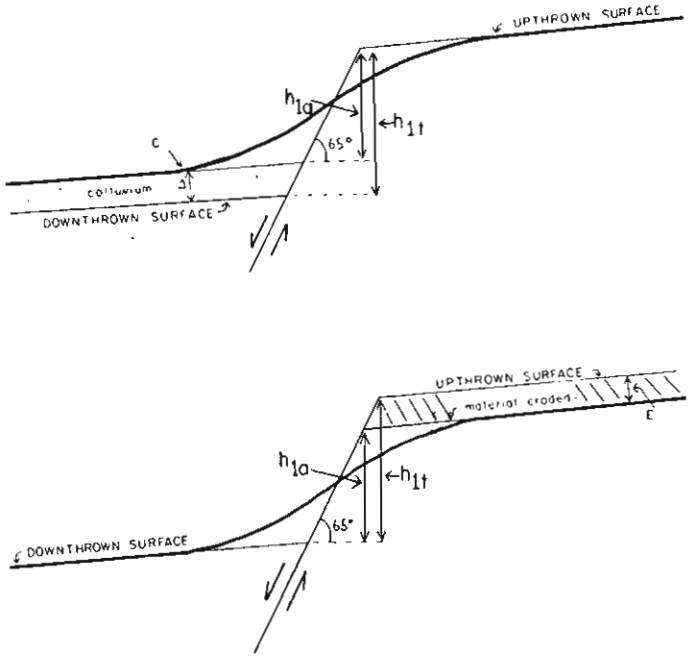

Figure 43.—Geomorphic complications to the simple scarp geometric model. Terms defined in Glossary.
(a) Colluviation at base. (b) Erosion of the upthrown surface.

SCARP MORPHOLOGY

Scarp Production and Degradation

Because the formation of scarps on the SCFZ and VGFZ was not observed or recorded by man, a tectonic origin must be inferred from available geologic data. First, trench exposures reveal stratigraphic displacements under surface scarps in three locations (described later). Secondly, the traces of studied scarps are coincident with a known master fault with over 7015 m of Cenozoic vertical displacement (Huntley 1979, page 87). Finally, field studies after major earthquakes elsewhere in the Basin and Range province (Jones 1915; Gianella and Callaghan 1934; Tocher 1956; Slemmons 1957) have shown indisputably that at least some range-bounding and intrabasin scarps in alluvium are created by tectonic displacement. The coincidence of fresh, historic scarps with subdued, rounded scarps along a fault zone (Page 1934; Wallace 1977) imply that the latter are results of prehistoric tectonic displacements. Scarps of the SCFZ and VGFZ are similar in position, geometry, and morphology to such subdued tectonic scarps.

Recent studies have suggested that linear escarpments in alluvium can also be caused by groundwater decline and subsidence in alluvial basins (Holzer and others 1979). However, reported water-table declines of up to 100 m have produced scarps only on the order of 0.4 m high (Holzer 1977). Much of the subsidence results from compaction of highly compressible clays interbedded with coarser alluvium near valley axes (Freeze and Cherry 1979, page 371). At the Sangre de Cristo Range front, scarps up to 87 m high are underlain by coarse gravels of low compressibility. Fluctuations of groundwater table between late Pleistocene glacial and interglacial stades may have occurred in the San Luis Valley. However, magnitude of such water-table rises in glacial stades was almost certainly less than about 30 m (the maximum depth of the present groundwater table), since rises larger than this would have created lake conditions, and none are known of in late Pleistocene time (Powell 1958). Thus neither the sedimentologic setting nor the magnitude of inferred late Pleistocene groundwater fluctuations in the study area seem appropriate for differential compaction generation of large scarps at the range front.

For smaller interbasin scarps of the VGFZ that are developed in finer sediments with a shallower water table, scarp production could possibly be related to differential compaction. Two factors suggest a tectonic origin, however: (1) the fault scarps trend diagonally from range front to valley axis (plate 1), cross-cutting sedimentologic facies have boundaries which should control compaction, and (2) the scarp zone coincides with the flank of a deep gravity low, interpreted by Huntley (1977) to be a subsurface graben *within* the San Luis Valley.

Fault scarps of the SCFZ and VGFZ are sufficiently eroded that the abrupt scarp face has been replaced by a smooth vegetated scarp slope. Existing maximum scarp slope angles range from 3° to 34°. Post-fault degradation of scarps is inferred to have generally followed the five-step conceptual model of Wallace (1977) for scarp decline in unconsolidated materials (figure 44). All fault scarps of the VGFZ, and most scarps of the SCFZ, are now in Stage E (figure 44), with maximum scarp slope angles of 3°-30°. A few of the higher scarps of the SCFZ are in Stage D, and debris-flow processes occur on long scarp slopes at over 30°.

Trench exposures show that the average near-surface fault dip is 70°-85° valleyward. In addition, preserved parts of the lower

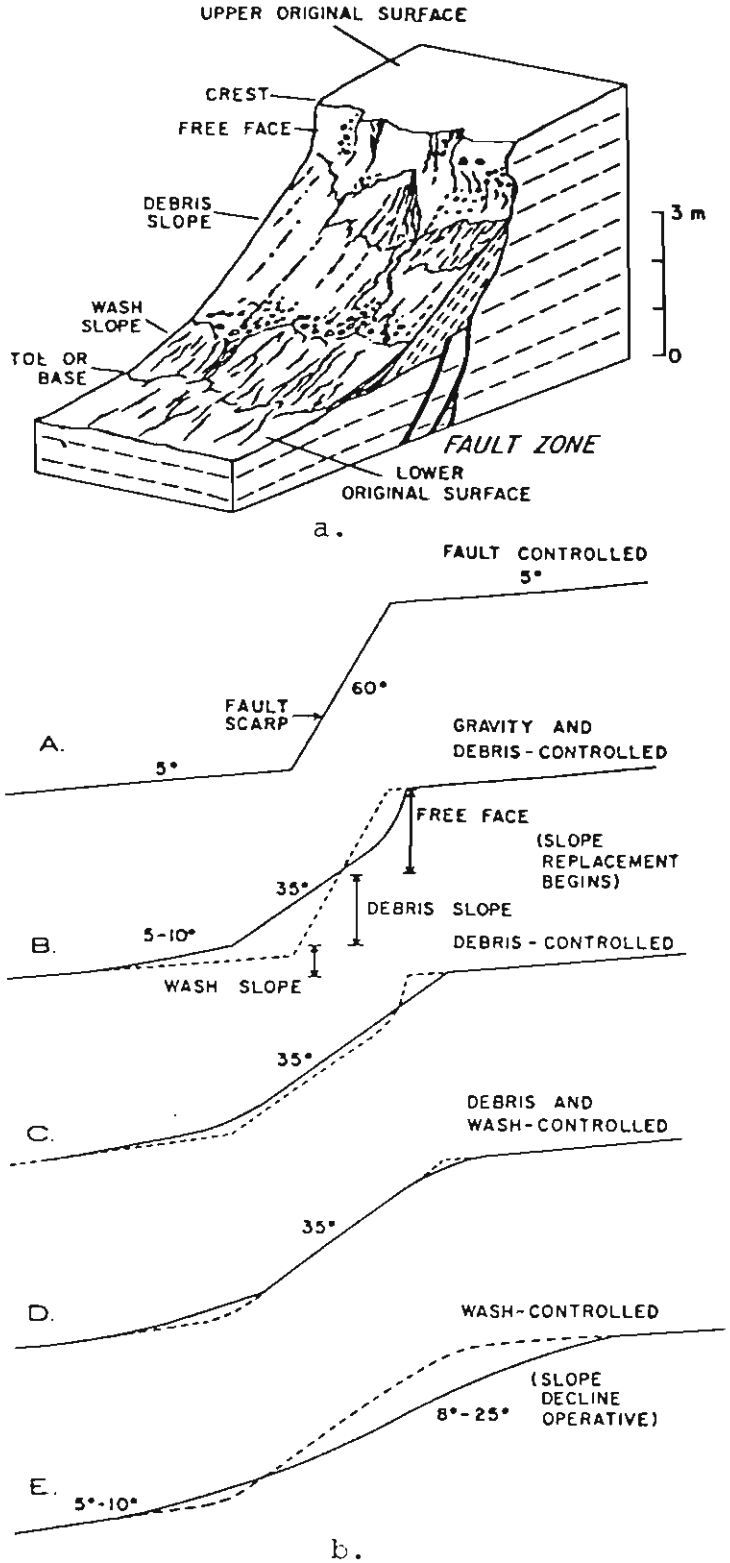

Figure 44.—Conceptual model of scarp morphology and degradation.
(a) Fault scarp morphologic terms for young scarps. (b) Conceptual model of fault scarp decline (from Wallace 1977, page 1269).

scarp face buried by colluvium dip from 55°-60° in gravels and from 20°-25° in sands. The scarp decline sequence implied by these values is as follows: (1) a fresh scarp is produced with a 70°-85° free face; (2) rapid gravity fall brings the free face to 55°-60° in gravels, 20°-25° in sands and colluvium fills fractures and small graben at scarp base; (3) gravity- and debris-stage decline (60°-35°) continue and colluvium builds into a wedge and buries lower 55°-60° scarp face; and (4) debris and wash decline of the scarp face continue to present angles (3° to 34°).

Subsurface exposures indicate the modern colluvial wedge usually contains a larger volume of sediment than appears to have been removed from the scarp crest. Further, the colluvium is rich in silt and fine sand, but the faulted alluvial gravels contain little sediment finer than coarse to medium sand. Where did the extra material come from? Most of the colluvium volumetrically in excess of crest removal is probably reworked loess and sand initially deposited as a thin veneer on alluvial fans. These materials were probably transported downslope by sheetwash and redeposited at the scarp-base slope break. Such eolian-augmented colluvial wedges grow with time. Sparse subsurface data from natural and artificial cuts show that the thickness of the wedge, as a fraction of scarp size, increases with the $\log_{10}$ of scarp age (figure 45). This is reasonable since, as the wedge grows in area, a given volume of deposition per time yields a smaller thickness increment.

Morphologic Effects of Recurrent Movement

Renewed displacement on a degraded fault scarp results in drastic modification of prevailing slope form and process. Rejuvenation creates: (1) an increased scarp height, (2) a new free face, (3) a sharp crest, (4) a renewal of gravity-fall erosion, and (5) a new colluvial wedge. Continued weathering modifies the fresh signs of scarp rejuvenation so that identification becomes increasingly difficult with time. Wallace (1977) lists five criteria which characterize modified multi-event scarps: (1) breaks in scarp profile, (2) terraces and/or knick points in dissecting drainages, (3) scarp heights exceeding the maximum recorded for single events, (4) complex erosion-sedimentation records, and (5) greater displacements of older than of younger deposits.

Not all criteria are applicable in the study area. Criterion (2) was not observed. Criterion (4) requires subsurface exposures, which are rare. Criterion (3) suggests that scarps larger than the recorded maxima (10.7 m; Richter 1958) result from multiple events, but it does not necessarily follow that scarps smaller than the maximum result from only one event. The next section discusses the utility of Criterion (5) for tectonic reconstruction. However, some scarps are restricted to a unit of single age. Where this occurs, the only viable criterion deals with details of scarp morphology (Criterion (1)).

A conceptual analysis of scarp rejuvenation following Wallace (1977), (figure 44) is shown in figure 46. The sharp break at the top of the free face (c′) constitutes a new scarp crest point. With continued erosion, the crest point migrates upslope; migration rate is probably controlled by the steepness of the prerejuvenation scarp profile. After sufficient scarp modification, c′ may approach and merge with c (after Stage E + D, figure 46). Field data from the SCFZ at Major Creek (described later) indicate that merger of crest points can occur within about 7700 years, in sandy sediments. A small percentage of scarp profiles on the SCFZ do show multiple profile breaks on the upper scarp face. The weakness of such breaks, and their proximity to one another, suggest that: (1) the latest displacement occurred at least 7000 years ago and (2) with continued weathering the two breaks will merge, and no evidence will remain of scarp rejuvenation.

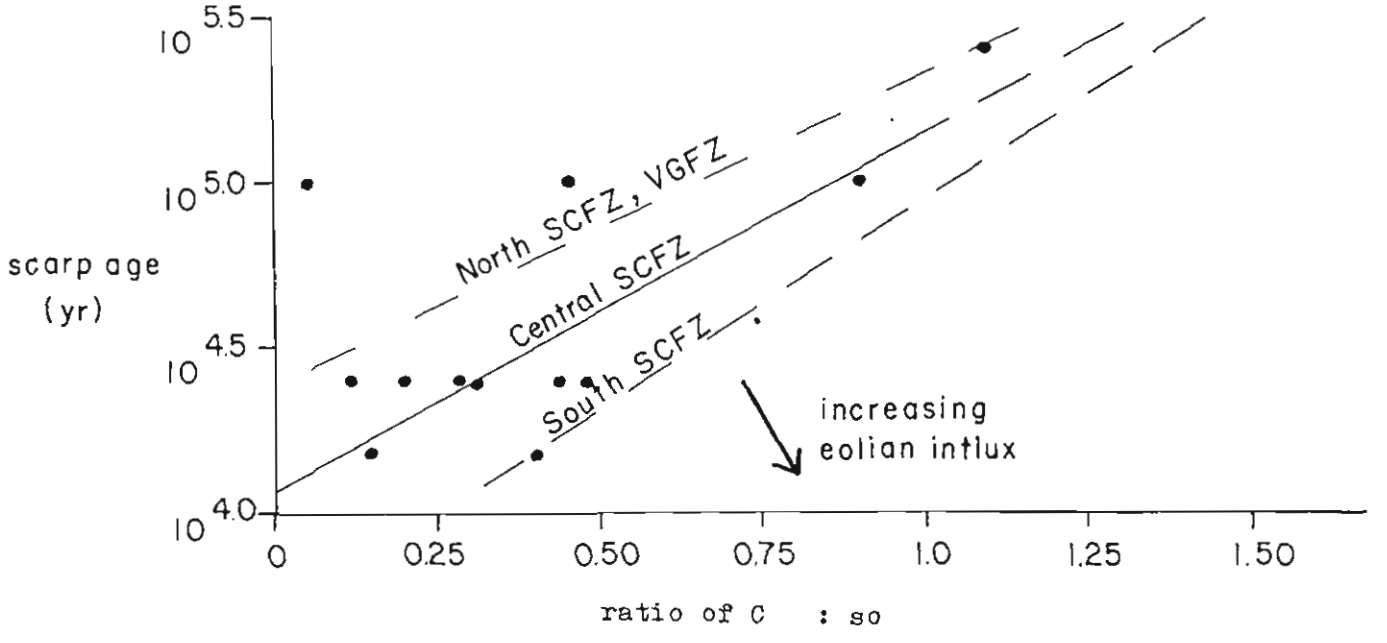

Figure 45.—Effect of time and eolian influx rates on scarp-base colluvium.

Geomorphic Relation to Quaternary Surfaces

When fault scarps interact with multilevel Quaternary surfaces, the resulting geometry yields important clues as to history of faulting. In the San Luis Valley, Quaternary surfaces can have two possible age-geometric relations: (1) younger deposits incised into older ones near fanheads, where erosion temporarily exceeds deposition, and (2) younger deposits at grade with, or overlapping, older deposits near the valley axis, where deposition exceeds or equals erosion. Single and multiple fault events offsetting the two possible geometries result in four possible fault scarp-alluvial scarp relations, summarized in figures 47 and 48.

Along the SCFZ, typical scarp geometry resembles figure 48. Multiple fault events (as many as 20) have repeatedly offset inset sequences of up to five terraces. On the VGFZ, all four possible geometries are represented as scarps traverse from the range front to the valley center. Change of scarp heights between successive surfaces is used as the prime tool in neotectonic reconstruction, where subsurface data are unavailable.

VILLA GROVE FAULT ZONE

Location and Tectonic Setting

The VGFZ is a 10-km long by 0.4 to 1.2-km wide, northwest-trending zone of about 40 discontinuous, parallel fault scarps which traverses the northern San Luis Valley from near Valley View Hot Springs to Villa Grove (figure 49). With minor exceptions, all scarps face southwest toward the valley center. Both seismic reflection surveys (Stoughton 1977) and gravity data (Huntley 1977, figure 34b, c) indicate surface scarps are coincident with the northeast edge of a deep gravity low in the valley, inferred to represent a buried graben.

Style of Deformation

Individual scarps in the VGFZ vary from 0.1 to 2.6 km in length. Trend of scarps roughly parallels the trend of the whole fault zone, with no clear expression of an en echelon pattern (figure 50). However, there is circumstantial evidence for hinge-type normal movement on the fault zone as a whole: (1) scarp heights in alluvium increase steadily from northwest (0.4-1.0 m) to southeast (14.0 m), and (2) depth to basement inferred by gravity data increases steadily from northwest to southeast.

Small antithetic (northeast-facing) scarps exist in two settings. In the first, low scarps define a narrow graben at the western margin of the fault swarm (scarps Q and M, figure 50). The surface graben is approximately centered on the axis of a large gravity low, implying a genetic association with deep graben formation. In the second setting, small oblique-trending scarps cut upthrown blocks into horsts (scarps K and G, figure 50). Antithetic scarp height increases toward the intersection with the main scarp, and then is abruptly truncated. Such structures are interpreted as a response to local ground extension, rather than to deep-seated antithetic displacement. Classic ramp structures serve to transfer displacement between rare en echelon scarps (figure 51).

Scarp Morphology

Fault scarps of the VGFZ are relatively small and subdued compared to range-front scarps. Scarp heights range from 0.2 m to 14.0 m, maximum scarp slope angles from 3°-23° (figure 52). Typical scarp morphology consists of five parts: (1) upper fan surface, (2) stripped fan surface near the scarp crest, (3) scarp face, (4) wash apron (surface expression of the colluvial wedge), and (5) lower fan surface (figure 53). Profiles are consistently asymmetric, in that the wash apron is usually much wider than the stripped fan surface. Much wash apron material is probably derived from reworked eolian sand, as previously discussed.

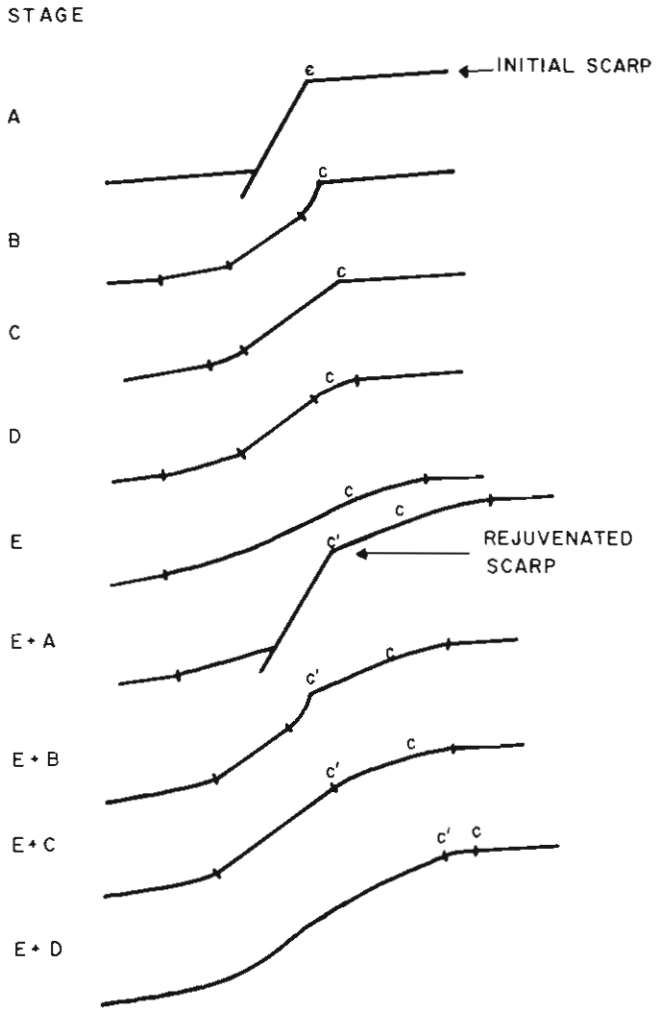

Figure 46.—Conceptual model for degradation of a rejuvenated fault scarp, based on the model of Wallace (1977, figure 2).

Modification of fault scarps increases with age. A plot of maximum scarp slope angle as a function of $\log_{10}$ of scarp height (h_2) shows that scarps offsetting older surfaces are progressively more gentle for similar heights (figure 54). Both separation of and slope of regression lines for dated scarps differ from those derived by earlier workers (e.g., Bucknam and Anderson 1979, page 11) for single-event scarps of a similar age range in Utah. Computer simulation of fault scarp decline using a diffusion-type equation (e.g., Nash 1980) shows that multiple-event scarps should have lower scarp angles than single-event scarps for similar heights and age of last faulting (Colman, McCalpin, and Ostenaa 1981). The more intervals of uplift (and erosion) that

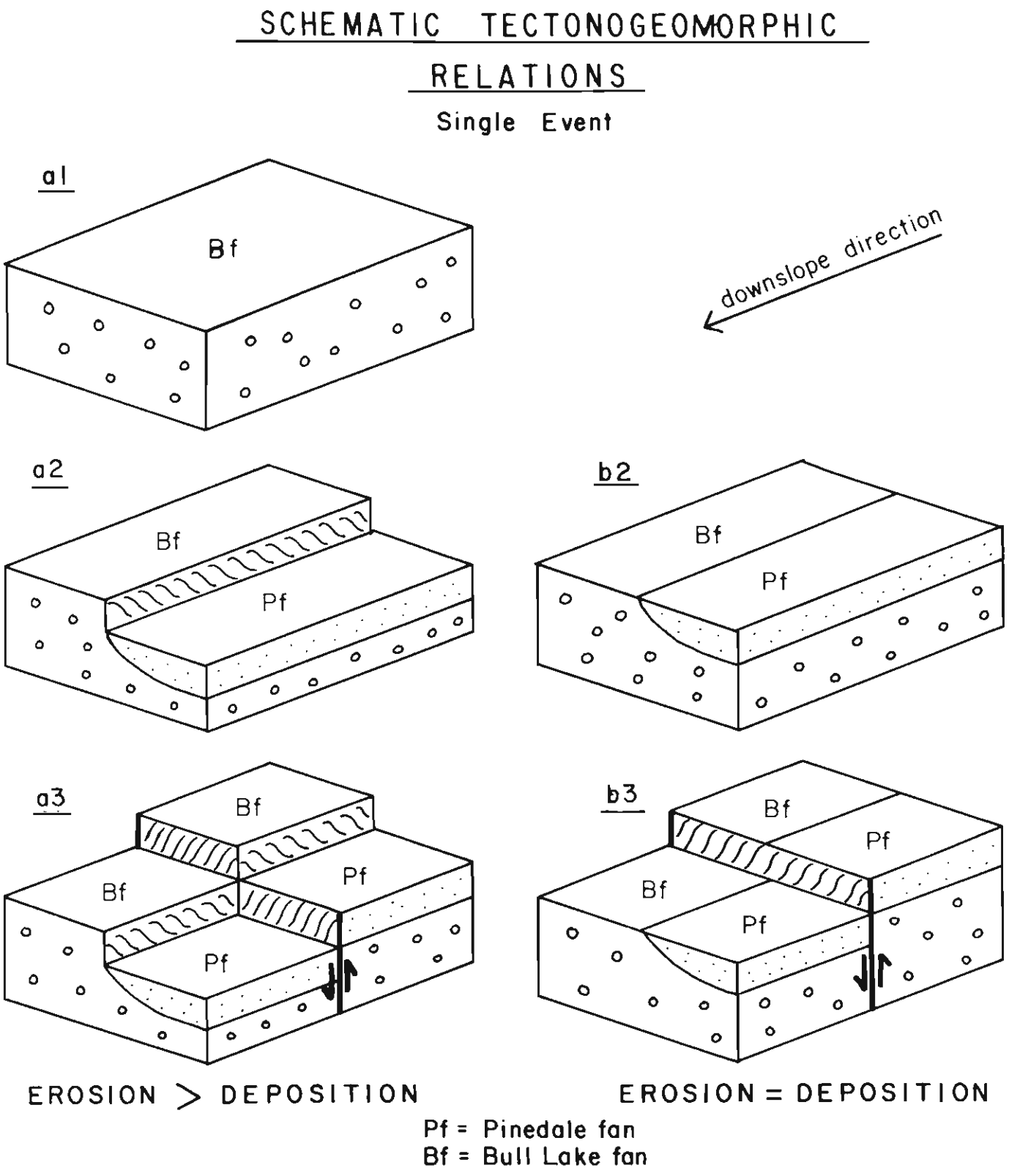

Figure 47.—Geometry of a hypothetical single-event fault scarp offsetting an alluvial terrace sequence.

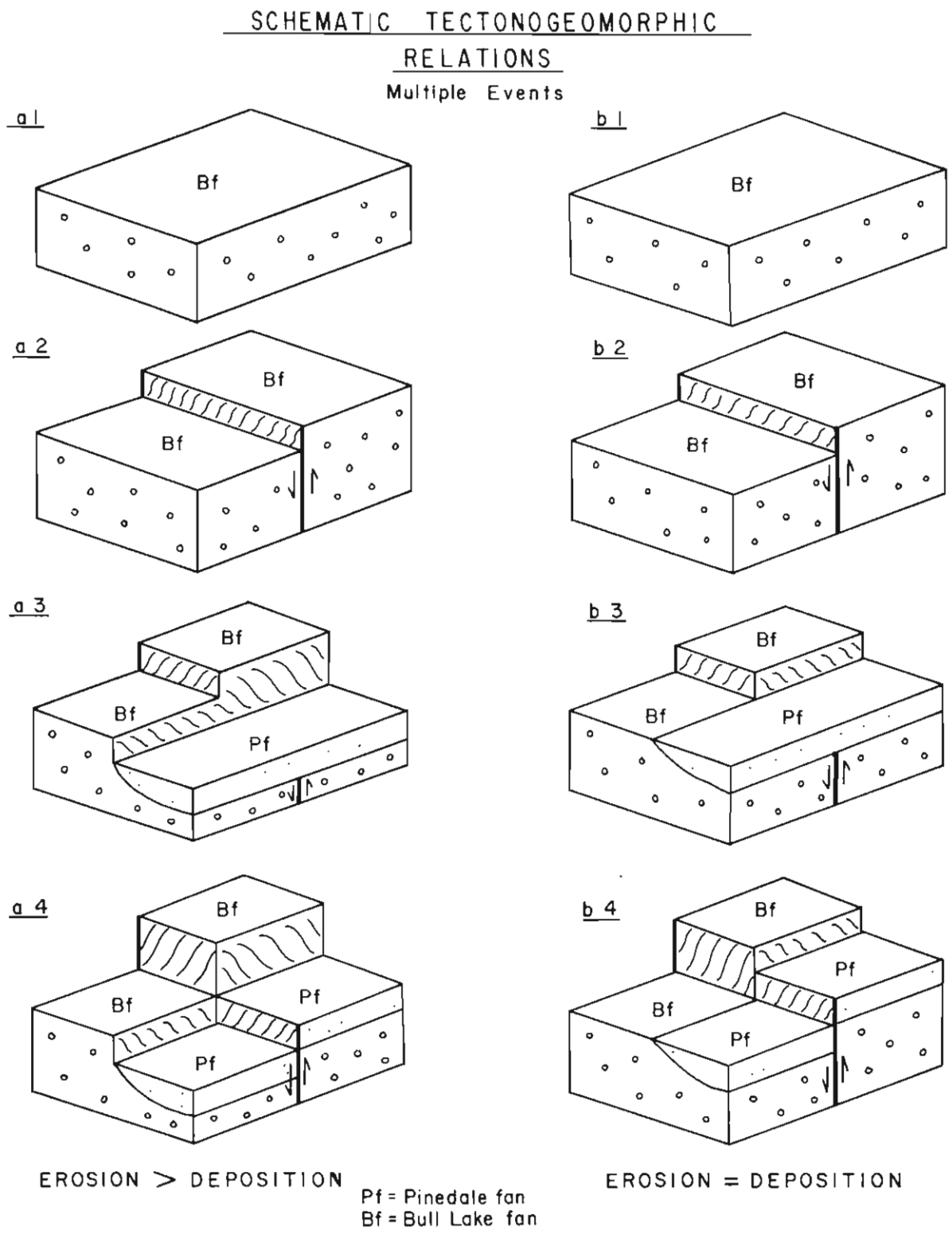

Figure 48.—Geometry of a hypothetical multiple-event fault scarp offsetting an alluvial terrace sequence.

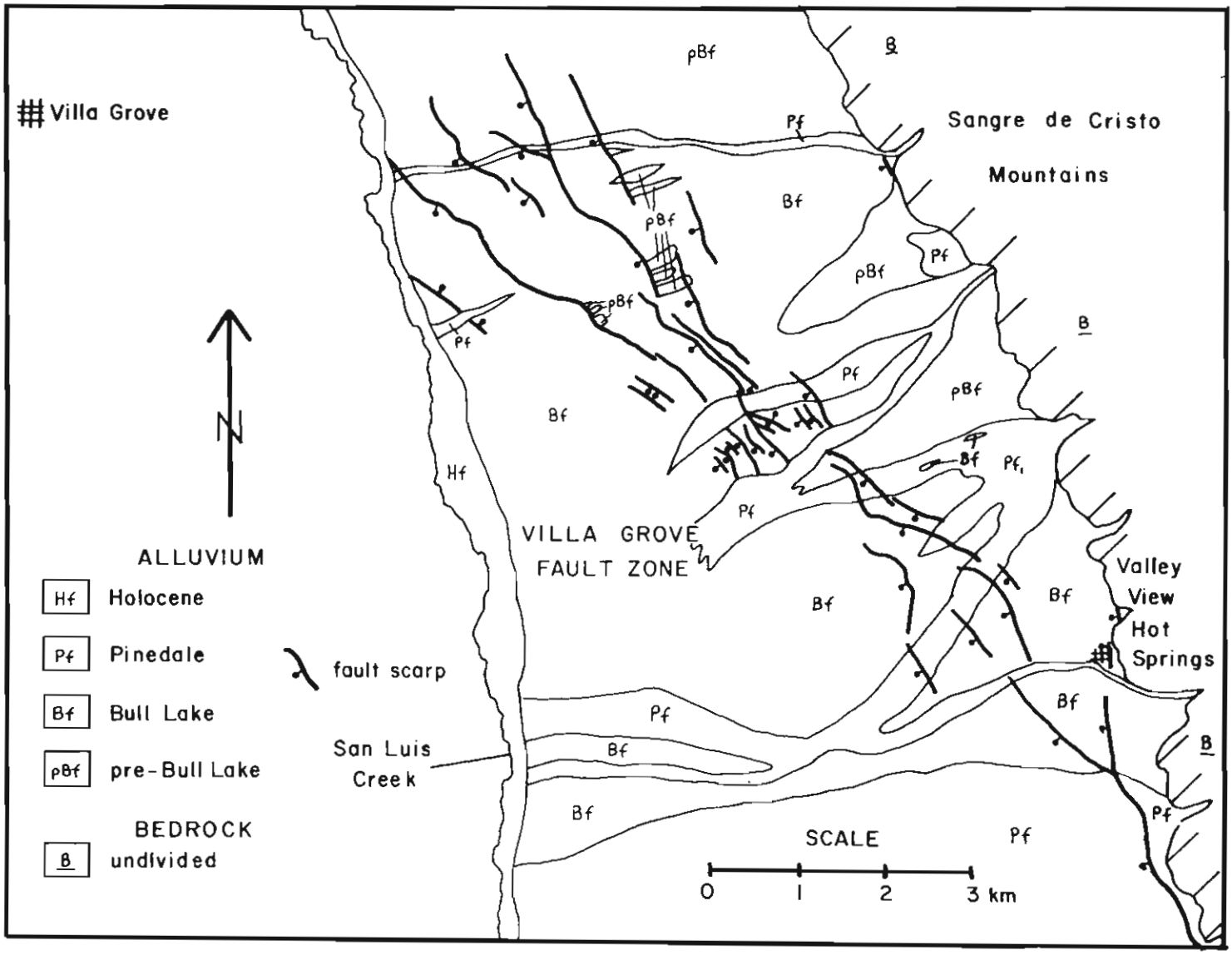

Figure 49.—Generalized geologic map of the VGFZ area, northern San Luis Valley.

have formed a scarp of a certain height, the lower its maximum scarp angle will be, assuming a similar age of latest faulting. Regression lines in figure 55 suggest that: (1) the latest fault event, which offset Pinedale deposits, occurred less than about 10,000 years ago by comparison to Utah single-event scarp data, and (2) scarps offsetting pre-Pinedale deposits were rejuvenated during the latest event, and are therefore steeper than assumed single-event scarps offsetting deposits of similar age in Utah. Both of the above conclusions are supported by geometric relations of scarps with alluvial terrace sequences, described in a subsequent section.

Field observations suggest that some of the scatter in figure 54 is due to the effect of alluvial textures on the rate of scarp decline. Consequently, two clast size parameters were measured on the scarp face of each profile: maximum clast diameter and modal clast diameter (i.e., most commonly occurring diameter). To test for systematic effects of clast size on the maximum angle-scarp height relation, the angle deviation of each data point from the least-squares regression line was compared to both maximum and modal diameters. As expected, scarps composed of larger-than-average clasts had steeper angles than did finer-grained scarps of the same height and age. However, the correlation of angle deviation with clast size is statistically quite variable (table 14). Better correlation is obtained with modal than with maximum diameter, and with younger scarps than with older scarps. A typical clast size-deviation plot is shown in figure 55 for scarps cutting Bull Lake deposits. The trend of the regression line suggests that an increase in modal diameter of ~6 cm will

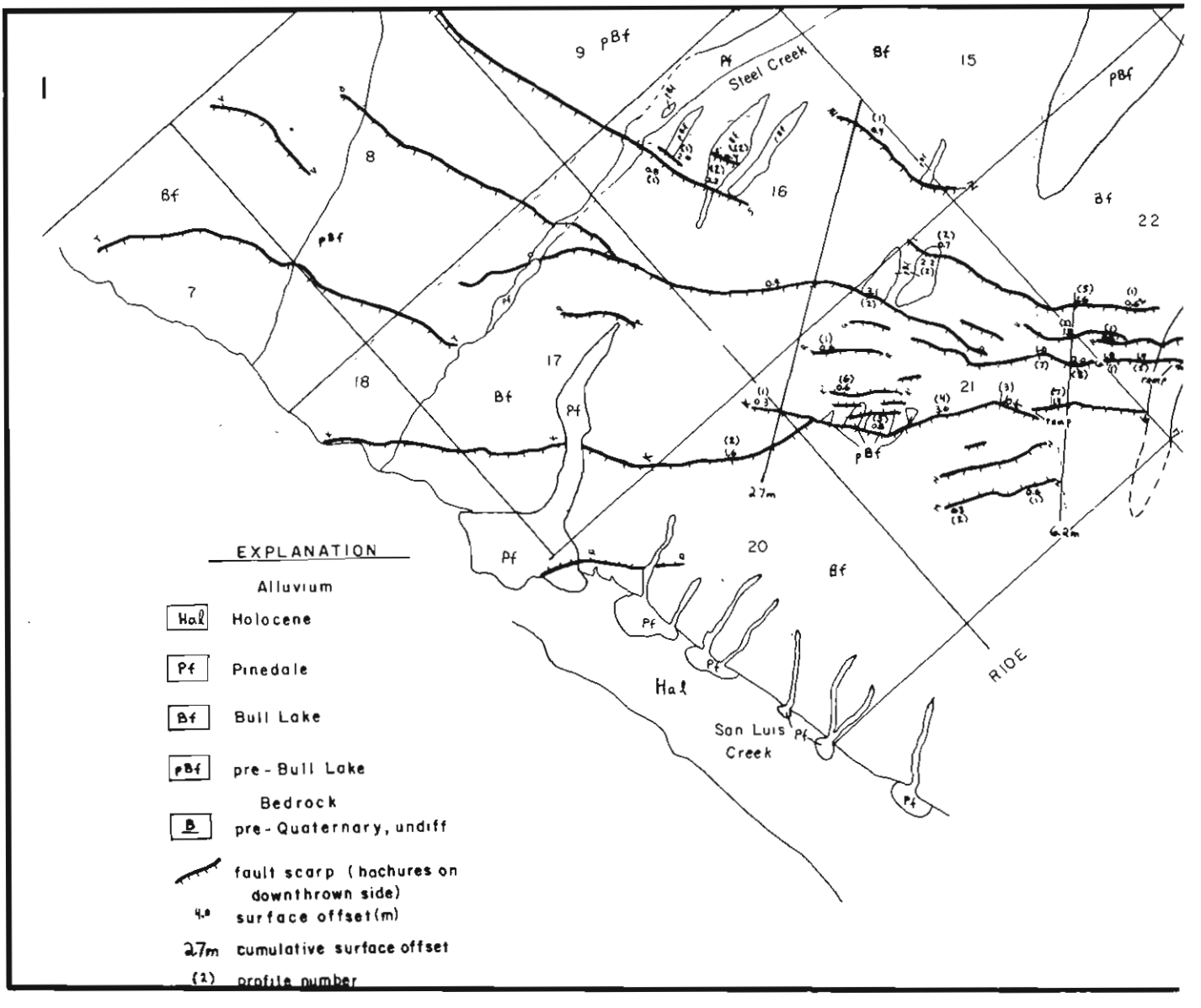

Figure 50.—Detailed scarp map of the VGFZ.

yield a 1° increase in maximum scarp slope angle, other factors (age, height) being constant.

Age differences are also noted in crest width and retreat of the scarp crest, as defined in this report (figure 37). The absolute values of both parameters are found to increase with age (table 15). However, since older, multi-event scarps are usually higher features than younger scarps, the absolute increase in crest width and retreat distance could be explained in terms of size alone. By dividing the absolute values by scarp surface offset we get a measure of the relative magnitude of crest retreat and width compared to overall scarp geometry. Resulting ratios of crest width/surface offset and retreat of crest/surface offset also increase with age (table 15). This can be interpreted as the crest zone involving a larger proportion of the scarp profile as modification progresses. Results in table 15 confirm the relative-age usefulness of the explicit definitions for crest width and retreat shown in figure 37.

Scarp Interaction with Geologic Units

Figure 50 shows that five categories of scarps exist in the VGFZ:

(1) Scarps that offset pre-Bull Lake fans only, and are truncated by Bull Lake surfaces (S').

(2) Scarps that front pre-Bull Lake fan remnants and continue across Bull Lake surfaces (K, L, O, S).

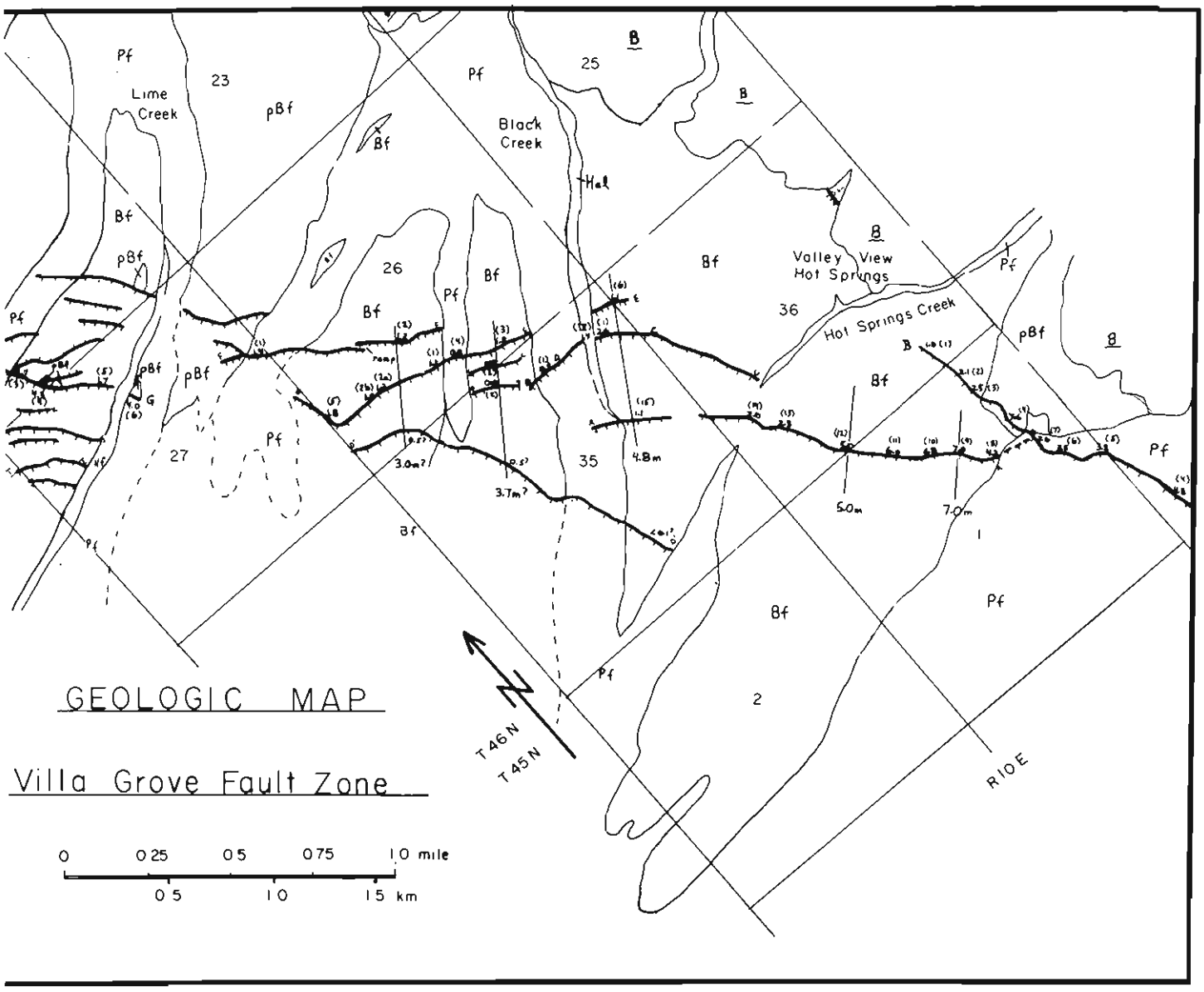

(3) Scarps that traverse only Bull Lake deposits, hence movement can be classified only as post-Bull Lake (K',M,N,P,Q,R,Z).

(4) Scarps that offset Bull Lake deposits but are truncated by Pinedale deposits (G, I, J).

(5) Scarps that offset both Bull Lake and Pinedale deposits but with much smaller scarp height across Pinedale deposits (A, B, C, D, E, F, H).

The existence of these five kinds of scarps implies recurrent movement on VGFZ faults from pre-Bull Lake to post-Pinedale time. A complex pattern emerges of displacement on different scarps within different time intervals. However, no apparent migration of displacement either along the trend or across the width of the VGFZ is noted.

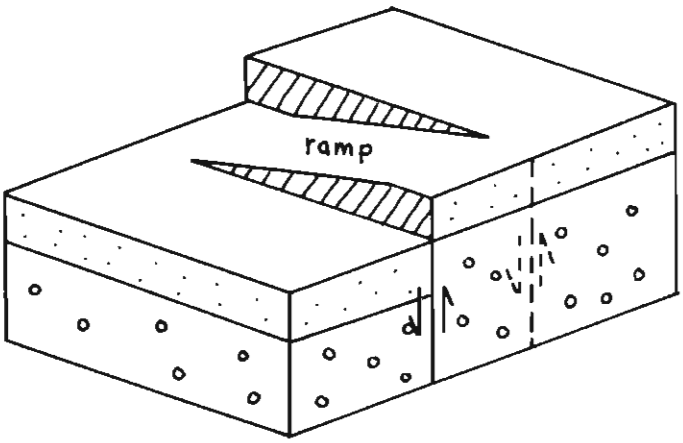

Figure 51.—Schematic block diagram of ramp structure as observed on the VGFZ.

Figure 52.—Low-sun-angle photograph looking east at the VGFZ.

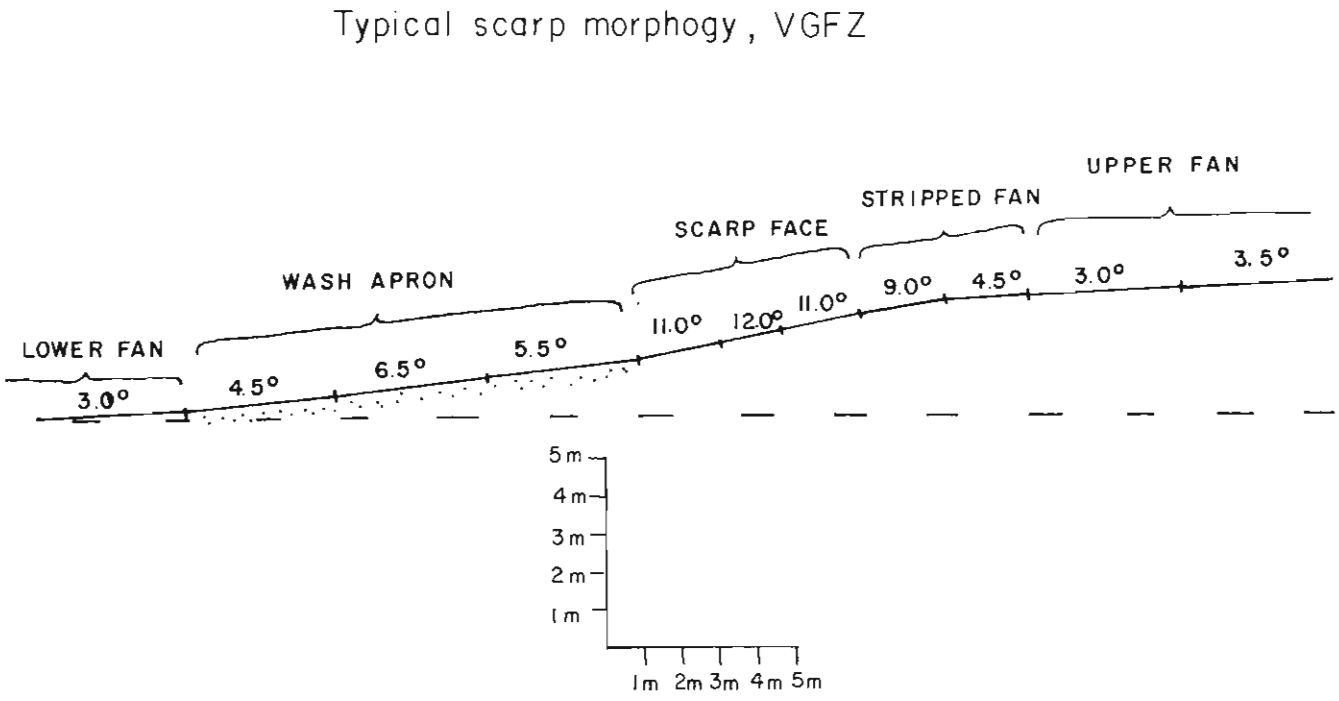

Figure 53.—Components of typical scarp morphology, VGFZ.

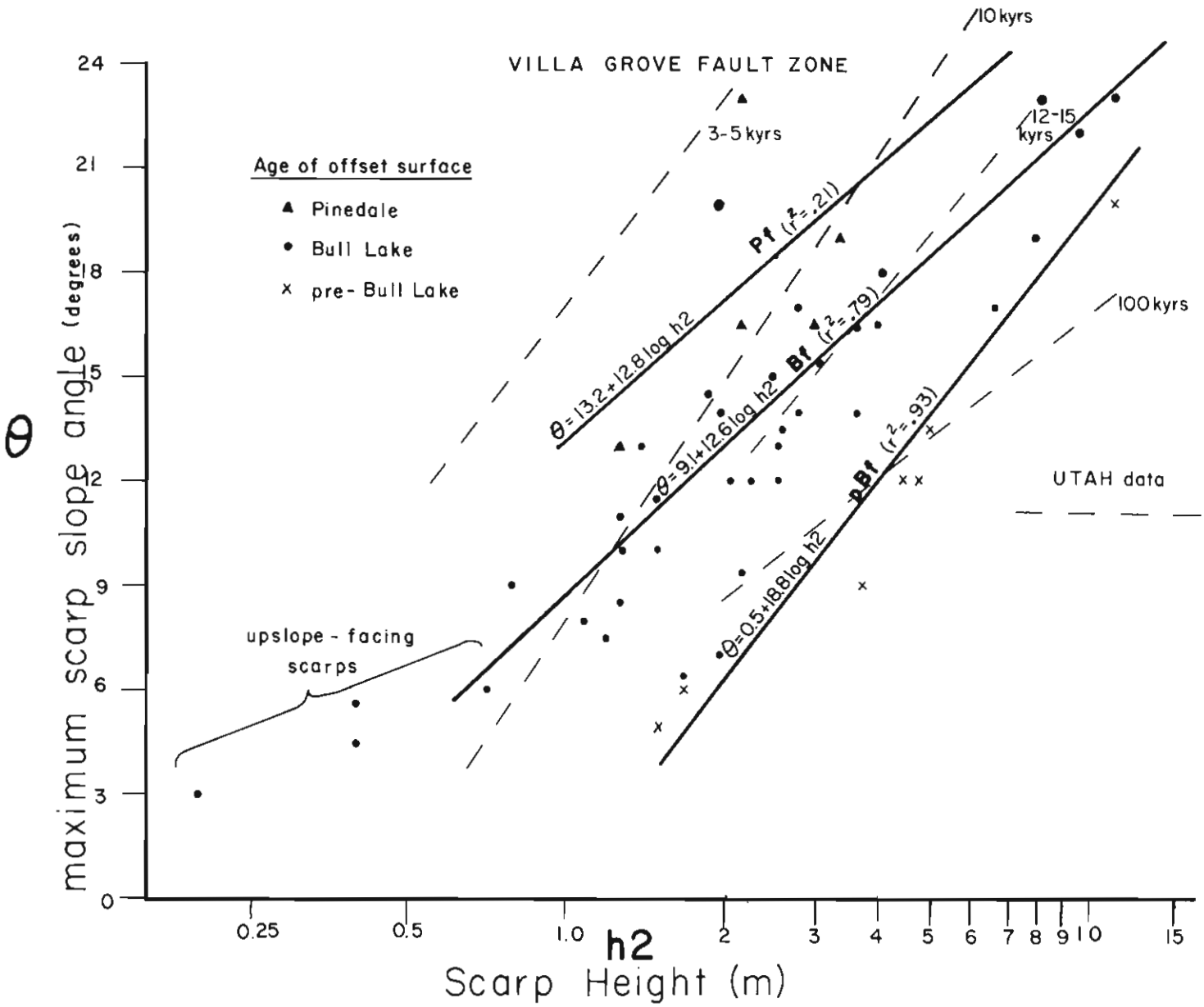

Figure 54.—Plot of maximum scarp slope angle as a function of $\log_{10}$ of scarp height, VGFZ.

Table 14.—Effect of maximum (M) and modal (m) clast diameter (in cm) for scarps on deviation (D) (in degrees) from the regression line of θ on log h_2[a]

Age of Offset Deposit	Maximum Diameter	VGFZ r^{2},[b]	Modal Diameter	r^{2},[b]	Maximum Diameter	SCFZ r^{2},[b]	Modal Diameter	r^{2},[b]
Holocene[c]								
Pinedale	D = −15.8 + 0.45M	0.75	D = 11.8 − 0.79m	0.24	D = −0.52 + 0.01M	0.02	D = −3.2 + 0.12m	0.25
Bull Lake	D = −.115 − 0.002M	0.01	D = −3.2 + 0.17m	0.22	D = −1.46 + 0.01M	0.12	D = −2.18 + 0.09m	0.09
pre-Bull Lake	D = −0.82 + 0.12M	0.04	D = −0.19 + 0.11m	0.01	[c]	[c]	[c]	[c]

[a] Relationship between deviation and clast diameter is calculated using a least-squares fit.
[b] r^2 = correlation coefficient squared.
[c] No data.

Displacement History: Spatial and Temporal Aspects

Fault displacements on all individual scarps have been summed across the VGFZ in seven locations (figure 50). Cumulative displacements represent the total offset across the fault zone since Bull Lake time. Spatial analysis of displacement along the length of the fault zone reveals generally increasing displacement toward the southeast. The data suggest a hinge-type movement on the VGFZ.

Temporal displacement trends were analyzed mainly by scarp geometric relationships with surfaces of different age. Youngest surfaces offset are those of mid-late Pinedale fans (about 13,000 years old). Single-event scarps have displacements of 0.8-1.4 m. Geometric relations on scarp C (profile C2, figure 50) indicate that a single pre-Pinedale fault event occurred, with displacement about 1.2 m followed by a post-Pinedale displacement of 1.4 m (figure 56). At several sites, an estimate of the number of fault events that formed multiple-event scarps can be made by dividing the calculated fault throw at successively higher profiles by the fault throw of a single-event scarp on the same fault strand (table 16). (Reduction of scarp height data to fault throw data has advantages discussed previously.) The implicit assumption that each fault event over a long period had the same throw as did the latest event is questionable, especially since evidence from trenches in the SCFZ shows throw varying through time from less than 1 m to about 2.3 m (discussed later). However, few alternatives to this assumption exist. If the latest event resulted in a throw near the long-term average, then the method should yield valid results. Scarps which offset both Bull Lake and pre-Bull Lake deposits suggest that while only one event occurred in post-Bull Lake time, two to three events occurred in the pre-Bull Lake interval (table 16).

To substantiate recurrent faulting, a trench was excavated across an inferred multiple-event pre-Bull Lake scarp (profile S2, figure 50). The trench log (figure 57) shows that the fault plane was not exposed. Instead, up to 3.0 m of colluvium was found in depositional contact with the buried lower scarp face. The colluvial wedge itself showed no evidence of multiple colluviation events; however, burrowing and disruption were extensive. Size of the total displacement (5 m) and the continuation of the scarp across Bull Lake deposits with smaller scarp heights indicate multiple events did occur.

Table 15.—Age trends in mean retreat (terms defined in Glossary) (R_c) and width of scarp crest (W_c), VGFZ

Fan Offset by Scarp	No. Averaged	Mean Surface Offset (m)	Mean Retreat (m)	Mean Width (m)	Retreat/ Offset Ratio	Width/ Offset Ratio
Pinedale fan	4	1.4	2.8	4.0	2.0	2.9
Bull Lake fan	34	1.6	5.6	6.1	3.5	3.8
pre-Bull Lake fan	6	2.6	11.6	10.0	4.5	4.0

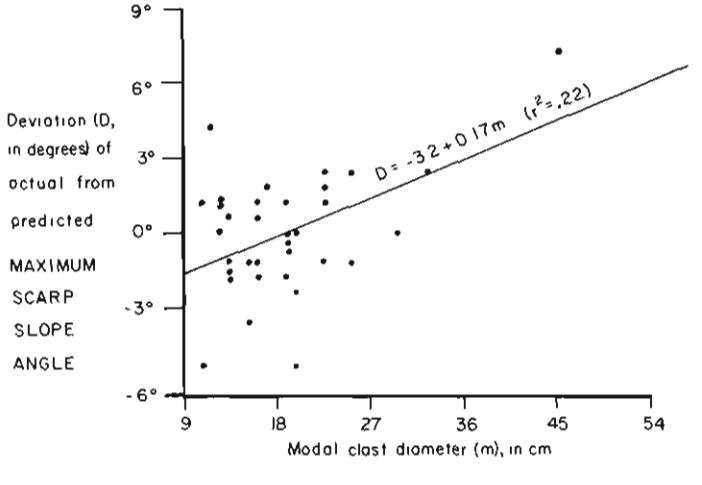

Figure 55.—Plot of the deviation of actual from predicted maximum scarp slope angle as a function of modal clast diameter on the scarp, post-Bull Lake scarps, VGFZ.

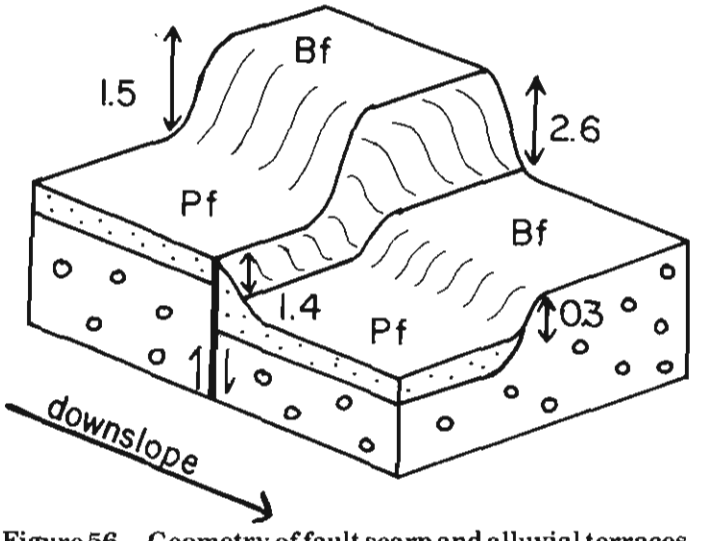

Figure 56.—Geometry of fault scarp and alluvial terraces at scarp profiles C1 and IV, VGFZ (location is on figure 50).

Timing of inferred multiple events can be roughly bracketed by pedologic evidence. On the upthrown block the buried B horizon predates, but the overlying K horizon postdates scarp production (figure 57). The B horizon is weaker than Bull Lake B horizons (i.e., developed over less than about 120,000 years), and K horizon is much better developed than in Bull Lake soils (perhaps twice as old). The evidence implies that faulting at the site may have begun approximately 300,000 to 250,000 years ago. The soil developed on the colluvial wedge has a weak textural B horizon, indicating it is roughly intermediate in development between Pinedale and Bull Lake soils. Thus, the colluvial wedge has probably been stable since about 60,000-80,000 years ago. In the time interval spanning roughly 300,000 to 60,000 years ago three or four displacements may have occurred, totalling about 5 m.

The inferred mid-late Pleistocene tectonic history for the VGFZ based on scarp heights, geometry, and trench exposures is summarized in figure 58. Frequency of events offsetting dated deposits suggests a recurrence interval on the order of 60,000 to 100,000 (?) years for earthquakes producing a measurable component of surface faulting.

Seismic Hazard

Magnitude of Quaternary earthquakes can be estimated from (1) size of fault displacement and (2) length of surface rupture. Fault displacements of 0.8-1.4 m calculated for single-event scarps on the VGFZ correspond to earthquakes of Richter magnitude (M_L) 6.6 to 7.0 (Bonilla and Buchanan 1970). The length of surface rupture due to any single event is uncertain, but post-Bull Lake scarps do traverse the entire 10 km length of the fault zone. A surface rupture length of 10 km corresponds to that produced by M_L 6.8 historic earthquakes (Mark and Bonilla 1977). Thus, both surface rupture and fault displacement data suggest that M_L 6.6 to 7.0 earthquakes are capable of occurring about every 60,000-100,000 years on VGFZ. If the latest earthquake, which occurred less than 13,000 years ago, represented a total strain release on the underlying faults, then the probability of a major surface-rupturing earthquake originating on the VGFZ in the near future seems low.

SANGRE DE CRISTO FAULT ZONE

Location and Tectonic Setting

The SCFZ separates the Northern Sangre de Cristo Mountains from the deep basin beneath the San Luis Valley (figure 59). Subsurface data indicate as much as 7015 m of normal-fault displacement on the fault zone since early to mid-Tertiary time (Huntley 1979). The SCFZ in the study area includes three distinct segments: (a) a 90-km long northwest-trending segment, (b) a 20-km long north-trending segment, and (c) a 10-km long segment which tends east-west at the south end of the Sierra Blanca (figure 59). Discontinuous fault scarps in alluvium, colluvium, and till at the range front indicate that normal displacement on the SCFZ has continued through Pleistocene and Holocene time. Analysis of scarps provides the main evidence for reconstructing Quaternary tectonism.

Style of Deformation

The SCFZ contains five different types of Quaternary fault scarps. Scarp types and lengths are: (1) scarps which cut across valley-mouth reentrants (245 m to 1100 m long), (2) scarps which parallel the range front, a few 10s to 100s of meters valleyward of the alluvium-bedrock contact (430 m to 2990 m long), (3) scarps which diverge from the range front and trend up to 1.2 km out onto the alluvial slope (365 m to 3170 m long), (4) scarps which parallel the range front as much as 0.8-1.6 km valleyward from the front (915 m to 1830 m long), and (5) transverse or oblique scarps connecting any of the types above (245 m to 730 m long).

It is not usually possible to trace scarps from one valley mouth to the next along the base of the intervening faceted spur. By contrast, historic fault breaks in the Basin and Range are com-

Table 16.—Sequence of faulting events deduced from scarps, VGFZ

Fan	Fault Throw		No. of Fault Events	Inferred Fault Events[a]	
	Scarp E	Scarp C			
Pinedale	0.8	1.4	1		Present
Bull Lake	1.8	2.6	2	X	Pinedale 2
					Pinedale 1
				X	Bull Lake
	Scarp S	Scarp G	Scarp O		
Bull Lake	0.8	1.7-2.7	0.4-1.0	1-2	Present
				X	
				X	
pre-Bull Lake	2.4	4.0-4.3	3.1	2-4	Bull Lake
				X	
				X	
				X?	pre-Bull Lake

[a] Position of X represents occurrence of fault event in time.

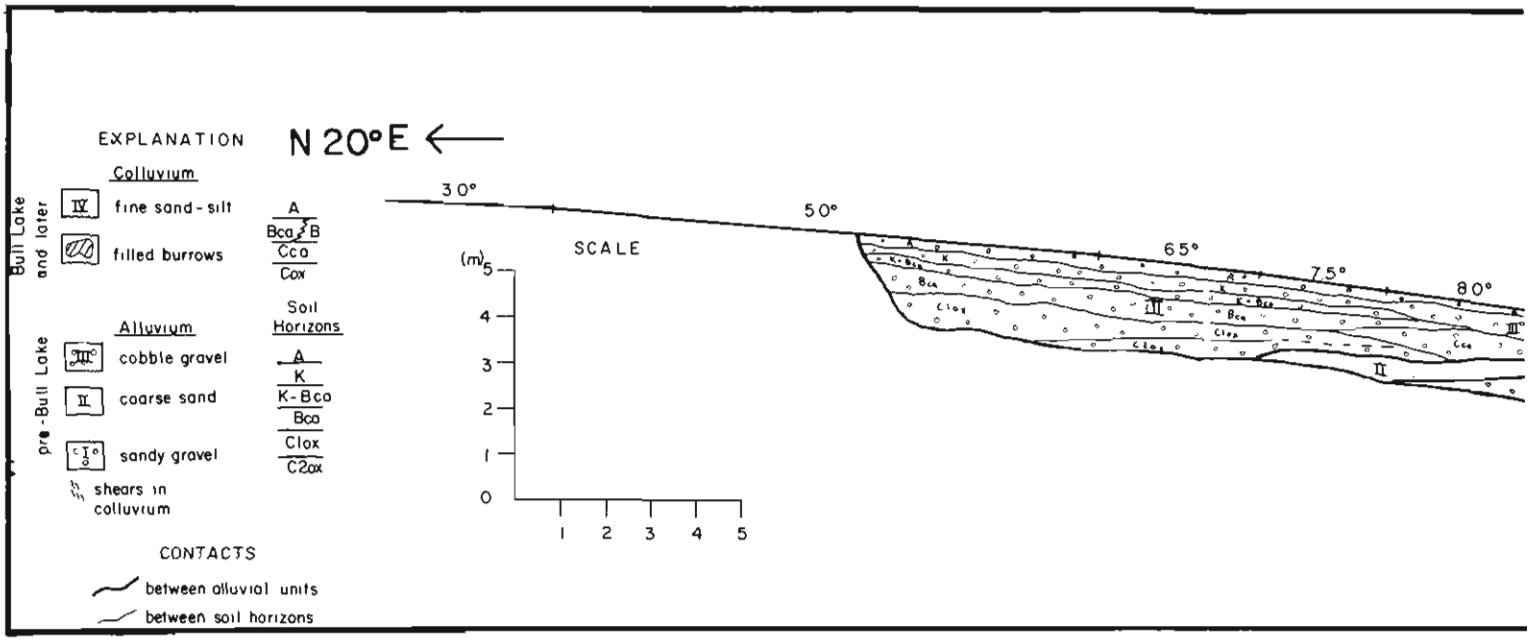

Figure 57.—Log of trench, profile S2, VGFZ.

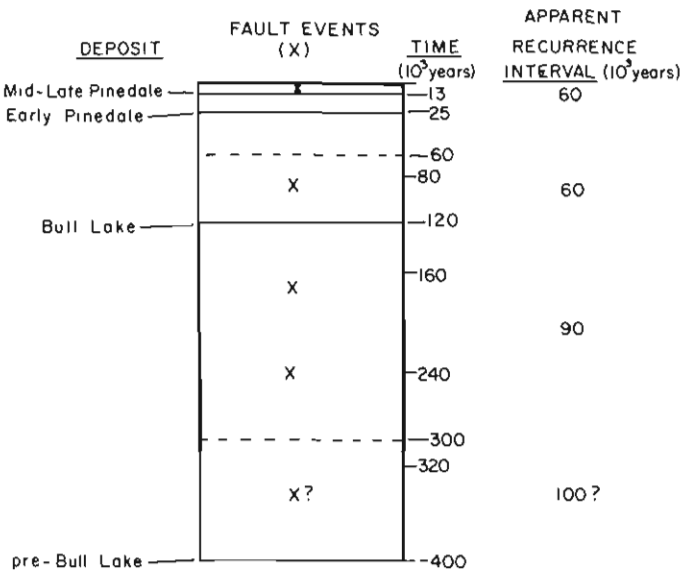

Figure 58.—Diagram of inferred tectonic history of the VGFZ in Quaternary time.

monly continuous across both valley mouths and the base of the intervening spurs (e.g., Page 1934). Well-defined scarps comparable in size to present valley-mouth scarps were almost certainly formed on the steep (20°-30°) colluvial slopes at the base of faceted spurs on the SCFZ. Two factors may have tended to eradicate the spur-base scarps much faster than the valley-mouth scarps: (1) greater erosion potential exists on the 20°-30° spur-base slopes than on the 5°-7° valley-mouth terraces, where scarps are preserved and (2) poorly sorted colluvium at the base is more erodible than coarse tightly packed outwash gravels in the valley mouths.

Scarp Morphology

Fault scarps of the SCFZ vary greatly in size, degree of modification, and geometry. Scarp heights range from 2 m in Holocene alluvium to 87 m in pre-Bull Lake deposits; maximum scarp slope angles range from 13° to 34°. Simple faulting and complex faulting involving surface rotation, graben formation, and step-faulting were all observed.

Relative-age differences between scarps are revealed in the plot of maximum scarp slope angle *versus* $\log_{10}$ of scarp height (figure 60). Scarps offsetting older deposits plot farther to the right on the diagram, signifying greater volume of erosion from the scarp. The position of data points from single- and double-event scarps offsetting Pinedale deposits of the SCFZ indicates that latest faulting occurred roughly between 5000 and 10,000 years ago, by comparison with similar dated scarps in Utah. The regression line is similar to that defined by post-Pinedale scarps

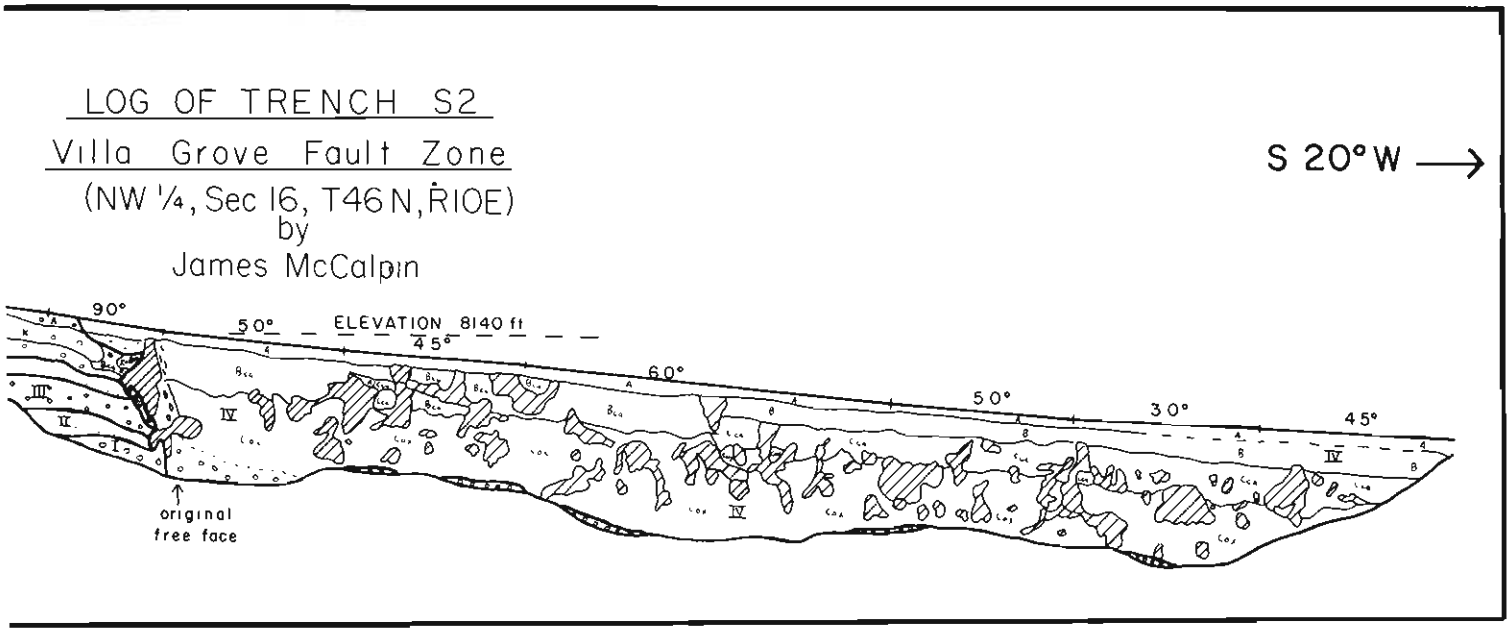

on the VGFZ, suggesting that the youngest scarps on the VGFZ and SCFZ may have resulted from the same fault event, or from events closely spaced in time. Multiple-event scarps in Bull Lake and pre-Bull Lake deposits are much steeper for a given height than are single-event scarps in comparable deposits in Utah, confirming the steepening influence of late rejuvenating event(s) on pre-existing scarps.

All three regression lines on figure 60 merge when maximum scarp angles exceed about 30° and debris processes occur on the scarp face. For multi-event scarps, the slope angle-scarp height relation apparently holds only for scarps which have reached the wash stage of development (Stage E, figure 44). If a gravity-or debris-controlled face exists on a rejuvenated scarp, the maximum angle on that face is not related to scarp height.

Scarps where debris processes are still active are distinct morphologically from wash-dominated scarps (figure 61). A broad, planar scarp face sloping from 27°-34° dominates the debris-controlled scarp. The face is inferred to be the direct result of slope regrading after renewed faulting and creation of a near-vertical free face (see figure 46, Stages E and A, E and B). The abundance of debris-controlled faces (maximum scarp slope angle greater than 30°) on larger scarps of the SCFZ implies that the transition from gravity to debris stage after rejuvenation may be rapid, but from debris to wash stage is much slower. As successive rejuvenation increases scarp height the area of the scarp face also increases, so that for each increment of slope decline a greater volume of material must be removed before wash processes become dominant. If rejuvenation occurs frequently enough, the scarp may never have time to progress beyond the debris-controlled stage.

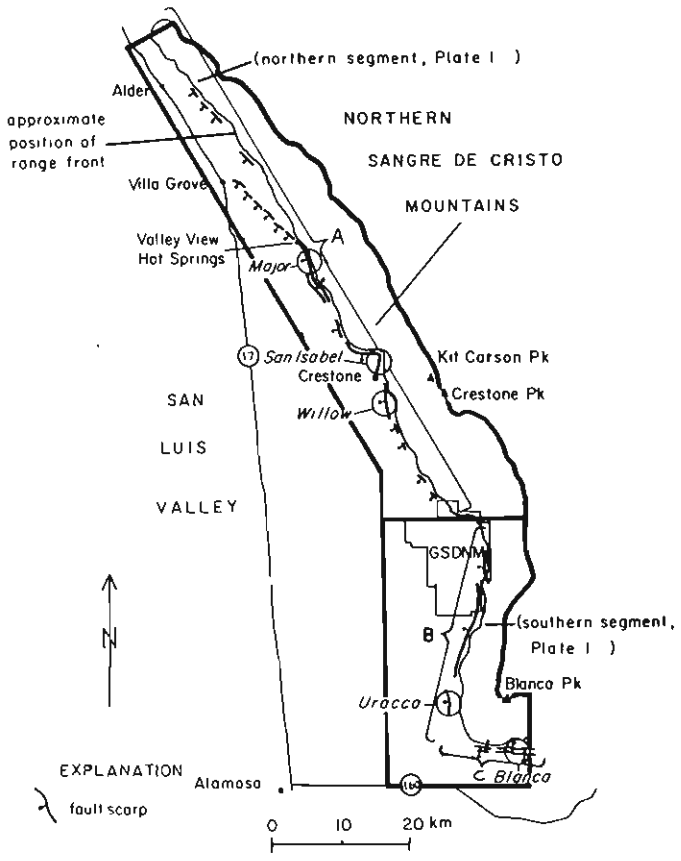

Figure 59.—Index map of the SCFZ.

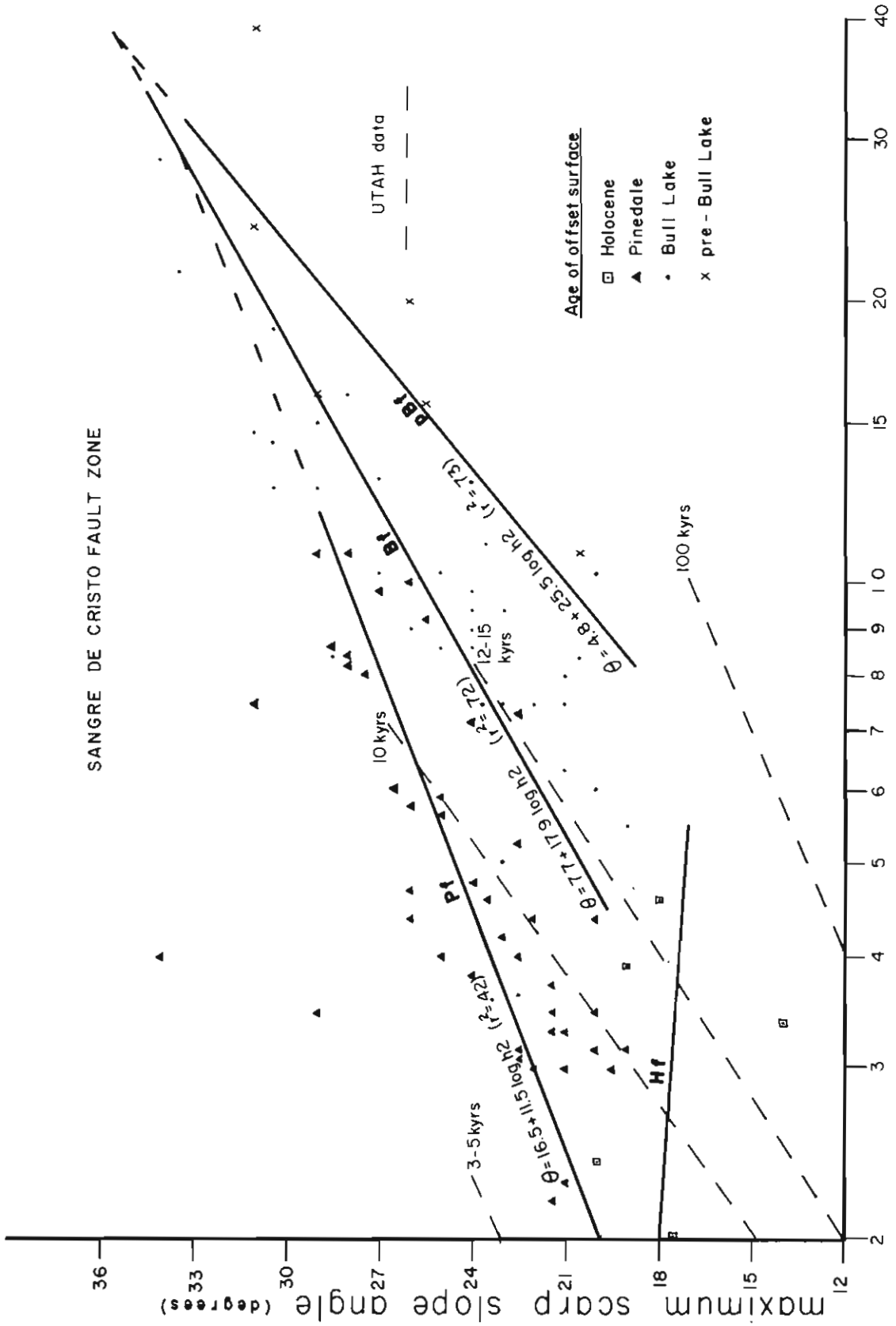

Figure 60.—Plot of maximum scarp slope angle as a function of $\log_{10}$ of scarp height, SCFZ.

The crest width and crest retreat of scarps increase, in both absolute and relative terms, with increasing scarp age (table 17). Some profiles display several crests suggestive of multiple events (figure 62). Both scarps in figure 62 have lesser offset in younger deposits along trend than the total offset at the profiled sites, indicating recurrent movement. Multiple crests can also be formed by boulders, roots, or other textural discontinuities on the scarp face—these should always be avoided during profiling.

Alluvial texture also exerts control on scarp morphology on the SCFZ. Scarps offsetting coarse gravels (modal diameter 50-60 cm) are steeper than scarps of the same age and height which offset finer alluvium (modal diameter 20-30 cm). A plot of angular deviation from the regression lines of figure 60, as a function of modal clast size, is shown for post-Pinedale scarps in figure 63. The trend of the data suggests that an increase of roughly 8.6 cm in modal clast diameter will result in a 1° increase in maximum scarp slope angle, all other scarp parameters remaining equal. However, the low regression coefficient ($r = 0.50$) suggests that other factors are also responsible for details of scarp morphology.

The majority of SCFZ scarps profiled (53 of 90) are simple scarps (figure 64a). However, complex scarps are common (37 of 90 profiles), perhaps because of relatively large displacements on the SCFZ. Graben structures are abundant (15 of 90 profiles; figure 64b), dominating the fault zone between Cotton and Wild Cherry Creeks, and between Tobin and Blanca Creeks (figure 2, plate 1). Traces of rotated downthrown blocks are also fairly common (13 of 90 profiles; figure 64c). More complex scarps may have existed but are now buried under large colluvial wedges. Longitudinal step faults also occur (figure 64d).

Several complications can occur in a small area. At Pole Creek (figure 2) two scarps obliquely intersect and continue past the intersection. Each scarp retains its offset and morphologic properties through the intersection (figure 65). The larger north-trending scarp plots older than the smaller northwest-trending scarp on the scarp height-slope angle diagram (figure 60). Furthermore, displacement on the north-trending scarp decreases to the north, but on the cross-cutting scarp displacement remains constant. A tentative interpretation suggests two movements on the north-trending fault, followed by one movement on the northwest-trending scarp. All events post-date the stabilization of the early Pinedale alluvial fan (roughly 25,000 years BP).

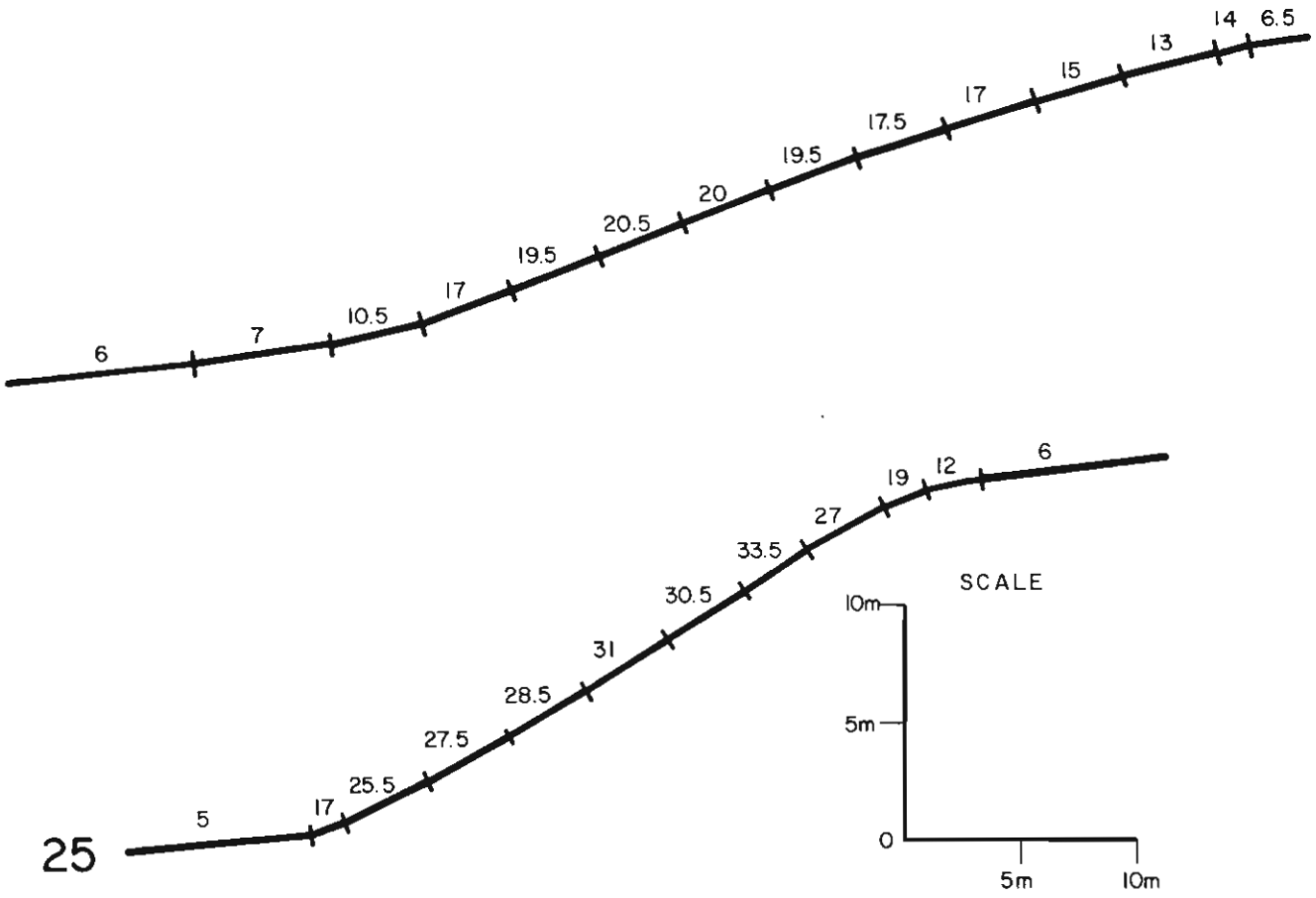

Figure 61.—Comparison of the morphology of wash-dominated versus debris-dominated fault scarps, SCFZ. (a) Wash-dominated scarp. (b) Debris-dominated scarp. Segment slopes are in degrees.

Table 17.—Age trends in retreat and width of scarp crest, SCFZ (terms defined in Glossary)

Surface Offset by Scarp	No. of Profiles Averaged	Mean Surface Offset (so) (m)	Mean Retreat (R_c) (m)	R_c/so	Mean Width (W_c) (m)	W_c/so
Holocene fan	5	2.0	3.6[a]	1.8[a]	4.6[a]	2.3[a]
post-Pinedale fan	5	2.2	4.5	2.1	5.6	2.5
Pinedale fan	36	3.5	4.0	1.1	5.2	1.5
post-Bull Lake fan	2	10.0	8.1	.8	7.0	.7
Bull Lake fan	33	5.2	8.3	1.6	9.8	1.9
pre-Bull Lake fan	6	10.5	23.9	2.3	13.7[b]	1.3[b]

[a] Anomalously large values due to easily erodible nature of fine-grained alluvium.
[b] Anomalously small values due to severe dissection of upthrown block into ridges.

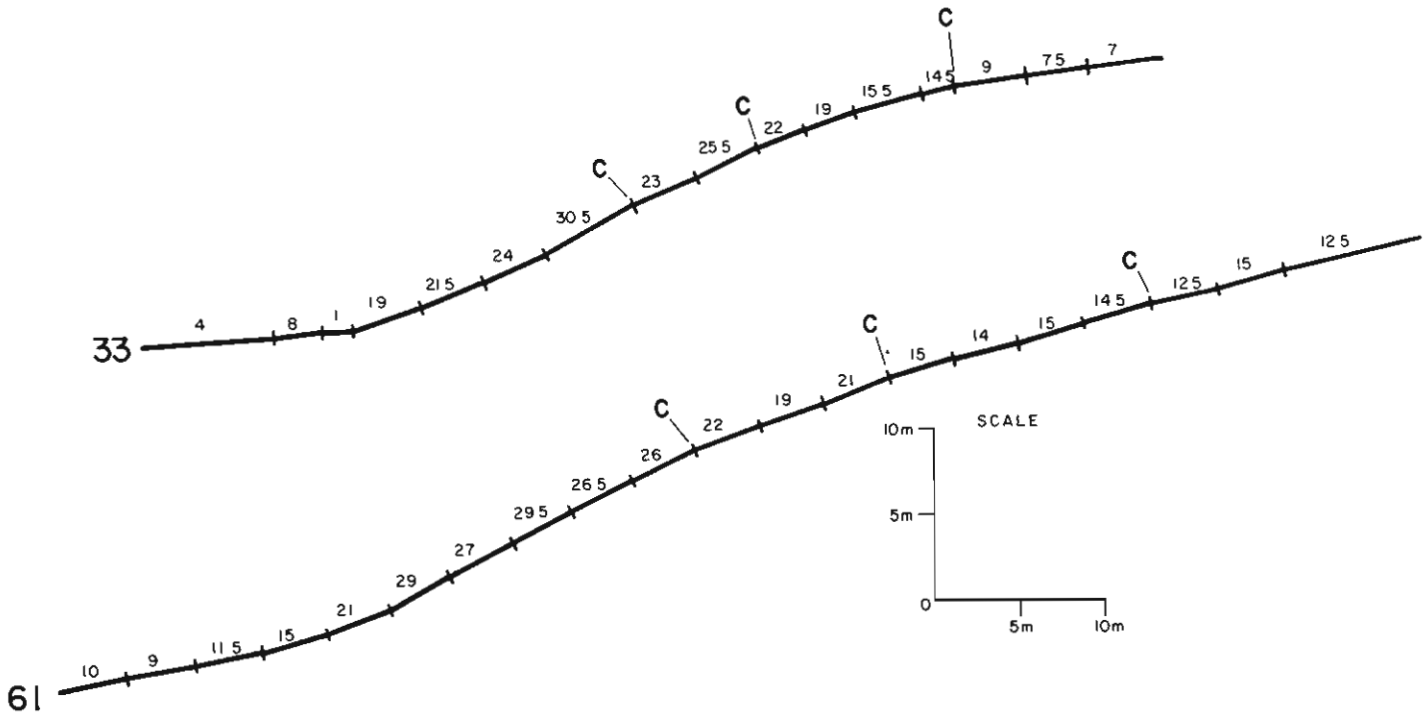

Figure 62.—Fault scarps displaying multiple crests on the SCFZ.

Morphology of Range Front Spurs

The steep range front rising above the SCFZ exhibits well-developed faceted spurs on ridge lines, features long identified with recently active block-faulted mountains (Wallace 1978). Between narrow faceted ridges elongate drainage basins extend perpendicular to the range crest. The faceted ridge ends commonly exhibit multiple benches and steps. Multiple facets are well preserved in the area between Major and San Isabel Creeks, where four dominant levels of facets are observed (figure 66a). A typical facet profile at the Sangre de Cristo Range front, showing steps and benches, is shown in figure 66b. Steep steps sloping valleyward at 20° to 34° are separated by lower-angled ridge crests with 7° to 15° slopes. The main facets have crests at 3277 m to 3338 m elevation, and facet faces are severely gullied. Two lower facet sets (2881-2971 m, 2805-2830 m) are inset within the larger facet, and are correspondingly less gullied and eroded. The lowest facet set (2658-2683 m) includes numerous very fresh, ungullied facets which rise directly above fault scarps in Quaternary alluvium and colluvium.

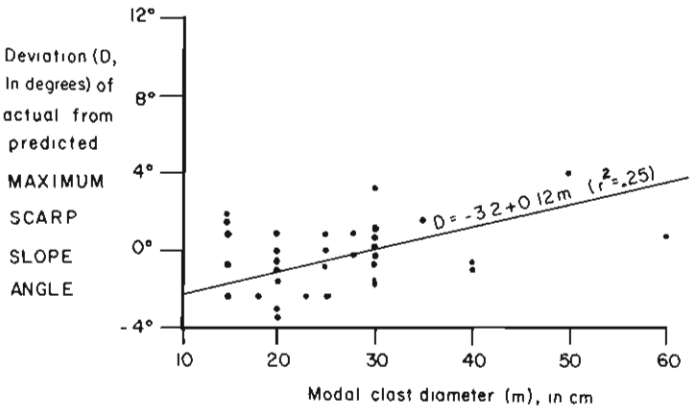

Figure 63.—Plot of the deviation of actual from predicted maximum scarp slope angles as a function of modal clast diameter on the scarp, post-Pinedale scarps, SCFZ.

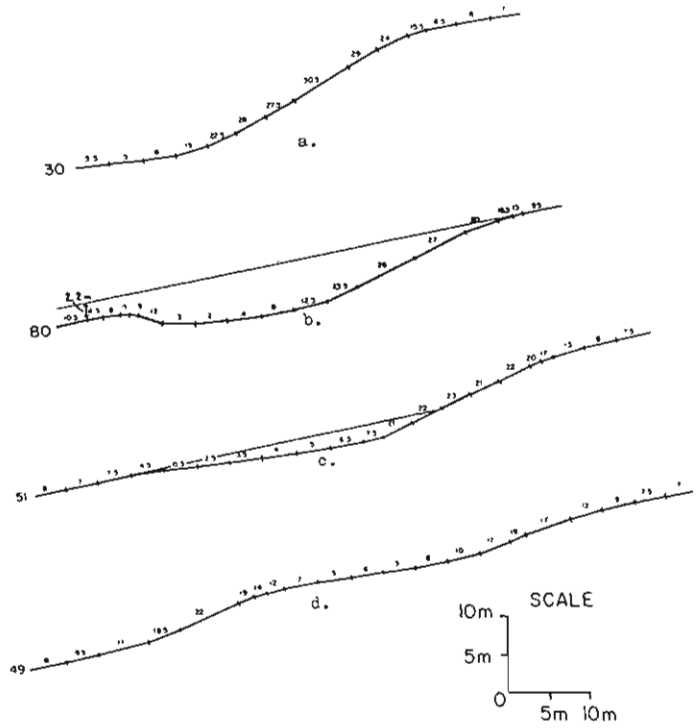

Figure 64.—Scarp morphologic types of the SCFZ.
(a) Simple scarp. (b) Scarp with graben. (c) Scarp with lower surface rotation. (d) Scarp with step-faulting. Segment slopes are in degrees.

Multiple facets elsewhere in the Basin and Range province have been interpreted as resulting from episodes of mountain block uplift (forming steps) alternating with episodes of no uplift (forming benches by slope retreat and pediment formation) (Hamblin and Best 1978; Wallace 1978). The geometry of facets at the Sangre de Cristo Range front indicates that three episodes of uplift have occurred since the beginning of facet formation. Scarps in Quaternary deposits at the base of the lowest facet set indicate that the latest uplift episode has continued through late Quaternary time, and is probably continuing today.

Interaction with Geologic Units

Scarps of the SCFZ offset multiple terrace sequences in five key valley mouths along the range front. Changes in scarp height and morphology at each location, plus four trenches, provide data on the magnitude and frequency of Quaternary tectonic events. A detailed map, scarp profiles, and brief analysis of each area follow.

Alluvium of five ages is offset by a scarp of the SCFZ at the mouth of Major Creek (figure 67). The scarp is progressively higher and more degraded fronting older deposits (figure 68). Data from a trench along the line of Profile 35 (figure 67) in mid-late Pinedale alluvium indicated that the 4.6-m high scarp resulted from two displacement events. Total vertical displacement across the deformation zone is close to 3.6 m, although stratigraphic correlation across the deformed buried graben is speculative (figure 69). Charcoal from graben sediments dates the first movement as occurring before 10,100 ± 110 years BP and the second event as occurring shortly before 7660 ± 120 years BP.

At the mouth of San Isabel Creek, a prominent 3.2-km long scarp offsets five surfaces, ranging from pre-Bull Lake to mid-late Pinedale age (figure 70). Scarps range from 4.4-m high in mid-late Pinedale alluvium to 39.1-m high in pre-Bull Lake alluvium (figure 71). Single-event displacement, based on the calculated throw of the smallest and youngest scarp, is roughly 2.5 m.

In the Willow Creek area, a single fault scarp trending north-south roughly 0.8 km valleyward of the range front offsets four Quaternary glaciofluvial units (figure 72). Scarp heights range from 2.3 m cutting early Holocene alluvium to 87 m fronting pre-Bull Lake deposits (figure 73). Because of good evidence for recurrent movement and easy access, the Willow Creek area was studied in detail. Two trenches were dug along Profiles 9 and 10 (figure 72) to investigate deformation styles and recurrence intervals.

The small scarp offsetting early Holocene alluvium at Profile 9 shows clear evidence of a single fault movement. Stratigraphic displacement at the fault plane was measured as 1.35 to 1.45 m

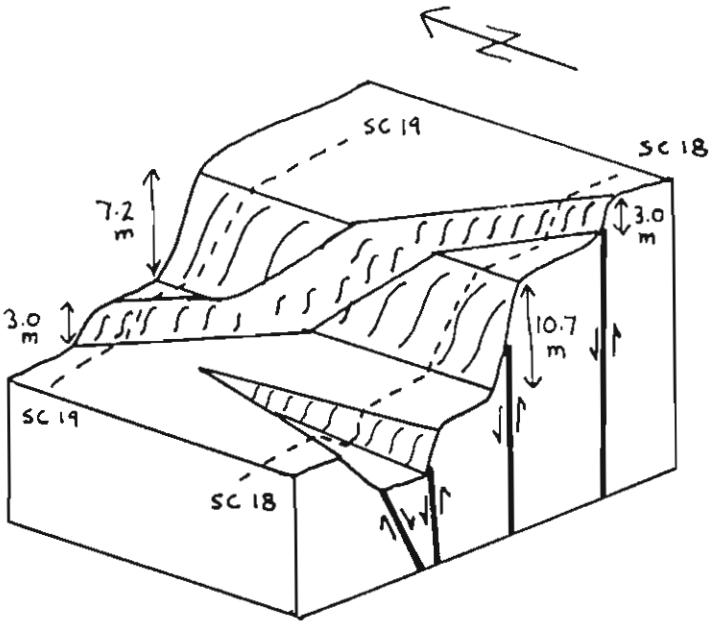

Figure 65.—Schematic block diagram of cross-cutting fault scarps that offset the Pole Creek alluvial fan (early Pinedale).

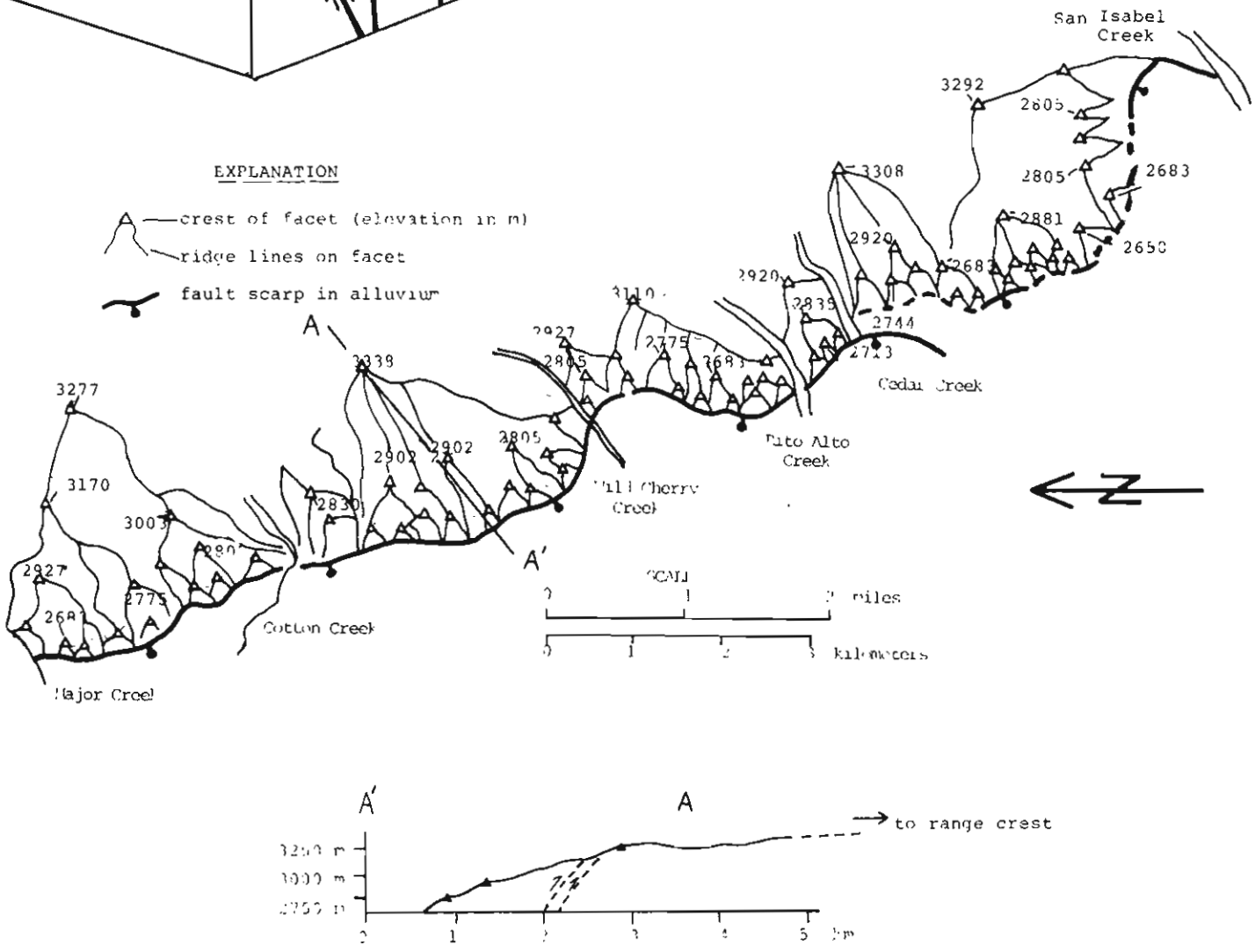

Figure 66.—Plan view and profile of a typical faceted range-front spur between Major and San Isabel Creeks.

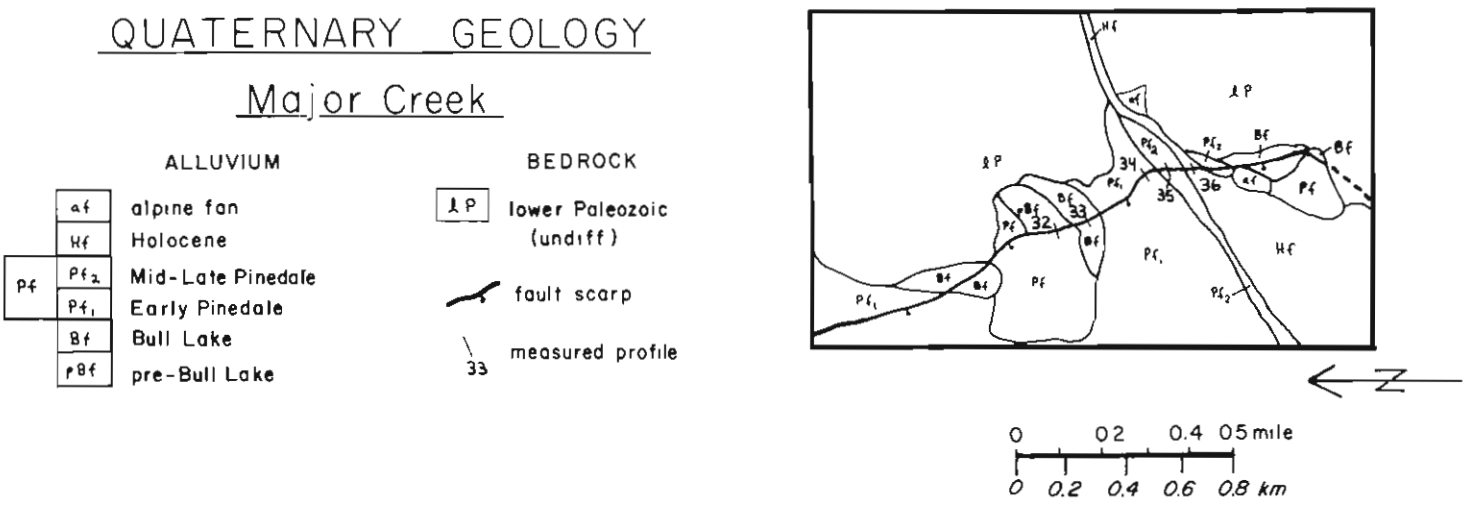

Figure 67.—Quaternary geologic map, Major Creek area.

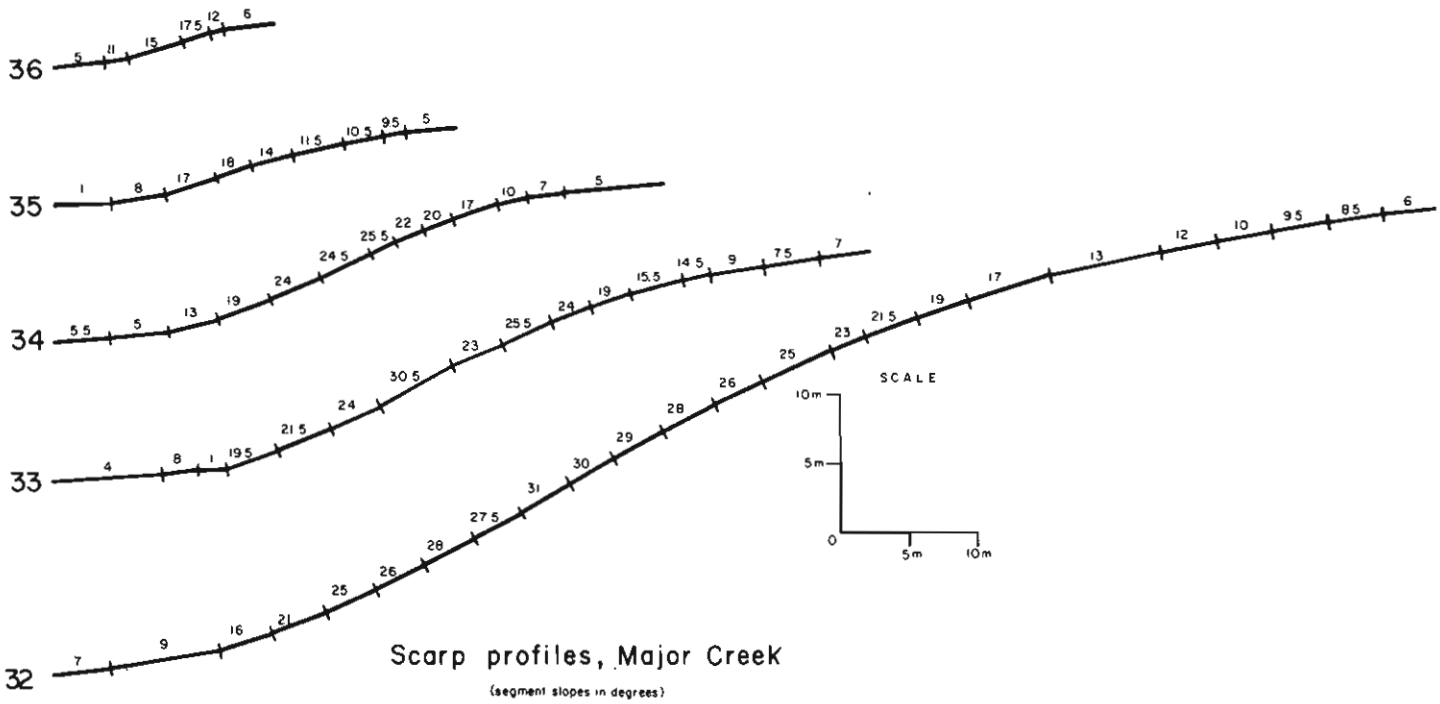

Figure 68.—Fault scarp profiles, Major Creek area.

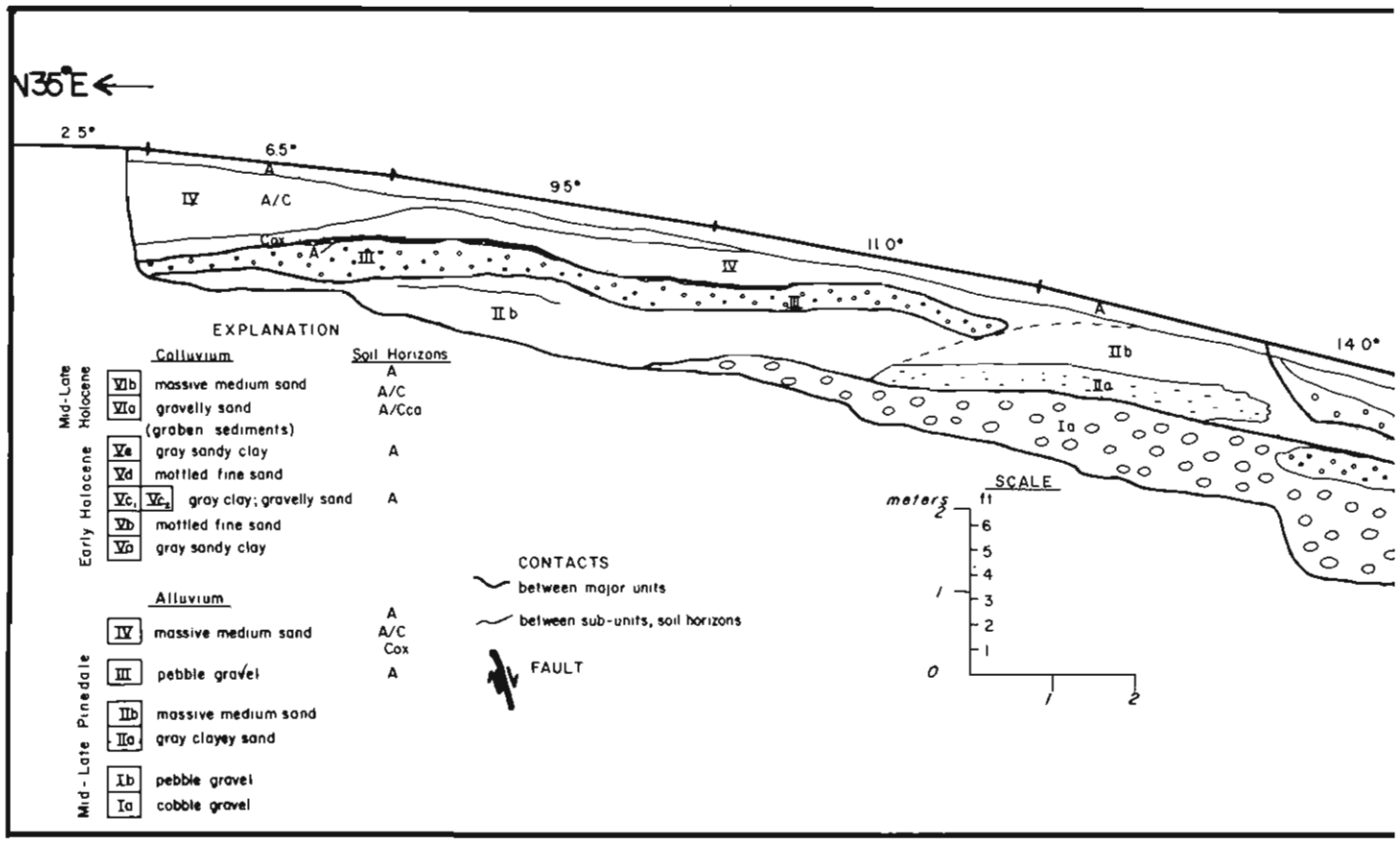

Figure 69.—Log of trench, Profile 35, Major Creek area.

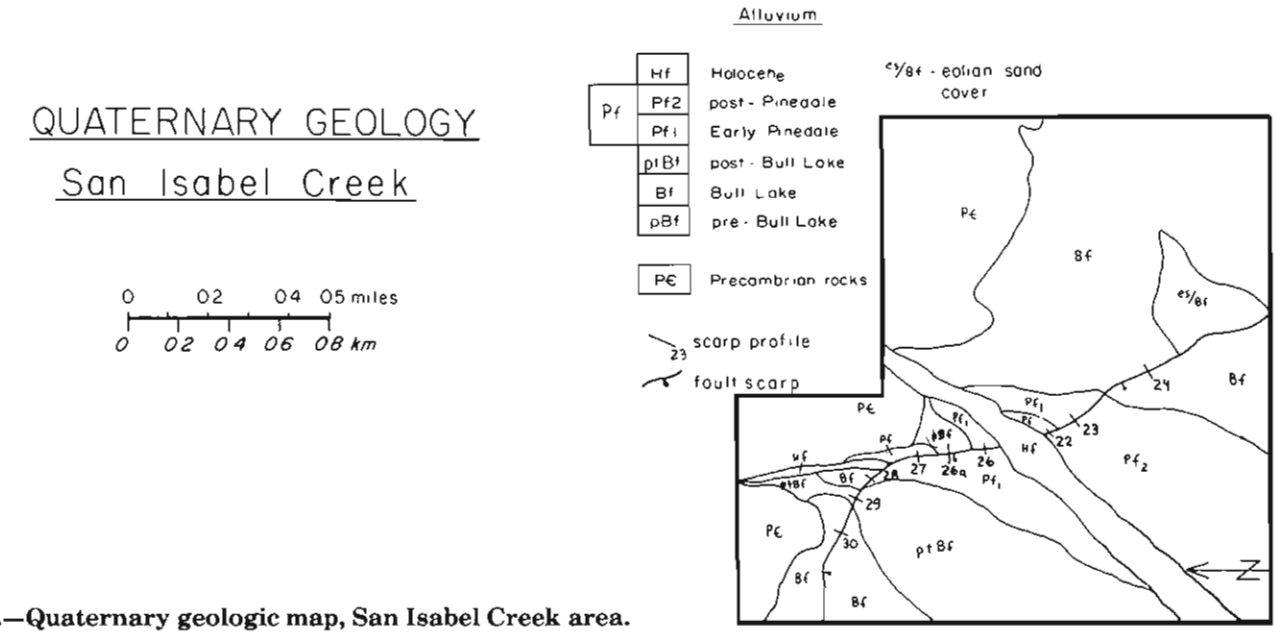

Figure 70.—Quaternary geologic map, San Isabel Creek area.

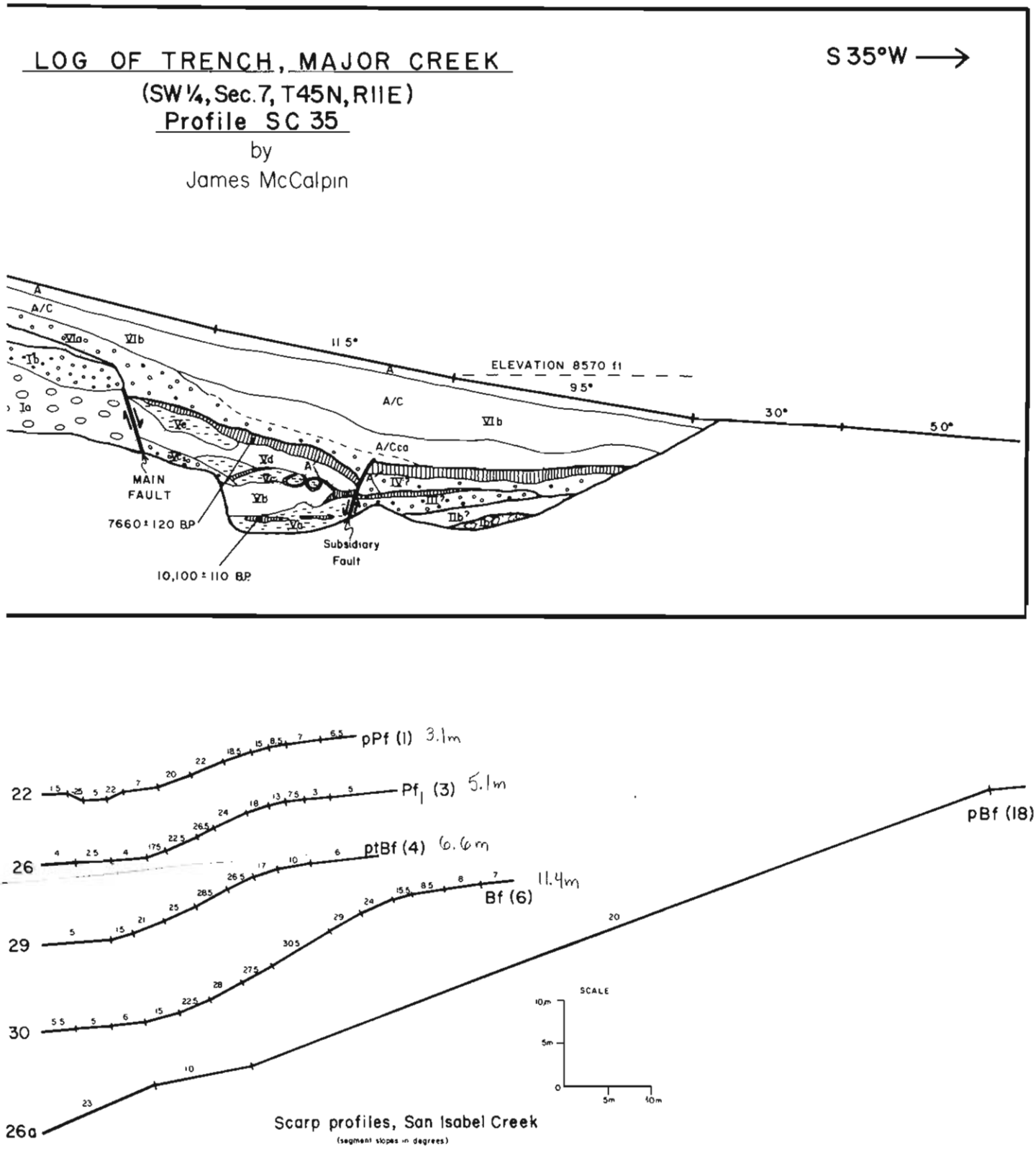

Figure 71.—Fault scarp profiles, San Isabel Creek area.

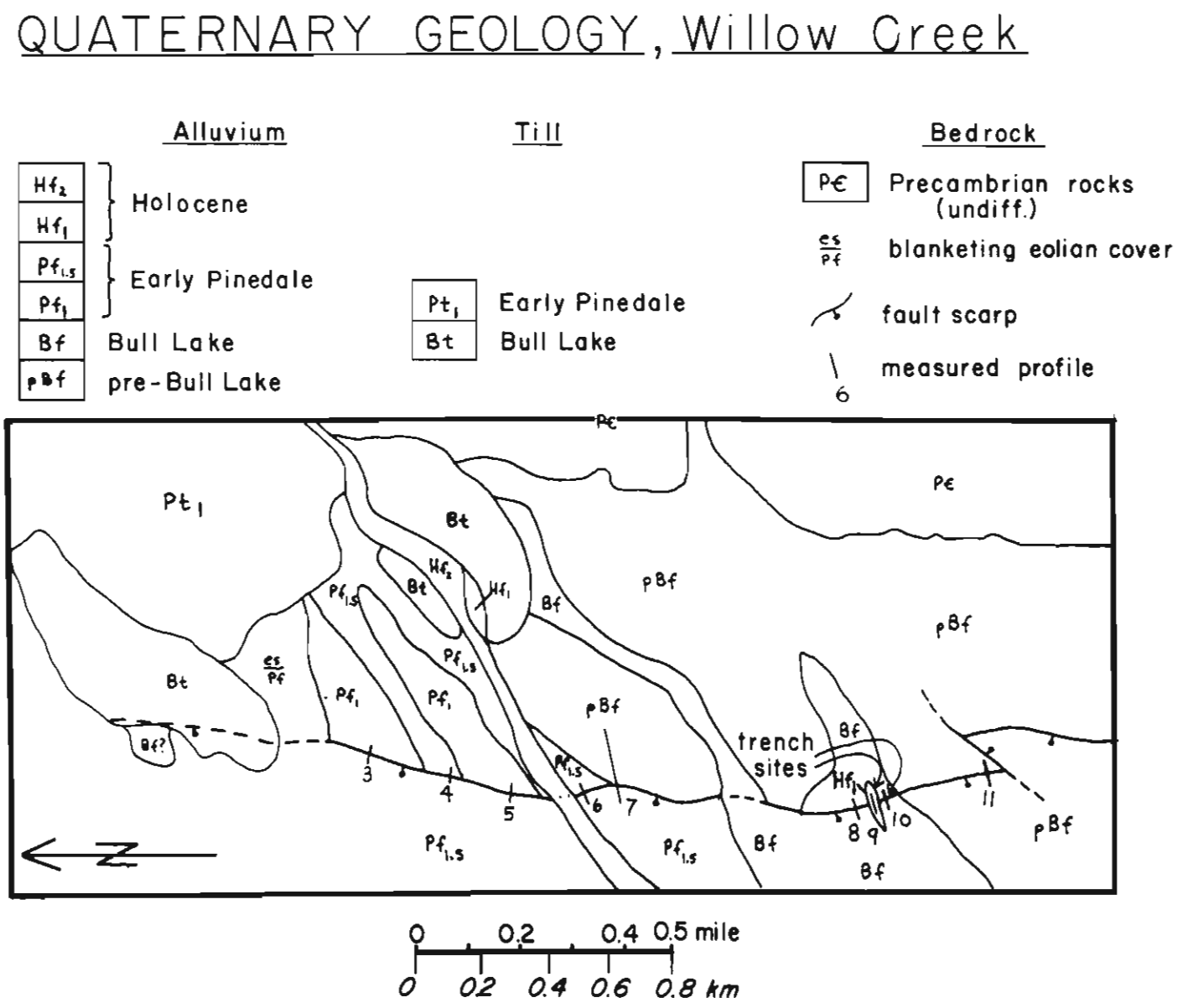

Figure 72.—Quaternary geologic map, Willow Creek area.

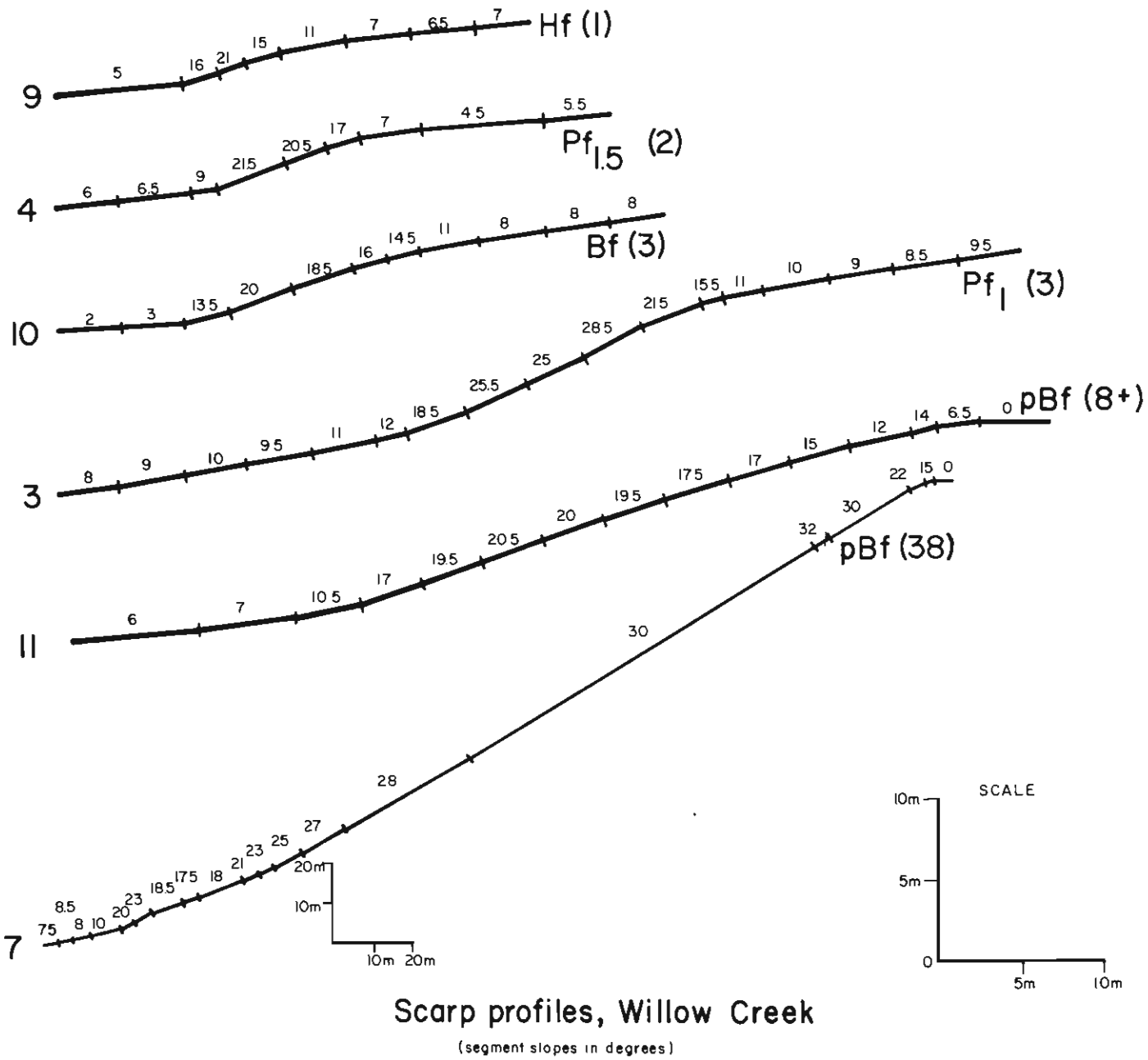

Figure 73.—Fault scarp profiles, Willow Creek area.

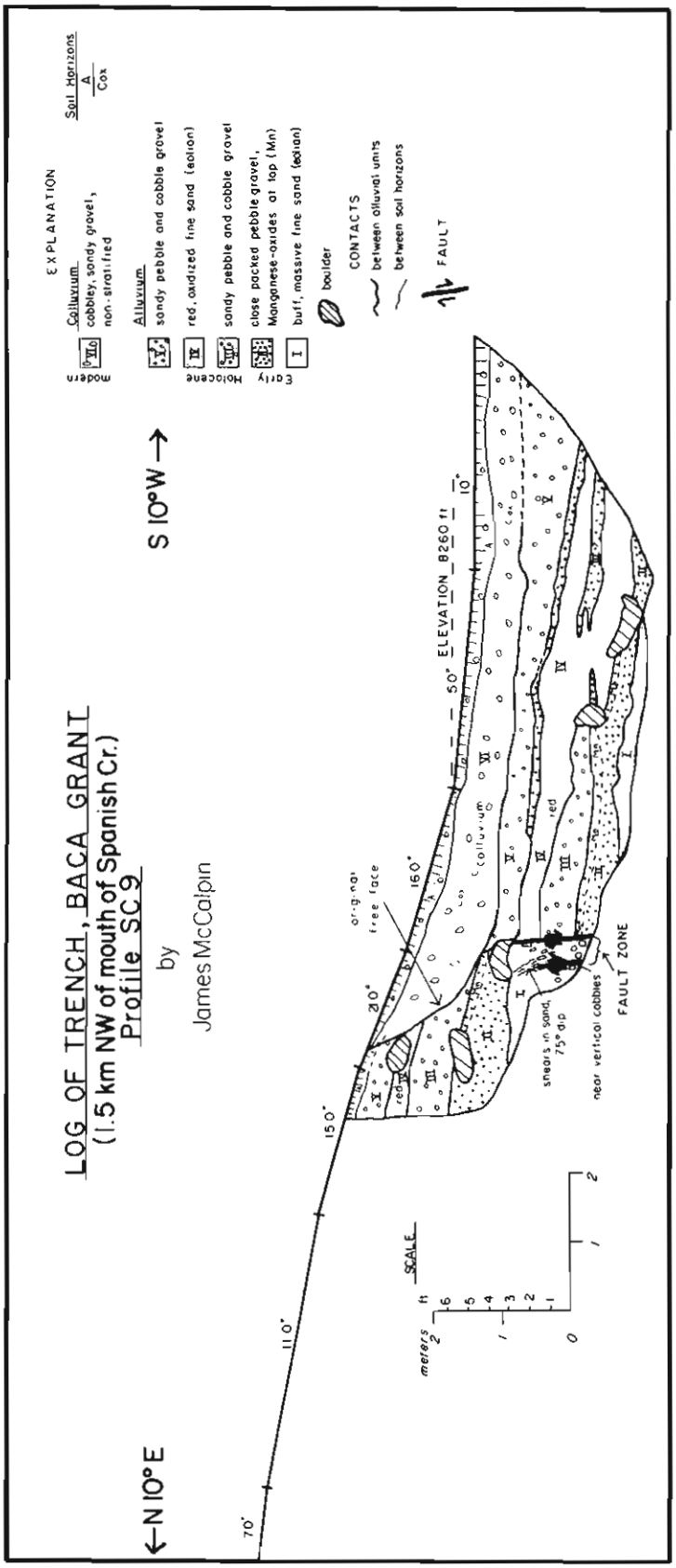

Figure 74.—Log of trench, Profile SC9, Baca Grant.

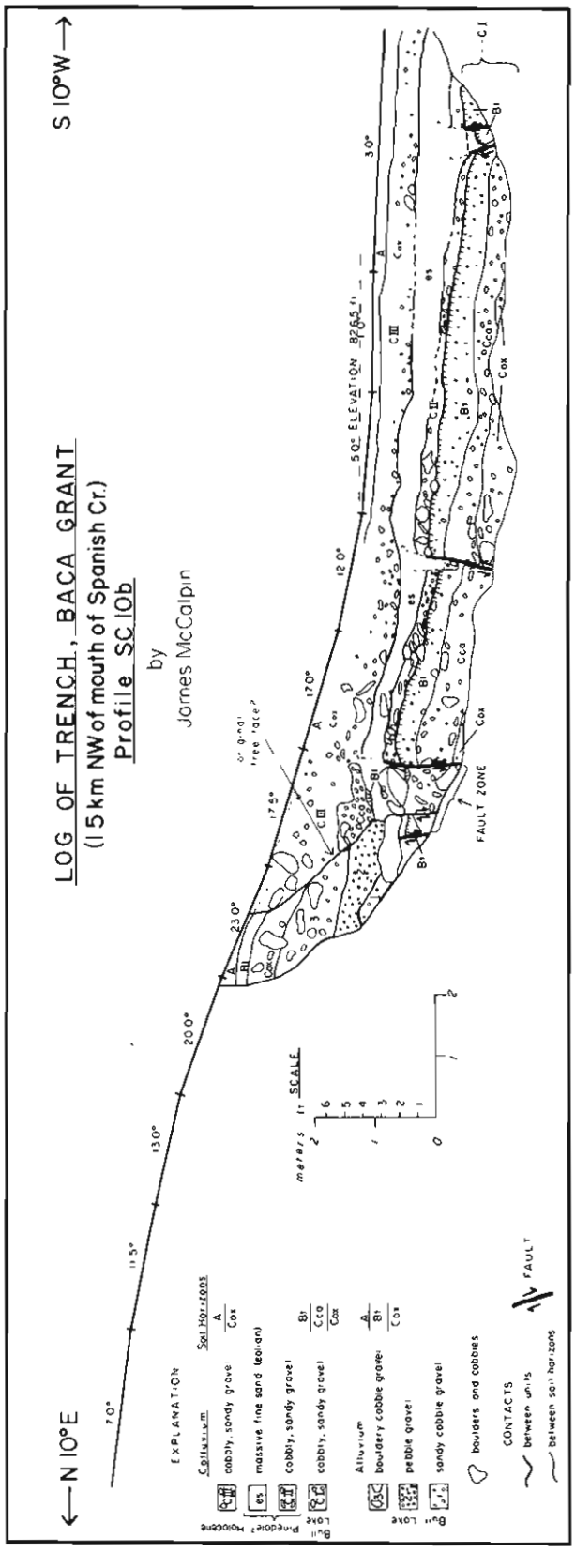

Figure 75.—Log of trench, Profile SC10b, Baca Grant.

(figure 74). The upthrown surface was dragged into the fault plane with a vertical drag component of 0.9 m. Thus, of the net 2.3 m of displacement across the fault zone, 0.9 m was contributed by drag and 1.4 m by abrupt offset on the fault plane. The larger scarp offsetting Bull Lake alluvium was fronted by a complex colluvial wedge containing three colluvial units, each grading to coarse-grained toward its base (figure 75). The colluviums contain soil profiles in their upper parts that can be compared in development to other soils observed throughout the study area. Colluvium I carries a soil with a well-developed textural B horizon and an underlying C_{ca} horizon; overall the soil is similar to soils developed on relict Bull Lake fan surfaces. The middle colluvium carries no soil, indicating that insufficient time for soil development occurred between its deposition and that of overlying Colluvium III. Colluvium III carries a weakly developed A/C profile which is similar in development to soils on mid-late Pinedale or early Holocene deposits.

Displacements due to individual fault events can also be estimated, using several assumptions: (1) total displacement of all events (probably three) must equal the net displacement of 5.3 m; (2) the latest event had a displacement of about 2.3 m, according to the trench in the single-event scarp directly to the north; and (3) each displacement must have been equal to or greater than the thickness of the colluvial wedge resulting from renewed faulting. The degree of soil formation and deformation in the colluvial units indicates the sequence of fault events diagrammed in figure 76. This sequence is also compatible with geomorphic relations along the scarp north of the trench site (figure 72). A graphical representation of displacement through time suggests that uplift is eposodic, with recurrence ranging from approximately 58,000 to 9,000 years (figure 77). Estimated displacements for single events range from less than 1 m to 2.3 m.

On the west flank of the Sierra Blanca at Uracca Creek, a scarp 1.2 km west of the range front offsets early Holocene through pre-Bull Lake alluvium (figure 78). Scarps range from 2.9-m high in Holocene alluvium to 20.0-m high in Bull Lake alluvium (figure 79). A trench across the Holocene scarp at Profile 48 revealed evidence of a single movement with a measured minimum fault throw of about 2.0 m (figure 80). Charcoal from a soil horizon developed on the scarp profile dated at 5640 ± 100 years BP. This date roughly brackets faulting as occurring between early Holocene deposition (8,000 years BP) and 5640 years BP.

At the mouth of Blanca Creek on the south flank of the Sierra Blanca, a large 2.1-km long scarp-graben system disrupts glacial and alluvial deposits of five ages (figure 81). The deformation zone, which stays within 200 m of the range front, consists of a large basin-facing scarp fronted by a graben 30-50 m wide (figure 82). Arroyo cuts show the graben is filled with massively bedded sandy sediments (partly eolian?) at least 2-m deep. Scarp heights, which range from 3.2 m in mid-late Pinedale alluvium to 28.3 m in Bull Lake alluvium, greatly exaggerate net fault throw across the fault zone (figure 83).

To determine long-term recurrence at these five key sites on the SCFZ, we must again assume that the latest single-event scarps represent "typical" events. Despite the potential weakness in the assumption, the inferred number of events is surprisingly consistent for deposits of several ages within fault segments A and B. Early Holocene or mid-late Pinedale deposits appear to have been offset by one event, early Pinedale deposits by three to five events, Bull Lake deposits by three to seven events, and pre-Bull Lake deposits by 13 to 18 events (table 18, column 4). A graphical portrayal of tectonic history for segment A of the SCFZ is shown in figure 84; compare this to the similar history in figure 58 for the VGFZ. Data presented in table 18 form the basis for an analysis of spatial and temporal variation in fault activity along the SCFZ, as described in the next section.

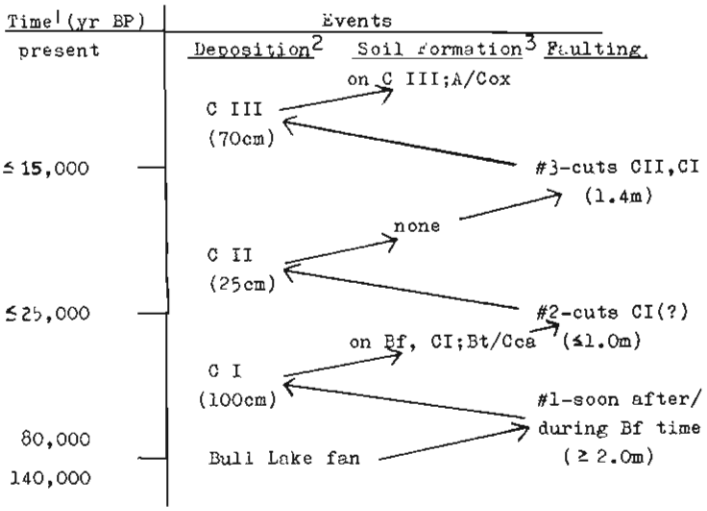

Figure 76.—Inferred sequence of geologic events, Baca Grant trenches.

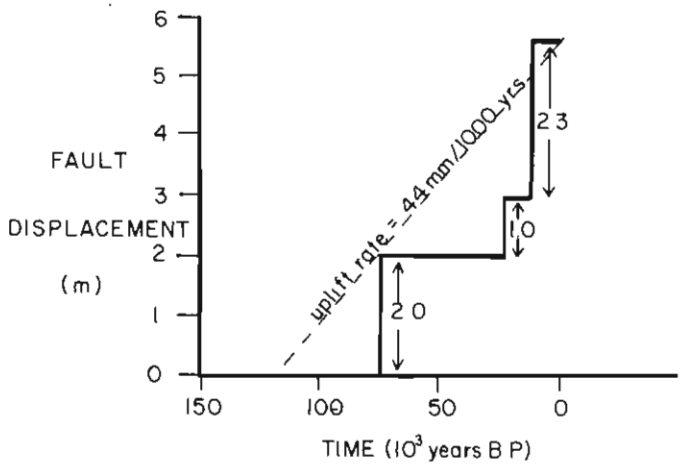

Figure 77.—Inferred displacement history, Baca Grant trenches.

Displacement History: Spatial and Temporal Aspects

The Sangre de Cristo Fault Zone consists of three prominent segments in the study area, defined by different orientations as previously described (figure 59). The record of faulted Quaternary surfaces within each segment has been used to reconstruct its tectonic history independent of its flanking segments. Calculated recurrence intervals between surface faulting events (figure 85) are quite variable along the length of the SCFZ. Recurrence in post-early Pinedale time in the northern four sites has ranged from 5,000 to 11,700 years, compared to 25,000 years at Blanca Creek. The implication is that faulting occurs only half as often on Segment C as on A or B. Comparison of recurrence intervals in post-Pinedale time with recurrence intervals in earlier times shows that fault events appear to have become increasingly frequent on all segments of the SCFZ since early Pinedale time. The Pinedale-Bull Lake interval has the longest recurrence values, suggesting that this time period was one of relative tectonic quiescence, especially compared to post-Pinedale time. Recurrence values in pre-Bull Lake time represent the longest record of Quaternary uplift, and may be nearer to true long-term average figures.

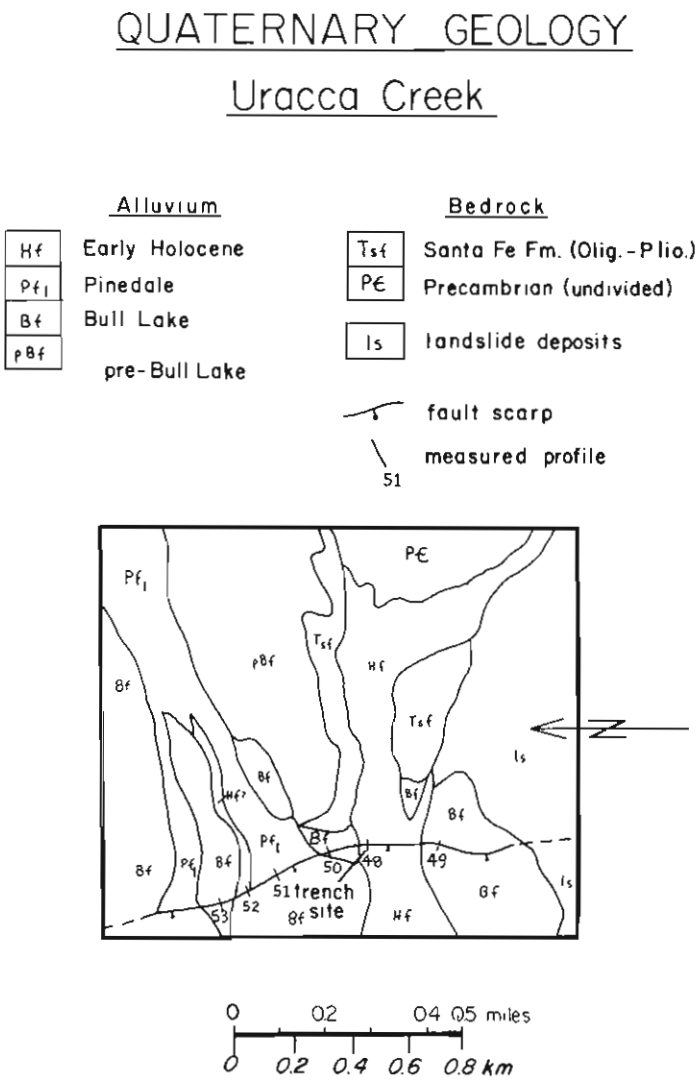

Figure 78.—Quaternary geologic map, Uracca Creek area.

The spatial trend of uplift at the Sangre de Cristo Mountains has been compiled into a graph (figure 86) which plots calculated fault throw of all measured profiles from both the SCFZ (90 profiles) and the VGFZ (63 profiles). An average fault dip of 70° is assumed in the calculations. Fault throw values for units of equivalent age along the fault zones are connected by continuous lines, which display a graphical record of uplift variation along the length of the range front.

Segment A, the longest (90 km) and most prominent segment of the SCFZ, contains the best-peserved and largest geomorphic evidence for Quaternary uplift. Uplift vectors reconstructed from scarp profiles remain high in the central portion of Segment A, but drop rapidly north of the Major Creek-Kerber Creek Fault Zone (MKFZ) (figure 86). The MKFZ is a major Laramide structure (Knepper 1974), which separated the San Luis Arch (south and west) from an adjoining structural basin (north and east); it was cross-cut by Neogene rifting. In addition, the scarcity of fault scarps at the range front opposite the Villa Grove Fault Zone suggests that some of the differential uplift of the mountain mass may be taken up on the VGFZ. However, adding displacements from the VGFZ to interpolated values from the SCFZ still shows a considerable decrease in uplift north of the MKFZ (figure 86). The data suggest that Segment A should be considered as two segments: Segment A1 south of the MKFZ, characterized by high uplift rates, and with the range-front fault developed in fractured Precambrian basement of the ancestral Uncompahgre Highland and San Luis Arch; and Segment A2 north of the MKFZ, typified by lower uplift rates, with the range-bounding fault developed through perhaps more rigid Precambrian basement underlying a persistently basinal area.

Older deposits show this decrease in uplift amount across the MKFZ much better than do younger deposits. There is little difference between uplift of Pinedale, and no difference between uplift of Holocene, deposits across the MKFZ (figure 86). One explanation for this contrast is that a certain percentage of surface-faulting events on Segment A1 may terminate at the MKFZ over a long period of time. The longer the period observed, the more striking the drop in uplift across the MKFZ would appear. In the relatively short time since Pinedale deposition, at least two surface-faulting events have occurred which apparently did not terminate at the MKFZ.

Fault scarps are not well-preserved in deposits older than Pinedale age in the southern part of Segment A. However, scarps in Pinedale deposits (undivided) are similar in size to scarps in contemporaneous deposits in the central portion of Segment A, suggesting no significant tectonic boundaries between the two areas (figure 86).

Segment B is a 20-km long fault segment which trends N 5°-10° E from Medano Creek to Holbrook Creek (figures 59 and 86). A 10-km long continuous scarp at the range front offsets a coalescing series of Pinedale (undivided) alluvial fans, with scarp heights ranging from 3.3 m to 8.5 m. These heights are similar to those recorded in the southern part of Segment A1, implying that, despite the large difference in strike between Segments A and B, uplift rates (at least since Pinedale time) have been similar on both segments (figures 81 and 86). The only data

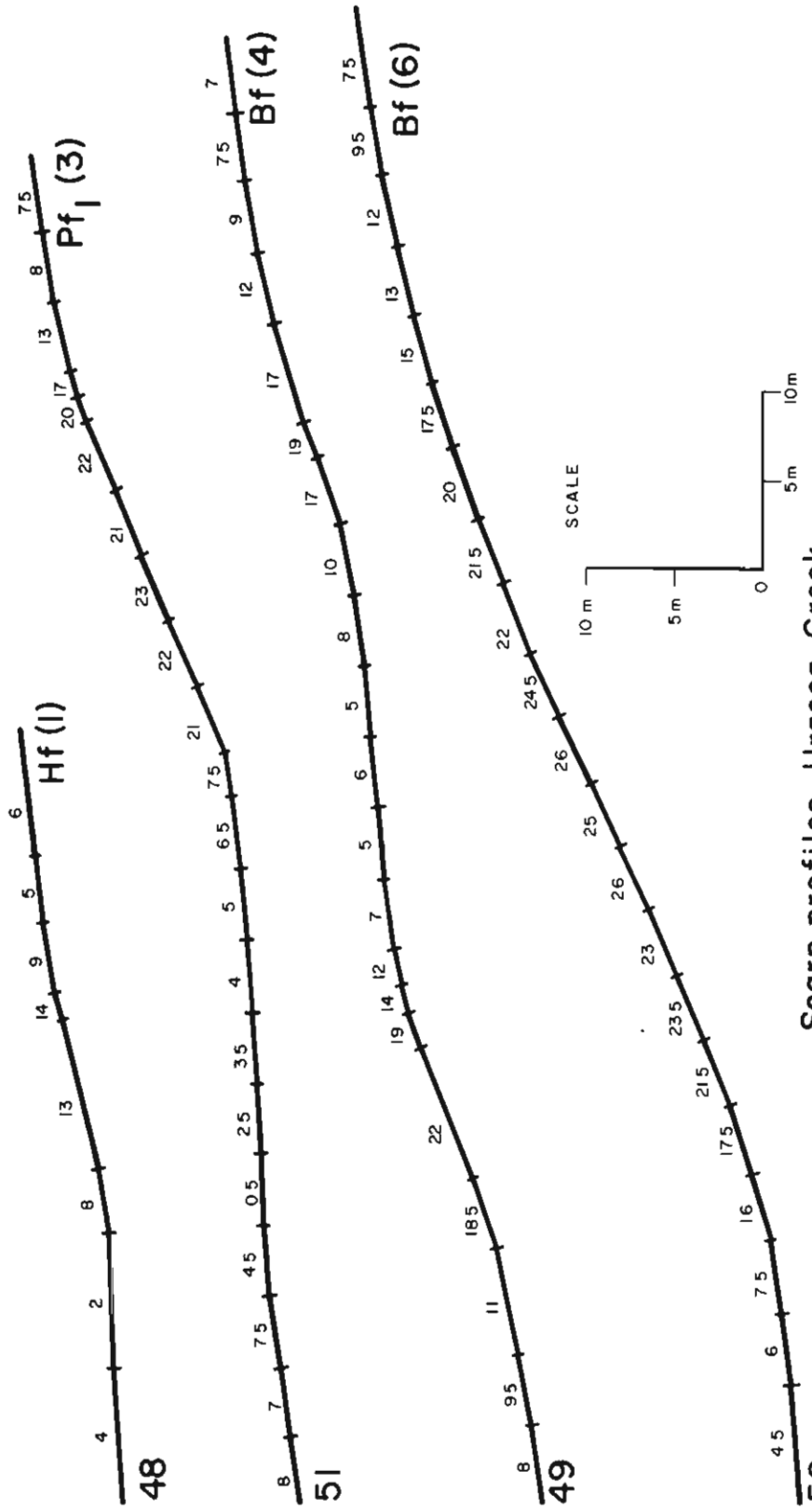

Figure 79.—Fault scarp profiles, Uracca Creek area.

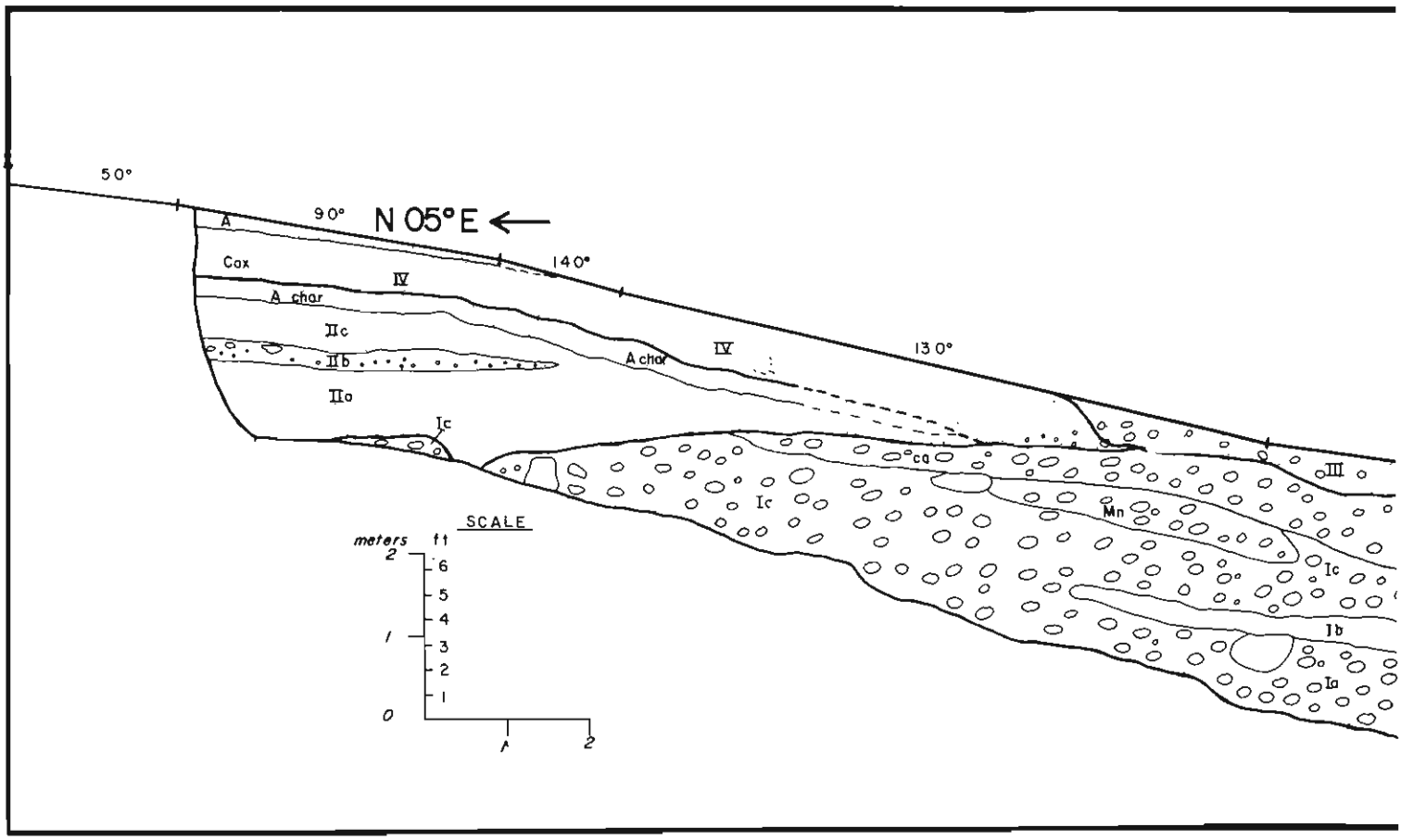

Figure 80.—Log of trench, Profile SC48, Uracca Creek area.

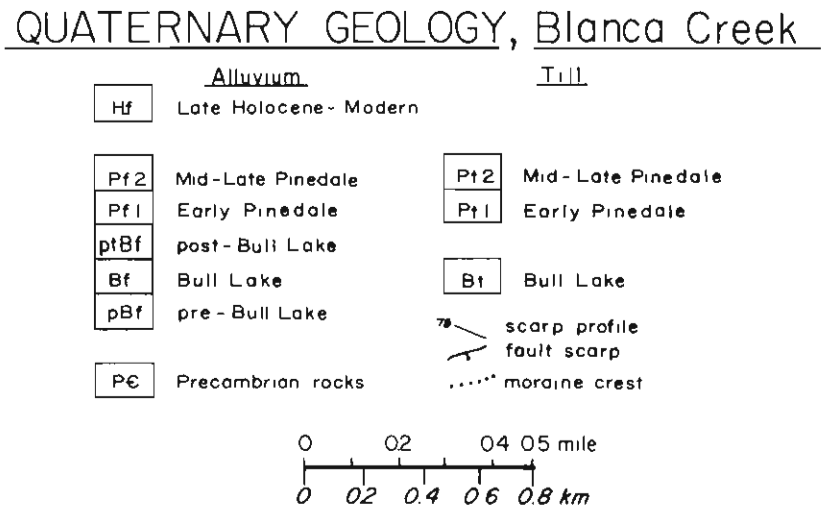

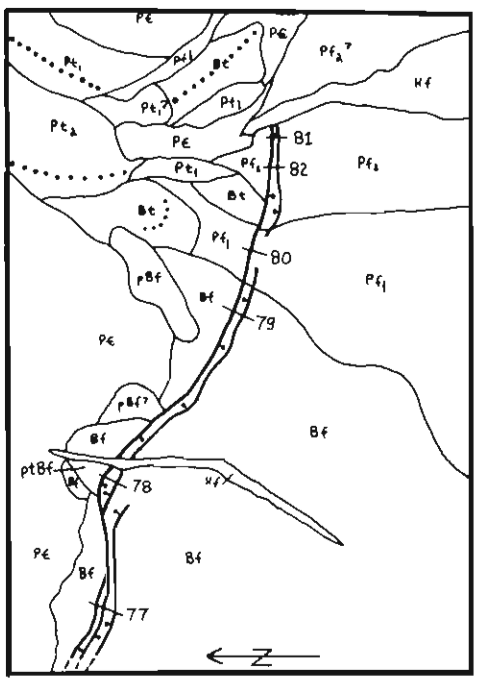

Figure 81.—Quaternary geologic map, Blanca Creek area.

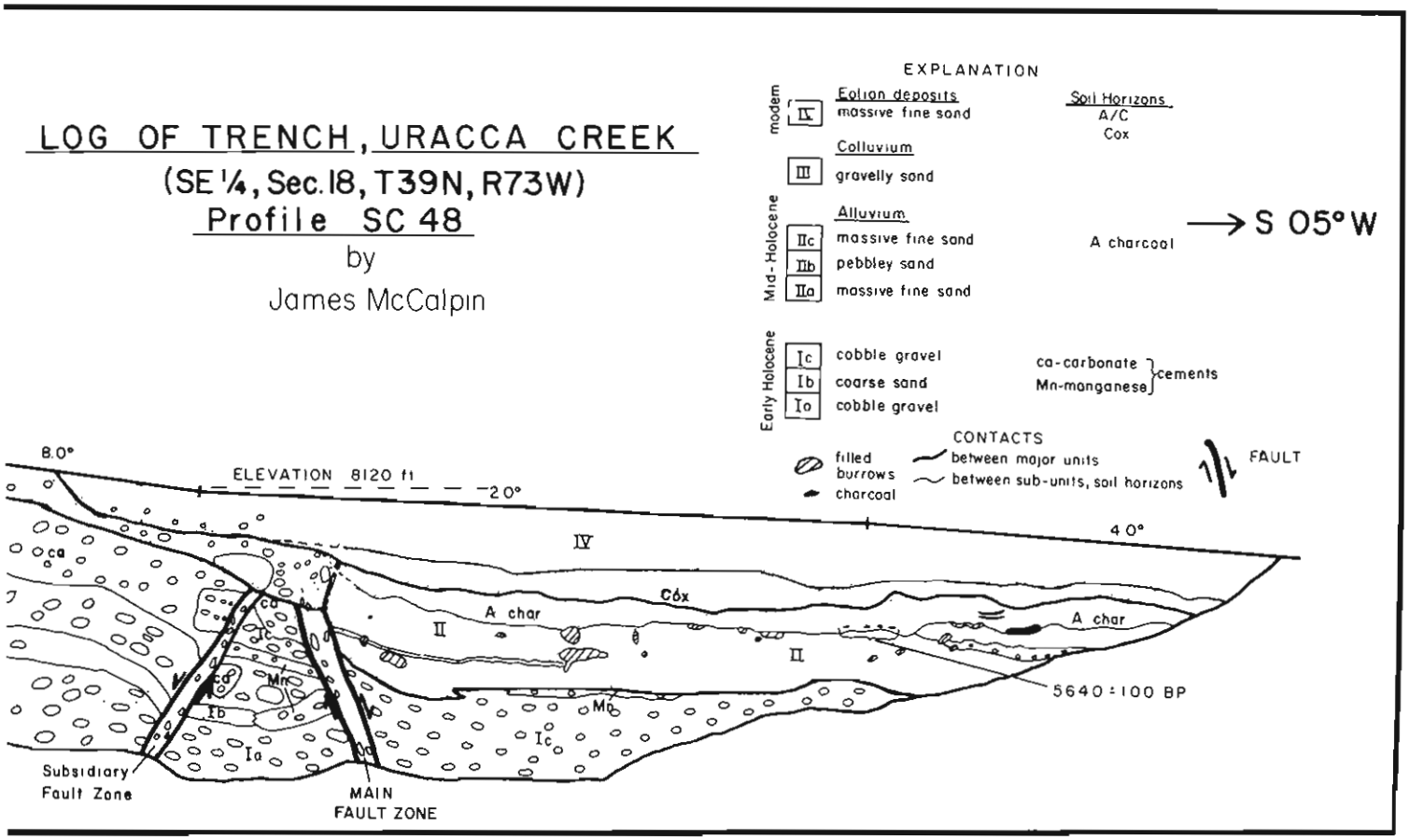

on long-term fault behavior of Segment B come from the Uracca Creek area (figures 78 and 79), where a subsidiary fault 1.2 km west of the range front offsets Quaternary deposits of five ages. Uplift rates calculated at this locality are similar to those calculated for Segment A. An unknown amount of uplift may have occurred at the range-front position 1.2 km to the east, for although young scarps were not observed at that position, the range-front displays well-developed faceted spurs. Early Holocene deposits of Segment B at Uracca Creek are offset an amount similar to contemporaneous deposits of Segment A1, suggesting similar Holocene uplift pattern. Faulting of 2.0 m at Uracca Creek (figure 79) is approximately bracketed as occurring between about 8,000 and 5640 ± 100 years ago. The time is sufficiently similar to the time of faulting at Major Creek on Segment A1 (before 7660 ± 120 years ago) that the two scarps may be contemporaneous. Even if they represent two surface-faulting events closely spaced in time, the evidence argues for similar Holocene uplift histories on Segments A and B.

Segment B has been mapped as the northern continuation of the larger northeast-trending Manassa Fault by Kirkham and Rogers (1978). However, no evidence of Quaternary surface-faulting exists along the 65 km of this inferred fault between the Rio Grande River and the southern part of Segment B of this report. Thus the main body of the Manassa Fault, which is inferred from subsurface and geomorphic data only, certainly

Figure 82.—Head-on view of fault scarp and basal-filled graben (foreground) at an unnamed drainage between Tobin and Blanca Creeks, Sierra Blanca. Rod at base is 2 m high.

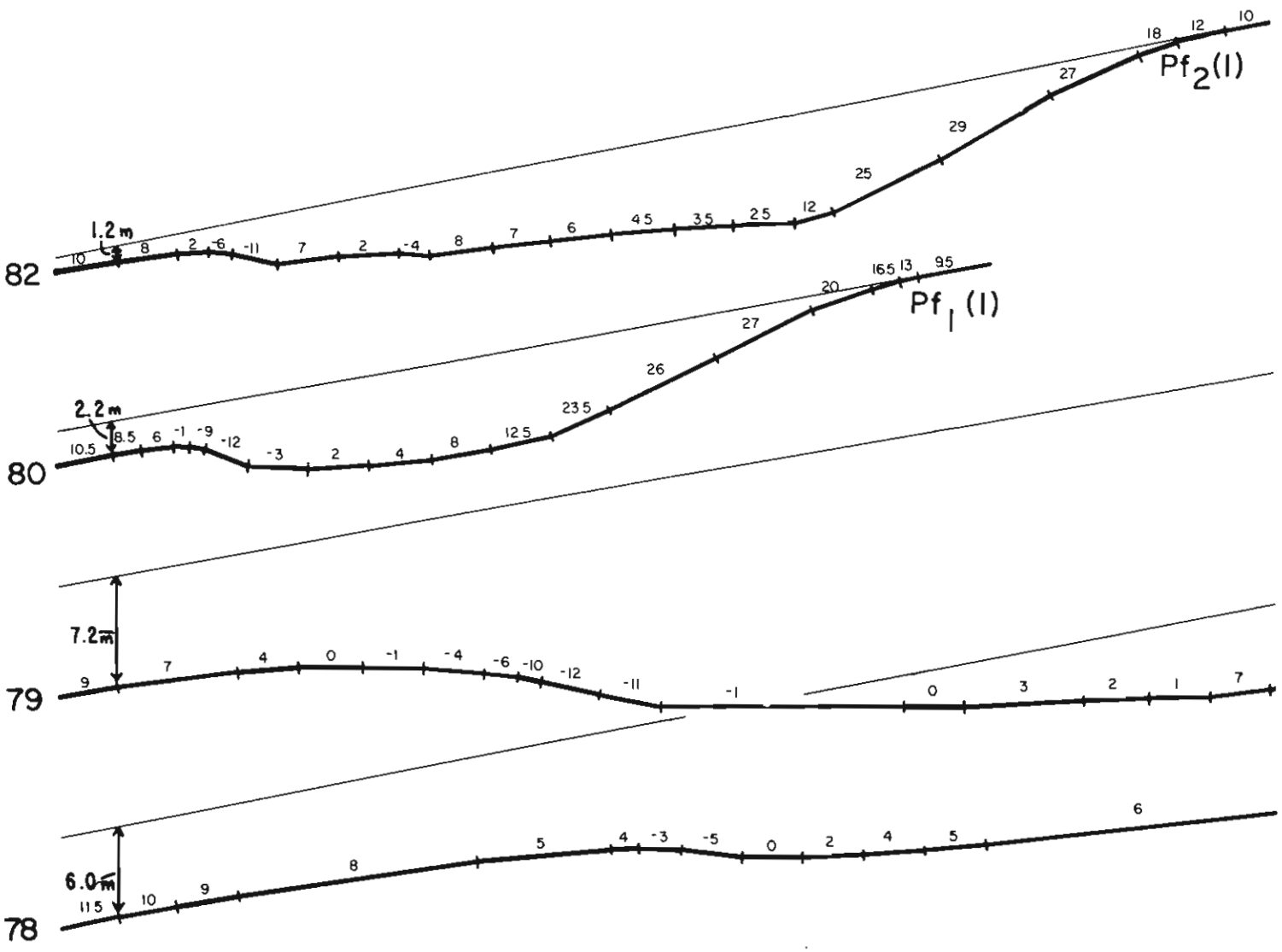

Figure 83.—Fault scarp profiles, Blanca Creek area.

exhibits a much lower rate of Quaternary activity than has Segment B of the Sangre de Cristo Fault Zone. Further detailed mapping of Quaternary deposits and tectonic features in the southern San Luis Valley is needed to define the relation of the Manassa Fault to structures farther north.

Segment C, the short (10-km long) fault segment which bounds the Blanca Massif on the south, is dominated by a large scarp-graben system at the range front (figure 81). Calculated uplift values on this segment for early Pinedale and Bull Lake time are about one-half the size of values on Segments A and B (figure 86). This segment is bounded on both ends by high-angle intersections with other larger faults, i.e., on the west by Segment B of the SCFZ and on the east by a north-south-trending cross fault. Scarps on the cross fault are as large as those measured on Segments A and B and are about twice the size of scarps on Segment C. Based on this evidence, it is concluded that Segment C represents a minor cross fault within the larger horst-graben system, which transfers displacements from north-trending master faults north and south of the Blanca Massif.

Quaternary uplift rates for Segment A, based on fault scarps, are compared in figure 87 to long-term Neogene uplift rates based on vertical displacement of Precambrian rocks due to rifting. All data come from the San Isabel-Willow Creek areas (figure 86). Uplift rates defined by scarps in pre-Pinedale deposits are considerably less than either the post-Oligocene average uplift rate or the minimum rate for a pulse of rapid uplift observed in the Salida, Colorado area by Taylor (1975). The post-Pinedale uplift rate is approximately equivalent to the long-term average uplift rate. The comparison of rates suggests that most of mid-late Quaternary time has been characterized by less tectonic activity than usual on the SCFZ, but in the post-Pinedale interval activity has increased to nearly average rates. The divergence of post-Pinedale from pre-Pinedale uplift rates may be a function of the short length of the post-Pinedale interval and of temporal variability in fault occurrence. Evidence from trenches on the SCFZ suggests that faulting recurrence is nonuniform in time (figure

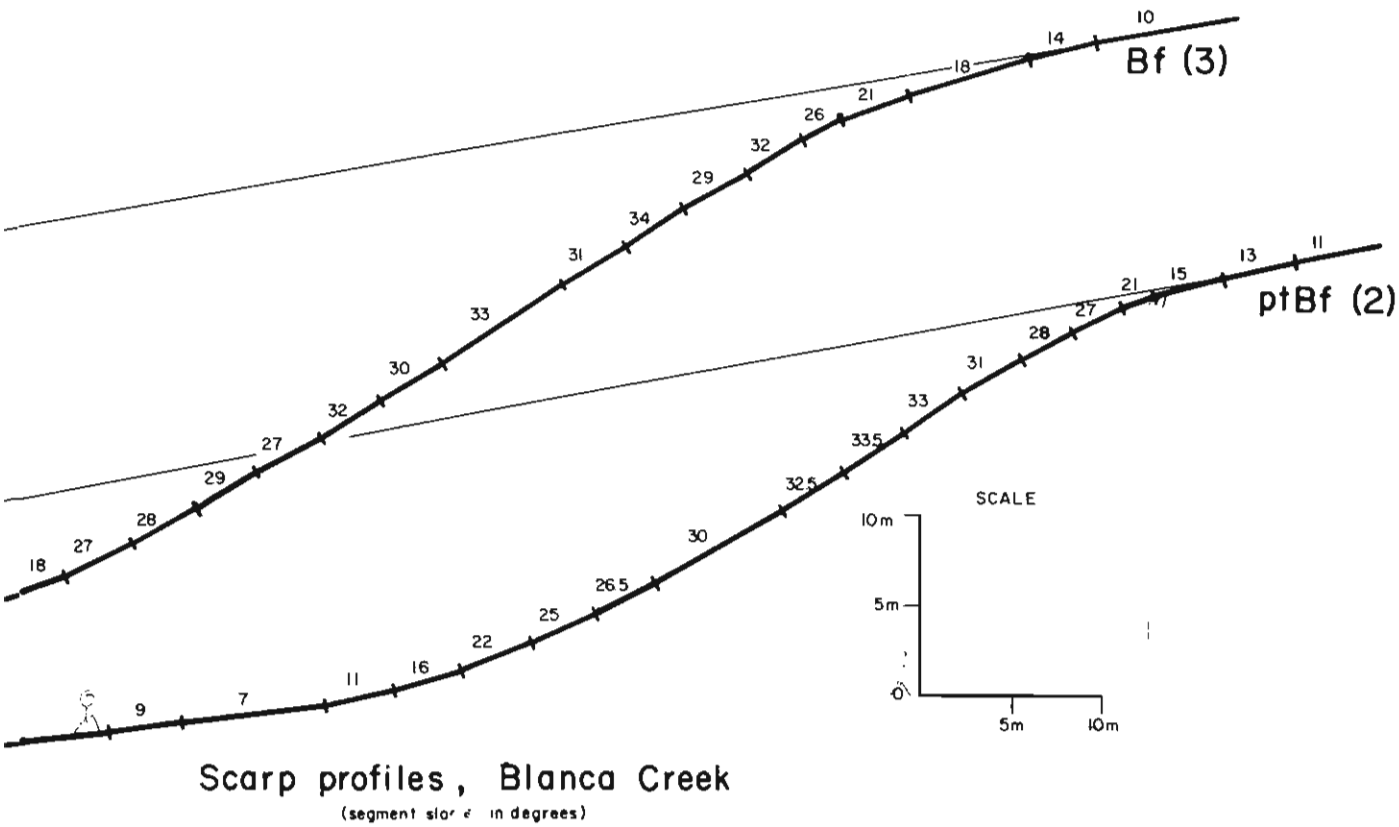

Scarp profiles, Blanca Creek

(segment slopes in degrees)

77). Long-term uplift rates such as the pre-Pinedale Quaternary rate may actually be composed of alternating periods of rapid uplift and relative tectonic quiescence, as shown by the hypothetical dotted lines in figure 86. For example, rapid uplift for 25,000 years (such as the observed post-Pinedale uplift) followed by quiescence for about 40,000 years would result in the long-term Quaternary uplift rate. Field data imply that quiescent periods in the last 120,000 years have been no longer than about 60,000 years and no shorter than about 2500 years (figures 69 and 76).

Seismic Hazard

The magnitude of Quaternary earthquake events which produced surface faulting can be estimated from measures of fault displacement and length of ground rupture. Displacements attributable to single fault events on the SCFZ range from 1.2 to 2.9 m, with the larger values at the center of the fault zone (figure 88). Empirical data for historic normal faulting (Bonilla and Buchanan 1970) suggest that displacements of 1.2 to 2.9 m are correlative with earthquake magnitudes M_L 6.8 to 7.4 (figure 89).

Magnitude estimates based on ground rupture length are less accurate because the extent of ground rupture due to a single fault event is not known. Maximum rupture length is constrained by the combined lengths of all fault segments (120 km); minimum rupture length is the longest single scarp (10 km). Geologic data suggest that the latest faulting event may have created scarps from Major Creek to Uracca Creek (figure 2), a distance of 70 km. This distance corresponds to historic rupture lengths accompanying M_L 7.3 earthquakes (Mark and Bonilla 1977).

In summary, geologic evidence indicates that M_L 6.8 to M_L 7.4 earthquakes occur on the SCFZ every 25,000 to 30,000 years on the average. However, faulting events may have occurred within as little as 2500 years of each other. Analysis of fault scarps cannot provide data on earthquakes that were smaller than the

Table 18.—Summary of fault displacement and recurrence intervals data, SCFZ

Area	Offset Deposit[a]	Profile Number	Vertical Fault Displacement[b] (m)	Number of Fault Events[c]	Deposit Age[d] (1000 yr)	Average Recurrence Interval[e] (1000 yr)
Major Creek	Hf1	36	1.4	1	8	8.0
	Pf2	35	3.8	2	13	6.5
	Pf1	34	8.9	5	25	5.0
	Bf	33	13.5	7	120	17.2
	pBf	32	23.4	13	400	30.8
San Isabel Creek	pPf	22	2.5	1	13?	13?
	Pf1	27	5.5+	3	25-35	8.3-11.7
	Pf1	26	6.2+	3	25-35	8.3-11.7
	Pf1	23	8.0−	3	25-35	8.3-11.7
	ptBf	29	9.2	4	60?	15?
	Bf	24	16.0	6	120	20.0
	Bf	28	14.2	6	120	20.0
	Bf	30	16.0	6	120	20.0
	pBf	26a	39.4	18	400	22.2
Willow Creek	Hf1	9	2.3	1	8	8.0
	Pf1.5	4	3.9	2	25	12.5
	Pf1.5	6	3.8	2	25	12.5
	Pf1	3	8.7+	3	35	11.7
	Pf1	5	6.5+	3	35	11.7
	Bf	8	5.5	3	120	40.0
	Bf	10	5.5	3	120	40.0
	pBf	7	87±	38	1,000	26
	pBf	11	14.0+	8+	400	50−
Uracca Creek	Hf1	48	2.0	1	8	8.0
	Hf1	52	2.2	1	8	8.0
	Pf1	51	5.2	3	25	8.3
	Bf	49	7.5+	4+	120	30.0−
	Bf	50	12.0−	6−	120	20.0−
	Bf	53	9.4	5	120	24.0
	pBf		(34)[f]	(17)[f]	400?	(23.5)[f]
Blanca Creek	Pf2	81	4.1?	1	13	13.0
	Pf2	82	1.2	1	13	13.0
	Pf1	80	2.4	1	25	25.0
	ptBf	78	6.4	2	60?	30.0?
	Bf	77	6.5	3	120	40.0
	Bf	79	7.8	3	120	40.0
	pBf2?		(20)[f]	(8)[f]	400	50

[a] Hf1 is early Holocene, pPf is post-Pinedale, Pf2 is mid-late Pinedale, Pf1 is early Pinedale, ptBf is post-Bull Lake, Bf is Bull Lake, pBf is pre-Bull Lake (undivided).

[b] Measured by the graphical projection method in all cases.

[c] Assuming average displacements per event calculated from one- and two-event scarps.

[d] Age in 10^3 years; from Rocky Mountain Chronology (figure 32).

[e] Interval in 10^3 years; derived by dividing age of deposit by number of fault events. These values are long-term *averages*, hence they cannot reveal variation in fault activity within specified time intervals.

[f] ( ) denotes estimates made from heights of fault-line escarpments.

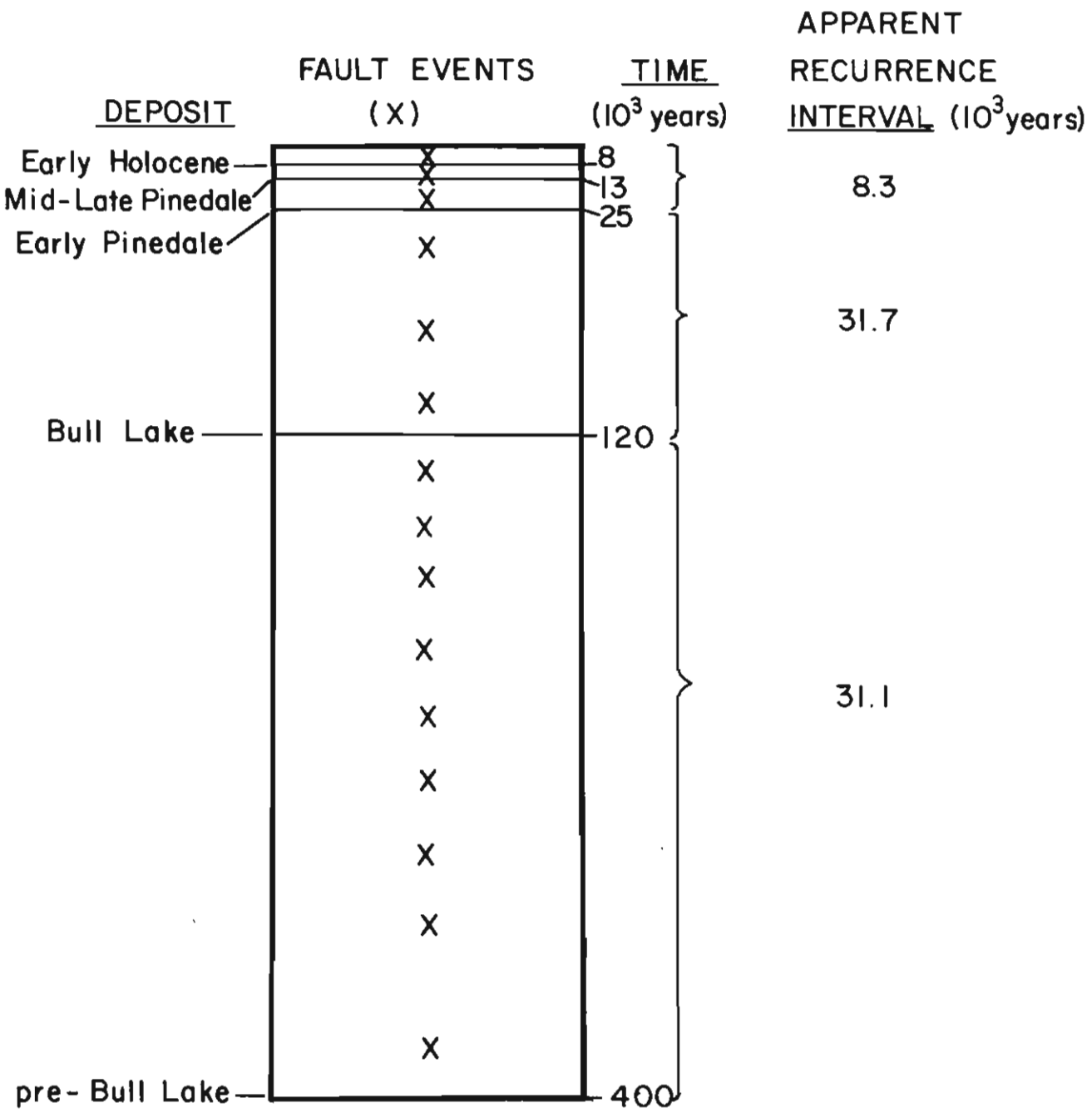

Figure 84.—Inferred tectonic history of the SCFZ in late Quaternary time, Segment A1.

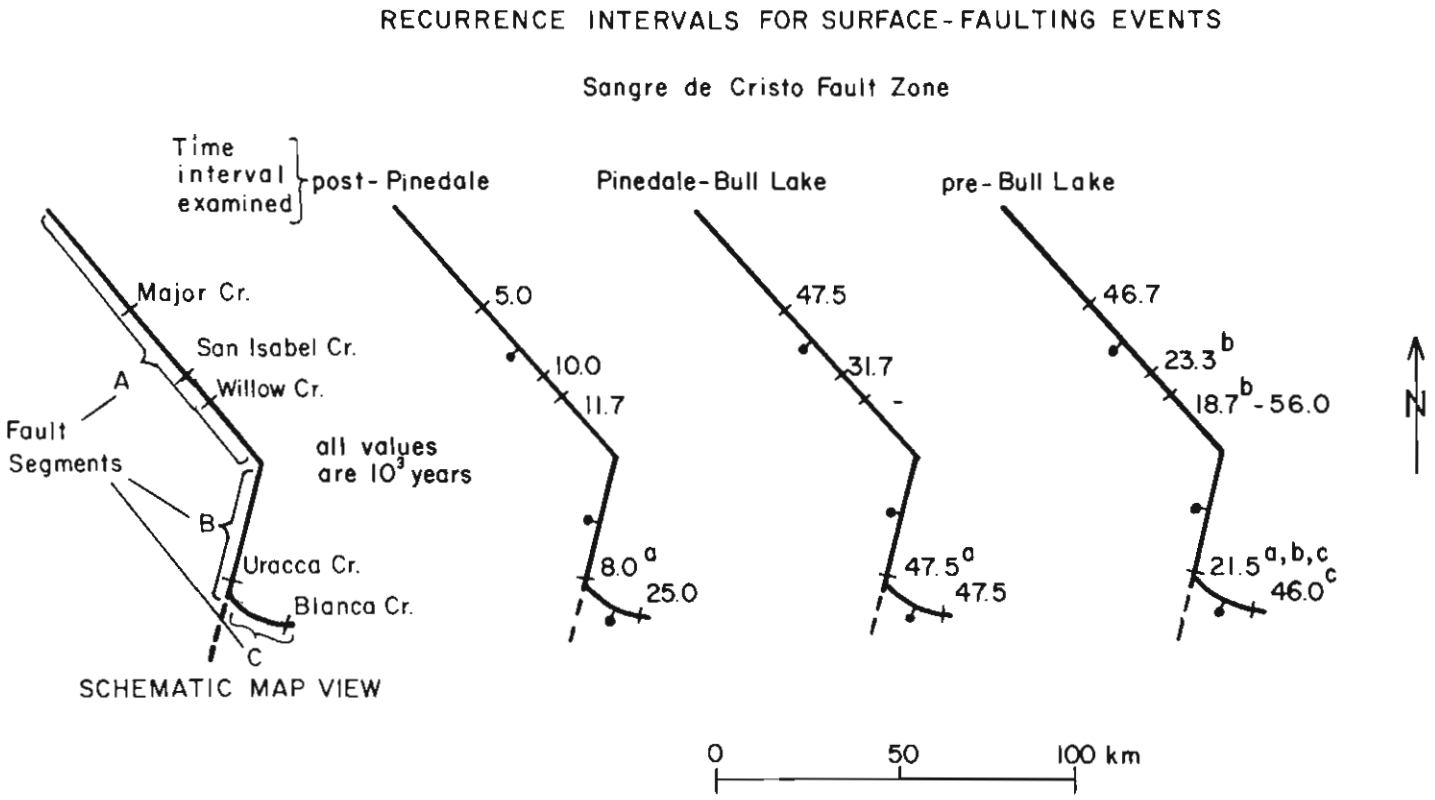

Figure 85.—Spatial and temporal trends in recurrence intervals for surface-faulting events of the SCFZ.

threshold magnitude needed to produce measurable surface rupture. For shallow-focus historic earthquakes, the threshold appears to be M_L 5.0 to 5.5 (Bonilla and Buchanan 1970). Earthquakes smaller than this may have occurred in the San Luis Valley in Quaternary time, but their recurrence relations are unknown.

It is also possible that slow aseismic "creep" on the SCFZ has contributed to scarp formation. Several lines of evidence argue against a creep origin for scarps, however: (1) colluvial wedges exhibit discrete multiple colluvial units indicative of discrete pulses of deposition accompanying scarp formation (figure 75); (2) alluvial strata maintain uniform thickness across the fault plane and do not thicken on the downthrown block as expected if offset was continuous during deposition (figure 74); (3) stratigraphic sequences in trenches are offset equally from bottom to top, but offset should be progressively greater in lower strata if fault movement was continuous (figure 74); and (4) study area scarps are similar morphologically to earthquake-generated scarps in Nevada (Wallace 1977). The above observations strongly suggest that scarps of the SCFZ resulted from discrete surface offsets events, and that slow fault "creep" has played little or no part in their formation.

SEISMICITY OF THE STUDY AREA

Introduction

One way to assess the validity of geologically derived estimates of earthquake magnitude, recurrence interval, and spatial distribution in the study area is to examine the evidence for modern seismicity. This evidence consists of: (1) instrumental records since 1960 A.D. and (2) historical records since 1870 A.D.

Instrumental Records

A detailed analysis of seven years of seismograms from Golden, Colorado failed to verify a single event (detection limit about Richter magnitude 3.0) in the study area (Presgrave 1977). An earlier microearthquake survey detected only one locatable event in the San Luis Valley in a three-week period (Keller and Adams 1976). [By comparison, more than one microearthquake per day was recorded in a more active portion of the RGRZ near Albuquerque, New Mexico (Jaksha and others 1981).] The scarcity of good seismic data in the study area precludes a confident

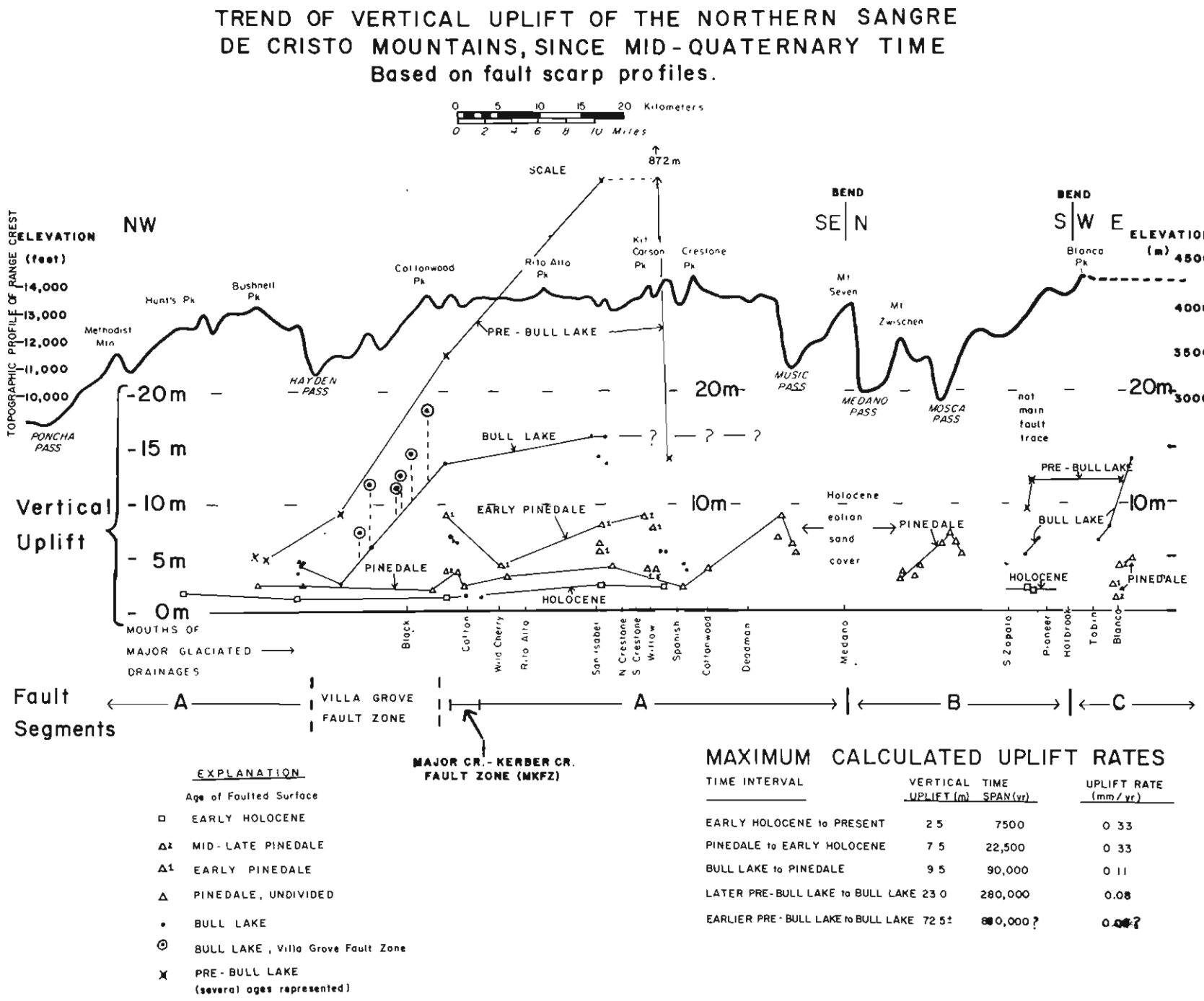

Figure 86.—Trend of vertical uplift of the northern Sangre de Cristo Mountains since mid-Quaternary time.

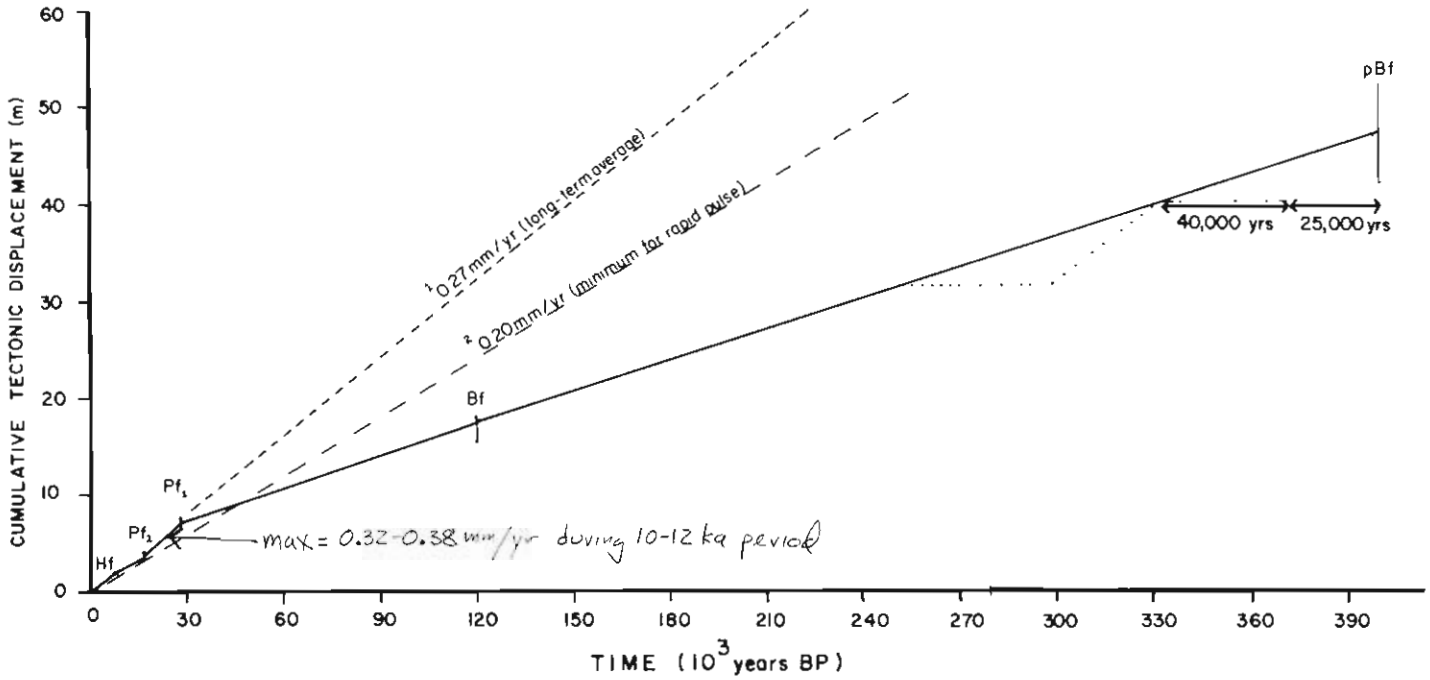

Figure 87.—Long- and short-term calculated uplift rates, SCFZ.

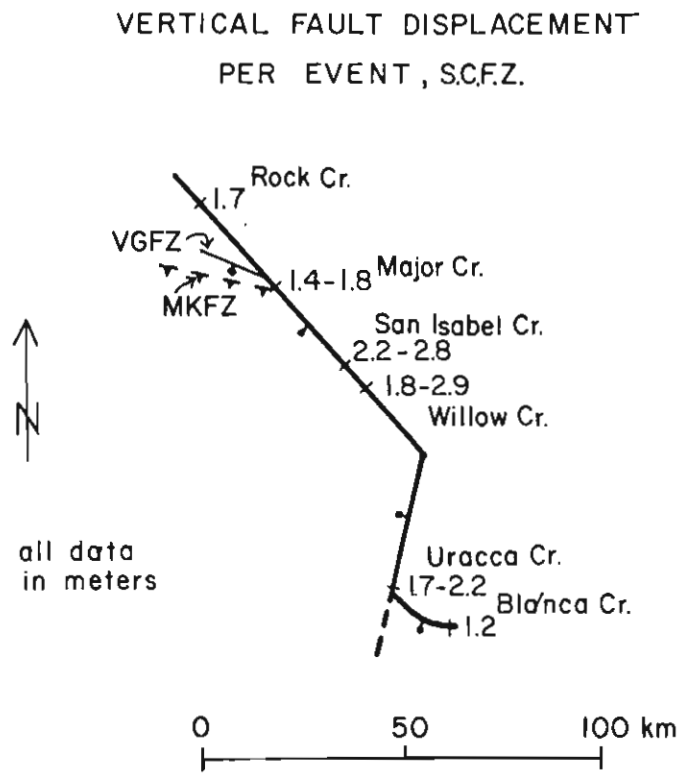

Figure 88.—Vertical displacement per surface-faulting events on the SCFZ.

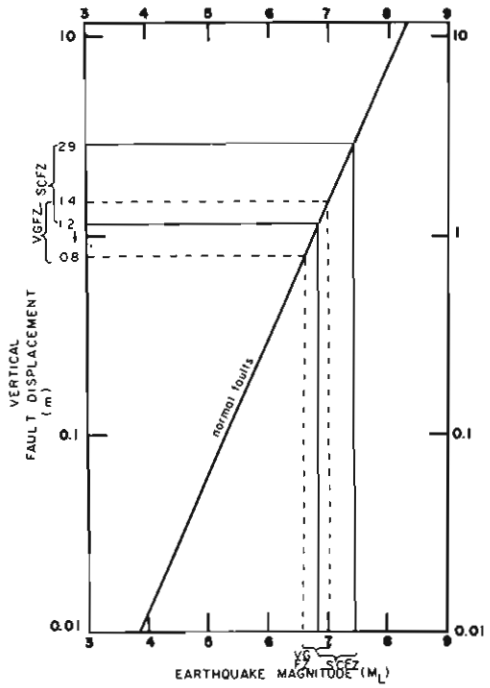

Figure 89.—Estimates of paleoearthquake magnitude on the VGFZ and SCFZ based on vertical displacements per event.

interpretation of the apparent low level of modern macro- and microseismicity. The lack of earthquakes greater than magnitude 3.0 in a seven-year period is not incompatible with deduced long-term Quaternary tectonism, if one assumes that faults obey standard frequency-magnitude relations as described by Richter (1958, page 325) for world-wide historic earthquakes (figure 90).

Historical Seismicity

Analysis of historical records reveals that no felt shocks have originated in either the San Luis Valley or Northern Sangre de Cristo Mountains since 1870 (Hadsell 1968; Simon 1969). [In contrast, the Rio Grande Rift Zone in the Albuquerque-Socorro, New Mexico region has experienced 16 large-to-moderate shocks since 1869 (Hoffman 1975; von Hake 1975).] Lack of small- to moderate-magnitude earthquakes in the study area in 110 years of historic record is not compatible with deduced frequency and magnitude of large prehistoric Quaternary faulting events, if standard frequency-magnitude relations are assumed for area faults (figure 90). Three explanations are possible: (1) the SCFZ and VGFZ do not conform to standard frequency-magnitude relations as derived by Richter (1958) for historically active faults; (2) small-to-moderate shocks did occur but were not observed, reported or recorded; and (3) rapid uplift in post-Pinedale time has temporarily relieved strain on the faults. Explanations (1) and (3) are the most plausible. The Neogene extensional faults in the study area may resemble other Basin and Range faults which exhibit a "seismic cycle" of thousands of years from one large earthquake to the next (Ryall 1977). Between large events, seismicity and earthquake energy release may fall to very low levels, from 0.001 to 0.0001 of that typifying main shock sequences.

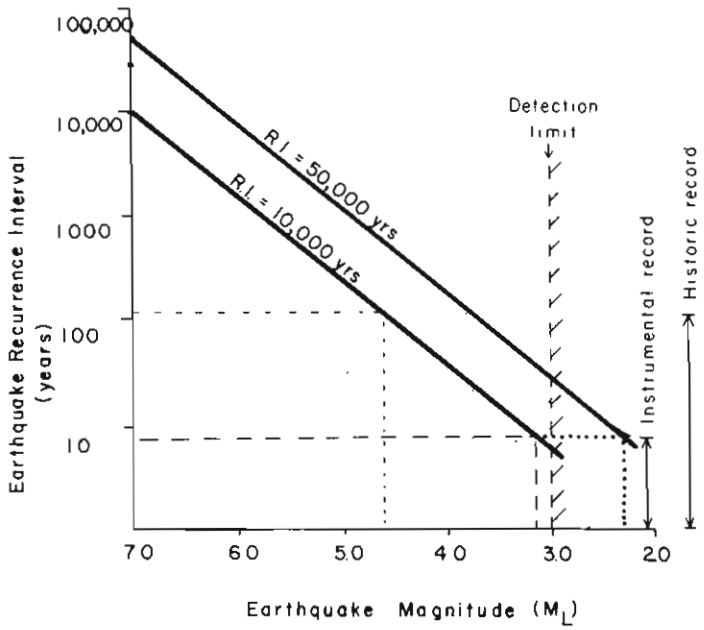

Figure 90.—Hypothetical earthquake frequency-mangnitude relations for the SCFZ.

SUMMARY OF NEOTECTONICS

Geomorphic analysis of Quaternary fault scarps reveals that surface-faulting events have periodically occurred on the Sangre de Cristo and Villa Grove Fault Zones since at least mid-Pleistocene time. Geometric models developed in this study allowed reduction of all scarp height data to fault throw values, which could then be compared along the length of the fault zones and between different time periods. Fault events with throws of 1.2 to 2.9 m have apparently occurred roughly every 10,000 to 50,000 years on the SCFZ. On the VGFZ, smaller displacements (0.8 to 1.4 m per event) occur approximately every 60,000 to 10,000 years. No earthquakes comparable in size to the inferred Quaternary earthquakes have been recorded anywhere in Colorado in historic time (Hadsell 1968). Furthermore, not even minor shocks have been detected from either fault zone in the 110 years of recorded history. Geologic evidence indicates that large fault events with long recurrence intervals may be the normal style of tectonic activity in this part of the Rio Grande Rift Zone.

SYNTHESIS AND CONCLUSIONS

This study describes in detail the Quaternary geology of a 2000 km^2 area in the Rio Grande Rift Zone of south-central Colorado. Glacial moraines of the northern Sangre de Cristo Mountains and alluvial fans of the adjacent San Luis Valley formed in response to Quaternary climate fluctuations. During and after their deposition, earthquakes originating on rift faults offset the deposits and formed prominent fault scarps which are visible today. Detailed surficial geologic mapping and measurement of 153 scarp profiles over the 120-km-long fault zone in this study represent a pioneering attempt to use Quaternary geologic techniques for reconstructing the tectonic history of a structurally important area.

Quaternary Deposit

Judging by distribution, morphology, and surface clast weathering characteristics, Quaternary deposits of the west flank of the Sangre de Cristo Mountains fall into five distinct groups. Highly dissected and weathered remnants of alluvial fans near the range front, commonly fault-bounded, date from pre-Bull Lake time. Slightly less weathered, less dissected areas of alluvium near the range front date from Bull Lake time, and are correlated by means of physical continuity and weathering characteristics with subdued, eroded Bull Lake moraines in the lower parts of glacial valleys. Large symmetrical alluvial fans of early Pinedale age dominate the alluvial slope fronting the Sangre de Cristo Range and are traceable to massive, youthful early Pinedale terminal moraines at the mouths of several valleys. Extensive, more youthful fan surfaces adjacent to early Pinedale fans resulted from mid-late Pinedale outwash deposition, when multiple nested moraines were forming behind massive terminals, and farther up valley as Pinedale ice retreated into cirques. Small areas flanking present drainage channels are composed of Holocene alluvium. Although no direct connection exists now, much of this alluvium is probably contemporary with early Neoglacial moraines and rock glaciers that record a small post-Pinedale ice advance in cirques.

Relative-dating (RD) parameters collected at 75 stations on the crests of moraines and on rock glaciers quantitatively define the local relative-age groupings of deposits as described above. Of the 15 RD parameters measured at each station, moraine crest width, average and maximum weathering rind thickness, and percentage of stones with rinds yielded the most consistent separation of age groups. RD parameters that measure percentages ("percent-limited") commonly have values near the absolute limit of 100 percent and the range of values is "telescoped." RD parameters that measure physical dimensions of objects ("unlimited") suffer no such constraints, and commonly the magnitude of absolute and relative differences between these parameters for various age groups is larger than for percent-limited parameters. In addition, differences in elevation and lithology strongly affect RD parameters. Rock glaciers and recessional moraines at high elevations (3400-3700 m) commonly display equivalent or *greater* surface clast oxidation, pitting and weathering rind thickness, than do much *older* terminal deposits at valley mouths (2900-3100 m). An increase of precipitation and available moisture at higher elevations may be responsible for this phenomenon, suggesting that surface clast weathering is dependent on hydration as well as oxidation processes (as suggested by Birkeland and others 1979a). Clast weathering is also more advanced on Precambrian hornblende gneisses of the southern segment than on Upper Paleozoic sandstones of the northern segment, on glacial deposits of equivalent age. Values for maximum and average weathering rind thickness and percentage of stones with rinds show the most difference. The larger percentge of mafic minerals susceptible to chemical weathering

in the gneisses as opposed to the sandstones probably causes the difference in rate of rind formation; however, differences in local climate between the northern (cooler, wetter) and the southern (warmer, drier) segments may also play a part. Importantly, morphologic RD parameters such as moraine crest width and slope angles do not seem to be affected by variations in elevation or lithology and therefore can be used as true relative-age indications across a wide range of topographic and geographic situations.

Comparison of RD data from Quaternary deposits of the Sangre de Cristo Mountains with data from Quaternary sequences elsewhere in the Rocky Mountains (e.g., Richmond 1962, 1965; Pierce and others 1976) indicates a rough equivalence in number of age subdivisions and in absolute RD values. Due to differences in lithology and climate between this study area and those areas previously studied, RD values do not match exactly. However, the magnitude of RD differences between deposits of different age is similar in this area to that in other areas. Comparison of weathering rind and moraine slope angle data between the Sangre de Cristo Range (this study) and the Sierra Nevada (Burke and Birkeland 1979) shows that the difference between Bull Lake and Pinedale deposits is almost identical to that between the Tahoe and Tioga deposits, respectively. Rinds are slightly thicker and more abundant, and slope angles are slightly lower for the Sange de Cristo deposits in both age groups, suggesting that the rock type of the Sangre de Cristo is more susceptible to both chemical and physical weathering processes than is that of the Sierra Nevada. Because the RD-based correlation of local deposits with other deposits is so good, limiting dates on deposits from throughout the Rocky Mountains and Sierra Nevada are inferred to apply to the local sequence as well. Five ^{14}C dates collected locally are consistent with the composite Quaternary chronology (modified from Blackwelder 1915, and Richmond 1965), and further support correlation.

NEOTECTONICS

To determine the neotectonic history of the Sangre de Cristo Range, well-preserved fault scarps offsetting Quaternary deposits were studied intensively. Two independent lines of evidence were brought to bear on scarp age and history: (1) the interaction of scarps with dated Quaternary glacial and alluvial deposits described previously, and (2) the age-dependent features of scarp morphology as revealed by detailed surface profiling. Conceptual block diagrams of scarps offsetting multiple Quaternary surfaces show that each temporal permutation of offset, erosion, and deposition results in a unique scarp-terrace geometry. Because the absolute age of Quaternary depositional terraces can be estimated, the relative and absolute timing of faulting can be deduced from scarp-terrace geometry. Scarp morphologic analyses (in particular, the maximum scarp slope angle-scarp height relation) were performed on 153 detailed profiles of scarps. When compared to similar slope angle-scarp height data for other dated scarps, resulting scarp age estimates are consistent with those derived from scarp-terrace geometry. However, two complications are noted to the unrestricted use of the slope angle-scarp height relation for scarp age estimation. First, multiple-event scarps offsetting old Quaternary deposits are steeper for equivalent heights than are old single-event scarps across the same deposits, due to the rejuvenating effect of repeated faulting. Secondly, scarps of a given age and height offsetting coarser gravels have steeper maximum scarp slope angles than do identical scarps offsetting finer material. Therefore the slope angle-scarp height relation as proposed by Bucknam and Anderson (1979) can be used for age estimation only when either single- or multiple-event scarps are compared, and when deposit texture is more or less uniform on all measured scarps.

A simple displacement on a fault at depth can be translated into varying styles and sizes of fault scarps at the surface. As each of these scarp types degrade with time, scarp morphology changes further. In order to examine variations in true fault displacement along the length of a fault, one must "go back in time" and remove the complicating effects of scarp degradation and complex styles of surface faulting. This has been accomplished herein by development of geometric models based on trigonometric identities which give unique solutions for original fault displacement given present scarp morphology. Once all fault scarp height measurements are converted to fault displacement (throw) values, uplift vectors can be compared in both time and space on the major fault zones. The geometric method developed herein is a potentially powerful tool for differentiating zones of neotectonic uplift activity on different faults, or on different segments of a single fault.

Evidence from scarp-terrace geometry, scarp morphology, and from five trenches excavated through fault scarps reveals a wealth of data on the neotectonics of the Sangre de Cristo Mountains. On the Villa Grove Fault Zone scarps with present heights of 0.3 to 14.0 m have resulted from inferred fault offsets of 0.8-1.4 m occurring roughly every 60,000-100,000 years in the last 400,000 years. The last such event offsets mid-late Pinedale alluvium and thus post-dates about 13,000 years B.P. On the Sangre de Cristo Fault Zone scarps with present heights of 2 to 87 m have resulted from fault offsets of 1.2 to 2.9 m recurring about every 10,000-50,000 years since at least mid-Pleistocene time. Two recent events are well-controlled by ^{14}C dates and occurred: (1) between 13,000 and 10,100 $\pm$ years B.P.; and (2) shortly before 7660 $\pm$ 120 years B.P. Recurrent Holocene movement such as that documented for the SCFZ has been previously reported (Kirkham and Rogers 1978) and marks the SCFZ as one of the few faults that could be considered "active" in the state.

The amount of displacement attributable to individual fault events, and the length of surface rupture on the two fault zones, suggest (by analogy to historic scarp-producing earthquakes) that earthquakes of magnitude (M_L) 6.8 to 7.4 have typified the SCFZ. Smaller earthquakes *may* have also occurred in Quaternary time that did not result in surface rupture, but no geologic evidence remains of any such events. Field evidence from trenches strongly suggests that scarps result from episodic, discrete faulting events and that slow aseismic fault creep has played little or no part in their formation.

No earthquakes have occurred in the study area in its 110-year recorded history (Hadsell 1968; Simon 1969). Empirical earthquake frequency-magnitude relations derived from historic earthquakes (Richter 1958) indicate that, if M_L 7.0 earthquakes have recurrence intervals of 10,000-50,000 years on the SCFZ, then we should expect to have experienced earthquakes up to M_L 4.6 in the period 1870-1980. Because no such events have occurred, it is possible that the standard frequency-magnitude relations do not hold for the SCFZ. Instead, large earthquakes with large recurrence intervals may be separated by long tectonically quiescent periods without the occurrence of frequent small-to-medium-magnitude earthquakes. Similar fault behavior has been attributed to other Basin and Range faults in Nevada by Ryall (1976), and may be the tectonic style typical of such faults.

The current tectonic regime of the Sangre de Cristo Mountains is undoubtedly influenced by extensional normal faulting associated with Rio Grande rifting (Tweto 1979). Faceted spurs at the range front indicate that rapid uplift began in Late Tertiary (Pliocene?) time, after a long period of slow uplift represented by gently sloping, accordant ridge crests. Three periods of rapid uplift, interspersed with slower uplift, have occurred since facet formation began . The well-preserved fault scarps in alluvium studied in this report are evidence that the lowest facet set represents the latest rapid uplift episode. However, uplift rates deduced from Quaternary scarps are generally lower than average long-term uplift rates prevailing since the beginning of Rio Grande Rift formation (approximately 7000 m in 26 m.y.). It therefore appears that, at least since about 400,000 years B.P., uplift of the Sangre de Cristo Mountains has slowed and that we are presently in a period of *relative* tectonic quiescence. This accords with observations farther south in the rift zone (Chapin and Seager 1975).

Several intriguing lines of inquiry remain in the study area. One deals with the problem of Early Tertiary continental sediments accumulating in the San Luis Basin 10 to 20 million years *before* the supposed inception of rift valley development about 26 m.y. (Lipman and Mehnert 1975). If these sediments accumulated in early rift basins then inception of rifting may be pushed back to Eocene or to Paleocene time, as suggested by Tweto (1979). Another speculation concerns the possible effect of Pleistocene climatic fluctuations on earthquake activity. The weight of glacier ice on the Sangre de Cristo horst might have retarded uplift of the block, whereas rising pluvial groundwater levels in the San Luis graben may have increased pore pressures and promoted fault slippage. The two questions outlined above pertain not only to the Rio Grande Rift Zone, but to the Basin and Range Province as a whole.

Finally, the methods of neotectonic reconstruction used in this study might profitably be applied wherever a distinct sequence of Quaternary deposits occur. Where independent evidence of deposit or scarp age is not available, scarp-terrace geometry and scarp morphology can still give evidence of local relative-age histories of faulting, erosion, and deposition. If paleotectonic reconstruction is desired, then reduction of scarp height data to fault throw values as described herein is desirable. Application of these geometric techniques to fault scarp sets in the western United States (as in Swan and others 1981) and elsewhere in the world may yield invaluable (and perhaps surprising) new data on the Quaternary tectonic history of many diverse terrains.

REFERENCES

Allen, C.R., 1975, Geological criteria for evaluating seismicity: Geological Society of America Bulletin, volume 86, pages 1041-1057.

Anderson, L.W., 1978, Late Quaternary chronology of the Fourth of July cirque, Front Range, Colorado: Geological Society of America, Abstracts with Programs, volume 10, number 4, page 209.

Atwood, W.W., 1940, The physiographic provinces of North America: Ginn and Company, Boston, 536 pages.

Benedict, J.B., 1973, Chronology of cirque glaciation, Colorado Front Range: Quaternary Research, volume 3, number 4, pages 584-599.

Birkeland, P.W., 1973, Use of relative-age dating methods in a stratigraphic study of rock glacier deposits, Mount Sopris, Colorado: Arctic and Alpine Research, volume 5, number 4, pages 401-416.

—— 1974, Pedology, weathering, and geomorphological research: Oxford Press, London, 285 pages.

Birkeland, P.W., Burke, R.M., and Walker, A.L., 1979a, Variation in chemical parameters of Quaternary soils with time and altitude, Sierra Nevada, California: Geological Society of America, Abstracts with Programs, volume 11, number 7, page 388.

Birkeland, P.W., Colman, S.M., Burke, R.M., Shroba, R.R., and Meierding, T.C., 1979b, Nomenclature of alpine glacial deposits, or what's in a name?: Geology, volume 7, number 11, pages 401-406.

Blackwelder, Eliot, 1915, Post-Cretaceous history of the mountains of central western Wyoming: Journal of Geology, volume 23, pages 307-340.

Bonilla, M.G., and Buchanan, J.M., 1970, Interim report on worldwide historic surface faulting: U.S. Geological Survey, Open-File Report, 32 pages.

Bryan, Kirk, 1938, Geology and ground-water conditions in Rio Grande depression in Colorado and New Mexico, *in* Regional Planning, Part 6, Rio Grande Joint Investigation in the Upper Rio Grande Basin, volume I, section 1, pages 197-225. National Research Commission, Washington, D.C.

Bucknam, R.C., and Anderson, R.E., 1979, Estimation of fault-scarp ages from a scarp-height-slope-angle relationship: Geology, volume 7, pages 11-14.

Burbank, W.S., and Goddard, E.N., 1937, Thrusting in Huerfano Park, Colorado, and related problems of orogeny in the Sangre de Cristo Mountains: Geological Society of America Bulletin, volume 48, number 7, pages 931-976.

Burke, R.M., and Birkeland, P.W., 1979, Reevaluation of multiparameter relative dating techniques and their application to the glacial sequence along the eastern escarpment of the Sierra Nevada, California: Quaternary Research, volume 11, number 1, pages 21-51.

Chapin, C.E., and Seager, W.R., 1975, Evolution of the Rio Grande Rift in the Socorro and Las Cruces area: New Mexico Geological Society, 26th Field Conference Guidebook, pages 297-321.

Church, Michael, 1972, Baffin Island sandurs: a study of arctic fluvial processes: Geological Survey of Canada Bulletin, number 216, 208 pages.

Clement, Jean M., 1952, The geology of the northeastern Baca Grant area, Saguache County, Colorado: M.S. thesis, Colorado School of Mines, Golden.

Colman, S.M., McCalpin, J.P., and Ostenaa, D.A., 1981, Morphology of fault scarps in the Rio Grande Rift, Colorado, as an indicator of age of faulting (abs.). Seismic Hazards in Colorado—A Symposium. Association of Engineering Geologists, Denver.

Cooke, R.V., and Warren, Andrew, 1973, Geomorphology in deserts: University of California Press, Berkeley, 394 pages.

Currey, D.R., 1974, Probable pre-Neoglacial age of the type Temple Lake moraine, Wyoming: Arctic and Alpine Research, volume 6, number 3, pages 293-300.

—— 1980, Events associated with the last cycle of Lake Bonneville-Idaho, Nevada, and Utah: American Quaternary Association, 6th Biennial Meeting, Abstracts, page 59.

Davis, L., and Stoughton, Dean, 1979, Interpretation of seismic reflection data from the northern San Luis Valley, south-central Colorado, *in* Riecker, R.E., ed., Rio Grande Rift: Tectonics and Magmatism, pages 185-194. American Geophysical Union, Washington, D.C.

DeVoto, R.H., Peel, F., and Pierce, W.H., 1971, Pennsylvanian and Permian stratigraphy, tectonism, and history, northern Sangre de Cristo Range, Colorado, *in* James, H.L., ed., Guidebook to the San Luis Basin, Colorado, pages 141-163, New Mexico Geological Society, 22nd Field Conference Guidebook.

Dixon, H.N., 1971, Flora of the San Luis Valley, *in* James, H.L., ed., Guidebook to the San Luis Basin, Colorado, pages 133-135. New Mexico Geological Society, 22nd Field Conference.

Embleton, C., and King, C.A.M., 1975, Glacial geomorphology, 2nd edition: John Wiley and Sons, New York, 573 pages.

Epis, R.C., Scott, G.R., Taylor, R.B., and Chapin, C.E., 1976, Cenozoic volcanic, tectonic, and geomorphic features of central Colorado, *in* Professional Contributions of the Colorado School of Mines, number 8, pages 323-338, Colorado School of Mines Press, Golden.

Freeze, R.A., and Cherry, J.A., 1979, Groundwater: Prentice-Hall, Englewood Cliffs, New Jersey, 604 pages.

Gableman, J.W., 1952, Structure and origin of the northern Sangre de Cristo Range, Colorado: American Association of Petroleum Geologists Bulletin, volume 36, number 8, pages 1574-1612.

Gaca, J.R., and Karig, D.E., 1966, Gravity survey of the San Luis Valley area, Colorado: U.S. Geological Survey Open-File Report, 21 pages.

Gianella, V.P., and Callaghan, E., 1934, The Cedar Mountain, Nevada earthquake of December 20, 1934: Bulletin of the Seismological Society of America, volume 24, pages 367-384.

Gilbert, G.K., 1890, Lake Bonneville: U.S. Geological Survey Monograph number 1.

Gile, L.H., Peterson, F.F., and Grossman, R.B., 1966, Morphological and genetic sequences of carbonate accumulation in desert soils: Soil Science, volume 101, pages 347-360.

Hadsell, F.A., 1968, History of earthquake activity in Colorado: Colorado School of Mines Quarterly, volume 63, number 1, pages 57-72.

Hamblin, W.K., and Best, M.G., 1978, Patterns and rates of recurrent movement along the Wasatch-Hurricane-Sevier Fault Zone, Utah, during late Cenozoic time: U.S. Geological Survey, National Earthquake Hazards Reduction Program, Summaries of Technical Reports, volume V, pages 70-71.

Hawley, J.W., ed., 1978, Guidebook to the Rio Grande Rift: New Mexico Bureau of Mines and Mineral Resources, Circular 163.

Hoffman, J.P., 1975, The seismic history of the Rio Grande Rift: U.S. Geological Survey Earthquake Information Bulletin, volume 7, number 3, pages 8-13.

Holzer, T.L., 1977, Active surface faulting caused by groundwater extraction near Picacho, Arizona: Geological Society of America, Abstracts with Programs, volume 9, number 4, page 437.

Holzer, T.L., Davis, S.N., and Lofgren, B.E., 1979, Faulting caused by ground-water extraction in south-central Arizona: Journal of Geophysical Research, volume 84, number B2, pages 603-612.

Huntley, David, 1977, Ground-water recharge to the aquifers of the northern San Luis Valley: a remote-sensing investigation: Ph.D. dissertation, Colorado School of Mines, Golden.

——— 1979, Cenozoic faulting and sedimentation in northern San Luis Valley, Colorado: Geological Society of America Bulletin, volume 90, number 1, part 1, pages 8-10.

Hurst, C.T., 1941, A Folsom location in the San Luis Valley, Colorado: Southwestern Lore, volume 7, number 2, pages 31-34.

Jaksha, L.H., Locke, J., and Gebhart, H.J., 1981, Microearthquakes near the Albuquerque volcanoes, New Mexico: Geological Society of America Bulletin, volume 92, part 1, pages 31-36.

Johnson, R.B., 1967, The Great Sand Dunes of southern Colorado: U.S. Geological Survey Professional Paper 575-C, C117-C183.

Jones, J.C., 1915, The Pleasant Valley, Nevada, earthquake of October 2, 1915: Bulletin of the Seismological Society of America, volume 5, pages 190-205.

Jordan, M., 1974, Geothermal investigations in the San Luis Valley, south-central Colorado: M.S. thesis, Colorado School of Mines, Golden.

Karig, D.E., 1964, Structural analysis of the Sangre de Cristo Range, Venable Peak to Crestone Peak, Custer and Saguache Counties, Colorado: M.S. thesis, Colorado School of Mines, Golden.

Keller, G.R., and Adams, H.E., 1976, A reconnaissance micro-earthquake survey of the San Luis Valley, southern Colorado: Bulletin of the Seismological Society of America, volume 66, pages 345-347.

Kirkham, R.M., and Rogers, W.P., 1978, Earthquake potential in Colorado: Colorado Geological Survey, Open-File Report 78-3, 196 pages.

Knepper, D.H., Jr., 1974, Tectonic analysis of the Rio Grande Rift Zone, central Colorado: Ph.D. dissertation, Colorado School of Mines, Golden.

Koch, R.W., 1963, Geology of the Venable Peak area, Sangre de Cristo Mountains, Colorado: M.S. thesis, Colorado School of Mines, Golden.

Lineback, A., and Wickham, T., 1978, Is the Illinoian a super stage? Geological Society of America, Abstracts with Programs, volume 10, number 3, page 445.

Lipman, P.W., and Mehnert, H.H., 1975, Late Cenozoic basaltic volcanism and development of the Rio Grande depression in the Southern Rocky Mountains: Geological Society of America Memoir 144, pages 119-154.

Litsey, L.R., 1954, Geology of the Hayden Pass-Orient area, Sangre de Cristo Mountains, Custer, Fremont, and Saguache Counties, Colorado: Ph.D. dissertation, University of Colorado, Boulder.

Madsen, D.B., and Currey, D.R., 1979, Late Quaternary glacial and vegetation changes, Little Cottonwood Canyon area, Wasatch Mountains, Utah: Quaternary Research, volume 12, number 2, pages 254-270.

Mahaney, W.C., 1973, Neoglacial chronology in the Fourth of July cirque, central Colorado Front Range: Geological Society of America Bulletin, volume 84, pages 161-170.

Marchand, D.E. and Harden, Jennifer, 1976, Soil chronosequences, northeastern San Joaquin Valley, California: American Quaternary Association, 4th Biennial Meeting, Abstracts, page 110.

Mark, R.K., and Bonilla, M.G., 1977, Regression analysis of earthquake magnitude and surface fault length using the 1970 data of Bonilla and Buchanan: U.S. Geological Survey Open-File Report 77-614, 8 pages.

McCalpin, James, 1981, Quaternary geology and neotectonics of the west flank of the northern Sangre de Cristo Mountains, south-central Colorado: Ph.D. dissertation, Colorado School of Mines, Golden.

Merriam, C.H., 1898, Life zones and crop zones of the United States: U.S. Department of Agriculture, Division of Biological Survey, Bulletin 10, 79 pages.

Miller, C.D., 1971, Quaternary glacial events in the northern Sawatch Range, Colorado: Ph.D. dissertation, University of Colorado, Boulder.

Morris, S.E., 1979, Holocene periglacial facies—a model of location, relative development, and environmental history, Blanca Massif, southern Colorado: M.A. thesis, University of Iowa, Iowa City.

Munger, R.D., 1959, Geology of the Spread Eagle Peak area, Sangre de Cristo Mountains, Saguache and Custer Counties, Colorado: M.S. thesis, University of Colorado, Boulder.

Nelson, A.R., 1976, Late Quaternary glacial chronology in the Upper Fraser Valley, Grand County, Colorado: Geological Society of America, Abstracts with Programs, volume 8, number 5, page 614.

Nolting, R.M., 1970, Pennsylvanian-Permian stratigraphy and structural geology of the Orient-Cotton Creek area, Sangre de Cristo Mountains, Colorado: M.S. thesis, Colorado School of Mines, Golden.

Page, B.M., 1934, Basin-range faulting of 1915 in Pleasant Valley, Nevada: Journal of Geology, volume 43, pages 690-707.

Pearl, R.J., and Barrett, J.K., 1976, Geothermal resources of the Upper San Luis and Arkansas valleys, Colorado, *in* Epis, R.C., and Weimer, R.J., eds., Studies in Colorado Field Geology, pages 439-445. Professional Contributions of the Colorado School of Mines, number 8, Colorado School of Mines Press, Golden.

Peterson, R.E., 1979, Tectonic geomorphology of the northern Sangre de Cristo Mountains near Villa Grove, Colorado: M.S. thesis, University of Arizona, Tucson.

Pierce, K.L., Obradovich, J.D., and Friedman, I., 1976, Obsidian hydration dating and correlation of Bull Lake and Pinedale glaciations near West Yellowstone, Montana: Geological Society of America Bulletin, volume 87, number 5, pages 703-710.

Powell, W.J., 1958, Ground water resources of the San Luis Valley,

Colorado: U.S. Geological Survey Water Supply Paper 1379, 284 pages.
Presgrave, B.W., 1979, Seismicity of Colorado from instrumental data: M.S. thesis, Colorado School of Mines, Golden.
Richmond, G.M., 1960, Glaciation of the east slope of Rocky Mountain National Park, Colorado: Geological Society of America Bulletin, volume 71, pages 1371-1382.
——1962, Quaternary stratigraphy of the La Sal Mountains, Utah: U.S. Geological Survey Professional Paper 324, 135 pages.
——1965, Glaciation of the Rocky Mountains, *in* Wright, H.E., and Frey, D.G., eds., The Quaternary of the United States, Princeton University Press, Princeton, New Jersey, pages 217-230.
——1972, Appraisal of the future climate of the Holocene in the Rocky Mountains: Quaternary Research, volume 2, number 3, pages 315-322.
Richmond, G.M., and Obradovich, J.D., 1972, Radiometric correlation of some continental Quaternary deposits—a review: American Quaternary Association, 2nd Biennial Meeting, Abstracts, pages 47-49.
Richter, C.F, 1958: Elementary seismology, W.H. Freeman, San Francisco, California.
Riecker, R.E., ed., 1979, Rio Grande Rift: tectonics and magmatism: American Geophysical Union, Washington, D.C., 438 pages.
Roy, W.R., and Hall, R.D., 1980, Re-evaluation of the Bull Lake glaciation through restudy of the type locality and study of other localities: Geological Society of America, Abstracts with Programs, volume 12, number 6, page 302.
Ryall, Alan, 1977, Earthquake hazard in the Nevada region: Bulletin of the Seismological Society of America, volume 67, number 2, pages 517-532.
Schumm, S.A., 1965, Quaternary paleohydrology, *in* Wright, H.E., and Frey, D.G., eds., The Quaternary of the United States, Princeton University Press, Princeton, New Jersey, pages 783-794.
Scott, G.R., 1970, Quaternary faulting and potential earthquakes in east-central Colorado: U.S. Geological Survey Professional Paper 700-C, C11-C18.
Scott, G.R., and Taylor, R.B., 1975, Post-Paleocene Tertiary rocks and Quaternary volcanic ash of the Wet Mountain Valley, Colorado: U.S. Geological Survey Professional Paper 868, 15 pages.
Scott, G.R., Taylor, R.B., Epis, R.C., and Wobus, R.A., 1976, Geologic map of the Pueblo 1° by 2° quadrangle, south-central Colorado: U.S. Geological Survey Map MF-775, volume 1, pages 187, 500.
Scott, W.E., McCoy, W.D., Shroba, R.R., and Miller, R.D., 1980, New interpretations of the Late Quaternary history of Lake Bonneville, western United States: American Quaternary Association, 6th Biennial Meeting, Abstracts, pages 168-169.
Siebenthal, C.E., 1907, Notes on the glaciation of the Sangre de Cristo Range, Colorado: Journal of Geology, volume 15, pages 15-22.
——1910, Geology and water resources of the San Luis Valley, Colorado: U.S. Geological Survey Water Supply Paper 240, 128 pages.
Simon, R.B., 1969, Seismicity of Colorado: consistency of recent earthquakes with those of historical record: Science, volume 165, number 3896, pages 897-899.
Slemmons, D.B., 1957, Geological effects of the Dixie Valley-Fairview Peak, Nevada, earthquakes of December 16, 1954: Seismological Society of America Bulletin, volume 47, number 4, pages 353-375.
Soil Survey Staff, 1975, Soil taxonomy: a basic system of soil classification for making and interpreting soil surveys: U.S. Department of Agriculture, Agricultural Handbook number 436, 754 pages.
Speight, J.G., 1963, Late glacial historical geomorphology of the Lake Pukaki area, New Zealand: New Zealand Journal of Geology and Geophysics, volume 6, pages 160-188.
Sterr, H.M., 1980, Seismotectonic history and morphological evolution of Late Quaternary fault scarps in southwestern Utah: Ph.D. dissertation, University of Colorado, Boulder.
Stoughton, Dean, 1977, Interpretation of seismic reflection data from the San Luis Valley, south-central Colorado: M.S. thesis, Colorado School of Mines, Golden.
Swan, F.H., III, Schwartz, D.P., and Cluff, L.S., 1980, Recurrence of moderate-to-large magnitude earthquakes produced by surface faulting on the Wasatch Fault Zone, Utah: Bulletin of the Seismological Society of America, volume 70, number 5, pages 1431-1462.
Taylor, R.B., 1975, Neogene tectonism in south-central Colorado, *in* Curtis, B.F., ed., Cenozoic history of the Southern Rocky Mountains: Geological Society of America Memoir 144, pages 211-216.
Tocher, Don, 1956, Movement on the Rainbow Mountain fault: Bulletin of the Seismological Society of America, volume 465, pages 10-14.
Toulmin, P., III, 1953, Petrography and petrology of the Rito Alsto Stock, Custer and Saguache Counties, Colorado: M.S. thesis, University of Colorado, Boulder.
Tweto, O.L., 1964, Geology, *in* Mineral and water resources of Colorado, U.S. 88th Congress, 2nd Session, Committee print, pages 11-27.
——1979, The Rio Grande Rift System in Colorado, *in* Riecker, R.E., ed., Rio Grande Rift: tectonics and magmatism: American Geophysical Union, Washington, D.C., pages 33-56.
Upson, J.E., 1938, Late Tertiary and Quaternary faulting in the San Luis Valley, Colorado: Geological Society of America, Abstracts, pages 316-317.
——1939, Physiographic subdivisions of the San Luis Valley, southern Colorado: Journal of Geology, volume 47, pages 721-736.
——1941, The Vallejo Formation: new Early Tertiary red-beds in southern Colorado: American Journal of Science, volume 239, number 8, pages 577-589.
Volckmann, R.P., 1965, Geology of the Crestone Peak area, Sangre de Cristo Range, Colorado: Ph.D. dissertation, University of Michigan, Ann Arbor.
Von Hake, C.A., 1975, Earthquake history of New Mexico: U.S. Geological Survey Earthquake Information Bulletin, volume 7, number 3, pages 23-26.
Wallace, R.E., 1977, Profiles and ages of young fault scarps, north-central Nevada: Geological Society of America Bulletin, volume 88, pages 1267-1281.
——1978, Geometry and rates of change of fault-generated range fronts, north-central Nevada: U.S. Geological Survey, Journal of Research, volume 6, number 5, pages 637-650.
West, M.W., 1978, Quaternary geology and reported surface faulting along east flank of Gore Range, Summit County, Colorado: Colorado School of Mines Quarterly, volume 73, number 2, pages 1-66.
Wychgram, D.C., 1972, Geology of the Hayden Pass-Orient Mine area, northern Sangre de Cristo Mountains, Colorado: a geologic remote sensing evaluation: M.S. thesis, Colorado School of Mines, Golden.

APPENDIX A

Appendix A.—Soil Profile Symbols and Abbreviations.

textural B horizon

A horizon	
color B horizon	
weak, subangular blocky (sbk) structure	wk weak
moderate subangular blocky structure	mod moderate
strong subangular blocky to prismatic structure	str strong
Stage I carbonate (discontinuous coats on stone bottoms)	f fine
Stage I-II carbonate (continuous coats on stone bottoms)	med medium
Stage II carbonate (continuous coats on stone bottoms and sides; carbonate blebs in matrix)	cse coarse
Stage III-III+ carbonate (matrix engulfed by carbonate; laminar structure)	sbk subangular blocky
	abk angular blocky

APPENDIX B

Appendix B.—Fault scarp measurements VGFZ.

Scarp Profile Number[a]	Maximum Scarp Slope Angle (deg)	Ambient Fan Surface Slope (deg)	Scarp Height h_2 (m)	Surface Offset (m)	Width of Crest (m)	Retreat of Crest (m)	Clast Diagram Max. (cm)	Clast Diagram Av. (cm)	Age[b]
A1	23.0	6.5	6.1	3.0	13.0	1.0	65	17.5	P
A2	27.5	2.5	7.2	5.2	3.5	0.5	50	15	P
A4	22.0	4.5	7.3	4.8	5.5	6.5	55	16	P
A5	23.0	4.0	6.5	3.8	3.5	9.0	55	17.5	P
A6	20.5	6.0	6.8	3.5	7.5	13.5	70	22.5	P
A7	18.5	5.0	4.4	2.6	7.5	5.2	65	17.5	B
A8	19.0	7.5	8.0	4.2	7.5	14.5	35	16	B
A9	23.0	6.0	11.3	7.0	11.0	10.5	35	16	B
A10	22.0	6.0	9.6	6.8	12.0	6.5	—	—	B
A11	27.0	4.0	8.2	6.0	9.5	11.5	95	22.5	B
A12	21.0	5.0	6.6	5.0	7.5	6.0	40	18.5	B
A13	14.0	4.5	3.6	2.3	7.2	13.5	40	13.5	B
A14	16.5	4.0	3.0	2.0	6.6	6.3	35	16	? B
A15	7.0	4.0		1.1					
B1	10.0	7.5		1.0			35	11	B
B2	18.5	7.0	3.7	2.1	6.6	9.2	40	16	B
B3	19.0	7.0	3.4	2.5	7.4	6.1	45	17.5	B
B4	22.5	4.5	11.2	7.6	14.0	25.0	60	17.5	pB
C1	16.5	5.0	4.0	2.6	6.5	4.5	110	30	B
C2	13.0	5.0	1.4	0.8	2.5	4.5	100	32.5	B
D1	8.0	5.0	1.1	0.4	4.0	1.8	35	15	B
D2	11.0	5.0	1.3	0.6	2.5	2.0	55	22.5	B
E1	14.0	4.5	4.5	3.5	2.0	1.2	25	12.5	B
E2a	20.0	4.0	2.0	1.3	5.5	2.0	110	45	B
E2b	12.0	4.0	2.1	1.0	6.5	6.5	35	13.5	B
E3	17.0	4.5	2.8	1.8	3.2	1.1	55	25	B
E4	13.0	4.5	1.3	0.8	2.4	1.7	30	17.5	P

E5	14.0	5.0	2.8	1.8	5.5	6.0	45	18.5	B
E6		5.0		1.1					
F1	16.5	5.0	2.2	1.4	3.5	2.0	30	12.5	P
F2	14.5	4.0	1.9	1.2	6.5	5.2	55	22.5	B
G1	15.5	3.5	3.1	1.8	9.0	6.5	35	12.5	B
G2	15.0	3.0	2.5	1.9	5.5	3.5	30	11	B
G3	13.0	2.0	2.6	1.7			130	25	B
G4u	13.5	3.0	5.1	4.3	8.5	3.5	100	17.5	pB
G4l	6.0	3.0	1.7	1.2	6.0	6.0	—	—	pB
G5	12.0	3.0	2.6	1.7	4.5	5.0	75	20	B
G6	12.0	1.5	4.5	4.0	7.0	11.5	75	25	pB
G7	12.0	3.0	2.3	1.0	7.0	3.5	30	16	B
G8	18.0	2.5		2.0					
H1	10.0	3.0	1.5	0.8	5.5	4.5	90	22.5	B
H2	10.0	2.5		1.8					B
K1	4.5	1.0	0.4	0.3			25	12.5	B
K2	9.5	1.0	2.2	1.6			40	15	B
K3	18.5	3.0	2.6	1.6	4.4	0.5	30	12	B
K4	18.0	2.0	4.1	3.0	8.0	7.5	45	16	B
K5	11.5	3.0	1.5	0.8	0.7	1.0	60	13.5	B
K'6	5.5	−2.0	0.4	0.3			35	13.5	B
K7	10.0	2.0		1.4					B
L1	7.0	4.5	2.0	0.6	12.0	15.5	50	11	B
L2u	13.5	−1.0	2.6	2.2	9.5	0.5	75	18.5	B
L2l	8.5	2.5	1.3	0.7	2.0	0.5	75	18.5	B
L3	10.0	3.0		1.6					B
M1	6.0	−1.0	0.7	0.6	6.5	3.5	30	13.5	B
M2	3.0	−2.0	0.2	0.3	4.5	1.0	25	11	B
O1	9.0	3.0	0.8	0.4	5.5	7.5	45	17.5	B
O2	12.0	3.0	4.8	3.1	5.5	3.0	65	17.5	pB
R1	7.5	3.0	1.2	0.6	6.0	1.5	35	13.5	B
S1u	16.5	4.0	3.6	2.6	8.5	7.0	35	16	B
S1l	10.0	3.0	1.3	0.8	6.0	1.0	55	20	B
S2u	5.0	3.0	1.5	0.4	12.0	9.5	45	15	pB
S2l	9.0	3.0	3.6	2.6	21.0	23.0	35	12.5	pB
Z1	6.5	3.5	1.7	0.4	12.5	20.5	140	20	B

[a] Identified in figure 50.
[b] Age of offset alluvium: P is Pinedale, B is Bull Lake, pB is pre-Bull Lake.

APPENDIX C

Appendix C.—Fault scarp measurements, SCFZ.

Scarp Profile Number[a]	Maximum Scarp Slope Angle (deg)	Ambient Fan Surface Slope (deg)	Scarp Height h_2 (m)	Surface Offset (m)	Width of Crest (m)	Retreat of Crest (m)	Clast Diameter Max. (cm)	Clast Diameter Av. (cm)	Age[b]	Calculated Fault Throw[c] (m)	Scarp Type[d]
1	19.5	9.0	3.0	2.0	7.0	9.2	70	22.5	B	2.1	S
2	21.0	8.0	8.0	5.3	15.5	8.5	120	35	B	5.9	S
3	28.0	9.0	8.4	5.5	6.2	1.1	450	60	P_1	8.7	S
4	21.5	5.5	3.3	2.8	5.0	5.7	180	40	$P_{1.5}$	3.9	S
5	25.0	7.0	5.9	4.7	8.0	4.0	150	40	P_1	6.5	S
6	21.5	7.0	3.7	2.7	4.0	4.2	280	35	$P_{1.5}$	3.8	S
7	32.0	7.0		81.2	3.0	22.5	400	32.5	pB	85.1	S
8	25.0	8.0	4.0	2.8	4.5	5.0	200	35	P	5.5	S
9	21.0	7.0	2.3	1.6	4.0	4.2	120	25	H	2.3	S
10	20.0	8.0	4.4	2.8	7.5	9.0	90	20	B	5.3	S
11	20.5	6.5	10.7	7.2	3.5	24.5	300	20	pB	14.0	S
12	34.0	7.0	4.0	3.4	5.5	4.0	120	55	P	2.3	Cg
13	20.0	6.0	6.1	4.2	6.0	14.2	120	25	B	4.2	S
14u	23.0	9.0	5.0	3.1	8.0	2.5	65	25	B	3.6	Csf
14l	13.0	8.5	1.2	0.5	3.0	4.0	65	25	B		Csf
15	24.0	7.0	4.8	3.6	5.0	5.0	60	20	P	4.0	S
16	27.5	12.0	8.1	5.0	5.5	4.5	140	30	P	5.4	S
17	31.0	8.0	7.5	5.7	3.5	0.5	120	50	P	6.1	S
18u	22.0	9.0	3.0	1.8	4.5	4.0	80	30	P	2.4	Csf
18l	28.0	8.0	10.7	7.9	7.0	0.7	110	40	P	4.4	Cg
19u	22.5	6.0	7.2	6.4	6.7	6.5	130	35	P	8.8	Csf
19l	21.0	6.0	3.0	2.2	3.2	2.6	100	30	P		Csf
20	31.0	6.0		25.0					Bdrk		S
21	24.0	7.0	3.8	2.9	2.7	2.1	100	27.5	P	4.2	S
22	22.0	7.0	4.4	3.1	5.0	6.7	130	25	P_2	2.5	Cg
23	26.0	6.0	10.0	7.7	5.2	11.5	40	15	P	8.0–	Cr
24	29.0	7.5	14.9	11.4	20.0	11.0	190	40	B	16.0	Cr
25	33.5	6.0	14.4	12.0	7.0	3.5	270	35	B	13.5	Cr

	Scarp Δ	Fan Δ	Scarp Ht	Surface offset	Crest width	Crest Retreat	Clast Diam max	Clast Diam avg	Age	Throw	Scarp Type
26	26.5	4.0	6.1	5.1	8.0	3.7	110	30	P	6.2+	S
27	25.0	6.0	5.6	4.3	3.6	3.0	125	30	P	5.5+	S
28	29.0	6.0	12.7	10.2	10.0	12.5	160	30	B	14.2	S
29	28.5	6.0	8.3	6.6	6.5	4.0	90	25	ptB	9.2	S
30	30.5	8.0	14.2	11.4	7.5	8.6	160	40	B	160	S
31	24.0	10.0	7.0	4.1	11.0	6.5	80	15	B	—	S
32	31.0	10.0	24.2	16.5	27.0	33.0	60	17.5	pB	23.4	S
33	30.5	8.0	12.5	9.6	20.0	10.5	180	25	B	13.5	Cr
34	25.5	6.0	9.1	7.6	6.5	7.5	55	17.5	P_1	8.9	S
35	18.0	5.0	4.6	3.5	5.3	12.0	18	0.2	P_2	3.8	S
36	17.5	6.0	2.0	1.4	2.6	2.0	12	0.2	H	1.4	S
37	19.0	5.0	5.0	3.6					P	3.7–	S
38	23.0	7.0	7.5	5.2	6.5	7.0	50	12.5	B	6.4	S
39	24.0	7.0	8.5	6.0	7.7	4.0	60	15	B	6.5	S
40	23.5	10.0	11.0	6.3	9.1	8.7	40	15	B	6.8	S
41	19.0	4.0	3.2	2.8	4.2	3.0	60	20	P	2.4	Cg
42	24.0	8.0	9.9	6.2	8.5	6.0	90	22.5	B	1.5	Cg
43u	30.5	12.5	18.8	10.0	9.5	6.5	250	20	B	1.4	Cg
44	27.0	10.0	10.3	7.5	10.0	8.5	60	20	B	——	Cr
45u	25.0	5.0	10.2	8.7	4.5	9.5	90	17.5	B	4.2	Cg
46	30.0	12.0	9.0	4.7	9.0	9.2	220	32.5	B	2.3	Cg
47	27.0	7.5	4.0	2.9	5.0	2.5	70	30	P	3.2	Cr
48	14.0	5.0	3.4	2.0	4.0	0.5	12	0.2	H	2.0	S
49u	19.0	7.5	5.5	2.9	10.5	5.5	60	15	B	6.7	Csf
49l	22.0	7.5	6.2	4.2	6.5	6.5	50	25	B		Csf
50	26.0	12.0	20.0	8.4	16.0	20.5	70	20	pB	12.0–	Cr
51	23.0	8.0	9.3	6.1	6.5	14.5	70	20	B	5.2	Cr
52	19.0	8.0	3.9	2.1	6.3		50	22.5	H	2.2	S
53	25.5	9.0	15.4	10.6	13.5	21.5	50	20	pB	9.4	Cr
54	21.5	9.0	2.2	1.2	5.0	5.0	75	30	P	1.3	S
55	21.0	9.0	6.3	3.4	6.0	8.0	95	25	B	3.5	S
56	25.0	12.0	8.5	3.8	7.5	10.5	70	25	B	4.3	S
57l	24.0	11.0	9.0	4.6	14.5	14.0	90	25	B	4.6	S
58	22.0	10.0	7.4	4.4	14.5	3.5	120	25	B	4.5	S
59	20.0	8.0	3.5	2.1					B	2.4	S
60	22.5	9.0	3.6	2.2	6.6	2.5	170	30	B	2.5	S
61	29.0	12.5	15.8	8.7	19.0	21.5	80	20	pB	9.0	S
62	21.0	7.0	7.4	5.0	12.7	5.0	120	30	B	5.1	S
63	20.5	11.0	8.4	4.2	11.0	5.2	200	25	B	4.9	S
64	22.5	7.0	3.1	2.2	4.0	2.2	150	30	P	2.5	S
65	21.5	7.0	3.5	2.6	3.0	0.5	70	20	P	3.0	S
66	23.5	7.0	4.6	3.4	3.1	1.0	80	25	P	3.6	S
67	26.0	7.0	5.8	4.6	4.0	4.7	40	20	P	0.8– net?	Cg
68	22.5	5.0	4.0	3.2	9.5	5.0	30	15	P	3.4	Cg
69	21.0	5.0	3.3	2.8	4.6	3.4	70	20	P	3.2	S
70	28.0	11.0	8.2	5.2	5.6	5.5	60	16	P	6.3	S
71u	23.0	6.0	4.2	3.2	5.0	4.5	50	20	P	5.2	Csf,r
71l	22.5	5.0	3.2	2.7	4.0	4.0	50	20	P		Csf,r
72	28.5	9.5	8.5	6.0	6.3	3.7	65	25	P	6.4	S
73u	26.0	5.0	4.7	3.6	3.7	4.5	40	15	P	7.2	Csf
73l	26.0	5.0	4.4	3.6	3.7	1.7	40	15	P		Csf
74	20.0	7.5	2.4	1.5	4.7	2.8	70	20	H	1.8	S
75	30.0	5.0	15.9	12.9	8.2	16.7	75	25	B	14.0	S

76	22.5	1.5	5.3	5.0	5.0	6.0	75	25	P	4.9	S
77u	27.0	11.0	12.8	8.4	16.0	8.3	180	30	B	6.5	Cg, sf
77l	24.0	8.0	9.4	6.2	7.5	9.0	120	30	B		Cg, sg
78	33.5	11.0	21.5	15.0	7.5	12.2	220	35	ptB	6.4	Cg
79	34.0	10.0	28.3	20.8	14.0	13.0	130	35	B	7.8	Cg
80	27.0	10.0	9.9	6.4	8.1	2.5	60	30	P_1	2.4	Cg
81u	29.0	9.0	3.5	2.5	6.7	0.6	150	30	P_2	4.1	Csf
81l	20.0	9.0	3.2	1.6	7.5	5.4			P_2		Csf
82	29.0	10.0	10.8	7.0	8.0	9.2	90	30	P_1	1.2	Cg

[a] Profiles are located on 1:50,000 scale map in McCalpin (1981).

[b] Age of offset alluvium: H is early Holocene, P_2 is mid-late Pinedale, P_1 is early Pinedale, $P_{1.5}$ is later early Pinedale, P is Pinedale (undivided), ptB is post-Bull Lake, B is Bull Lake, pB is pre-Bull Lake (undivided), Bdrk is faulted bedrock, no estimate made.

[c] Scarp type: 53 profiles of simple scarp (S); 9 profiles of complex scarp, surface rotation (Cr); 15 profiles of complex scarp, graben formation (Cg); 13 profiles of complex scarp, step faulting (Csf). Total of 90 profiles.

[d] Graphically calculated fault throw based on the assumptions that the fault plane intersects the center of the steepest scarp segment, and that the fault dip is 70°. Throw values are corrected for basal deposit thickness where data are available.